

LmxMPK3, a mitogen-activated protein
kinase involved in length control of a
eukaryotic flagellum

DISSERTATION

submitted for the doctoral degree

- Dr. rer. nat. -

Department of Biology,

Faculty of Mathematics, Informatics and Natural Sciences,

University of Hamburg, Germany

by

Maja Erdmann

Hamburg, Germany

May 2009

Genehmigt vom Department Biologie
der Fakultät für Mathematik, Informatik und Naturwissenschaften
an der Universität Hamburg
auf Antrag von Priv.-Doz. Dr. M. WIESE
Weiterer Gutachterin der Dissertation:
Frau Professor Dr. I. BRUCHHAUS
Tag der Disputation: 06. Mai 2009

Hamburg, den 16. April 2009



A handwritten signature in black ink, appearing to read 'Jörg Ganzhorn'.

Professor Dr. Jörg Ganzhorn
Leiter des Departments Biologie

Confirmation

I hereby confirm that the thesis „LmxMPK3, a mitogen-activated protein kinase involved in length control of a eukaryotic flagellum” submitted by Maja Erdmann is written in linguistically correct English.

A handwritten signature in black ink that reads "Craig Roberts". The signature is written in a cursive, slightly slanted style.

Dr. Craig Roberts
Reader
Strathclyde Institute of Pharmacy and Biomedical Sciences
University of Strathclyde

We absolutely must leave room for doubt or there is no progress and no learning. There is no learning without having to pose a question. And a question requires doubt.

Richard P. Feynman, 1918 - 1988, US-American physicist, Nobel Prize 1965

Table of contents

1 Introduction	1
1.1 <i>Leishmania</i> and leishmaniasis	1
1.1.1 Taxonomy of <i>Leishmania</i> species	1
1.1.2 Clinical manifestation and epidemiology of leishmaniases	1
1.1.3 Current anti-leishmanial chemotherapies	3
1.1.4 <i>Leishmania</i> life cycle	4
1.1.5 Genome organisation and gene regulation in <i>Leishmania</i>	7
1.2 The eukaryotic flagellum	10
1.2.1 Structure and function of the flagellum	10
1.2.2 Intraflagellar transport (IFT)	12
1.3 Signal transduction in eukaryotic cells	15
1.3.1 Different signalling pathways	15
1.3.2 Protein phosphorylation and protein kinases	17
1.3.3 The MAP kinase cascade	19
1.3.4 Signal transduction in trypanosomatids	20
1.4 LmxMPK3 - State of knowledge and project aims	26
1.4.1 State of knowledge	26
1.4.2 Project aims	27
2 Materials	29
2.1 Laboratory equipment	29
2.2 Plastic and glass wares, other materials	30
2.3 Chemicals	30
2.4 Culture media, stock and buffer solutions	33
2.5 Bacterial strains	37
2.6 <i>Leishmania</i> strains	38
2.7 Mouse strain	38
2.8 DNA vectors and plasmid constructs	38
2.9 Oligonucleotides	39
2.10 Antibodies	40
2.11 Enzymes	40
2.12 Molecular biology kits	41
2.13 DNA and protein molecular weight markers	41

3 Methods	42
3.1 Cell biology methods	42
3.1.1 Culturing of <i>E. coli</i>	42
3.1.1.1 Culturing on medium plates	42
3.1.1.2 Culturing in liquid medium	42
3.1.1.3 Preparation of glycerol stocks	42
3.1.2 Culturing of <i>Leishmania</i>	42
3.1.2.1 Culturing of <i>L. mexicana</i> and <i>L. major</i> promastigotes	42
3.1.2.2 <i>In vitro</i> differentiation to <i>L. mexicana</i> axenic amastigotes	42
3.1.2.3 <i>In vitro</i> differentiation to <i>L. mexicana</i> promastigotes	43
3.1.2.4 Preparation of <i>Leishmania</i> stabilates	43
3.1.3 <i>Leishmania</i> cell counting	43
3.1.4 Fluorescence-activated cell sorting (FACS) of <i>Leishmania</i> promastigotes	43
3.2 Molecular biology methods	43
3.2.1 Preparation of competent bacteria	43
3.2.1.1 Method of Hanahan (1983)	43
3.2.1.2 Preparation of competent BL21 (DE3) [pAP/lacI ^Q]	44
3.2.2 Transformation of <i>E. coli</i>	44
3.2.3 Transfection of <i>Leishmania</i>	44
3.2.3.1 Gene Pulser transfection (<i>BIO RAD</i>)	44
3.2.3.2 Nucleofector transfection (<i>Amaxa</i>)	45
3.2.4 Isolation of plasmid DNA from <i>E. coli</i>	45
3.2.4.1 Plasmid DNA mini-preparation (Zhou <i>et al.</i> , 1990)	45
3.2.4.2 Plasmid DNA mini-preparation using <i>Macherey & Nagel</i> and <i>Qiagen</i> Kits	46
3.2.4.3 Plasmid DNA midi-preparation using <i>Invitrogen</i> , <i>Macherey & Nagel</i> and <i>Qiagen</i> Kits	46
3.2.5 Isolation of genomic DNA from <i>Leishmania</i> (Medina-Acosta and Cross, 1993)	46
3.2.6 Isolation of total RNA from <i>Leishmania</i> using a <i>Macherey & Nagel</i> Kit	47
3.2.7 Determination of DNA and RNA concentrations	47
3.2.8 Reactions with DNA-modifying enzymes	47
3.2.8.1 Cleavage of DNA using type II restriction endonucleases	47
3.2.8.2 Complete fill-in of a 5'-overhang to create blunt end DNA using Klenow enzyme	47
3.2.8.3 Dephosphorylation of DNA 5'-ends	47
3.2.8.4 Ligation of DNA fragments	48
3.2.9 Phenol/chloroform extraction of aqueous DNA solutions	48
3.2.10 Ethanol precipitation of DNA	48
3.2.11 Agarose gel electrophoresis	48

3.2.12 DNA extraction from agarose gels using <i>Macherey & Nagel</i> and <i>Qiagen</i> Kits	48
3.2.13 Insertion mutagenesis using complementary 5'-phosphorylated oligonucleotides	49
3.2.14 Polymerase chain reaction (PCR)	49
3.2.15 Reverse transcription-polymerase chain reaction (RT-PCR)	50
3.2.16 Cloning of a PCR product using the TOPO TA Cloning Kit (<i>Invitrogen</i>)	50
3.2.17 DNA sequencing	50
3.2.18 Southern blot analysis	50
3.2.18.1 Cleavage of genomic DNA and agarose gel electrophoresis	50
3.2.18.2 Denaturation, capillary blotting and cross-linking of DNA to nylon membrane	51
3.2.18.3 Pre-hybridisation, hybridisation and stringency washing	51
3.2.18.4 Detection of the DIG-labelled hybridisation probe	51
3.2.18.5 Stripping-off the hybridisation probe	52
3.3 Protein and immunochemical methods	52
3.3.1 Expression of recombinant proteins in <i>E. coli</i>	52
3.3.2 Preparation of <i>E. coli</i> cell lysates for protein purification	52
3.3.3 Affinity purification of recombinant proteins	53
3.3.3.1 Purification of GST-fusion proteins	53
3.3.3.2 Purification of His-tag fusion proteins	53
3.3.4 Thrombin cleavage of a GST-fusion protein to remove the GST-tag	53
3.3.5 Phosphoprotein purification from <i>Leishmania</i> using a <i>Qiagen</i> Kit	53
3.3.6 Determination of protein concentrations using Bradford reagent	54
3.3.7 Preparation of <i>Leishmania</i> lysates for immunoblot analysis	54
3.3.8 Preparation of <i>Leishmania</i> S-100 lysates for <i>in vitro</i> kinase assays	54
3.3.9 Discontinuous SDS polyacrylamide gel electrophoresis (SDS-PAGE)	54
3.3.10 Staining of SDS-PA gels	54
3.3.10.1 Coomassie staining	54
3.3.10.2 Silver staining	55
3.3.11 Drying of SDS-PA gels	55
3.3.12 Immunoblot analysis	55
3.3.12.1 Electroblotting of proteins using the semi-dry method	55
3.3.12.2 Immunological detection of proteins	56
3.3.12.3 Stripping-off the antibodies	56
3.4 <i>In vitro</i> kinase assays	56
3.4.1 Standard kinase assay with recombinant proteins	56
3.4.2 <i>In vitro</i> activation of recombinant kinases	56

3.4.3 Kinase assays with an activated recombinant kinase on <i>Leishmania</i> S-100 lysates	57
3.5 Mouse foot pad infection studies	57
3.6 Isolation of <i>Leishmania</i> amastigotes from mouse lesions	57
3.7 Microscopy techniques and flagellar length determination	58
3.7.1 Immunofluorescence analysis	58
3.7.2 Fluorescence microscopy on living <i>Leishmania</i> promastigotes	58
3.7.3 Transmission electron microscopy	59
3.7.4 Flagellar length determination	59
4 Results	60
4.1 The phenotype of the <i>LmxMPK3</i> null mutants and the <i>LmxMPK3</i> add back mutants	60
4.1.1 Generation of the <i>LmxMPK3</i> add back mutants	60
4.1.2 <i>LmxMPK3</i> expression levels of the <i>LmxMPK3</i> mutants	60
4.1.3 Measurements of the flagellar lengths of the <i>LmxMPK3</i> mutants	61
4.1.4 Analysis of the ultrastructure using transmission electron microscopy	62
4.1.5 Quantification of PFR-2 in the <i>LmxMPK3</i> null mutants	64
4.1.5.1 Immunofluorescence analysis	64
4.1.5.2 Immunoblot analysis	64
4.1.6 Mouse infection studies with the <i>LmxMPK3</i> mutants	65
4.2 The expression profile of <i>LmxMPK3</i> during differentiation of <i>L. mexicana</i>	66
4.3 Generation and characterisation of a GFP- <i>LmxMPK3</i> and a GFP- <i>LmxMKK</i> mutant	67
4.3.1 Preparation of the different transfection constructs	67
4.3.2 Transfection and verification of obtained clones	68
4.3.3 Measurements of the flagellar lengths of the GFP- <i>LmxMPK3</i> and GFP- <i>LmxMKK</i> mutants	70
4.3.4 Localisation studies of <i>LmxMPK3</i> and <i>LmxMKK</i> using fluorescence microscopy on living cells	71
4.3.5 Determining the correlation between <i>LmxMPK3</i> amount and flagellar length using fluorescence-activated cell sorting	72
4.4 Generation and characterisation of an inhibitor-sensitised <i>LmxMPK3</i> mutant	73
4.4.1 Preparation of the transfection construct	74
4.4.2 Transfection and verification of obtained clones	74
4.4.3 Measurements of the flagellar lengths of the inhibitor-sensitised <i>LmxMPK3</i> mutants	75
4.4.4 Inhibitor test on the inhibitor-sensitised <i>LmxMPK3</i> mutant	76

4.5 Biochemical characterisation of GST-LmxMPK3 and GST-LmxMPK3-KM	78
4.5.1 Generation of the expression constructs	78
4.5.2 Recombinant expression and affinity purification of GST-LmxMPK3 and GST-LmxMPK3-KM	78
4.5.3 Optimisation of the kinase assay reaction conditions for GST-LmxMPK3	79
4.5.4 Kinase assays with GST-LmxMPK3 and GST-LmxMPK3-KM	80
4.6 Analysis and optimisation of the activation of LmxMPK3 and LmxMPK3-KM by LmxMKK-D	81
4.6.1 Kinase assays with <i>in vitro</i> -activated GST-LmxMPK3 and GST-LmxMPK3-KM	81
4.6.2 Optimisation of the LmxMPK3 activation using an <i>in vivo</i> system	82
4.6.2.1 Generation of the co-expression constructs	82
4.6.2.2 Recombinant co-expression and affinity purification of His-LmxMPK3 and His-LmxMPK3-KM	83
4.6.2.3 Optimisation of the kinase assay reaction conditions for <i>in vivo</i> -activated His-LmxMPK3	84
4.6.2.4 Kinase assays with His-LmxMPK3 and His-LmxMPK3-KM derived from the different co-expressions	85
4.7 Analysis of the activation mechanism of LmxMPK3	86
4.7.1 <i>In vitro</i> studies	87
4.7.1.1 Generation of the co-expression constructs	87
4.7.1.2 Recombinant co-expression and affinity purification of the different His-LmxMPK3-TDY mutants	88
4.7.1.3 Kinase assays and subsequent analysis of the tyrosine phosphorylation state of the different His-LmxMPK3-TDY mutants	89
4.7.1.4 Analysis of the phosphorylation state of the different His-LmxMPK3-TDY mutants by mass spectrometry	92
4.7.2 <i>In vivo</i> studies	93
4.7.2.1 Generation of the different transfection constructs	93
4.7.2.2 Transfection and verification of obtained clones	95
4.7.2.3 Measurements of the flagellar lengths of the LmxMPK3-TDY mutants	98
4.8 Substrate search for LmxMPK3	100
4.8.1 PFR-2 as a potential LmxMPK3 substrate	101
4.8.1.1 Immunoblot analysis of PFR-2 in <i>L. mexicana</i> phosphoprotein fractions	101
4.8.2 A <i>PFR-2</i> mRNA regulating protein as a potential LmxMPK3 substrate	102
4.8.2.1 RT-PCR analysis of <i>PFR-2</i> mRNA in <i>LmxMPK3</i> null mutants	102
4.8.3 An OSM3-like kinesin as a potential LmxMPK3 substrate	103
4.8.3.1 Generation of the expression construct	104
4.8.3.2 Recombinant expression and affinity purification of GST-LmxKin32	104
4.8.3.3 Kinase assays with GST-LmxKin32 and <i>in vitro</i> -activated GST-LmxMPK3	105

4.8.4 The outer dynein arm docking complex (ODA-DC) subunit DC2 as a potential LmxMPK3 substrate	106
4.8.4.1 Immunoblot analysis of LmxDC2 in <i>L. mexicana</i> phosphoprotein fractions	106
4.8.4.2 Kinase assays with His-LdDC2 and <i>in vivo</i> -activated His-LmxMPK3	107
4.8.5 Glutamine synthetase as a potential LmxMPK3 substrate	108
4.8.5.1 Immunoblot analysis of LmxGS in <i>L. mexicana</i> phosphoprotein fractions	108
4.8.6 Kinase assays with <i>in vitro</i> -activated GST-LmxMPK3 on <i>Leishmania</i> lysates	109
4.8.7 <i>In silico</i> substrate search for LmxMPK3 using PREDIKIN	111
4.8.7.1 Features of LmjHS and its homologues	112
4.8.7.2 Testing the predicted LmjHS peptide as an LmxMPK3 substrate <i>in vitro</i>	113
4.8.7.3 Testing an N-terminal part of LmjHS as a LmxMPK3 substrate <i>in vitro</i>	116
4.8.7.4 Testing an N-terminal part of LmxHS as a LmxMPK3 substrate <i>in vitro</i>	118
5 Discussion	122
5.1 The phenotype of the <i>LmxMPK3</i> null mutants and the <i>LmxMPK3</i> add back mutants	122
5.1.1 The morphology and structure of the flagellum	122
5.1.2 The ability to complete the life cycle	127
5.2 The expression profile of LmxMPK3 during differentiation of <i>L. mexicana</i>	128
5.3 The subcellular localisation of LmxMPK3 and its activator LmxMKK	129
5.4 Characterisation of an inhibitor-sensitised LmxMPK3 mutant - an inducible system for selective kinase silencing	131
5.5 The correlation between LmxMPK3 amount and activity, and flagella length	133
5.6 Biochemical characterisation of LmxMPK3 and LmxMPK3-KM	134
5.7 The activation of LmxMPK3 and its molecular mechanism	135
5.7.1 Phosphorylation and activation of LmxMPK3 and LmxMPK3-KM	135
5.7.2 Phosphorylation and activation of different LmxMPK3-TDY mutants	138
5.7.2.1 <i>In vitro</i> studies	139
5.7.2.2 <i>In vivo</i> studies	142
5.8 Substrate search for LmxMPK3	144
5.8.1 Testing potential candidate proteins for LmxMPK3 substrate function	145
5.8.1.1 PFR-2 and a <i>PFR-2</i> mRNA regulating protein	145
5.8.1.2 The OSM3-like kinesin LmxKin32	146
5.8.1.3 The outer dynein arm docking complex (ODA-DC) subunit DC2	148
5.8.1.4 Glutamine synthetase	148
5.8.2 Screening the entire <i>Leishmania</i> proteome for LmxMPK3 substrates	149
5.8.2.1 <i>In vitro</i> kinase assays with activated LmxMPK3 on <i>Leishmania</i> lysates	149
5.8.2.2 <i>In silico</i> substrate search for LmxMPK3 using PREDIKIN	150

5.9 LmxMPK3 as a target for blocking leishmanial transmission to the insect vector	155
5.10 <i>LmxMPK3</i> mutants as model systems to study human ciliopathies	156
6 Summary	159
7 References	162
8 Appendix	178
8.1 Nucleotide and amino acid sequences	178
8.1.1 LmxMPK3	178
8.1.2 PFR-2C	181
8.1.3 LmxKin32	182
8.1.4 LmjDC2	183
8.1.5 LmxGS	184
8.1.6 LmjHS and LmxHS	184
8.1.7 IFT57	188
8.2 Plasmid maps	189
8.3 MALDI-TOF MS and MS/MS spectra	193

Abbreviations

-/-	double-allele deletion
+/-	single-allele deletion
°C	degree Celsius
1-NA-PP1	1-naphthyl-pyrazolo[3,4d]pyrimidine
A	ampère
aa	amino acids
ADP	adenosine diphosphate
Amp	ampicillin
APS	ammonium persulfate
ARE	AU-rich element
ATP	adenosine triphosphate
BBS	Bardet-Biedl syndrome
<i>BLE</i>	phleomycin resistance marker gene
BNI	Bernhard Nocht Institute for tropical medicine
bp	base pairs
BSA	bovine serum albumine
<i>C. elegans</i>	<i>Caenorhabditis elegans</i>
<i>C. reinhardtii</i>	<i>Chlamydomonas reinhardtii</i>
CaBP	Ca ²⁺ -binding proteins
cAMP	cyclic adenosine monophosphate
CD-domain	common docking domain
cDNA	complementary DNA
cGMP	cyclic guanosine monophosphate
CL	cutaneous leishmaniasis
CPB	cysteine protease B
CSPD	disodium 3-(4-methoxyspiro {1,2-dioxetane-3,2-(5-chloro)tricyclo [3.3.1.1 ^{3,7}]decan}-4-yl)phenyl phosphate
Da	Dalton
DABCO	1,4-diazabicyclo[2.2.2]octane
DAG	diacylglycerol
DAPI	4',6-diamidino-2-phenylindole dilactate
DB	database
DCL	diffuse cutaneous leishmaniasis
ddH ₂ O	double distilled water
D-domain	docking domain
DGC	directional gene cluster

DHFR-TS	dihydrofolate reductase-thymidylate synthase
DIC	differential interference contrast
DIG	digoxigenin
DMF	N,N-dimethylformamide
DMSO	dimethyl sulfoxide
DNA	deoxyribonucleic acid
dNTP	deoxyribonucleotide triphosphate
DTT	1,4-dithiothreitol
<i>E. coli</i>	<i>Escherichia coli</i>
EDTA	ethylenediamine tetraacetic acid
EGF	epidermal growth factor
EGTA	ethylene glycol bis(β -aminoethylether) tetraacetic acid
EPB	electroporation buffer
ER	endoplasmic reticulum
ERK	extracellular signal-related kinase
F	Farad
FACS	fluorescence-activated cell sorting
FAZ	flagellar attachment zone
FCaBP	flagellar Ca^{2+} -binding protein
FCS	fetal calf serum
FML	fucose mannose ligand
g	gramme
$\times g$	times gravity
gDNA	genomic DNA
GFP	green fluorescent protein
GIPL	glycoinositol phospholipids
gRNA	guide RNA
GS	glutamine synthetase
GSK	glycogen synthase kinase
GST	glutathione-S-transferase
GTP	guanosine triphosphate
h	hours
HEPES	N-2-hydroxyethylpiperazine-N'-2-ethanesulfonic acid
His	histidine
HPLC	high performance liquid chromatography
HRE	hormone response element
HRP	horse radish peroxidase

HS	hypothetical substrate
HSP	heat-shock protein
<i>HYG</i>	hygromycin B resistance marker gene
IF	immunofluorescence
iFCS	heat-inactivated FCS
IFT	intraflagellar transport
IgG	immunoglobulin G
iNOS	inducible nitric oxide synthase
InsP	Inositol phosphate
InsP ₃	inositol 1,4,5-triphosphate
IPS	<i>myo</i> -inositol-1-phosphate synthase
IPTG	isopropyl-β-D-thiogalactopyranoside
IR	intergenic region
JNK	c-Jun N-terminal kinase
kb	kilo base pairs
kDa	kilo Dalton
kDNA	kinetoplast DNA
l	litres
<i>L.</i>	<i>Leishmania</i>
LB	lysogeny broth
LPG	lipophosphoglycan
M	molar
<i>m/z</i>	mass-to-charge ratio
MALDI-TOF	matrix-assisted laser desorption/ionisation - time of flight
MAP	mitogen-activated protein
MAPK	MAP kinase
MAPKAPK	MAPK-activated protein kinase
MAPKK	MAP kinase kinase
MAPKKK	MAP kinase kinase kinase
MBP	myelin basic protein
MCL	mucocutaneous leishmaniasis
MCS	multiple cloning sites
MDA	mass drug administration
MES	morpholinoethane sulfonic acid
min	minutes
MOPS	morpholinopropane sulfonic acid
mRNA	messenger RNA

MS	mass spectrometry
MS/MS	tandem MS
<i>NEO</i>	neomycin resistance marker gene
OD	optical density
ODA-DC	outer dynein arm docking complex
ORF	open reading frame
<i>PAC</i>	puromycin resistance marker gene
PBS	phosphate-buffered saline
PCR	polymerase chain reaction
PFR	paraflagellar rod
PH	pleckstrin homology
PhD	<i>Philosophiae Doctor</i>
PKA	protein kinase A
PKD	polycystic kidney disease
PKDL	post kala azar dermal leishmaniasis
PM	peritrophic membrane
PMSF	phenylmethyl sulfonyl fluoride
PSG	promastigote secretory gel
PTB	phosphotyrosine binding
PtdIns	phosphatidylinositol
PtdInsP	phosphatidylinositol phosphate
PV	parasitophorous vacuoles
PVDF	polyvinylidene fluoride
RNA	ribonucleic acid
RNAi	RNA interference
RP	retinitis pigmentosa
rpm	revolutions per minute
rRNA	ribosomal RNA
RT	reverse transcriptase
RT	room temperature
RTK	receptor tyrosine kinases
RT-PCR	reverse transcription-polymerase chain reaction
s	seconds
SAP	shrimp alkaline phosphatase
SDR	substrate-determining residue
SDS	sodium dodecyl sulphate
SDS-PA	SDS-polyacrylamide

SDS-PAGE	SDS-PA gel electrophoresis
SH	Src homology
SL	spliced leader
SSC	standard saline citrate
<i>T.</i>	<i>Trypanosoma</i>
TBS	Tris-buffered saline
TBV	transmission-blocking vaccines
TEM	transmission electron microscopy
TEMED	N,N,N',N'-tetramethylethylenediamine
TLCK	N α -tosyl-L-lysine chloromethyl ketone hydrochloride
TPR	tetratricopeptide repeat
Tris	tris(hydroxymethyl)aminomethane
TRP	transient receptor potential
U	units
UTR	untranslated region
UV	ultraviolet
V	volt
v/v	volume per volume
VL	visceral leishmaniasis
w/v	weight per volume
WHO	World Health Organisation
X-Gal	5-Bromo-4-chloro-3-indolyl- β -D-galactopyranoside

1 Introduction

1.1 *Leishmania* and leishmaniasis

Leishmania are parasitic protozoa and the etiological agents of the leishmaniasis, a group of diseases transmitted to mammals by sand flies. The parasites were first discovered in India by the British tropical physician Sir W.B. Leishman and the Irish tropical physician C. Donovan in 1901. Leishmaniasis belongs to the currently 14 neglected tropical diseases listed by the World Health Organization (WHO).

1.1.1 Taxonomy of *Leishmania* species

Leishmania belong to the order Kinetoplastida named for the presence of the kinetoplast, a distinct region of the single mitochondrion containing coiled DNA filaments, which is always closely associated with the basal body of the flagellum. Kinetoplastida can be divided into two suborders according to the number of flagella per cell. While Bodonina reveal two flagella and are mostly free-living, Trypanosomatina possess only a single flagellum and are predominantly parasitic. The latter comprise the family Trypanosomatidae consisting of nine different genera. While some of them use plants, insects or reptiles as their main hosts, the genera *Endotrypanum*, *Trypanosoma* and *Leishmania* infect mammals. Besides *Trypanosoma brucei* (*gambiense* and *rhodesiense*) causing sleeping sickness and *Trypanosoma cruzi* causing Chagas disease, also 21 of the almost 30 known *Leishmania* species are pathogen to humans.

1.1.2 Clinical manifestation and epidemiology of leishmaniasis

Since *Leishmania* parasites are transmitted to mammals by sand flies, their endemic region is consistent with the habitat of their vectors, predominantly rural areas in the tropics and subtropics. Sand flies of the genus *Phlebotomus* are found in the old world (Africa, Asia and Europe), whereas the genus *Lutzomyia* is found in the new world (America). Both genera belong to the family of Psychodidae (moth fly) in the order of Diptera. Leishmaniasis occurs in 88 countries worldwide distributed on all continents except Australia. 72 of those nations belong to the developing countries including the 13 poorest countries in the world. However, leishmaniasis is also found in 16 European countries like France, Spain, Italy and Greece. Over the last 10 years endemic regions have been spreading, and a significant increase in the number of recorded cases of the disease has been reported. The WHO estimates that 2 million new cases occur annually, 12 million people are presently infected and 350 million people are currently threatened by the disease worldwide.

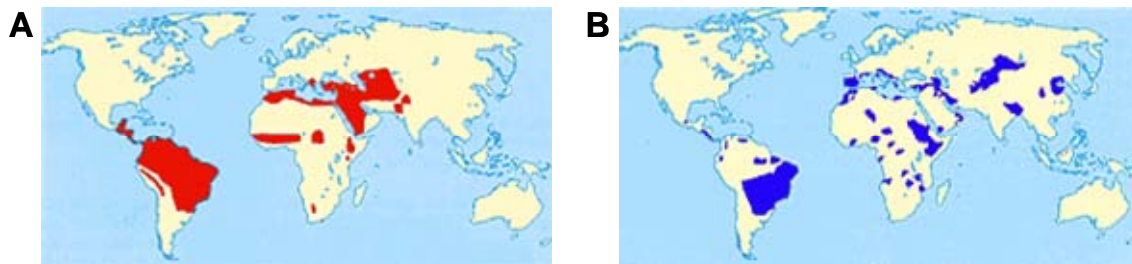


Figure 1: Geographical distribution of leishmaniases

A: cutaneous and mucocutaneous leishmaniasis; B: visceral leishmaniasis.

(Source: <http://www.infektionsbiologie.ch/modellparasiten/leishmania.htm>, 2004)

There are three different forms of leishmaniasis differing in their clinical symptoms. The clinical manifestation and the severity of the disease depend on the *Leishmania* species as well as on the genotype and immune status of the host.

Cutaneous leishmaniasis (CL)

CL, also known as Aleppo boil, Bagdad boil or oriental boil, is the most common form of leishmaniasis which exclusively affects the skin. A lesion develops at the site of bite typically located on exposed areas such as the face, arms and legs and mostly remains restricted to this site. The lesion often spontaneously heals with scarring accompanied by a lifelong immunity against the *Leishmania* species which caused the disease. CL accounts for ca. 75% of new *Leishmania* infections. 90% of the cases of CL are found in Iran, Afghanistan, Syria, Saudi Arabia, Brazil and Peru. The CL-causing species in the old world are predominantly *L. major*, *L. tropica* and *L. aethiopica*. CL in the new world is mainly caused by members of the *L. mexicana* complex, *L. panamensis* and *L. guyanensis*.

A more severe form of CL is the diffuse cutaneous leishmaniasis (DCL) resulting in widely spread and chronic skin lesions which may cover an individual's entire body. This form of CL is difficult to treat and patients do not self-cure. DCL is found in Africa and America and is caused by some members of the *L. mexicana* complex and *L. aethiopica*.

Mucocutaneous leishmaniasis (MCL)

MCL, also called Uta or Espundia, is exclusively found in America and is mostly caused by members of the *L. braziliensis* complex. This form of leishmaniasis can lead to an extensive destruction of the nasal, pharyngeal and laryngeal mucosa and their surrounding tissues. It develops as a complication of CL with parasites disseminating from the primary cutaneous lesion via lymphatic and blood vessels to reach the upper respiratory tract mucosa. MCL is difficult to treat and can be fatal especially if superinfections occur.

Visceral leishmaniasis (VL)

VL is the most severe form of leishmaniasis and also known as kala azar or Dum-Dum fever. After infection the parasite migrates to the internal organs such as liver, spleen and bone

marrow. Typical symptoms include fever, weight loss, anaemia and substantial swelling of the liver and spleen. If left untreated the disease results in the death of the host within two years. VL is caused by members of the *L. donovani* and *L. infantum* complex. 90% of the cases of VL are found in Bangladesh, India, Nepal, Sudan and Brazil.

Patients who have recovered from VL may suffer from post kala azar dermal leishmaniasis (PKDL). PKDL is a chronic form of CL beginning with a nodular rash appearing on the face which then spreads to other parts of the body. The disease is particularly severe if the lesions spread to the mucosal surfaces.



Figure 2: Clinical picture of leishmaniasis
A: CL; B: MCL; C: VL. (Source: WHO/TDR/Crump/Kuzoe)

1.1.3 Current anti-leishmanial chemotherapies

Since over 60 years pentavalent antimonials have been used to treat all forms of leishmaniasis, especially CL and VL. The primary mode of action has not been clarified to date. Pentostam[®] (sodium stibogluconate, *GlaxoSmithKline*) and Glucantime[®] (meglumine antimoniate, *Aventis*) are the most conventional products. A disadvantage of this “first line drug” is the long period of parenteral administration for 20 to 28 days as well as severe side effects such as heart and liver damages (Lee and Hasbun, 2003). Moreover, antimonial resistance has been observed in India since 1980. As a consequence, 65% of Indian patients are not responsive to antimonial treatment any more (Sundar, 2003).

Due to the increasing resistance to pentavalent antimonials several “second line drugs” have been recommended or newly developed. The diamidine pentamidine was introduced in 1952 and is used to treat all forms of leishmaniasis in cases of antimonial resistance. The primary mode of action is unclear to date. The use of pentamidine is mainly restricted by several serious side effects such as hyperkalaemia, renal and gastrointestinal dysfunctions, and also the development of an insulin-dependent diabetes mellitus.

Amphotericin B is a highly effective polyene antibiotic which is used for treatment of antimonial resistant VL and certain cases of MCL (Croft and Coombs, 2003). The compound is selective towards ergosterol which is the predominant sterol over cholesterol in *Leishmania* (Croft *et al.*, 2006). However, severe side effects such as hypokalaemia, liver

and kidney damages, and myocarditis have been observed. Therefore, numerous lipid formulations of Amphotericin B were developed in the 1980s showing a reduced toxicity. AmBisome[®] (Gilead Sciences), the liposomal formulation of Amphotericin B, was first shown to be effective against VL in 1991. However, high costs restrict its use as an anti-leishmanial drug.

In 2002 Miltefosine (hexadecylphosphocholine) was registered in India for treatment of VL and CL in cases of antimonial resistance. It was the first anti-leishmanial drug for oral administration. However, Miltefosine has exhibited teratogenicity and thus should not be administered to women of child-bearing age (Croft and Coombs, 2003). Moreover, there are concerns regarding the long half-life which might support drug resistance. Therefore, a combination therapy treatment is recommended.

The aminoglycoside antibiotic paromomycin was registered in 2006 to treat VL in India. It is also used to treat CL in topical or parenteral formulations. Occurring side effects are mostly relatively harmless.

Due to the risk of occurring drug resistances the development of new anti-leishmanial drugs is paramount. New drugs should be orally administerable, financially affordable, well tolerated by patients and should optimally aim at more than one target structure to counteract against the development of drug resistances.

1.1.4 *Leishmania* life cycle

Leishmania parasites undergo profound biochemical and morphological changes when passing through their digenetic life cycle, whereby they survive in their sand fly vector as well as in their mammalian host. Different cell surface glycoconjugates play an important role in the survival strategy of the parasite. The insect-stage promastigotes are spindle-shaped cells, 10 to 20 μm in length, which possess a flagellum, reaching up to 20 μm in length, protruding from the flagellar pocket at the anterior end of the cell. In contrast, the amastigotes living in the phagocytes of their mammalian host are spherical-shaped cells, only 2 to 4 μm in diameter, which reveal only a very short flagellum limited to the flagellar pocket. Both forms of the parasite multiply by binary fission.

Promastigotes assume different morphological forms in the gut of the sand fly (see Table 1). At different stages lipophosphoglycan (LPG), the main cell surface glycoconjugate of promastigotes, binds to lectin receptors of the gut epithelium to prevent expulsion of the parasite during defecation. Procyclic promastigotes are present in the abdominal midgut of the female sand fly and develop from amastigotes within 48 h after the blood meal while still enclosed by the peritrophic membrane (PM) protecting the parasite from digestive enzymes (Pimenta *et al.*, 1997). They are an oval-shaped, flagellated, slightly motile and replicative form of promastigotes. During the following 24 h the procyclic forms slow down their

replication and transform into the non-dividing, long, slender and strongly motile nectomonad promastigotes which escape from the PM by secretion of a chitinase (Schlein *et al.*, 1991) to anchor themselves to the midgut epithelium. They subsequently migrate towards the anterior midgut until reaching the stomodeal valve located at the junction between midgut and foregut. By day four the nectomonad forms develop into leptomonad promastigotes, shorter forms of the parasite which initiate a second growth cycle resulting in a massive infection. Leptomonads produce the promastigote secretory gel (PSG) which blocks the anterior midgut and ensures the transmission of the parasite to the mammalian host at a later stage. After day five leptomonad promastigotes differentiate into mammalian-infective, non-dividing metacyclic promastigotes. Additionally, leaf-like haptomonad forms with short flagella are observed at the stomodeal valve forming a parasite plug. Directly before the next blood meal the PSG plug has to be regurgitated by the female sand fly, thereby transmitting the metacyclic promastigotes into the skin of the mammalian host. It is assumed that an induced enzymatic damage of the stomodeal valve, an occurrence of parasites in the salivary glands and an excretion of parasites from the anus of infected sand flies additionally contributes to the transmission of the parasite.







Morphological form	Criteria	Schematic illustration
Amastigote	ovoid body, flagellum not visible	
Procyclic promastigote	BL 6.5 - 11.5 µm, flagellum < BL	
Nectomonad promastigote	BL ≥ 12 µm, flagellar length variable	
Leptomonad promastigote	BL 6.5 - 11.5 µm, flagellum ≥ BL	
Haptomonad promastigote	disc-like expansion of flagellar tip, body form and flagellar length variable	
Metacyclic promastigote	BL ≤ 8 µm, flagellum > BL	

Table 1: Morphological forms of *L. mexicana*

BL, body length. (modified from Rogers *et al.*, 2002)

In the skin of the mammalian host the metacyclics avoid the complement-mediated lysis using different strategies. On the one hand, the insertion of the lytic C5b-C9 complex into the promastigote membrane is effectively blocked (Puentes *et al.*, 1990). On the other hand, a serine/threonine protein kinase (LPK-1) is secreted by the metacyclics which leads to an inactivation of C3, C5 and C9 (Hermoso *et al.* 1991). At the same time, however, the promastigotes depend on fixation of opsonic complement factors to enter the host macrophages. Thus, the leishmanial surface metalloprotease gp63, also called leishmanolysin, rapidly converts bound C3b into iC3b favouring phagocytic clearance rather than lytic clearance. The uptake by macrophages is mediated by the complement receptors

CR1 and CR3 (Brittingham *et al.*, 1995; Rosenthal *et al.*, 1996) as well as by mannosyl-fucosyl receptors and fibronectin receptors in the macrophage membrane which bind to LPG and gp63 (Kane and Mosser, 2000).

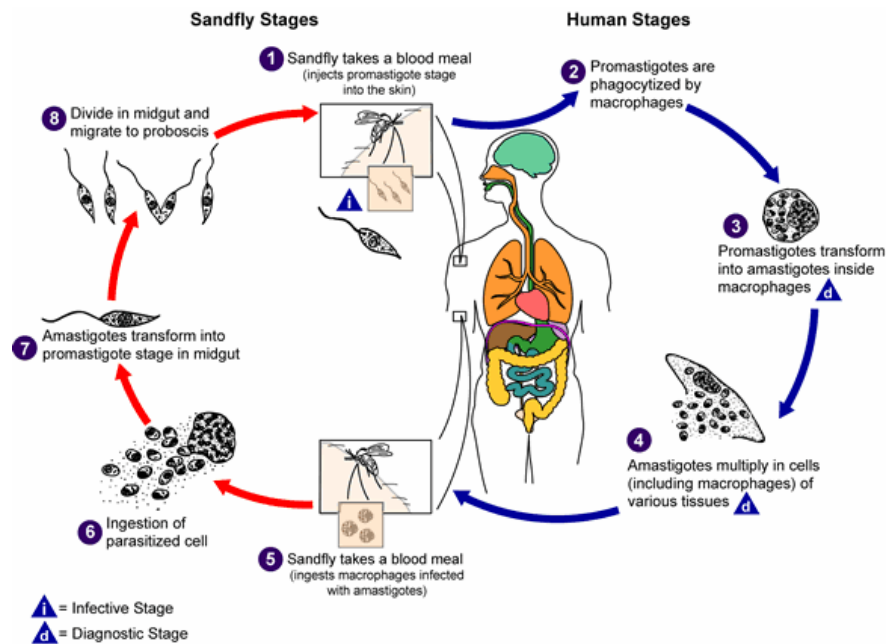


Figure 3: *Leishmania* life cycle

(Source: <http://www.dpd.cdc.gov/dpdx>)

The *Leishmania*-filled phagosomes subsequently fuse with lysosomes to form phagolysosomes which are also termed parasitophorous vacuoles (PVs). The PVs contain acid hydrolases at a local pH of 4.7 to 5.2 and vary in number, size and shape according to the respective *Leishmania* species. While numerous *L. mexicana* and *L. amazonensis* parasites share one PV, each *L. major* and *L. donovani* parasite is individually located in a small PV (Antoine *et al.*, 1998). Triggered by the low pH and the elevated temperature in the mammalian host, the metacyclic promastigotes differentiate into amastigotes within 2 to 5 days (Shapira *et al.*, 1988; Zilberstein *et al.*, 1991). Subsequent proliferation of the amastigotes eventually leads to lysis of the macrophage and infection of neighbouring macrophages with the released amastigotes.

An early response of macrophages to the infection with pathogens is the respiratory burst, a rapid release of reactive oxygen species such as the hyperoxide anion (O_2^-) and hydrogen peroxide (H_2O_2), and the generation of nitric oxide (NO). *Leishmania* parasites evade those defence mechanisms using different strategies. It was found that LPG reduces the production of O_2^- by inhibiting protein kinase C. In addition, gp63 was shown to be involved in the suppression of the respiratory burst (Sørensen *et al.*, 1994). In addition, it was found that the inducible nitric oxide synthase (iNOS) is inhibited in early infection by both LPG and glycoinositol phospholipids (GIPLs), the major constituents of the amastigote surface

(Proudfoot *et al.*, 1995). Moreover, the release of pro-inflammatory cytokines by the macrophage is prevented by affecting the phosphorylation state of MAP (mitogen-activated protein) kinases such as p38 and ERK 1/2 (Martiny *et al.*, 1999; Prive and Descoteaux, 2000; Junghae and Raynes, 2002).

Apart from macrophages, other cell types are able to phagocytose *Leishmania* parasites. During the early phase of infection parasites are taken up by dendritic cells (Caux *et al.*, 1995) as well as polymorphonuclear neutrophil granulocytes. The latter are believed to act as host cells before macrophages are infected (Laufs *et al.*, 2002; Laskay *et al.*, 2003). Moreover, fibroblasts presumably serve as host cells for persisting *Leishmania* parasites in the clinically latent disease (Bogdan *et al.*, 2000).

1.1.5 Genome organisation and gene regulation in *Leishmania*

Supported by the WHO the sequencing of the *L. major* genome was started in 1994 by the *Leishmania* Genome Network and was finished in 2003 (Ivens *et al.*, 2005). Thereafter, the *L. infantum* and *L. braziliensis* genome sequencing was completed by the Sanger Institute (Peacock *et al.*, 2007). Currently, sequencing of the *L. mexicana* genome is in progress, and shotgun reads are already available on the website of the Sanger Institute.

The haploid genome of *Leishmania* comprises 3.2 to 5×10^7 base pairs (bp) which are arranged on 34 (e. g. *L. mexicana*; Britto *et al.*, 1998) to 36 chromosomes depending on the *Leishmania* species. As the chromosomes do not condense during the mitotic cycle, the number of chromosomes was determined by pulsed field gel electrophoresis (Stiles *et al.*, 1999). Like in other eukaryotes, chromosomes in *Leishmania* reveal telomeric sequences at their ends (Myler *et al.*, 1999), however, they lack typical centromeric sequences. Chromosomal sizes range from 0.3 to 2.8×10^7 bp in *L. major*. Number and size of chromosomes can change rapidly, since repetitive DNA sequences (30% of the genome) can cause amplifications or deletions of DNA regions by homologous intramolecular recombination. In addition to the standard complement of chromosomes, *Leishmania* parasites can contain linear or circular multi-copy minichromosomes which can constitute 5 to 10% of the total cellular DNA. They can form spontaneously or as a response to drug selection or nutrient stress and are the result of the amplification of DNA regions (Beverley, 1991; Segovia, 1994) which is likely to occur by homologous intramolecular recombination supported by flanking repetitive sequences (Olmo *et al.*, 1995; Grondin *et al.*, 1996). *Leishmania* organisms are predominantly diploid as indicated by the need of two consecutive rounds of electroporation for the generation of null mutants (Cruz *et al.*, 1991) and the presence of restriction site polymorphisms (Hendrickson *et al.*, 1993). However, contrary to *T. brucei*, genetic (sexual) exchange in *Leishmania* seems to be an infrequent feature (Panton *et al.*, 1991), and its mechanism is unclear (Gibson and Stevens, 1999). The amount

of sequence polymorphisms in the *Leishmania* genome is very low (< 0.1%), contrasting with the genomes of *T. brucei* and *T. cruzi* (Ivens *et al.*, 2005). The G/C content of the *Leishmania* genome is noticeably high (57%; Alonso *et al.*, 1992) compared to the mammalian genome (40 to 45%), especially in the third (wobble) position of the amino acid codons (ca. 85%). So far, 8370 protein-coding genes have been identified in the *L. major* genome (<http://www.genedb.org/genedb/leish>).

Apart from the genomic DNA (gDNA) of the nucleus, *Leishmania* organisms contain the kinetoplast DNA (kDNA) which is located in the single, large mitochondrion of the parasite and makes up 10 to 15% of the total cellular DNA. The kDNA consists of several thousand circular, non-supercoiled DNA molecules which are catenated to generate a highly condensed planar network. There are two types of circular DNA molecules. Minicircles are present in 5000 to 10000 non-identical copies per cell ranging from 0.5 to 2.8 kilo base pairs (kb). So far, their only known genetic function is to encode guide RNAs (gRNAs) which are involved in the editing of maxicircle transcripts (see below). The maxicircles exist in 25 to 50 identical copies per cell, and their size ranges from 20 to 39 kb. They encode rRNAs, mitochondrial proteins and a small number of gRNAs.

Generally, *Leishmania* genes do not contain introns, and hence *cis*-splicing mechanisms are not expected to occur. So far, only four genes subjected to *cis*-splicing have been identified in trypanosomatids, among them an RNA helicase (Ivens *et al.*, 2005). Almost one third of the *Leishmania* protein-coding genes is clustered into families of related genes. While smaller families have most likely developed by tandem gene duplication, genes of larger families have multiple loci consisting of single genes and/or tandem arrays and often represent *Leishmania*-specific genes. Genes of highly expressed proteins such as α - and β -tubulins, flagellar proteins, heat shock proteins (HSPs), proteases, transporters and surface proteins are present in multiple copies. Those genes are often organised as direct tandem repeats which most likely serves as a mechanism to increase the abundance of the primary transcripts. Some correlation between the gene copy number and the intracellular protein concentration was demonstrated for some heat shock proteins in *Leishmania* promastigotes (Brandau *et al.*, 1995; Hübel *et al.*, 1995).

Although trypanosomatids reveal a range of chromatin-remodelling activities, the mechanisms regulating RNA polymerase II-directed transcription seem to differ strongly from those of other eukaryotes. The chromosomes are organised into directional gene clusters (DGCs) of tens to hundreds of genes with unrelated predicted functions which can reach up to 1259 kb in size (Ivens *et al.*, 2005). Those clustered genes are co-transcribed thus generating a polycistronic pre-mRNA. A common spliced leader (SL) sequence of 39 nucleotides, also known as mini-exon, is subsequently attached to the 5'-end of all messages by a mechanism called *trans*-splicing. The SL is encoded separately by

approximately 200 gene copies which are predominantly organised in a tandem array. The 5'-end of the SL contains a 7-methylguanosine cap which is essential for the splicing reaction. *Trans*-splicing is controlled by polypyrimidine (CT) tracts in the 5'-UTR of genes and usually occurs at the first AG dinucleotide downstream of the CT tract. In *Leishmania* 3'-end polyadenylation eventually releasing monocistronic mRNA is coupled to *trans*-splicing of the downstream gene neighbour (Ullu *et al.*, 1993). Polyadenylation occurs 100 to 500 nucleotides upstream of the splice-acceptor site (Stiles *et al.*, 1999; Clayton, 2002). Therefore, unlike other eukaryotes, poly(A) site selection is not determined by consensus poly(A) signal sequences. The 5'- and 3'-UTR of *Leishmania* transcripts are mostly longer than those of other eukaryotes reaching up to 688 bp and 2973 bp, respectively. The initiation mechanism of RNA polymerase II-directed transcription has not been clarified to date. The only known RNA polymerase II promoter belongs to the SL gene and is located upstream of each SL gene copy (Saito *et al.*, 1994). Several homologues of RNA polymerase II basal transcription factors have been identified, however, the majority of those factors is missing (Ivens *et al.*, 2005). By contrast, the trypanosomatid genomes contain a noticeably high number of genes encoding proteins with potential RNA binding properties. Current knowledge strongly suggests that gene expression in trypanosomatids is primarily regulated on the posttranscriptional level, contrasting higher eukaryotes controlling gene expression mainly by regulating transcription. Transcript abundance depends on sequences in the 3'-UTR and the downstream intergenic region (IR) affecting mRNA processing and/or stability and is mediated by labile protein factors (Stiles *et al.*, 1999). The 3'-UTR is also known to control translation efficiency. In some cases, posttranslational modifications affect intracellular protein amounts (Clayton, 1999).

Another characteristic of trypanosomatids is the extensive sequence modification of the mitochondrial transcripts by a process known as RNA editing. The genes on the maxicircles generate transcripts lacking numerous uracil (U) units. The gRNA (see above) serves as a template for the insertion (or less frequently the deletion) of uracil into the pre-mRNA recruiting different enzymes. The process of RNA editing is essential for converting the mitochondrial transcripts into mature mRNAs ready for translation.

There are different ways for the analysis and manipulation of genes in *Leishmania* organisms. The generation of null mutants can be achieved by sequentially replacing both alleles of the gene to be analysed by different resistance marker genes in two consecutive rounds of electroporation. Gene replacement occurs by the mechanism of homologous recombination. A different strategy of gene introduction is the addition of an expression vector carrying the gene of interest in addition to selected IR sequences and a resistance marker gene. In contrast to *T. brucei*, the mechanism of RNA interference (RNAi) has not been applied successfully to *Leishmania* to date. However, while most *Leishmania* species

lack essential components involved in this process (Robinson and Beverley, 2003), *L. braziliensis* has been found to contain all components necessary for RNAi (Peacock *et al.*, 2007).

1.2 The eukaryotic flagellum

1.2.1 Structure and function of the flagellum

Flagella and cilia are eukaryotic organelles conserved from protists to mammals. They function in a variety of biological processes such as single cell movement, sensory reception and fluid movement in complex multicellular organisms. Flagella show the same construction as cilia, however, they are much longer. They typically project from the cell surface and are composed of a microtubule backbone (axoneme) surrounded by a membrane contiguous with the plasma membrane. According to the axonemal organisation of microtubule pairs two main ciliary types, namely “9+2” (motile) and “9+0” (primary, non-motile), have been defined. The “9+2” axoneme is composed of nine microtubule doublets surrounding a central pair of singlets which is absent in the “9+0” axoneme. However, this classical distinction is obsolete since organisation of microtubules can vary within one organelle as shown for the cilia of sensory neurons of *Caenorhabditis elegans* displaying middle segments composed of nine microtubule doublets and distal segments of nine microtubule singlets. In addition, the classification of “9+2” and “9+0” as motile or sensory is strongly simplified. Examples of motile primary cilia (e.g. in the renal epithelium; Ong and Wagner, 2005) as well as motile cilia/flagella with sensory roles (see below) have been reported. The axonemal microtubules are linked to numerous other proteins such as the inner and outer dynein arms responsible for flagellar beating, the radial spokes and the nexin bridges (see Figure 4). It was found that the axoneme of *Chlamydomonas* species is composed of at least 250 proteins (Piperno *et al.*, 1977).

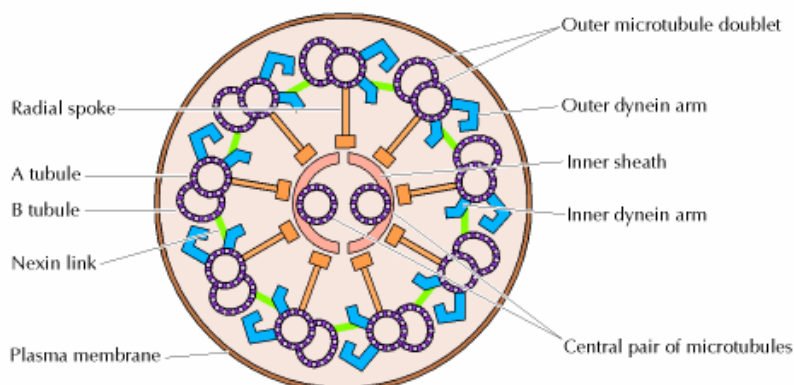


Figure 4: Schematic illustration of a “9+2” axoneme

(Source: Cooper G. M.: The Cell - A Molecular Approach, Sinauer Associates, 2nd edition, 2000)

A unique feature of the flagellum in trypanosomatids is the presence of a lattice-like structure called the paraflagellar rod (PFR) which is attached to the axoneme and runs along the length of the flagellum (Gull, 1999). A PFR has so far been identified in three groups of protists: kinetoplastids, euglenoids and dinoflagellates. The PFR consists of a short proximal, an intermediate and a more developed distal domain (see Figure 5). Filaments of the intermediate domain link the proximal and distal domains which are both composed of plate-like structures stacked parallel to each other. Moreover, the proximal domain of the PFR is connected to the axonemal microtubule doublets 4 to 7 by fibres. Although the complete composition of the PFR is still unknown, two closely related proteins could be identified as the major components. Their homologues are PFR-1 and PFR-2 in *Leishmania*, PFR-C and PFR-A in *T. brucei*, and PAR-3 and PAR-2 in *T. cruzi*, respectively. The corresponding genes are organised in tandem arrays of several gene copies. Some other proteins have been shown to localise to the PFR. Among them are calmodulin (Ruben and Patton, 1986; Ridgley *et al.*, 2000) and some calflagins (flagellar calcium-binding proteins; Wu *et al.*, 1994; Bastin *et al.*, 1999a). In addition, several proteins involved in the nucleotide metabolism, namely adenylate kinases (Pullen *et al.*, 2004; Ginger *et al.*, 2005) and cAMP phosphodiesterases (Zoraghi and Seebeck, 2002; Oberholzer *et al.*, 2007), have been identified as PFR-associated components. Several examples show that the PFR has an essential role in the motility of the parasite. *PFR-2* null mutants of *L. mexicana* still display a residual PFR containing PFR-1 subunits, however, they reveal an approximately 4-fold reduced velocity of forward motility (Santrich *et al.*, 1997). The flagellar beat pattern is altered showing a reduced wavelength and a decreased beat frequency. The impaired motility might result from a reduced elastic bending resistance of the flagella lacking most of the PFR. A more dramatic phenotype could be generated in *T. brucei* in which the *PFR-A* mRNA was ablated by RNAi (Bastin *et al.*, 1998; Bastin *et al.*, 1999a; Bastin *et al.*, 2000). The PFR seemed to be disrupted resulting in paralysed cells which sedimented to the bottom of the tissue culture flask. Besides its function in cell motility the PFR might serve as a scaffold for regulatory and metabolic proteins of the flagellum (Ralston and Hill, 2008).

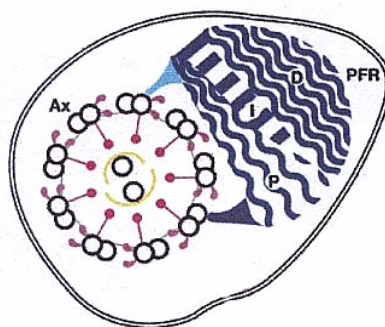


Figure 5: Schematic illustration of the PFR next to the axoneme

Ax, axoneme; D, distal; I, intermediate; P, proximal. (modified from Bastin *et al.*, 2000)

The trypanosomatid flagellum is involved in other biological activities than cell motility such as the attachment to host surfaces (see 1.1.4) and intracellular signalling. The latter might be supported by several identified flagellar proteins with a potential role in environmental sensing or intracellular signal transduction. In *T. brucei* the adenylate cyclase ESAG4 is exclusively found in the flagellar membrane (Paindavoine *et al.*, 1992), however, neither its function nor the corresponding signalling pathway have been identified to date. In addition, an EF-hand flagellar Ca^{2+} -binding protein (FCaBP) was found to associate with the flagellar membrane in a Ca^{2+} -dependent manner in *T. cruzi* (Engman *et al.*, 1989). An analogous mechanism can be found in the plasma membrane of mammalian retinal rod cells where the EF-hand Ca^{2+} -binding protein recoverin mediates signal transduction by changes in intracellular Ca^{2+} levels (Dizhoor *et al.*, 1991; Calvert *et al.*, 1995). Another example of a flagellum-specific receptor is the glucose transporter ISO1 which was analysed by Piper *et al.* (1995). Its possible role in glucose sensing is supported by observations made on yeast and human orthologues (Ozcan *et al.*, 1996; Bandyopadhyay *et al.*, 2000). An example for the presence of motile cilia with sensory roles in mammals are the cilia of the female reproductive tract in mice which contain transient receptor potential (TRP) channels involved in environmental sensing (Teilmann *et al.*, 2005). The flagellum of trypanosomes is additionally involved in regulating cell size, shape, polarity and division (Kohl *et al.*, 2003). Those functions are likely to be mediated by the flagellar attachment zone (FAZ), a structure which is exclusively found in trypanosomes and is probably involved in the attachment of the flagellum to the cell body. It is therefore unlikely that the unattached flagellum of *Leishmania* has similar functions.

The flagellum of trypanosomatids exits from a deep invagination of the plasma membrane at the anterior end of the cell known as the flagellar pocket. Its opening is surrounded by the “zone of adhesion” (Overath *et al.*, 1997), a desmosome-like thickening which might prevent the flow of material into and out of the flagellar pocket. However, macromolecules have been shown to pass this border (Landfear and Ignatushchenko, 2001). The flagellar pocket is the only site of the whole cell where endocytosis and the secretion of proteins take place. Moreover, membrane proteins are first delivered to the flagellar pocket from where they are differentially targeted to different membrane domains (Bastin *et al.*, 2000).

1.2.2 Intraflagellar transport (IFT)

Intraflagellar transport (IFT) is the motor-dependent bidirectional movement of IFT particles along the length of eukaryotic flagella and cilia. It is a highly conserved process essential for the construction and maintenance of those organelles and has been excessively studied in *Chlamydomonas*. Although many proteins involved in IFT have yet to be identified (Haycraft *et al.*, 2003), 17 protein subunits belonging to two different IFT complexes (A and B)

conserved among green algae, nematodes and vertebrates have been identified. Morphologically similar particles are also present in the flagella of trypanosomatids (Sherwin and Gull, 1989). Using an *in silico* approach twelve of the conserved protein subunits could be identified in *Leishmania* (Gouveia *et al.*, 2007) while at least 10 IFT complex proteins were found in *T. brucei* (Briggs *et al.*, 2004; Absalon *et al.*, 2008). IFT complex subunits are rich in protein-protein interaction domains of the tryptophan-aspartic acid (WD)-40, tetratricopeptide repeat (TPR) protein and coiled coil families (Cole, 2003) which allow complex assembly as well as binding of cargo and motor proteins.

Anterograde movement of IFT complex B (from base to tip) is driven by a heterotrimeric motor protein complex of the kinesin-2 family, consisting of two heterodimerised kinesin motor subunits and an accessory subunit termed kinesin-2-associated protein (KAP) (Cole *et al.*, 1993; Wedaman *et al.*, 1996). Retrograde movement of IFT complex A (from tip to base) is driven by the cytoplasmic motor protein complex dynein 1b (Pazour *et al.*, 1999; Porter *et al.*, 1999; Signor *et al.*, 1999) consisting of at least two subunits, namely a dynein heavy chain (DHC1b) and a light intermediate chain (D2LIC) (Cole, 2003; Perrone *et al.*, 2003).

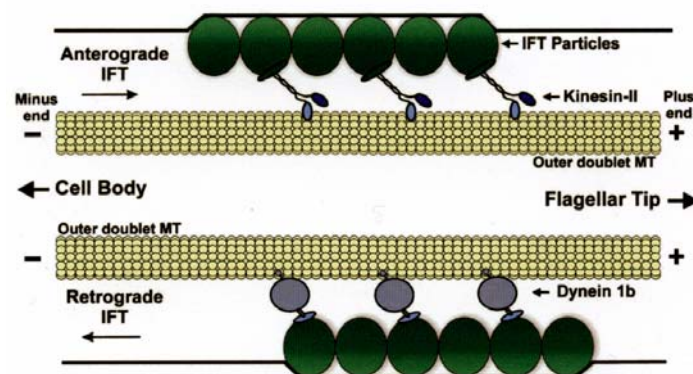


Figure 6: Schematic illustration of intraflagellar transport (IFT)
(Source: Cole, 2003)

Cilia contain multiple kinesins in addition to heterotrimeric kinesin-2 (Fox *et al.*, 1994). Analysis of the IFT in chemosensory cilia of *C. elegans* revealed that besides heterotrimeric kinesin-2, termed kinesin-II, a second kinesin-2 family member, known as OSM-3, drives anterograde IFT as a homodimeric complex (Signor *et al.*, 1999; Snow *et al.*, 2004). While kinesin-II and OSM-3 function together to assemble the middle segment of the axoneme composed of microtubule doublets (with each motor being able to work in the absence of the other motor), OSM-3 alone extends the distal end consisting of microtubule singlets. However, OSM-3 only extends distal singlets in some ciliary types, since it is also active in amphid wing cilia of *C. elegans* which only reveal microtubule doublets (Scholey, 2008). KIF17, a close relative of OSM-3, is known to target cyclic nucleotide-gated channels to mammalian primary cilia (Jenkins *et al.*, 2006). In *C. elegans* the kinesin-3 family member KLP-6 was shown to be essential for ciliary targeting of polycystins forming mechanosensory

ion channels in the membranes of cilia on male-specific sensory neurons (Peden and Barr, 2005). The microtubule-depolymerising kinesin-13 is supposed to cooperate with the IFT machinery at the flagellar tip to control the length of the flagellum in *Leishmania* (Blaineau *et al.*, 2007) and *Giardia* (Dawson *et al.*, 2007). It is generally assumed that accessory kinesins such as OSM-3 confer cilia-specific functions. They might be involved in modulating IFT, target specific proteins to the organelle or function as stable ciliary components (Scholey, 2008). In *Leishmania* a putative Unc104-like kinesin as well as a kinesin-2 subunit have been identified as IFT-related factors (Gouveia *et al.*, 2007). In addition, the *L. major* genome DB (Ivens *et al.*, 2005) reveals two putative OSM-3-like kinesins.

IFT is essential for the delivery of large numbers of different cargo proteins to the flagellum and back to the cell body. Axonemal subunits are transported from the basal body region to the tip of the flagellum, where the axoneme is assembled (Johnson and Rosenbaum, 1992). Additionally, IFT is responsible for the delivery of flagellar matrix and membrane proteins to the flagellum, with the latter proposed to be moved in the plane of the flagellar membrane (Qin *et al.*, 2005). Also IFT complex A proteins and the inactive dynein motor complex are delivered to the flagellar tip to be unloaded, thereby keeping up retrograde IFT (Absalon *et al.*, 2008). In trypanosomatids the PFR has to be assembled as a separate structure apart from the axoneme. Construction of the PFR is dependent upon IFT (Kohl *et al.*, 2003), and PFR subunits are attached primarily at the flagellar tip (Bastin *et al.*, 1999b). In return, kinesins, IFT complex B proteins as well as used axoneme and PFR subunits are transported back to the cell body for recycling or degradation. Anterograde and retrograde IFT proceed simultaneously resulting in a continuous turnover of flagellar subunits at the distal tip of the flagellum. Flagellar length might therefore be regulated by shifting the ratio between the rates of assembly and disassembly (Stephens, 1997; Marshall and Rosenbaum, 2001; Song and Dentler, 2001).

Likewise in *Chlamydomonas*, IFT particles have been localised to the space between the flagellar membrane and the axoneme in trypanosomes (Bastin *et al.*, 2000). Remarkably, IFT particles are preferentially transported along the axonemal microtubule doublets 3 and 4, or 7 and 8, and thus along both sides of the PFR (Absalon *et al.*, 2008). Although several IFT complex proteins have been localised along the length of the flagellum, a significant proportion is found around the area of the basal body (Cole *et al.*, 1998; Deane *et al.*, 2001; Pedersen *et al.*, 2005). However, IFT-like particles are absent from the transition zone of the basal body (Absalon *et al.*, 2008). It has been shown that IFT proteins are docked onto the transition fibers running between the basal body and the membrane (Deane *et al.*, 2001). Therefore, the transition fibers might act as a staging area for IFT particle formation where IFT could be involved in the selection of proteins entering the flagellum (Cole, 2003).

Moreover, IFT seems to play a role in signal transduction (Sloboda, 2005) probably by moving sensor molecules to the flagellar tip where they might become modified. Returning the modified sensor molecules to the cell body would provide the cell with information about the state of the flagellum or the environment outside the cell (Pazour and Rosenbaum, 2002a). Actually, 93 signal transduction proteins could be identified in purified flagella of *C. reinhardtii* which include 21 protein kinases (Pazour *et al.*, 2005).

Several observations suggest that protein kinases are critically involved in flagellar length control. The aurora protein kinase CALK (Pan *et al.*, 2004), the glycogen synthase kinase GSK3 β (Wilson and Lefebvre, 2004), the CDK (cyclin-dependent kinase)-related kinase LF2 (Tam *et al.*, 2007), the NIMA-related kinase Cnk2p (Bradley and Quarmby, 2005) and the MAP (mitogen-activated protein) kinase LF4 (Berman *et al.*, 2003) have been shown to control flagellar length in *Chlamydomonas*. Also the MAP kinase DYF-5 in *C. elegans* has a role in flagellar length regulation (Burghoorn *et al.*, 2007). Furthermore, the MAP kinases LmxMPK3 (Erdmann, diploma thesis, 2004; Erdmann *et al.*, 2006), LmxMPK9 (Bengs *et al.*, 2005), LmxMPK13 (the homologue of LF4) and LmxMPK14 (Scholz, PhD thesis, 2008), as well as the MAP kinase kinases LmxMKK (Wiese *et al.*, 2003a) and LmxPK4 (Kuhn, PhD thesis, 2004) have been shown to regulate flagellar length in *L. mexicana*. Actually, more than 80 phosphorylated flagellar components have been identified in *Chlamydomonas* (Tuxhorn *et al.*, 1998).

1.3 Signal transduction in eukaryotic cells

1.3.1 Different signalling pathways

Cells have to sense their environment to adapt or react to changes outside the cell. This feature is essential for single cell organisms such as *Leishmania* parasites as well as for cells in tissues or organs of multicellular organisms.

When *Leishmania* parasites pass through their digenetic life cycle they have to undergo profound biochemical and morphological changes to survive in the sand fly vector or in the mammalian host and to prepare for the next phase of their life cycle. Although it is not clear how environmental signals are sensed and transmitted into the cell, it is very likely that signal transduction processes are critically involved. Protein kinases are likely candidates, since *Leishmania* parasites reveal stage-specific changes in protein phosphorylation (Dell and Engel, 1994).

Multicellular organisms are further dependent on the efficient communication between single cells which are sometimes separated by long distances. Thus, hormones have taken over the task as extracellular chemical messengers transporting a signal from one cell to another.

Hormones can bind to different cellular receptors either being integral membrane proteins, cytoplasmic or nuclear proteins.

Hydrophobic hormones such as steroid hormones can pass the plasma membrane by passive diffusion and generally bind to nuclear receptors, a class of ligand-activated transcription factors, initially located in the cytosol. The hormone receptor complexes are subsequently translocated into the nucleus where they bind to specific nucleotide sequences known as hormone response elements (HREs), thereby regulating the transcription of different genes. Also soluble gases such as carbon monoxide (CO) and nitric oxide (NO) are able to diffuse into the cell where they activate a guanylate cyclase producing cyclic guanosine monophosphate (cGMP) as an intracellular messenger.

Hydrophilic hormones such as adrenalin act as “first messengers” by binding to a cell surface receptor resulting in a conformational change of the cytoplasmic receptor domain which eventually leads to the production of an intracellular signalling molecule, termed “second messenger”. This messenger triggers the intracellular release of Ca^{2+} , alters gene expression or activates different enzymes, which finally leads to changes in the metabolism or the cytoskeleton of the cell. Since those signal transduction pathways involve ordered sequences of biochemical reactions, they are also referred to as signalling cascades.

There are three main classes of cell surface receptors inducing specific intracellular responses:

Ligand-gated ion channel receptors mediate the quickest responses to extracellular signalling molecules. Binding of the messenger initiates temporary opening of the channel which leads to a change of ion concentrations over the membrane. The ion flow itself relays the signal and thus no “second messenger” is needed. An example for this mechanism is found in the post-synaptic cell of a neural synapse.

Seven-helix receptors such as the adrenergic receptor possess seven membrane-spanning α -helices and act through heterotrimeric GTP (guanosine triphosphate)-binding proteins which can switch between an active and an inactive form, thereby serving as molecular switches. The adenylate cyclase cascade is initiated generating cyclic adenosine monophosphate (cAMP) as a “second messenger”. In addition, the phosphoinositol cascade can be activated releasing inositol 1,4,5-triphosphate (InsP_3) and diacylglycerol (DAG) as “second messengers”. Both signalling pathways eventually lead to an increase of cytosolic Ca^{2+} levels. Ca^{2+} itself functions as an important intracellular messenger.

The third group describes the cell surface receptors with tyrosine kinase activity such as the epidermal growth factor (EGF) receptor. Those receptors are either linked with non-receptor tyrosine kinases on the cytosolic side of the plasma membrane or possess a cytoplasmic tyrosine kinase domain themselves. The latter are referred to as receptor tyrosine kinases (RTKs). Binding of the respective ligand to an RTK generally induces an oligomerisation of

the monomeric receptors. This leads to a crosswise tyrosine phosphorylation of the cytoplasmic receptor domains and to the phosphorylation of other submembraneous proteins on specific tyrosine residues. The phosphorylated tyrosine residues of the RTKs are recognised by proteins containing SH (Src homology)² or PTB (phosphotyrosine binding) domains. Those proteins are adapter proteins, enzymes or subunits of the cytoskeleton. In addition, they often contain SH3 domains which bind to proline-rich sequence motifs of further cytoplasmic proteins. Eventually, the small (monomeric) GTP-binding protein Ras, a key component and switchpoint of different signalling pathways, is activated. Among others, the MAP (mitogen-activated protein) kinase cascade can be activated which is achieved by binding of activated Ras to the MAPKKK (MAP kinase kinase kinase) Raf, thereby triggering a conformational change and thus its activation. The MAP kinase cascade culminates in the phosphorylation of different substrate proteins such as enzymes and transcription factors. Signal silencing is an important feature of intracellular signalling mainly occurring through an inactivation of intracellular signalling components. Another characteristic is the organisation of individual pathways into complex networks leading to a “cross talk” between different signalling cascades. Thus, signals can be spread out to further pathways or can be joined and integrated resulting either in the amplification or in the attenuation of the signal (Frost *et al.*, 1997; Ganiatsas *et al.*, 1998; Pearson *et al.*, 2001; Sundaram, 2006).

1.3.2 Protein phosphorylation and protein kinases

Intra- and extracellular signals often lead to a change in the phosphorylation state of specific proteins in order to regulate important molecular processes within the cell. Phosphorylation is the most frequent posttranslational modification, with approximately one third of mammalian proteins being phosphorylated. Reversible phosphorylation can change the properties of a protein in many different ways by forming ionic and hydrogen bonds. Conformational changes as well as the generation or masking of binding motifs can result in an alteration of the enzymatic activity, protein stability, binding properties or the subcellular localisation.

Protein kinases represent one of the largest gene families constituting 2% of all known mammalian genes. Those enzymes catalyse the transfer of the γ -phosphoryl group of adenosine triphosphate (ATP) or GTP to a hydroxyl group in their substrates. Most protein kinases belong to one of the three main groups named according to the amino acid residues being phosphorylated. While serine/threonine kinases are active toward serine and threonine residues, tyrosine kinases are highly specific for the phosphorylation of tyrosine residues. Dual-specificity kinases act on both aliphatic and aromatic amino acid residues. The latter group is only composed of MAPKKs (MAP kinase kinases) and LAMMER kinases (Hanks *et al.*, 1988; Lee *et al.*, 1996). The occurrence of phosphorylation differs over three orders from

serine, threonine to tyrosine with a ratio of 1800:200:1 in eukaryotic cells (Hubbard and Cohen, 1993).

The structure of protein kinases is highly conserved and is composed of two domains flanking the catalytic cleft where ATP (or GTP) and the substrate can bind (see Figure 7). The smaller N-terminal lobe consists of a five-stranded antiparallel β -sheet (β 1- β 5) and an α -helix (α C) where the latter is involved in the orientation of the nucleotide substrate. The larger C-terminal lobe mostly consists of α -helices and is responsible for binding of the substrate and transferring the γ -phosphoryl group of ATP (or GTP) to a hydroxyl group in the substrate. The catalytic domain of protein kinases comprises approximately 300 amino acid residues and reveals twelve conserved subdomains separated by regions of lower homology (see Figure 8). While subdomains I to IV are located in the N-terminal lobe, subdomain V is found within the deep catalytic cleft and subdomains VI to XI in the C-terminal lobe.

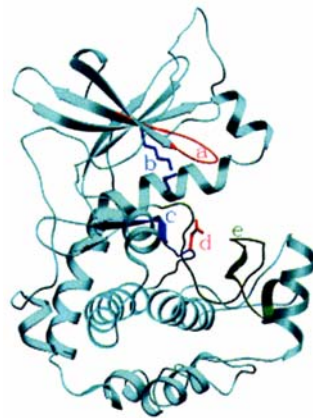


Figure 7: 3D structure of the catalytic domain of a protein kinase

a: phosphate anchor ribbon; b: Lys-Glu ionic bond; c: catalytic loop; d: catalytic Asp of subdomain VIb; e: activation loop. (Source: Krupa *et al.*, 2004)

Several conserved residues or secondary structures in both domains of protein kinases contribute to the orientation of the nucleotide substrate. Involved are the phosphate anchor ribbon which is a glycine-rich loop located between the β 1- and β 2-strands in subdomain I, an asparagine and an aspartate residue in subdomains VIb and VII, respectively, which bind divalent cations involved in nucleotide recognition, and a lysine residue in subdomain II which forms an ionic bond with a glutamate residue in the α C-helix and coordinates the α - and β -phosphoryl groups of the nucleotide substrate. The lysine residue is essential for the transfer of the γ -phosphoryl group of ATP. The so-called activation loop, typically 20-30 residues in length, provides a platform for the peptide substrate to bind in an extended conformation close to the γ -phosphoryl group of ATP. However, the activation loop has to be phosphorylated to be stabilised in an open and extended conformation which allows substrate binding and catalysis (Hubbard, 1997). The aspartate residue mentioned above is part of the highly conserved DFG motif located at the base of the activation loop. The

structure of this motif is tightly coupled to the phosphorylation of the activation loop. A different aspartate residue located in the so-called catalytic loop in subdomain VIb interacts with the hydrogen atom of the attacking hydroxyl group of the substrate (Huse and Kuriyan, 2002; Krupa *et al.*, 2004).

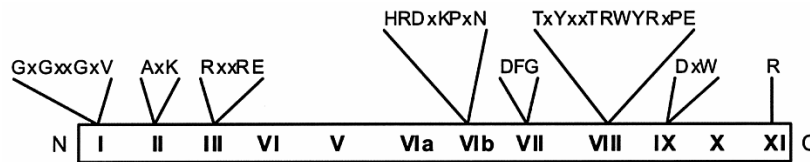


Figure 8: Schematic illustration of the catalytic domain in MAP kinases

Roman numerals indicate the twelve conserved subdomains. Consensus sequences in the subdomains are shown. (Source: Wiese *et al.*, 2003b)

1.3.3 The MAP kinase cascade

MAP (mitogen-activated protein) kinases play a central role in proliferation, differentiation and apoptosis of eukaryotic cells. They are also critically involved in stress and immune responses. The MAP kinase cascade can be activated by different signalling molecules such as hormones or cytokines and the respective cell surface receptors such as receptor tyrosine kinases (RTKs), seven-helix receptors and cytokine receptors. Five distinct classes of MAP kinases have been characterised, namely ERK (extracellular signal-related kinase) 1/2, JNK (c-Jun N-terminal kinase) 1/2/3, p38 $\alpha/\beta/2/\gamma/\delta$, ERK 3/4 and ERK5. While the ERKs are mainly associated with proliferation and differentiation, JNK and p38 are more involved in stress and immune responses.

The core module of the MAP kinase cascade is well conserved between different MAP kinase families and among all eukaryotes. It is composed of three kinases: a MAPKKK (MAP kinase kinase kinase), which - when activated - phosphorylates and thereby activates a MAPKK (MAP kinase kinase), which in turn phosphorylates and thus activates a MAPK (MAP kinase). MAPKKs are activated after phosphorylation by Ste20-like kinases or by interacting with a small GTP-binding protein of the Ras or Rho family which leads to a conformational change. MAPKKs are dedicated serine/threonine kinases which phosphorylate one or a few MAPKKs on two conserved serine and/or threonine residues. MAPKKs belong to the dedicated dual-specificity kinases and phosphorylate one or very few MAPKs on the threonine and the tyrosine residue of the highly conserved TXY motif located on the activation loop in subdomain VIII. MAPKs are multifunctional serine/threonine kinases which can phosphorylate many different substrate proteins in the cytoplasm or in the nucleus. Since transcription factors are typical MAPK substrates in higher eukaryotes, MAP kinase signalling often culminates in an altered gene transcription. RNA polymerase II, cytoskeletal proteins and further protein kinases such as MAPKAPKs (MAPK-activated

protein kinases) are also phosphorylated and thus regulated by MAPKs. Eventually, dual-specificity MAPK phosphatases deactivate distinct MAPKs by removing the phosphate groups from the TXY activation motif (Camps *et al.*, 2000). So far, 22 MAPKs, 7 MAPKKs and 20 MAPKKKs have been identified in mammals.

There are several primary sequence determinants which are typical for MAPK substrates. The phosphorylation site (serine or threonine) defined as position 0 is usually followed by a proline residue in position +1 (Pearson *et al.*, 2001). This preference is due to the corresponding binding pocket in the active site of the MAPK which is occupied by phosphotyrosine. Proline is preferred because its favoured backbone conformation places the side chain away from the kinase surface. Particularly ERK 1/2 substrates often reveal another proline residue at position -2 resulting in the phosphorylation motif PXS/TP (Pearson *et al.*, 2001). In addition, MAPK substrates often contain docking domains (D-domains) which support the selective interaction with MAP kinases (Enslin *et al.*, 2000). Those domains can also be found in MAPKKs, MAPK phosphatases and scaffold proteins. The D-domain consensus is (K/R)₂-X₂₋₆-I/L/V-X-I/L/V with at least two basic residues separated by 2-6 residues from a “hydrophobic-X-hydrophobic” sequence, where the hydrophobic residues are either leucine, isoleucine or valine. Sometimes the sequence is C-terminally extended by another X-I/L/V motif. The D-domain interacts with a stretch of negatively charged residues (see below) of the MAPK. A different docking site specifically mediating the interaction with ERK 1/2 is the FXFP motif (Jacobs *et al.*, 1999).

MAPKs also contain docking sites such as the “common docking (CD) domain” which contains the negatively charged DXXD/E motif and is usually situated C-terminally to the catalytic domain. The so-called ED site located nearby additionally contributes to the binding specificity of the MAPK (Tanoue and Nishida, 2003).

Moreover, MAPKs and their activators are often co-localised on scaffold proteins which link the protein kinases into linear pathways, thus inhibiting undesired cross talks and supporting pathway specificity (Marcus *et al.*, 1994).

1.3.4 Signal transduction in trypanosomatids

When trypanosomatids pass through their digenetic life cycle they have to adapt to environmental changes to survive in the different hosts and to prepare for the next phase of their life cycles. It is very likely that signal transduction processes are involved in this process, and indeed evidence for intracellular signalling has been obtained for *Leishmania*, *T. brucei* and *T. cruzi* (Parsons and Ruben, 2000). While signalling processes of mammals or model organisms such as *Saccharomyces cerevisiae* are well studied, very little is known about signal transduction of organisms which diverged early in evolution from other eukaryotes. Although similarities between signalling processes of mammals and

trypanosomatids are suggested, the latter apparently lack several components with key roles in higher eukaryotes. Moreover, little is known about the types of extracellular molecules which induce signal transduction in trypanosomatids. Secretion proteins of the host or the parasite itself are likely candidates, and indeed growth factors (Hide *et al.*, 1989), cytokines (Barcinski *et al.*, 1992) and adrenergic ligands (De Castro and Luz, 1993) have been reported to have physiological effects on trypanosomatids.

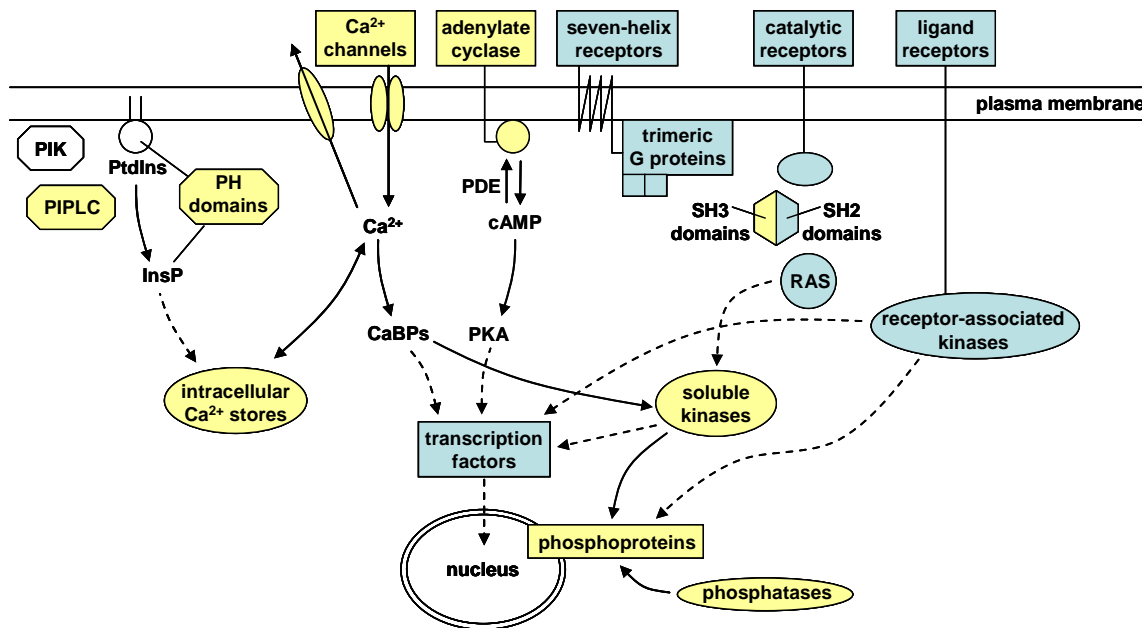


Figure 9: Signal transduction pathways in trypanosomatids and higher eukaryotes

PDE, cAMP phosphodiesterase; PIK, phosphatidylinositol kinases; PIPLC, phosphoinositide phospholipase C.

Dashed arrows and blue symbols indicate connections and components missing in trypanosomatids, solid arrows and yellow symbols indicate connections and components present in trypanosomatids. (modified from Parsons and Ruben, 2000)

So far, receptor adenylate cyclases are the only known transmembrane receptors in trypanosomatids (Ross *et al.*, 1991; Sanchez *et al.*, 1995). They possess a putative extracellular ligand-binding domain and a cytoplasmic adenylate cyclase domain and are encoded by a multigene family in *Leishmania* and *T. brucei*. Family members differ significantly in the extracellular domain suggesting an interaction with different ligands to regulate adenylate cyclase activity. The formation of cAMP has been shown to be tightly correlated with proliferation and differentiation processes in trypanosomes (De Castro and Luz, 1993; Rolin *et al.*, 1993). In many different organisms cAMP is an important “second messenger” which mainly works by activating protein kinase A (PKA) as a further component of the adenylate cyclase cascade. Actually, genes encoding PKA-related proteins have been identified in trypanosomatids (Huang *et al.*, 2002). Phosphodiesterases, enzymes breaking down cAMP, have also been found in trypanosomatids (al-Chalabi *et al.*, 1989). However, the substrates of the PKA-related proteins are not yet known.

In trypanosomatids, as in all other eukaryotes, Ca^{2+} functions as an important “second messenger”. The plasma membrane and the membranes of the mitochondrion, the ER and the acidocalcisomes are capable of transporting Ca^{2+} ions (Zilberstein, 1993; Nolan *et al.*, 1994), thereby maintaining low cytoplasmic Ca^{2+} concentrations (Xiong and Ruben, 1998). Acidocalcisomes might be the most distinctive homeostatic organelles with an additional role in the regulation of the intracellular pH (Docampo and Moreno, 1999). Trypanosomatids contain numerous Ca^{2+} -binding proteins (CaBPs) converting the Ca^{2+} signal into a physiological outcome. Among them are the universal regulator calmodulin, a protein kinase (Flawiá *et al.*, 1997) and an endonuclease (Gbenle, 1990). Moreover, EF-hand CaBPs can be found within the flagellum (Engman *et al.*, 1989). It remains unclear which extracellular signals induce Ca^{2+} flux and thus Ca^{2+} pathways. However, changes in cytoplasmic Ca^{2+} concentrations occur during cell invasion of *T. cruzi* (Docampo and Moreno, 1996) and development processes of *T. brucei* (Stojdl and Clarke, 1996).

In addition, components of the phosphoinositol cascade have been identified in trypanosomatids. Inositol phosphates (InsPs) act as the corresponding “second messengers”. They are usually produced by phosphorylation of membrane-bound phosphatidylinositol (PtdIns) by enzymes including phosphatidylinositol 3-kinase (PI3K) generating phosphatidylinositol phosphates (PtdInsPs) which are subsequently cleaved by phospholipase C producing cytoplasmic InsPs. Indeed, genes encoding PI3K (Bringaud *et al.*, 1998) and phospholipase C (Nozaki *et al.*, 1999) have been identified in *T. brucei* and *T. cruzi*, respectively. Different PtdInsPs and InsPs have been analysed in *T. cruzi* (Docampo and Pignataro, 1991) and *T. brucei* (Moreno *et al.*, 1992). While in higher eukaryotes inositol 1,4,5-triphosphate (InsP_3) causes the intracellular release of Ca^{2+} , no such effect was detectable in trypanosomes (Moreno *et al.*, 1992). However, several PH (pleckstrin homology) domain proteins have been found which are able to interact with different PtdInsPs and InsPs (Shaw, 1996). This interaction leads to a specific targeting of the PH domain proteins to the membrane or the cytoplasm and/or to a modulation of protein function. Several protein kinases of trypanosomatids contain PH domains (Parsons and Ruben, 2000).

There are some features in signalling mechanisms which greatly differ between higher eukaryotes and trypanosomatids. The latter lack heterotrimeric GTP-binding proteins, seven-helix receptors and receptor tyrosine kinases (RTKs) (Parsons and Ruben, 2000) although a few protein kinases with predicted transmembrane domains are present. However, such proteins could act as ectokinases phosphorylating molecules of the extracellular environment rather than mediating sensory functions (Parsons *et al.*, 2005). Nevertheless, it is interesting to note that all plant receptor kinases are serine/threonine kinases (Shiu and Bleecker, 2001) and that trypanosomatids could use similar strategies in environmental sensing. No tyrosine

kinases and phosphatases have been identified in trypanosomatids; however, respective enzymatic activities have been documented (Parsons *et al.*, 1994; Bakalara *et al.*, 1995). It has been suggested that tyrosine phosphorylation is carried out by atypical tyrosine kinases such as Wee1 and dual-specificity kinases (Parsons *et al.*, 2005). Moreover, in proteins of trypanosomatids SH (Src homology)² domains have not been found, while SH3 domains seem to be rare. Those domains usually mediate the interaction with phosphotyrosine and proline-rich sequence motifs, respectively. The culmination of signalling cascades is unlikely to be at the transcriptional level as it is mostly the case in higher eukaryotes. Since gene expression in trypanosomatids is probably regulated on the posttranscriptional level, intracellular signalling could eventually lead to the modulation of proteins with a role in mRNA processing, turnover or translation.

Consistent with stage-specific changes in protein phosphorylation (Parsons *et al.*, 1990, 1993, 1995; Aboagye-Kwarteng *et al.*, 1991; Dell and Engel, 1994), trypanosomatids possess numerous protein kinases. A genome-wide analysis revealed a total of 199 protein kinases in *L. major*, 190 in *T. cruzi* and 176 in *T. brucei* among which are 17, 19 and 20 atypical protein kinases, respectively, lacking the twelve conserved subdomains of eukaryotic protein kinases (Parsons *et al.*, 2005). The protein kinase genes comprise approximately 2% of the entire genome of trypanosomatids. Compared to the human host, a relative expansion of the CMGC (cyclin-dependent kinases (CDKs), mitogen-activated protein (MAP) kinases, glycogen synthase kinases (GSK) and CDK-like kinases), STE (homologues of yeast Sterile 7, Sterile 11 and Sterile 20 kinases) and NEK (NIMA (never in mitosis/Aspergillus)-related kinase) groups can be observed constituting 56% of the *Leishmania* kinome.

Trypanosomatids have to coordinate their cell cycle in accordance with life cycle differentiation and thus, there is a relatively large number of CDKs. Six classes of cdc2-related kinases (CRKs) have been identified, namely CRK 1-6 (Mottram, 1994). The roles of CRKs in cell cycle control are complex and vary depending on life cycle stage and the presence of different cyclins. CRK3 and CRK1 have been shown to be essential in *L. mexicana* (Hassan *et al.*, 2001; Mottram *et al.*, 1996).

Even in popular model organisms relatively little is known about NEKs; however, they appear to function in controlling the cell cycle (O'Connell *et al.*, 2003) and the cytoskeleton (Liu *et al.*, 2002; Mahjoub *et al.*, 2004). Several NEKs of trypanosomatids contain accessory domains such as coiled coils or PH domains. In *T. brucei* one NEK has been found to be involved in basal body separation (Pradel *et al.*, 2006).

Trypanosomatids possess a large number of MAPKs which are suggested to coordinate responses to environmental changes. In *T. brucei* four ERK homologues have been analysed so far. While Kfr1 might mediate the interferon- γ -induced proliferation of bloodstream forms (Hua and Wang, 1997), TbMAPK2 has been shown to be involved in cell cycle progression

of procyclic forms (Müller et al., 2002). TbECK1, which shares characteristics with both ERKs and CDKs, has a role in parasite growth (Ellis *et al.*, 2004), whereas TbMAPK5 seems to be involved in the differentiation of bloodstream forms (Domenicali Pfister *et al.*, 2006).

The first MAPK identified in *L. mexicana* was LmxMPK1 which was found to be encoded on the intergenic region between two SAP (secreted acid phosphatase) genes (Wiese, 1998) and is the homologue of Kfr1 in *T. brucei*. Later, eight additional MAPKs of *L. mexicana* were identified (LmxMPK 2-9) using degenerate oligonucleotide primers specific for nucleotide sequences corresponding to the MAPK activation loop and were cloned from a genomic DNA library of *L. mexicana* (Wiese *et al.*, 2003b). Shortly afterwards, the *L. major* genome sequencing was completed (Ivens *et al.*, 2005), and the *L. major* genome DB revealed six additional MAPK homologues which could also be identified in *L. mexicana* (LmxMPK 10-15). All of those new MAPK homologues of *L. mexicana* have already been cloned (Wiese, 2007). While the genomes of both *L. infantum* and *L. braziliensis* contain all of the 15 MAPK homologues, *T. brucei* and *T. cruzi* lack the homologues of LmxMPK7 and LmxMPK8. In addition, two atypical MAPKs have been identified in the *L. major* genome DB (LmjF03.0210 and LmjF13.0780; Parsons *et al.*, 2005).

The physiological function of several *L. mexicana* MAPKs has already been described in our laboratory. Deletion experiments showed that LmxMPK1 is essential for the proliferation of amastigotes and thus for parasite survival in the mammalian host (Wiese, 1998). Moreover, extensive analysis of the LmxMPK1 activation mechanism revealed that phosphorylation of the threonine in the TXY activation motif is both necessary and also sufficient for the full activation of the kinase (Melzer, PhD thesis, 2007). Likewise, deletion analysis of *LmxMPK2* also revealed an essential role of the kinase in establishing an infection in the mammalian host. Additionally, the promastigote mutants showed severe morphological defects (Wiese, 2007). It was also shown that *LmxMPK4*, the homologue of *TbMAPK2* in *T. brucei*, cannot be deleted from the genome of *L. mexicana* unless an extrachromosomal copy of the gene has been introduced in advance. Since this copy was retained in promastigotes and amastigotes even without antibiotic selection, LmxMPK4 is suggested to be essential in both promastigotes and amastigotes (Wang *et al.*, 2005). Null mutants of *LmxMPK5*, the homologue of *TbMAPK5* in *T. brucei*, showed a decreased ability to cause lesions in BALB/c mice, although parasites persisted at the site of inoculation (Wanders, MD thesis, 2004). In contrast, LmxMPK11 and LmxMPK12 are not essential for establishing an infection in the mammalian host (Windelberg, MD thesis, 2007). LmxMPK6 reveals a long C-terminal extension which could be involved in the regulation of kinase activity as it has been shown for TbECK1, its homologue in *T. brucei* (Ellis *et al.*, 2004). There are several *L. mexicana* MAPKs which play a role in the regulation of flagellar length. Deletion of *LmxMPK9* from the genome of *L. mexicana* generated promastigotes with significantly elongated flagella while

overexpression led to cells with shorter flagella (Bengs *et al.*, 2005). Likewise, promastigote deletion mutants for *LmxMPK13* and *LmxMPK14* displayed elongated flagella compared to the wild type (Scholz, PhD thesis, 2008). It was shown for *LmxMPK13* that this effect can be reversed by re-expressing the kinase in the deletion background. *LmxMPK13* is the homologue of LF4 in *C. reinhardtii* which also plays a critical role in flagellar length regulation as shown by null mutants displaying significantly elongated flagella (Berman *et al.*, 2003). In contrast, promastigote deletion mutants for *LmxMPK3* - which is the subject of this work - showed flagella reduced to one-fifth of the wild type length, and re-expression of *LmxMPK3* in the deletion background led to a regeneration of wild type flagella (Erdmann, diploma thesis, 2004; Erdmann *et al.*, 2006). All those MAPK homologues affecting flagellar length might be critically involved in regulating intraflagellar transport (IFT).

Seven potential MAPK kinase (MAPKK) genes (*LmxMKK* and *LmxPK 2-7*) belonging to the STE7 family have been identified in the *L. major* genome (Wiese *et al.*, 2003a; Kuhn, PhD thesis, 2004; Kuhn and Wiese, 2005; Parsons *et al.*, 2005). Like *LmxMPK3* null mutants, promastigote deletion mutants for *LmxMKK* displayed flagella reduced to one-fifth of the wild type length. No such effect has been observed in deletion studies for TbMEKg, the *LmxMKK* homologue in *T. brucei* (Vassella, personal communication). However, TbMEKg can reverse the *LmxMKK* null mutant phenotype (Scholz, PhD thesis, 2008). Indeed, it could be shown that *LmxMKK* is the physiological activator of *LmxMPK3* (Scholz, PhD thesis, 2008; Erdmann *et al.*, 2006). Mouse infection studies using *LmxMKK* null mutants revealed a delay in the onset of lesion development (Wiese *et al.*, 2003a). Contrasting to *LmxMKK*, deletion of *LmxPK4* from the genome of *L. mexicana* generated promastigotes with elongated flagella (Kuhn, PhD thesis, 2004). Actually, *LmxMPK13* - with a corresponding phenotype in deletion studies - has been shown to be activated by *LmxPK4* in *E. coli* (Scholz, PhD thesis, 2008). *LmxPK4* has also been suggested to be involved in differentiation from promastigotes to amastigotes thus affecting virulence (Kuhn and Wiese, 2005). The function of the remaining *L. mexicana* MAPKKs has not been determined yet.

Moreover, 23 potential MAPKK kinase (MAPKKK) genes of the STE11 family could be identified in the *L. major* genome (Parsons *et al.*, 2005). MRK1 is proposed to be essential in *L. major* as efforts to delete the gene from the genome failed (Agron *et al.*, 2005).

STE20 family kinases which often function as MAPKKK kinases and thus as MAPKKK activators are rare in trypanosomatids with only one candidate in *L. major* (Parsons *et al.*, 2005).

In summary, MAP kinase signalling mechanisms seem to be complex in trypanosomatids where both the activators and the downstream targets are yet unknown.

1.4 LmxMPK3 - State of knowledge and project aims

1.4.1 State of knowledge

LmxMPK3 has been identified as a MAP (mitogen-activated protein) kinase homologue in *Leishmania mexicana* revealing the twelve conserved subdomains of eukaryotic protein kinases, the conserved residues characterising serine/threonine protein kinases and the TXY activation motif highly conserved in MAP kinases (Wiese *et al.*, 2003b). In addition, LmxMPK3 carries a “common docking (CD) domain” located C-terminally to the catalytic domain. *LmxMPK3* is present as a single copy gene in the haploid genome, and its open reading frame (ORF) comprises 1164 bp encoding a protein of 388 amino acids with a calculated molecular mass of 43.7 kDa. Homologues of LmxMPK3 are present in other kinetoplastids such as *L. major*, *L. infantum*, *L. braziliensis*, *T. brucei* and *T. cruzi*. Moreover, homologues can also be found in *Solanum tuberosum*, *Dictyostelium discoideum* (ERK1; Gaskins *et al.*, 1994), *Chlamydomonas reinhardtii* as well as in *Toxoplasma gondii* (TgMAPK-1; Brumlik *et al.*, 2004). *LmxMPK3* mRNA levels are high in *L. mexicana* promastigotes, but tightly down-regulated in lesion-derived amastigotes indicating that LmxMPK3 is likely to play no role in the amastigote stage of the parasite (Wiese *et al.*, 2003b). In accordance, the protein was only detectable in promastigotes (Erdmann *et al.*, 2006).

An affinity-purified GST (glutathione-S-transferase)-fusion protein of LmxMPK3 which had been recombinantly expressed in *Escherichia coli* showed auto- and substrate phosphorylation activity in *in vitro* kinase assays. Maximal substrate phosphorylation was observed at 26°C and between 34 and 37°C (at 2 mM Mn²⁺, 10 mM Mg²⁺, and pH 7.2) and at the highest tested manganese concentration (10 mM Mn²⁺) in the absence of magnesium (at 27°C, and pH 7.2). Therefore, LmxMPK3 was classified as a manganese-dependent protein kinase (Erdmann, diploma thesis, 2004).

LmxMPK3 deletion studies revealed promastigotes with flagella strongly reduced in length (see Figure 10B). The flagellar beat frequency was irregular and much lower compared to the wild type resulting in reduced cell motility. Moreover, the cells were rather oval-shaped compared to the slender wild type promastigotes (Erdmann, diploma thesis, 2004). In contrast, overexpression of LmxMPK3 in *L. mexicana* generated promastigotes with elongated flagella (see Figure 10C). Those findings led to the conclusion that LmxMPK3 is involved in the regulation of flagellar length probably by affecting intraflagellar transport (IFT).

Indeed, the MAP kinase kinase LmxMCK - showing a very similar phenotype in deletion studies - had been found to be the physiological activator of LmxMPK3 as the latter was phosphorylated and thus activated by a constitutively active aspartate mutant of LmxMCK *in vitro*. Moreover, LmxMPK3 could only be found among the phosphorylated proteins of

L. mexicana promastigotes if LmxMCK was expressed. In addition, a feedback phosphorylation (of activated LmxMPK3 on LmxMCK) has been described *in vitro* (Scholz, PhD thesis, 2008; Erdmann *et al.*, 2006). The LmxMCK/LmxMPK3-pair was the first protein interaction of a signalling cascade described for *Leishmania*.

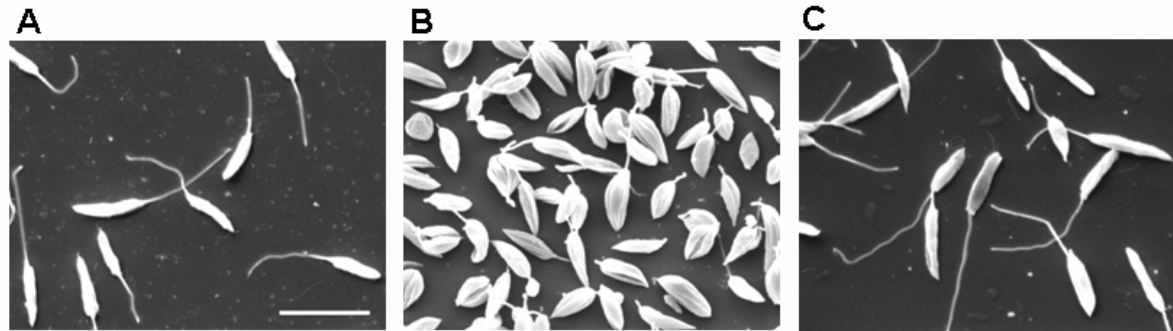


Figure 10: Scanning electron micrographs of *L. mexicana* wild type, *LmxMPK3* null mutant and *LmxMPK3* “overexpressor”

A: *L. mexicana* wild type; B: *LmxMPK3* null mutant; C: *LmxMPK3* “overexpressor”.
Bar, 10 μ m. (Source: Erdmann, diploma thesis, 2004)

1.4.2 Project aims

The overall aim of this work was to investigate the *in vivo* function of LmxMPK3 in more detail and to identify its physiological substrate(s). Furthermore, the activation mechanism of LmxMPK3 should be addressed *in vitro* and *in vivo*.

An *LmxMPK3* add back mutant should be generated in order to prove that the *LmxMPK3* null mutant phenotype is actually due to the lack of LmxMPK3 and can be reversed by the re-expression of LmxMPK3. Analysis of the *LmxMPK3* null mutants via transmission electron microscopy (TEM) should reveal structural abnormalities of the cell, especially within the flagellum and in its close proximity. Furthermore, mouse infection studies using the *LmxMPK3* null mutants would elucidate if the kinase has a role in establishing an infection in the mammalian host. To determine the subcellular localisation of LmxMPK3 and its activator LmxMCK, GFP mutants should be generated for both kinases for subsequent analysis on a fluorescence microscope.

Although the deletion of *LmxMPK3* from the genome of *Leishmania mexicana* was a successful approach for determining the function of the kinase, an inhibitor-sensitised *LmxMPK3* mutant of *L. mexicana* should be generated. The latter presents an inducible system in which immediate and transient effects can be studied as a response to the inactivation of a protein kinase. Another advantage over gene deletion mutants is that compensation mechanisms do not occur during the short time intervals used for inducible systems. Therefore, the “gate keeper” amino acid residue (threonine 116) located in the active site of LmxMPK3 should be replaced by glycine to create a small pocket in the

ATP-binding site (Bishop *et al.*, 2001). This functionally silent active-site mutation should sensitise the kinase to a synthetic inhibitor which does not inhibit wild type kinases. This system allows studying the *in vivo* function of a protein kinase and might also support the identification of its physiological substrates.

An enzymatically inactive mutant of LmxMPK3 for recombinant expression should be generated by replacing the highly conserved lysine (lysine 62) by a methionine to serve as a negative control in *in vitro* kinase assays. Moreover, the activation of recombinantly expressed LmxMPK3 by its activator LmxMKK should be optimised by establishing a co-expression system which allows an *in vivo* activation within *Escherichia coli* cells. The maximum activation of LmxMPK3 would be highly beneficial for *in vitro* analysis of the activation mechanism of LmxMPK3. The latter would be supported by introducing different mutations to the TDY activation motif. The enzymatic activities of the recombinantly expressed LmxMPK3-TDY mutants could be assessed by *in vitro* kinase assays, while the phosphorylation state could be determined by immunoblot analysis and mass spectrometry. For *in vivo* analysis of the activation mechanism the *LmxMPK3-TDY* mutants should be introduced into the *LmxMPK3* deletion background. Flagellar lengths of the obtained clones should be indicative for the activity of the LmxMPK3-TDY mutants *in vivo*.

Finally, different strategies should be used to identify the physiological substrate(s) of LmxMPK3. The opportunity to activate recombinantly expressed LmxMPK3 using its physiological activator should make an *in vitro* substrate search quite efficient. Since transcription factors - typical MAP kinase substrates in higher eukaryotes - are absent in *Leishmania* and gene expression is likely to be regulated on the posttranscriptional level, *Leishmania* MAP kinase substrates could be involved in processes such as mRNA processing, turnover or translation. Taking into account that LmxMPK3 is essential for flagellar assembly and flagellar length regulation, it is likely that the LmxMPK3 substrate either regulates the gene expression of components involved in processes such as intraflagellar transport (IFT) or that it is such a protein component itself. Identification of the LmxMPK3 substrate would contribute to the knowledge about flagellar length regulation and IFT in *Leishmania* which is still poorly understood. Moreover, it would provide new information about MAP kinase signalling and possibly gene regulation of trypanosomatids in general.

2 Materials

2.1 Laboratory equipment

<i>Description</i>	<i>Manufacturer</i>
<i>Centrifuges</i>	
Centrifuge 5415C/D/R	<i>Eppendorf, Hamburg</i>
GS-6KR Centrifuge (Rotor: GH3.8)	<i>Beckman Instruments, Munich</i>
HERMLE Z 400 K	<i>Hermle Labortechnik, Wehingen</i>
Optima TL Ultracentrifuge (Rotor: TLA 55)	<i>Beckman Coulter, Krefeld</i>
ProFuge 10 K	<i>Stratagene, La Jolla, CA, USA</i>
Sorvall RC-5B Refrigerated (Rotors: SS-34, GSA)	<i>Kendro Laboratory Products, Hanau</i>
<i>CO₂ incubator</i>	
BBK 6220	<i>Kendro Laboratory Products, Hanau</i>
<i>Electrophoresis equipment</i>	
Minigel(-Twin) Power supply: Consort E734	<i>Biometra, Göttingen Consort, Turnhout, Belgium</i>
Labtech Power supply: Gene Power Supply GPS 200/400	<i>Labtech International, Burkhardtsdorf Amersham Biosciences, Freiburg</i>
<i>FACS Sorter</i>	
FACSCalibur Flow Cytometer	<i>BD Biosciences, San Jose, CA, USA</i>
<i>Heat block</i>	
Thermomixer 5436	<i>Eppendorf, Hamburg</i>
<i>Microscopes</i>	
Axiovert 25	<i>Carl Zeiss, Jena</i>
Axioskop 2 plus Digital camera: C4742-95	<i>Carl Zeiss, Jena Hamamatsu Photonics, Herrsching am Ammersee</i>
Axiostar plus	<i>Carl Zeiss, Jena</i>
<i>pH Meter</i>	
Digital-pH-Meter CG 820	<i>Schott, Hofheim am Taunus</i>
<i>Photometer</i>	
BioPhotometer 6131	<i>Eppendorf, Hamburg</i>
Pharmacia LKB Ultrospec III	<i>Pharmacia, Milton Keynes, UK</i>
<i>Safety cabinet</i>	
HERAsafe HS15 (Heraeus)	<i>Kendro Laboratory Products, Hanau</i>
<i>Shaking incubators</i>	

Innova 4230/4400	<i>New Brunswick Scientific</i> , Edison, NJ, USA
<i>Shaking water baths</i>	
GFL 1083	<i>GFL</i> , Burgwedel
mgw LAUDA M3	<i>Heidolph Electro</i> , Kehlheim
<i>Sonifier</i>	
Branson Sonifier 250	<i>Branson</i> , Danbury, CT, USA
<i>Thermocycler</i>	
Gene Amp PCR System 9700	<i>PE Applied Biosystems</i> , Weiterstadt
<i>Transfectors</i>	
Gene Pulser 1652077	<i>BIO RAD Laboratories</i> , Munich
Pulse Controller	<i>BIO RAD Laboratories</i> , Munich
Capacitance Extender	<i>BIO RAD Laboratories</i> , Munich
Nucleofector II	<i>Amaxa Biosystems</i> , Gaithersburg, MD, USA
<i>UV linker</i>	
UV Stratalinker 1800	<i>Stratagene</i> , La Jolla, CA, USA
<i>Vortex</i>	
IKA-VIBRO-FIX VF2	<i>IKA Labortechnik</i> , Staufen

2.2 Plastic and glass wares, other materials

Plastic wares were purchased from the companies *Sarstedt* (Nümbrecht), *Eppendorf* (Hamburg), *VWR International* (Darmstadt), *Greiner Bio-One* (Solingen) and *Nunc* (Langenselbold).

10-well microscope slides and cover slips were obtained from *Menzel* (Braunschweig) and *Carl Roth* (Karlsruhe), respectively. The Neubauer chamber was purchased from *VWR International* (Darmstadt). The Biodyne A nylon membrane for Southern blots was produced by *Pall* (Dreieich). The Immobilon-P PVDF membrane for immunoblots was purchased from *Millipore* (Schwalbach). The X-ray films Retina XBA were obtained from *Fotochemische Werke* (Berlin).

2.3 Chemicals

<i>Description</i>	<i>Source</i>
Acetic acid	<i>Carl Roth</i> , Karlsruhe
Acrylamide 30% (w/v)/Bis-acrylamide 0.8% (w/v)	<i>Carl Roth</i> , Karlsruhe
Adenosine triphosphate (ATP)	<i>Roche Diagnostics</i> , Mannheim

Agar-Agar	<i>Carl Roth</i> , Karlsruhe
Agarose (<i>electrophoresis grade</i>)	<i>Amersham Biosciences</i> , Freiburg
Ammonium chloride	<i>Sigma-Aldrich</i> , Steinheim
Ammonium persulfate (APS)	<i>Sigma-Aldrich</i> , Steinheim
Ampicillin	<i>Sigma-Aldrich</i> , Steinheim
Bacto Tryptone	<i>Becton Dickinson</i> , Heidelberg
Blocking reagent	<i>Roche Diagnostics</i> , Mannheim
5-Bromo-4-chloro-3-indolyl- β -D-galactopyranoside (X-Gal)	<i>Roche Diagnostics</i> , Mannheim
Boric acid	<i>Sigma-Aldrich</i> , Steinheim
Bovine serum albumine (BSA)	<i>Sigma-Aldrich</i> , Steinheim
Bromophenol blue	<i>Sigma-Aldrich</i> , Steinheim
Calcium chloride	<i>Merck</i> , Darmstadt
Chloroform	<i>Carl Roth</i> , Karlsruhe
Cobalt chloride	<i>Carl Roth</i> , Karlsruhe
Coomassie Brilliant Blue G250	<i>Carl Roth</i> , Karlsruhe
Coomassie Brilliant Blue R250	<i>Serva</i> , Heidelberg
Disodium 3-(4-methoxyspiro {1,2-dioxetane-3,2-(5-chloro)tricyclo [3.3.1.1 ^{3,7}]decan}-4-yl) phenyl phosphate (CSPD)	<i>Roche Diagnostics</i> , Mannheim
1,4-Diazabicyclo[2.2.2]octane (DABCO)	<i>Sigma-Aldrich</i> , Steinheim
4',6-Diamidino-2-phenylindole dilactate (DAPI)	<i>Sigma-Aldrich</i> , Steinheim
N,N-Dimethylformamide (DMF)	<i>Merck</i> , Darmstadt
Dimethyl sulfoxide (DMSO)	<i>Carl Roth</i> , Karlsruhe
Disodium hydrogenphosphate	<i>Merck</i> , Darmstadt
1,4-Dithiothreitol (DTT)	<i>Biomol</i> , Hamburg
dNTP mix	<i>Roche Diagnostics</i> , Mannheim
Ethanol	<i>Carl Roth</i> , Karlsruhe
Ethidium bromide	<i>Sigma-Aldrich</i> , Steinheim
Ethylenediamine tetraacetic acid (EDTA)	<i>Carl Roth</i> , Karlsruhe
Ethylene glycol bis(β -aminoethylether) tetraacetic acid (EGTA)	<i>Sigma-Aldrich</i> , Steinheim
Fish sperm DNA	<i>Roche Diagnostics</i> , Mannheim
Formaldehyde 37% (Formaline)	<i>Carl Roth</i> , Karlsruhe
Formamide	<i>Merck</i> , Darmstadt
Fetal calf serum (FCS)	<i>Gibco BRL</i> , Eggenstein/ <i>PAN Biotech</i> , Aidenbach/ <i>Sigma-Aldrich</i> , Steinheim
Glucose	<i>Merck</i> , Darmstadt

L-Glutamine	<i>PAN Biotech, Aidenbach</i>
Glutardialdehyde	<i>Merck, Darmstadt</i>
Glutathione, reduced	<i>Sigma-Aldrich, Steinheim</i>
Glycerol	<i>Carl Roth, Karlsruhe</i>
Glycine	<i>Carl Roth, Karlsruhe</i>
Hemin	<i>Sigma-Aldrich, Steinheim</i>
Hoechst 33258 (10 mg/ml)	<i>Invitrogen Life Technologies, Karlsruhe</i>
N-2-Hydroxyethylpiperazine-N'-2-ethanesulfonic acid (HEPES)	<i>Merck, Darmstadt</i>
Hydrochloric acid	<i>Carl Roth, Karlsruhe</i>
Hygromycin B	<i>Merck Biosciences, Schwalbach</i>
Imidazole	<i>Merck, Darmstadt</i>
Isoamyl alcohol	<i>Carl Roth, Karlsruhe</i>
Isopropanol	<i>Carl Roth, Karlsruhe</i>
Isopropyl- β -D-thiogalactopyranoside (IPTG)	<i>Gerbu Biochemicals, Gaiberg</i>
Kanamycin sulfate	<i>Gerbu Biochemicals, Gaiberg</i>
N-Lauroyl sarcosine	<i>Sigma-Aldrich, Steinheim</i>
Leupeptin	<i>Sigma-Aldrich, Steinheim</i>
Lithium chloride	<i>Sigma-Aldrich, Steinheim</i>
Magnesium chloride	<i>Merck, Darmstadt</i>
Magnesium sulfate	<i>Merck, Darmstadt</i>
Maleic acid	<i>Serva, Heidelberg</i>
Manganese chloride	<i>Merck, Darmstadt</i>
β -Mercaptoethanol	<i>Sigma-Aldrich, Steinheim</i>
Methanol	<i>Carl Roth, Karlsruhe</i>
Milk powder	<i>Carl Roth, Karlsruhe</i>
Morpholinoethane sulfonic acid (MES)	<i>Serva, Heidelberg</i>
Morpholinopropane sulfonic acid (MOPS)	<i>Gerbu Biochemicals, Gaiberg</i>
Mowiol 4-88	<i>Merck, Darmstadt</i>
Neomycin (G418)	<i>Roche Diagnostics, Mannheim</i>
Okadaic acid	<i>Merck, Darmstadt</i>
Paraformaldehyde	<i>Sigma-Aldrich, Steinheim</i>
Penstrep (1000 U/ml Penicillin, 10 mg/ml Streptomycin)	<i>PAN Biotech, Aidenbach</i>
ortho-Phenanthroline	<i>Sigma-Aldrich, Steinheim</i>
Phenol, equilibrated in TE buffer pH 7.5-8.0	<i>Carl Roth, Karlsruhe</i>
Phenylmethyl sulfonyl fluoride (PMSF)	<i>Sigma-Aldrich, Steinheim</i>

Phleomycin (Bleocin)	<i>Merck Biosciences</i> , Schwalbach
ortho-Phosphoric acid	<i>Carl Roth</i> , Karlsruhe
Poly-L-Lysine hydrobromide	<i>Sigma-Aldrich</i> , Steinheim
Potassium acetate	<i>Merck</i> , Darmstadt
Potassium chloride	<i>Merck</i> , Darmstadt
Potassium dihydrogen phosphate	<i>Merck</i> , Darmstadt
Puromycin dihydrochloride	<i>Carl Roth</i> , Karlsruhe
Rubidium chloride	<i>Merck</i> , Darmstadt
Saponin	<i>Carl Roth</i> , Karlsruhe
Schneider's <i>Drosophila</i> medium	<i>PAN Biotech</i> , Aidenbach
SDM medium (Brun and Schönenberger, 1979)	<i>PAN Biotech</i> , Aidenbach
Silver nitrate	<i>Merck</i> , Darmstadt
Sodium acetate	<i>Carl Roth</i> , Karlsruhe
Sodium carbonate	<i>Merck</i> , Darmstadt
Sodium chloride	<i>Merck</i> , Darmstadt
Sodium citrate	<i>Merck</i> , Darmstadt
Sodium dihydrogen phosphate	<i>Merck</i> , Darmstadt
Sodium dodecyl sulfate (SDS)	<i>Serva</i> , Heidelberg
Sodium fluoride	<i>Merck</i> , Darmstadt
Sodium hydroxide	<i>Merck</i> , Darmstadt
Sodium orthovanadate	<i>Sigma-Aldrich</i> , Steinheim
Sodium thiosulfate	<i>Merck</i> , Darmstadt
N,N,N',N'-Tetramethylethylenediamine (TEMED)	<i>Sigma-Aldrich</i> , Steinheim
Tetracycline	<i>Sigma-Aldrich</i> , Steinheim
N _α -Tosyl-L-lysine chloromethyl ketone hydrochloride (TLCK)	<i>Sigma-Aldrich</i> , Steinheim
Tris base	<i>Carl Roth</i> , Karlsruhe
Triton X-100	<i>Sigma-Aldrich</i> , Steinheim
Tween 20	<i>Merck</i> , Darmstadt
Xylenecyanol	<i>Sigma-Aldrich</i> , Steinheim
Yeast extract	<i>Carl Roth</i> , Karlsruhe

2.4 Culture media, stock and buffer solutions

<i>Description</i>	<i>Composition</i>
Blocking solution 1 for immunoblots	5% (w/v) milk powder 20 mM Tris-HCl pH 7.5 in PBST

Blocking solution 2 for immunoblots	3% (w/v) BSA 20 mM Tris-HCl pH 7.5 in TBST
Bradford reagent	5% (v/v) ethanol 0.01% (w/v) Coomassie Brilliant Blue G250 10% (v/v) phosphoric acid filtered, stored at 4°C
Cobalt binding buffer/washing buffer 2	50 mM Tris-HCl pH 8.0 1 M NaCl 10% (v/v) glycerol 20 mM imidazole
Cobalt elution buffer	50 mM Tris-HCl pH 8.0 300 mM NaCl 10% (v/v) glycerol 500 mM imidazole 1 mM PMSF
Cobalt washing buffer 1	50 mM Tris-HCl pH 8.0 1 M NaCl 10% (v/v) glycerol 10 mM imidazole
Coomassie R250 destaining solution	30% (v/v) methanol 10% (v/v) acetic acid
Coomassie R250 staining solution	0.1% (w/v) Coomassie Brilliant Blue R250 40% (v/v) methanol 10% (v/v) acetic acid
Cryo medium for <i>Leishmania</i>	90% (v/v) iFCS 10% (v/v) DMSO
DAPI stock solution	160 µg/ml in methanol
Denaturing solution for Southern blotting	0.25 N HCl
DIG I buffer	0.1 M maleic acid 0.15 M NaCl adjusted to pH 7.5
DIG II buffer	1% (w/v) blocking reagent in DIG I buffer
DIG III buffer	50 mM MgCl ₂ 0.1 M NaCl 0.1 M Tris-HCl pH 9.5
DIG washing buffer	0.3% (v/v) Tween 20 in DIG I buffer
DNA loading buffer (10 ×)	0.5 × TBE 0.1 M EDTA pH 8.0 0.1% (w/v) bromophenol blue 0.1% (w/v) xylene cyanol 50% (v/v) glycerol
Electroporation buffer (EPB)	21 mM HEPES pH 7.5 137 mM NaCl 5 mM KCl

	0.7 mM Na ₂ HPO ₄ 6 mM glucose
Equilibration buffer for gel filtration	40 mM Tris-HCl pH 7.0 0.1% (v/v) β-mercaptoethanol 0.1 mM EGTA 0.1% (v/v) Triton X-100
Fixing solution for <i>Leishmania</i>	3.7% (w/v) formaldehyde in 1 × PBS
Gel drying solution	20% (v/v) ethanol 10% (v/v) glycerol
GST elution buffer	10 mM reduced glutathione 50 mM Tris-HCl pH 8.0
Hemin stock solution	2.5 mg/ml in 50 mM NaOH
Hybridising solution for Southern blots	50% (v/v) formamide 5 × SSC 0.1% (w/v) N-lauroyl sarcosine 0.02% (w/v) SDS 2% (w/v) blocking reagent
LB agar	1.5% (w/v) agar-agar in LB medium autoclaved for sterilisation (if required, antibiotics were added after LB agar had cooled down to ca. 50°C)
LB medium	1% (w/v) bacto tryptone 0.5% (w/v) yeast extract 1% (w/v) NaCl autoclaved for sterilisation (if required, antibiotics were added after LB medium had cooled down to ca. 50°C)
<i>Leishmania</i> lysis buffer for immunoblotting	1 × PBS 0.1% (w/v) SDS 50 mM DTT 1 × SDS-PAGE loading buffer 50 μM leupeptin 25 μM TLCK 1 mM PMSF 10 mM ortho-phenanthroline
<i>Leishmania</i> lysis buffer for kinase assays	50 mM MOPS pH 7.2 100 mM NaCl 1 mM EDTA pH 8.0 1 mM EGTA pH 7.3 30 mM MgCl ₂ 0.5% (v/v) Triton X-100 50 μM leupeptin 25 μM TLCK 1 mM PMSF 10 mM ortho-phenanthroline
Mowiol/DABCO	2.4 g Mowiol 6 g glycerol 12 ml 0.2 M Tris-HCl pH 8.5 6 ml ddH ₂ O

	2.5% (w/v) DABCO
Neutralising solution for Southern blotting	1.5 M NaCl 0.5 M NaOH
PBS (10 ×)	1.37 M NaCl 27 mM KCl 101 mM Na ₂ HPO ₄ 18 mM KH ₂ PO ₄
PBST	0.2% (v/v) Tween 20 in 1 × PBS
Pre-hybridising solution for Southern blots	100 µg/ml fish sperm DNA in hybridising solution
RF1	100 mM RbCl 50 mM MnCl ₂ 10 mM CaCl ₂ 30 mM potassium acetate 15% (v/v) glycerol adjusted to pH 5.8, filter-sterilised
RF2	10 mM RbCl 75 mM CaCl ₂ 10 mM MOPS 15% (v/v) glycerol adjusted to pH 6.8, filter-sterilised
Schneider's <i>Drosophila</i> medium complete	20% (v/v) iFCS 1% (v/v) penstrep 1% (v/v) L-glutamine 1.95 g MES/500 ml in Schneider's <i>Drosophila</i> medium adjusted to pH 5.5, filter-sterilised
SDM medium complete	5/10% (v/v) iFCS 1% (v/v) penstrep 7.5 µg/ml hemin in SDM medium
SDS-PAGE Electrophoresis buffer (10 ×)	0.25 M Tris base 1.92 M glycine 1% (w/v) SDS pH ~8.3 (do not adjust!)
SDS-PAGE Loading buffer (5 ×)	62.5 mM Tris-HCl pH6.8 20% (v/v) glycerol 2% (w/v) SDS 0.001% (w/v) bromophenol blue 200 mM DTT
SDS-PAGE Resolving gel buffer (4 ×)	1.5 M Tris base 0.4% (w/v) SDS adjusted to pH 8.8
SDS-PAGE Stacking gel buffer (4 ×)	0.5 M Tris base 0.4% (w/v) SDS adjusted to pH 6.8
Silver stain-developing solution	2.5% (w/v) Na ₂ CO ₃ 0.01% (v/v) formaldehyde

Silver stain-fixing solution	30% (v/v) ethanol 10% (v/v) acetic acid
Silver stain-sensitising solution	30% (v/v) ethanol 0.5 M sodium acetate 0.5% (v/v) glutardialdehyde 0.2% (w/v) Na ₂ S ₂ O ₃
Silver stain-staining solution	0.1% (w/v) AgNO ₃ 0.02% (v/v) formaldehyde
Silver stain-stopping solution	0.05 M EDTA
SSC (20 ×)	3 M NaCl 0.3 M sodium citrate adjusted to pH 7.0
Standard kinase reaction buffer (10 ×)	0.5 M MOPS pH 7.2 1 M NaCl 100 mM MgCl ₂ 20 mM MnCl ₂
TBE (5 ×)	0.45 M Tris base 0.45 M boric acid 10 mM EDTA pH 8.0
TBS (10 ×)	200 mM Tris-HCl pH 7.5 1.37 M NaCl
TBST	0.2% (v/v) Tween 20 in 1 × TBS
T ₁₀ E _{0.1}	10 mM Tris-HCl pH 8.0 0.1 mM EDTA pH 8.0
TELT	50 mM Tris-HCl pH 8.0 62.5 mM EDTA pH 8.0 2.5 M LiCl 4% (v/v) Triton X-100
TENS	10 mM Tris-HCl pH 8.0 1 mM EDTA pH 8.0 10 mM NaOH 0.5% (w/v) SDS
Transfer buffer for immunoblotting	25 mM Tris base 150 mM glycine 10% (v/v) methanol

2.5 Bacterial strains

<i>Description</i>	<i>Genotype</i>	<i>Source</i>
BL21 (DE3) [pAP/lacI ^Q]	<i>hsdS gal (λ.cts857 ind 1 Sam7 nin5 lacUV5-T7 gene 1) [pAP/lacI^Q]</i>	Joachim Clos, BNI, Hamburg
TOP10F'	F' [<i>lacI^q Tn 10 (Tet^R)mcrA Δ(mrr-hsdRMS-mcrBC) φ80lacZ ΔM15ΔlacX74 recA1 araD 139 Δ (ara-leu)7697 galU galK rpsL (Str^R) endA1 nupG</i>]	Invitrogen Life Technologies, Karlsruhe

XL1-Blue *recA endA gyrA96 thi-1 hsdR17 supE44 rel A1 lac [F' proAB lac^qZΔM15 Tn 10 (Tet^r)]* Stratagene, La Jolla, CA, USA

2.6 *Leishmania* strains

Leishmania major MRHO/IR/76/vaccine strain

Leishmania mexicana mexicana MNYC/BZ/62/M379, clone 2

2.7 Mouse strain

Infection studies were performed with 6 to 10 weeks old, female BALB/c mice which had either been bred in the BNI (Hamburg) or were purchased from *Charles River* (Sulzfeld).

2.8 DNA vectors and plasmid constructs

<i>Description</i>	<i>Source</i>
pB41ImmkkMut2	Wiese <i>et al.</i> , 2003a
pB5upLmxMPK3ds	Erdmann, diploma thesis, 2004
pBE2upds(MPK3)	Erdmann, diploma thesis, 2004
pCR2.1-23MPK3	Erdmann <i>et al.</i> , 2006
pCR2.1Immkk3	Wiese <i>et al.</i> , 2003a
pCR2.1-TOPO	<i>Invitrogen Life Technologies</i> , Karlsruhe
pGEX-KG5aBHLmxMPK3	Erdmann, diploma thesis, 2004
pGEX-KG(-P)	John von Freyend, unpublished
pJC45LdDC2	Harder, PhD thesis, 2005
pJCduet	Joachim Clos, BNI, Hamburg
pJCduet-LmxMPK13	Scholz, PhD thesis, 2008
pJCduet-LmxMPK13-LmxPK4	Scholz, PhD thesis, 2008
pSSU-int-Immkkgef-p-c1-lmcpbds-pac	Wiese <i>et al.</i> , unpublished
pTH6cGFPn	Dubessay <i>et al.</i> , 2006
pTH6nGFPc	Dubessay <i>et al.</i> , 2006
pX3ELmxMPK3	Erdmann, diploma thesis, 2004
pX63poIPAC	Bengs <i>et al.</i> , 2005

Plasmid constructs generated throughout the project are listed in 8.2 including plasmid maps which were drawn using Clone Manager 4.1 (*Sci-Ed Software*).

2.9 Oligonucleotides

The following oligonucleotides were synthesised by *Invitrogen Life Technologies* (Karlsruhe).

<i>Description</i>	<i>Nucleotide sequence</i>
EcoRI.for	5'-CGCATACGCGACGAATTC-3'
gln6.sense	5'-CTGGCTCTCCGGCAAAGAT-3'
gln9.rev	5'-ACGGAAACGCATTAACAGG-3'
Kin320680_1.for	5'-CCATGGAATTCGTGAAAGCGAACTCCGGGGCG-3'
Kin320680_1.rev	5'-AAGCTTCTAGACCCTAGGCTTGTTCGATCTGCTTGC-3'
LmjF36_2.for	5'-TCATGACNGAGTACGCTGGNACNCAG-3'
LmjF36_2.rev	5'-AAGCTTTCAGTGTGGGCACGCGTCATTTTCGTCG-3'
LmjF36pep1	5'-CATGTTGCGCGTGGGCAACTCTGCGCCTCCTCCGTTGACGCCGACAGCCTGA-3'
LmjF36pep2	5'-AGCTTCAGGCTGTGCGCGTCAACGGAGGAGGCGCAGAGTTGCCACGCGCAA-3'
LmxMPK3GFP-Nterm	5'-GGGCAATTGCACAAGAGCAACCAGGAGCTGAGC-3'
LmxMPK3GFP-Cterm	5'-GGGGTTAACGTGATGGTGACCGCTACCGTTCTTTGA-3'
LmxMPK3i.for	5'-GACGTGTACGTCGTCGGTCCGCTCATGGACGTAGA-3'
LmxMPK3i.rev	5'-ACGTCCATGAGCGGACCGACGACGTACACGTCTTC-3'
LmxMPK3KM.rev	5'-TCGCGACACTTCATGATGGACACCTTC-3'
MPK3-ADL.rev	5'-GGCGGTACCAGCGCGTGATGACTAAATCCGCAAGCTCCGA-3'
MPK3-ADY.rev	5'-GGCGGTACCAGCGCGTGATGACGTAATCCGCAAGCTCCGA-3'
mpk3c.rev	5'-GTGAAGCTTCTAGTGATGGTGACCGCT-3'
mpk3cXbal.rev	5'-GCTCTAGACTAGTGATGGTGACCGCT-3'
mpk3nClal.for	5'-CATCGATAAAATGCACAAGAGCAACC-3'
mpk3n.for	5'-CCAACATGTACAAGAGCAACCAGGAGC-3'
MPK3-TDL.rev	5'-GGCGGTACCAGCGCGTGATGACTAAATCCGTAAGCTC-3'
MscI.rev	5'-AGACGCCGACGGTGGCCA-3'
NcoIPAC.for	5'-CGACCTTCCATGGCGACCGAGTACAAGCCCACG-3'
NcoIPAC.rev	5'-GTAICTGGTCCGTCATGGAAGGTCGTCTCCTTG-3'
PFR2C_1.for	5'-CGTGCCTGTGCAACGAGGAG-3'
PFR2C_1.rev	5'-GTTTCATGCAGTCTCCAGGC-3'
pGEX-KG1.for	5'-CTATCCCACAAATTGATAA-3'
pXPHEO2	5'-AAACCGCTCGCGGTGTGTT-3'

2.10 Antibodies

Primary antibodies

<i>Antigen / Name (Characteristics)</i>	<i>Host</i>	<i>Dilution for Western / IF</i>	<i>Source</i>
AvGFP peptide mix	rabbit	1:100	<i>Clontech, BD Living Colors, Mountain View, CA, USA</i>
Digoxigenin (Fab fragments antibody, AP-conjugated)	sheep	1:10000	<i>Roche Diagnostics, Mannheim</i>
GST-LmxMCK	rabbit	1:100	<i>Wiese et al., 2003a</i>
IPS	rabbit	1:500	<i>Ilg, 2002</i>
LdDC2	chicken	1:1000	<i>Harder, PhD thesis, 2005</i>
LmxGS	rabbit	1:100	<i>Wiese et al., unpublished</i>
LmxMPK3 C-terminus	rabbit	1:500	<i>Erdmann et al., 2006</i>
PFR-A / L8C4 (hybridoma cell supernatant)	mouse	1:100 (1:1)	<i>Keith Gull, University of Oxford, UK</i>
Phosphotyrosine / 4G10 (hybridoma cell supernatant)	mouse	1:1	<i>Bernhard Fleischer, BNI, Hamburg</i>

Av = *Aequorea Victoria*; IF = immunofluorescence.

Secondary antibodies

<i>Antigen (Characteristics)</i>	<i>Host</i>	<i>Dilution</i>	<i>Source</i>
Chicken IgG (HRP-conjugated)	rabbit	1:1500	<i>Sigma-Aldrich, Steinheim</i>
Mouse IgG (HRP-conjugated)	rabbit	1:2000	<i>DAKO, Hamburg</i>
Mouse IgG (Alexa Fluor 488-conjugated)	goat	1:200	<i>Invitrogen Life Technologies, Karlsruhe</i>
Rabbit IgG (HRP-conjugated)	goat	1:5000	<i>Dianova, Hamburg</i>

2.11 Enzymes

<i>Description</i>	<i>Source</i>
Alkaline phosphatase, shrimp	<i>Roche Diagnostics, Mannheim</i>
<i>Expand High Fidelity PCR System</i>	<i>Roche Diagnostics, Mannheim</i>
Klenow enzyme	<i>Roche Diagnostics, Mannheim</i>

Restriction endonucleases	<i>New England Biolabs</i> , Frankfurt am Main
RNase A (bovine pancreas)	<i>Roche Diagnostics</i> , Mannheim
SuperScript II Reverse Transcriptase	<i>Invitrogen Life Technologies</i> , Karlsruhe
T4 DNA ligase	<i>Roche Diagnostics</i> , Mannheim
Thrombin	<i>Amersham Biosciences</i> , Freiburg

2.12 Molecular biology kits

<i>Description</i>	<i>Source</i>
<i>ECL Western Blotting Detection Kit</i>	<i>Amersham Biosciences</i> , Freiburg
<i>Human T Cell Nucleofector Kit</i>	<i>Amaxa Biosystems</i> , Gaithersburg, MD, USA
<i>Invitrogen Plasmid Purification Kit</i>	<i>Invitrogen Life Technologies</i> , Karlsruhe
<i>M&N NucleoSpin Extract II Kit</i>	<i>Macherey & Nagel</i> , Düren
<i>M&N NucleoSpin Plasmid Kit</i>	<i>Macherey & Nagel</i> , Düren
<i>M&N NucleoBond Xtra Midi Kit</i>	<i>Macherey & Nagel</i> , Düren
<i>M&N NucleoSpin RNA II Kit</i>	<i>Macherey & Nagel</i> , Düren
<i>PhosphoProtein Purification Kit</i>	<i>Qiagen</i> , Hilden
<i>QIAGEN Plasmid Midi Kit</i>	<i>Qiagen</i> , Hilden
<i>QIAprep Spin Miniprep Kit</i>	<i>Qiagen</i> , Hilden
<i>QIAquick Gel Extraction Kit</i>	<i>Qiagen</i> , Hilden
<i>SuperSignal West Pico Chemiluminescent Substrate Kit</i>	<i>Pierce/Perbio Science</i> , Bonn
<i>TOPO TA Cloning Kit</i>	<i>Invitrogen Life Technologies</i> , Karlsruhe

2.13 DNA and protein molecular weight markers

<i>Description</i>	<i>Source</i>
1kbp DNA Ladder	<i>Carl Roth</i> , Karlsruhe
PCR Marker	<i>New England Biolabs</i> , Frankfurt am Main
Prestained Protein Marker, Broad Range	<i>New England Biolabs</i> , Frankfurt am Main

3 Methods

3.1 Cell biology methods

3.1.1 Culturing of *E. coli*

3.1.1.1 Culturing on medium plates

A maximal volume of 250 μ l of (transformed) bacterial cells was plated on LB agar plates with a glass spreader sterilised in ethanol. For selection purposes the medium plates contained the required antibiotics (100 μ g/ml ampicillin, 50 μ g/ml kanamycin, 20 μ g/ml tetracycline). The medium plates with the bacteria were incubated upside down at 37°C overnight.

3.1.1.2 Culturing in liquid medium

Using a sterile inoculating loop, one single colony was used to inoculate the required volume of LB medium with the appropriate antibiotics (100 μ g/ml ampicillin, 50 μ g/ml kanamycin, 20 μ g/ml tetracycline). The cultures were grown in a shaking incubator (120-225 rpm) at 37°C overnight.

3.1.1.3 Preparation of glycerol stocks

500 μ l of the bacterial culture was added to the same volume of glycerol in a sterile cryo tube. After mixing the tube was incubated on ice for 10 min and subsequently stored at -70°C.

3.1.2 Culturing of *Leishmania*

3.1.2.1 Culturing of *L. mexicana* and *L. major* promastigotes

Promastigotes were grown in SDM medium (Brun and Schönenberger, 1979) (complete) at 27°C without CO₂. If required, the appropriate antibiotics were added to the medium (5 μ g/ml bleocin (phleomycin), 10 μ g/ml G418, 20 μ g/ml hygromycin B, 40 μ M puromycin). Cells were inoculated into fresh medium with a ratio of 1:500 to 1:1,000 using a disposable plastic pipette when cultures reached late log-phase or early stationary phase.

3.1.2.2 *In vitro* differentiation to *L. mexicana* axenic amastigotes

Cultured stationary phase promastigotes were sedimented by centrifugation at 2,050 \times g at 4°C for 5 min and washed with Schneider's *Drosophila* medium (complete). The cells were inoculated into fresh Schneider's *Drosophila* medium (complete) at 4 \times 10⁶ cells/ml and incubated at 34°C with 5% CO₂ (Bates *et al.*, 1992).

3.1.2.3 *In vitro* differentiation to *L. mexicana* promastigotes

Lesion-derived amastigotes were washed with SDM medium (complete), inoculated into fresh SDM medium (complete) at 1×10^7 cells/ml and incubated at 27°C without CO₂.

3.1.2.4 Preparation of *Leishmania* stabilates

10 ml of a log-phase *Leishmania* culture were centrifuged at $2,050 \times g$ at 4°C for 10 min. The sedimented cells were resuspended in 1.5 ml of ice-cold cryo medium and divided into three pre-chilled cryo tubes. The tubes were placed in the gas phase of liquid nitrogen for 24 h for gradual temperature reduction and were subsequently submerged into liquid nitrogen for long term storage.

For re-culturing the cells were thawed quickly in a 37°C water bath and immediately used to inoculate 10 ml of SDM medium (complete).

3.1.3 *Leishmania* cell counting

10 µl of the *Leishmania* culture were diluted in fixing solution to the appropriate ratio and the cell suspension was loaded onto a Neubauer chamber (0.1 mm, 0.0025 mm²) for cell counting using a light microscope. The whole area (two large squares) were counted and the average value was used to calculate the cell density using the following formula: number of cells/ml = number of counted cells \times diluting factor $\times 10^4$.

3.1.4 Fluorescence-activated cell sorting (FACS) of *Leishmania* promastigotes

Log-phase promastigotes were sorted directly from the culture using a BD FACSCalibur flow cytometer. Cell sorting was carried out by Claudia Sander-Jülch (FACS facility, BNI, Hamburg).

3.2 Molecular biology methods

3.2.1 Preparation of competent bacteria

3.2.1.1 Method of Hanahan (1983)

For the preparation of competent XL1-Blue cells a single colony was picked from an LB agar plate containing tetracycline and used to inoculate 3 ml of LB medium with 40 µg/ml tetracycline. The culture was grown in a shaking incubator at 37°C overnight. 500 µl of the culture were transferred into 100 ml of fresh LB medium containing 40 µg/ml tetracycline and the culture was grown until an optical density of 0.2 was reached at a wave length of 550 nm (OD₅₅₀). The culture was incubated on ice for 15 min, divided into two 50 ml tubes and centrifuged at $3,500 \times g$ at 4°C for 15 min. The harvested cells of each tube were carefully resuspended in 16 ml RF1, pooled and incubated on ice for 90 min. The cells were sedimented under the same conditions as before, carefully resuspended in 8 ml RF2 and

incubated on ice for 15 min. The competent cells were aliquoted in 200 µl volumes into 1.5 ml safe-lock tubes, quick-frozen in liquid nitrogen and stored at -70°C.

3.2.1.2 Preparation of competent BL21 (DE3) [pAP/aci^Q]

A single colony was picked from an LB agar plate containing kanamycin and used to inoculate 3 ml of LB medium with 10 µg/ml kanamycin. The culture was grown in a shaking incubator at 37°C overnight. 1ml of the culture was transferred into 200 ml of fresh LB medium containing 10 µg/ml kanamycin, and the culture was grown until an optical density of 0.3 was reached at a wave length of 600 nm (OD₆₀₀). The cells were harvested at 3000 × g at 4°C for 15 min and resuspended in 20 ml of a pre-chilled 50 mM CaCl₂ solution on ice. The cells were sedimented under the same conditions as before and carefully resuspended in 2 ml 50 mM CaCl₂, 50% (v/v) glycerol, and 7% (v/v) DMSO. The competent cells were aliquoted in 200 µl volumes into 1.5 ml safe-lock tubes, quick-frozen in a dry ice/ethanol bath and stored at -70°C.

3.2.2 Transformation of *E. coli*

An aliquot of competent bacteria was thawed on ice, and 0.5-10 µl of plasmid DNA were added to the cell suspension. After gentle mixing the cells were incubated on ice for 30 min. The cells were subsequently heat-shocked by incubation at 42°C for 90 s (XL1-Blue)/30 s (pAPlac) using a water bath and immediately placed on ice for 5 min. 800 µl (XL1-Blue)/500 µl (pAPlac) of LB medium were added and the cells were incubated in a shaking heat block (400 rpm) at 37°C for 40 min (XL1-Blue)/1h (pAPlac). 50-200 µl of the cell suspension were plated on an LB agar plate containing the relevant antibiotics for selection of positive clones, and the plate was incubated upside down at 37°C overnight.

If the transformed plasmid allowed a blue-white selection of cells carrying a positive recombinant plasmid, 40 µl X-Gal (40 mg/ml in DMF) and 40 µl IPTG (100 mM) were spread onto the LB agar plate which was subsequently pre-incubated at 37°C at least 30 min before plating the bacteria.

3.2.3 Transfection of *Leishmania*

3.2.3.1 Gene Pulser transfection (*BIO RAD*)

4×10^7 late log-phase promastigotes were sedimented at 5,600 × g for 20 s and washed with 500 µl of ice-cold EPB. The cells were centrifuged under the same conditions as before, resuspended in 400 µl of ice-cold EPB and transferred to a pre-chilled 4 mm-gap cuvette (*BIO RAD Laboratories*, Munich). 1-5 µg of linearised DNA or 5 µg of plasmid DNA were added to the cell suspension. After gentle mixing the cells were electroporated three times in a *BIO RAD* Gene Pulser at 1.5 kV, 200 Ω and 25 µF for 0.9-1.1 ms. The transfected cells were incubated on ice for 10 min and were subsequently transferred into 10 ml of SDM

medium (complete, with 10% iFCS) containing the antibiotics which had been used for culturing of the original clone. After incubation at 27°C for 24 h the culture was filled up to 40 ml with fresh SDM medium (complete, with 10% iFCS), and antibiotics were added according to the resistance marker gene of the transfected DNA fragment or plasmid. The diluted culture was distributed on two 96-well plates (200 µl/well) which were subsequently sealed with parafilm and incubated at 27°C until resistant cells grew (1-2 weeks). Positive cells were transferred into 2 ml of fresh medium containing the same antibiotics and were eventually passaged to the standard volume of 10 ml. If it was relevant to obtain a culture which originates from a single positive clone and the plate had shown positives on more than every third well, the cells were singled out on a 96-well plate once again.

3.2.3.2 Nucleofector transfection (*Amaxa*)

Transfections were carried out using the *Amaxa* Human T Cell Nucleofector Kit. 3×10^7 late log-phase promastigotes were sedimented at $5,600 \times g$ for 20 s and directly resuspended in 100 µl of Human T Cell Nucleofector solution containing the provided supplement. The cell suspension was transferred to the provided cuvette and 1-5 µg of linearised DNA or 5 µg of plasmid DNA were added. After gentle mixing the cells were electroporated in the *Amaxa* Nucleofector II using programme V-033. The transfected cells were incubated on ice for 10 min and were subsequently transferred into 10 ml of SDM medium (complete, with 10% iFCS) containing the antibiotics which had been used for culturing of the original clone. After incubation at 27°C for 24 h half of the culture (5 ml) was filled up to 20 ml with fresh SDM medium (complete, with 10% iFCS), and antibiotics were added according to the resistance marker gene of the transfected DNA fragment or plasmid. The diluted culture was distributed on a 96-well plate (200 µl/well). In addition, the cells were distributed with a 10-fold higher dilution on a second plate. Therefore, 0.5 ml of the original culture were filled up to 20 ml with fresh SDM medium (complete, with 10% iFCS) containing the same antibiotics as described above and distributed on a 96-well plate in 200 µl volumes. The plates were subsequently sealed with parafilm and incubated at 27°C until resistant cells grew (1-2 weeks). It was further proceeded as described in 3.2.3.1.

3.2.4 Isolation of plasmid DNA from *E.coli*

3.2.4.1 Plasmid DNA mini-preparation (Zhou *et al.*, 1990)

1.5 ml of an overnight culture were harvested at $15,800 \times g$ for 30 s, the supernatant was decanted, and the sedimented cells were resuspended in the residual supernatant (ca. 100 µl). 300 µl of TENS was added, and the cell suspension was vortexed at medium speed for 4 s and immediately placed on ice. Subsequently, 150 µl of 3 M sodium acetate pH 5.2 were added, and the cell lysate was vortexed at medium speed for 3 s and placed on ice again. The cell debris was sedimented at $15,800 \times g$ at 4°C for 10 min, and the particle-free

supernatant was transferred to a new 1.5 ml tube. 900 μ l of ice-cold 100% ethanol were added in order to precipitate the plasmid DNA, and the mixture was centrifuged at $15,800 \times g$ at 4°C for 15 min. The DNA pellet was washed with ice-cold 70% ethanol and centrifuged under the same conditions as before for 10 min. The supernatant was removed completely, and the pellet was allowed to dry (10-15 min) before it was dissolved in 40 μ l ddH₂O.

3.2.4.2 Plasmid DNA mini-preparation using *Macherey & Nagel* and *Qiagen* Kits

1.5 ml of an overnight culture were harvested at $15,800 \times g$ for 30 s and the supernatant was decanted. It was further proceeded according to the respective manufacturer's protocol chapter "Using a microcentrifuge".

3.2.4.3 Plasmid DNA midi-preparation using *Invitrogen*, *Macherey & Nagel* and *Qiagen* Kits

100 ml of an overnight culture were harvested at $4,000 \times g$ at 4°C for 15 min, and the supernatant was decanted. It was further proceeded according to the respective manufacturer's protocol chapter "High-copy plasmid purification" until the elution of the plasmid DNA was completed. For DNA precipitation 833 μ l volumes of the eluate were subsequently transferred to six 1.5 ml tubes, and 583 μ l of isopropanol were added to each tube. The mixture was centrifuged at $15,800 \times g$ at 4°C for 30 min. The DNA pellets were washed and dried as described in 3.2.4.1. Each DNA pellet was dissolved in 20 μ l ddH₂O, and the DNA solutions of the six tubes were finally pooled.

3.2.5 Isolation of genomic DNA from *Leishmania* (Medina-Acosta and Cross, 1993)

3 ml of a stationary phase *Leishmania* culture were centrifuged at $5,600 \times g$ for 30 s, and the sedimented cells were resuspended in 400 μ l of freshly prepared TELT in a 1.5 ml safe-lock tube. After incubation at room temperature for 5 min, 400 μ l of ice-cold TE-equilibrated phenol were added, and the mixture was end-over-end rotated at 4°C for 5 min. The mixture was centrifuged at $15,800 \times g$ at 4°C for 10 min, and the aqueous (upper) phase was transferred to a new 1.5 ml safe-lock tube. 400 μ l of chloroform/isoamyl alcohol (24:1) were added, and the mixture was end-over-end rotated and centrifuged as described above. The aqueous (upper) phase was again transferred to a new tube, and the genomic DNA was precipitated by adding 1 ml of ice-cold 100% ethanol. After incubation on ice for 5 min the tube was centrifuged at $15,800 \times g$ at 4°C for 10 min. The DNA pellet was washed with ice-cold 70% ethanol and centrifuged under the same conditions as before. The supernatant was removed completely, and the pellet was allowed to dry at room temperature (10-15 min) before it was dissolved in 200 μ l T₁₀E_{0.1}.

3.2.6 Isolation of total RNA from *Leishmania* using a *Macherey & Nagel* Kit

To prevent RNA degradation it was important to create an RNase-free working environment. Therefore, clean gloves were worn at all times during the preparation and were changed frequently. In addition, pipetting was carried out exclusively using RNase-free filter tips. Total RNA was isolated according to the manufacturer's protocol chapter "Total RNA purification from cultured cells and tissue". 1×10^8 late log-phase promastigotes were harvested at $5,600 \times g$ for 20 s and used as starting material for a single preparation. The incubation step with the supplied DNase was extended to 30 min. The total RNA was finally eluted with 50 μ l of the supplied RNase-free ddH₂O. For short term storage the RNA was frozen at -20°C, for long term storage it was kept at -70°C.

3.2.7 Determination of DNA and RNA concentrations

The nucleic acid solution was diluted 1:50 or 1:100 in ddH₂O and transferred to a UV cuvette (UVette, *Eppendorf*). The DNA or RNA concentration was determined using an *Eppendorf* BioPhotometer in the DNA or RNA mode, respectively.

3.2.8 Reactions with DNA-modifying enzymes

3.2.8.1 Cleavage of DNA using type II restriction endonucleases

The *NEB* restriction enzymes were used according to the manufacturer's recommendations with the supplied buffers and BSA solution. Analytical digests of plasmid DNA were carried out in a total volume of 15 μ l using 0.2-1.0 μ g of DNA and 5-10 U of enzyme and were incubated for 2-3 h at the recommended temperature. When the DNA was isolated using the Zhou method, 2 μ g of RNase A were also added to the digest. Preparative digests of plasmid DNA were performed in a total volume of 50-100 μ l using 10-20 μ g of DNA and 30-60 U of enzyme. When enzymes exhibiting no star activity were used, the incubation time of preparative digests was extended to 4-6 h or the digest was performed overnight.

3.2.8.2 Complete fill-in of a 5'-overhang to create blunt end DNA using Klenow enzyme

Fill-in reactions were carried out using the Klenow enzyme kit from *Roche*. The phenol/chloroform-extracted and ethanol-precipitated DNA was dissolved in 20 μ l of 1 \times filling buffer (provided). 0.75 μ l dNTPs (provided) and 1 U Klenow enzyme were added, and the mixture was incubated at 37°C for 15 min. The enzyme was finally inactivated by adding 0.5 μ l of 0.5 M EDTA pH 8.0.

3.2.8.3 Dephosphorylation of DNA 5'-ends

Linearised vector molecules revealing blunt ends or compatible sticky ends were treated with shrimp alkaline phosphatase (SAP) from *Roche*. The phenol/chloroform-extracted and ethanol-precipitated DNA was dissolved in 25.5 μ l of ddH₂O. 3 μ l of 10 \times dephosphorylation

buffer (provided) and 1.5 U SAP were added, and the mixture was incubated at 37°C for 2 h. The enzyme was finally inactivated at 65°C for 20 min.

3.2.8.4 Ligation of DNA fragments

Ligation reactions were carried out using the T4 DNA ligase kit from *Roche*. 50-100 ng vector DNA, the threefold molar excess of insert DNA, 1 µl of 10 × ligase buffer (provided) and 1 U T4 DNA ligase were mixed in a total volume of 10 µl and incubated at 13°C overnight. The reaction was kept on ice until it was used for bacterial transformation.

3.2.9 Phenol/chloroform extraction of aqueous DNA solutions

Using a 1.5 ml safe-lock tube 100 µl of TE-equilibrated phenol were added to 100 µl of DNA solution, and the mixture was vortexed at maximum speed for 30 s and centrifuged at 15,800 × g for 5 min. The aqueous (upper) phase was transferred to a new 1.5 ml safe-lock tube and 100 µl of chloroform/isoamyl alcohol (24:1) were added. The mixture was vortexed and centrifuged as described above. The aqueous (upper) phase was again transferred to a new tube, and the DNA was ethanol-precipitated.

3.2.10 Ethanol precipitation of DNA

11 µl (1/9 volume) 3 M sodium acetate pH 5.2 and 250 µl (2.5 volumes) of ice-cold 100% ethanol were added to 100 µl of an aqueous DNA solution. After incubation on dry ice or in the -70°C freezer for at least 20 min the tube was centrifuged at 15,800 × g at 4°C for 15 min. The DNA pellet was washed with ice-cold 70% ethanol and centrifuged for 10 min under the same conditions as before. The supernatant was removed completely, and the pellet was allowed to dry (10-15 min) before it was dissolved in the appropriate volume of ddH₂O.

3.2.11 Agarose gel electrophoresis

DNA (or RNA) was separated on 0.7-1.2% (w/v) agarose gels prepared with 0.5 × TBE and containing 0.3 µg/ml ethidium bromide. 1/10 volume of 10 × DNA loading buffer was added to the DNA (or RNA) samples, and the mixtures were loaded into the gel pockets. Separation of nucleic acids was performed at 1.4-10 V/cm in 0.5 × TBE until the dye front reached three quarters to full length of the gel. Nucleic acids were visualised by UV illumination and photographed for analysis. DNA molecular weight markers allowed an estimation of length and concentration of the separated DNA fragments.

3.2.12 DNA extraction from agarose gels using *Macherey & Nagel* and *Qiagen* Kits

To purify DNA from agarose gels the band of interest was excised under low intensity UV light ($\lambda = 365$ nm) using a clean scalpel. DNA extraction was performed according to the

respective manufacturer's protocol. The DNA was finally eluted with 15-50 μl of ddH₂O or elution buffer (supplied).

3.2.13 Insertion mutagenesis using complementary 5'-phosphorylated oligonucleotides

5 μl of each oligonucleotide solution (100 pmol/ μl) and 40 μl ddH₂O were mixed in a 200 μl PCR tube, and the annealing reaction was performed in a *PE* thermocycler using the following programme:

DNA denaturation	10 min	95°C	
gradual	}	65°C	
DNA		30 min	37°C
annealing		30 min	room temperature

The resulting DNA double-strand exhibiting sticky ends was subsequently ligated into a plasmid which had been linearised with appropriate restriction enzymes generating the respective complementary sticky ends. The ligation reaction was carried out with 2 μl of the annealed oligonucleotides and 50-100 ng vector DNA as described in 3.2.8.4.

3.2.14 Polymerase chain reaction (PCR)

PCRs were performed using the Expand High Fidelity PCR System from *Roche*. Reactions were carried out in a 200 μl PCR tube using a *PE* thermocycler.

Reaction mixture:

DNA template	10-200 ng
Primer A (10 μM)	1.5 μl
Primer B (10 μM)	1.5 μl
10 \times PCR buffer (15 mM MgCl ₂)	5 μl
dNTPs (20 mM)	1 μl
Enzyme mix	0.75 μl
ddH ₂ O	add up to 50 μl

Programme:

DNA denaturation	5 min	95°C	}	25-30 cycles
DNA denaturation	30 s	95°C		
Primer annealing	30 s	48-60°C		
DNA elongation	45 s - 2 min	72°C		
DNA elongation	7 min	72°C		
Cooling	unlimited	4°C		

The annealing temperature depended on the melting temperature of the oligonucleotides. The elongation time depended on the length of the DNA fragment to be amplified and was adjusted according to the manufacturer's recommendations.

3.2.15 Reverse transcription-polymerase chain reaction (RT-PCR)

Reverse transcription of RNA for first-strand cDNA synthesis was performed using the SuperScript II Reverse Transcriptase kit from *Invitrogen*. Subsequent PCR for second strand DNA synthesis and amplification was carried out using the Expand High Fidelity PCR System from *Roche* as described in 3.2.14. Reactions were carried out in 200 µl PCR tubes using a *PE* thermocycler.

First-strand cDNA synthesis:

100 ng total RNA, 0.5 µl of 10 µM gene-specific primer and HPLC-H₂O added up to 12 µl were incubated at 70°C for 10 min. 4 µl 5 × First-strand buffer (supplied), 2 µl 0.1 M DTT (supplied) and 0.5 µl 20 µM dNTPs were added before the mixture was incubated at 42°C for 2 min. 1 µl (200 U) SuperScript II RT was added followed by an incubation at 42°C for 1 h and 70°C for 10 min.

PCR:

2 µl of the cDNA solution were used for subsequent PCR which was performed as described in 3.2.14.

3.2.16 Cloning of a PCR product using the TOPO TA Cloning Kit (*Invitrogen*)

TOPO TA cloning allows the direct insertion of *Taq* polymerase-amplified PCR products into the plasmid vector pCR2.1-TOPO. The insertion reaction and subsequent transformation into competent cells of the *E. coli* strain TOP10F' (*Invitrogen*) were performed according to the manufacturer's protocol.

3.2.17 DNA sequencing

Plasmid sequencing was carried out by the company *Agowa* (Berlin).

3.2.18 Southern blot analysis

3.2.18.1 Cleavage of genomic DNA and agarose gel electrophoresis

3-5 µg of genomic DNA were incubated with 60-80 U of the appropriate *NEB* restriction enzyme in a total volume of 400 µl. The mixture also contained the supplied buffer and BSA solution according to the manufacturer's recommendations and 40 µg of RNase A. After end-over-end rotation at the recommended temperature (mostly 37 °C) overnight the cleaved DNA was ethanol-precipitated, dried at room temperature (10-15 min) and dissolved in 15 µl T₁₀E_{0.1}. 1.5 µl of 10 × DNA loading buffer were added to each of the DNA samples, and the

DNA was separated on a 0.7% (w/v) agarose gel at 7 V/cm until the dye front reached three quarters to full length of the gel. The separated DNA was visualised by UV illumination and photographed together with a ruler to allow a localisation of the marker bands on the blots.

3.2.18.2 Denaturation, capillary blotting and cross-linking of DNA to nylon membrane

To denature the DNA the gel was incubated with agitation in denaturing solution at room temperature for 20 min. For subsequent neutralisation the gel was incubated with agitation in neutralising solution at room temperature for 30 min. The DNA was transferred to a Biodyne A nylon membrane with a pore size of 0.2 μm (*Pall*) by capillary blotting (Figure 11) at 4°C overnight using 20 \times SSC as transfer buffer.

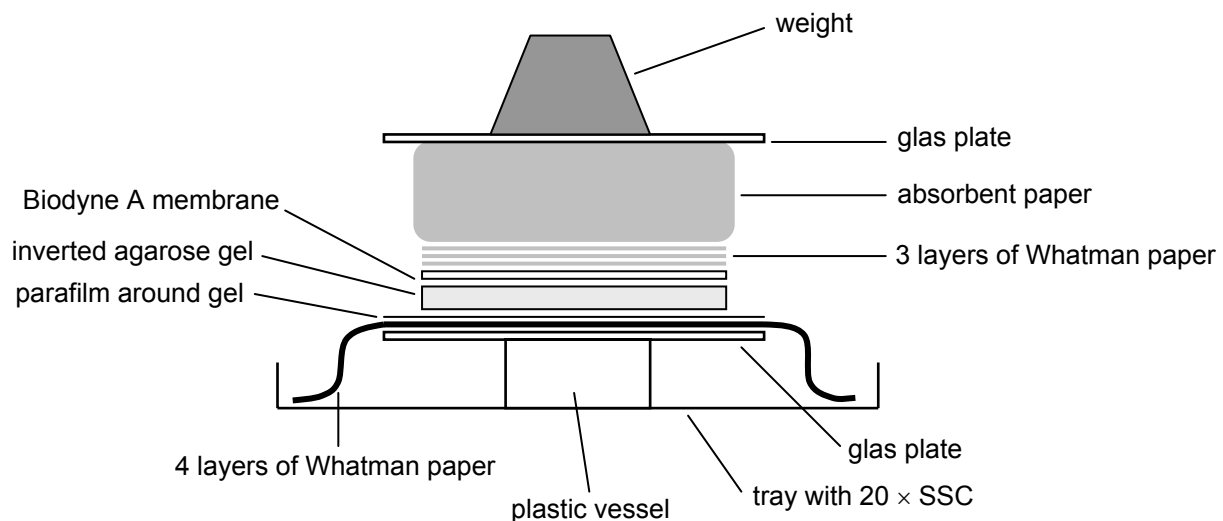


Figure 11: Schematic setup of a capillary blot

The gel pockets were marked on the membrane, and the DNA was cross-linked to the membrane using a UV linker (*Stratagene*) in the auto-cross-link mode.

3.2.18.3 Pre-hybridisation, hybridisation and stringency washing

The membrane was shrink-wrapped in thermoplastic foil with 50 ml pre-hybridising solution and incubated at 42°C in a shaking water bath for at least 3 h. The pre-hybridising solution was subsequently replaced by 50 ml hybridising solution containing the DIG-labelled hybridisation probe which had been heat-denatured at 95°C for 10 min beforehand, and the membrane was incubated overnight under the same conditions as before. The hybridising solution containing the probe was stored at -20°C for re-use. The membrane was washed twice in 200 ml 2 \times SSC/0.1% (w/v) SDS at room temperature for 5 min and twice in 200 ml 0.1 \times SSC/0.1% (w/v) SDS at 68°C for 10 min using a shaking water bath.

3.2.18.4 Detection of the DIG-labelled hybridisation probe

The membrane was washed in 200 ml DIG washing buffer at room temperature for 5 min and subsequently shrink-wrapped in thermoplastic foil with 50 ml DIG II buffer. After incubation at

37°C for 2 h in a shaking incubator the buffer was replaced by 40 ml DIG II buffer containing an AP-conjugated antibody against digoxigenin (*Roche*) in a 1:10,000 dilution, and the membrane was incubated for 45 min under the same conditions as before. It was washed twice with 200 ml DIG washing buffer at room temperature for 15 min before the membrane was equilibrated in DIG III buffer for 5 min. On a plastic foil each side of the membrane was incubated in 3-5 ml DIG III buffer containing CSPD (*Roche*) in a 1:100 dilution for 2.5 min. The membrane was dripped off using Whatman paper and placed in a radiographic cassette between two plastic foils. After pre-incubation at 37°C for 10 min Retina XBA X-ray films (*Fotochemische Werke*) were exposed at 37°C for 15-120 min using an incubator.

3.2.18.5 Stripping-off the hybridisation probe

The Southern blot membrane was washed in ddH₂O at room temperature for 10 min and twice in 0.2 M NaOH/0.1% (w/v) SDS at 37°C for 15 min using a shaking water bath. After incubation in 2 × SSC at 37°C for 5 min the membrane was stored at 4°C until re-hybridisation with a new probe.

3.3 Protein and immunochemical methods

3.3.1 Expression of recombinant proteins in *E. coli*

The bacterial colonies of freshly transformed cells were resuspended in 2 ml of LB medium directly on the LB agar plate and inoculated into 100-200 ml of LB medium containing the appropriate antibiotics. The culture was grown in a shaking incubator at 37°C until an optical density at a wave length of 600 nm (OD₆₀₀) of 0.9 was reached. The culture was cooled down to 18°C before the expression of the fusion protein was induced by adding IPTG in a final concentration of 100 µM. The culture was subsequently incubated in a shaking incubator at 18°C overnight before the cells were harvested at 3,500 × g at 4°C for 15 min. The sedimented cells were washed with 10 ml ice-cold 1 × PBS per sample, centrifuged as described before and could optionally be stored at -20°C until cell lysis.

3.3.2 Preparation of *E. coli* cell lysates for protein purification

Cells were resuspended in 5 ml ice-cold 1 × PBS per sample, transferred into 15 ml tubes and lysed on ice using a *Branson* sonifier with a 6 mm tip (4-6 constant impulses of 15 s duration; impulse intensity gradually increased from step 2 to 4). 600 µl 10% (v/v) Triton X-100 were added to each lysate, and the samples were rotated at 4°C for 30-60 min before the cell debris was removed by sedimentation at 15,800 × g at 4°C for 10 min.

3.3.3 Affinity purification of recombinant proteins

3.3.3.1 Purification of GST-fusion proteins

20 μ l bed volume of glutathione sepharose (Glutathione Uniflow Resin, *BD Biosciences*, Heidelberg) were prepared per 1 ml cell lysate. The appropriate volume of the 50% sepharose stock solution was centrifuged at $500 \times g$ at 4°C for 3 min, and the sepharose pellet was washed three times with ice-cold $1 \times$ PBS and sedimented under the same conditions as before. The cell lysate was added to the sepharose, and the bead suspension was rotated at 4°C for 1 h before it was centrifuged as described before. The sepharose was washed three times with ice-cold $1 \times$ PBS and sedimented as described before. The GST-fusion protein was finally eluted twice with one bed volume GST elution buffer by rotation at 4°C for 10 min and subsequent centrifugation under the same conditions as before.

3.3.3.2 Purification of His-tag fusion proteins

40 μ l bed volume of Chelating Sepharose (*Amersham Biosciences*, Freiburg) were prepared per 1 ml cell lysate. The appropriate volume of the 50% sepharose stock solution was centrifuged at $500 \times g$ at 4°C for 3 min, and the sepharose pellet was washed twice with ice-cold ddH₂O and sedimented under the same conditions as before. One bed volume 100 mM CoCl₂ solution was added, and the bead suspension was rotated at room temperature for at least 10 min. To remove free Co²⁺ the beads were washed twice with ice-cold ddH₂O and sedimented as described before. The cell lysate which had been diluted 1:1 with binding buffer was added to the sepharose, and the bead suspension was rotated at 4°C for 1 h before it was centrifuged as described before. The sepharose was washed with the used lysate volume of ice-cold washing buffer 1, with 5 bed volumes of ice-cold washing buffer 2 and once again with 5 bed volumes of ice-cold washing buffer 1 before it was sedimented as described before. The His-tag fusion protein was finally eluted twice with one bed volume cobalt elution buffer by rotation at 4°C for 10 min and subsequent centrifugation under the same conditions as before.

3.3.4 Thrombin cleavage of a GST-fusion protein to remove the GST-tag

250 μ g of the GST-fusion protein were incubated with 0.5 U thrombin (*Amersham*) in a total volume of 125 μ l at 20°C overnight.

3.3.5 Phosphoprotein purification from *Leishmania* using a Qiagen Kit

Phosphoproteins were purified from 2×10^9 late log-phase promastigotes which were washed with 10 ml 20 mM HEPES pH 7.5. It was further proceeded according to the manufacturer's protocol. The lysis step was extended to 1 h.

3.3.6 Determination of protein concentrations using Bradford reagent

10 μ l of the protein solution were added to 500 μ l Bradford reagent. After thorough mixing and incubation for 2-3 min the protein concentration was determined using an *Eppendorf* BioPhotometer in the calibrated Bradford mode.

3.3.7 Preparation of *Leishmania* lysates for immunoblot analysis

1×10^8 late log-phase promastigotes were harvested at $5,600 \times g$ for 20 s and washed with 1 ml $1 \times$ PBS followed by centrifugation under the same conditions as before. The cell pellet could optionally be stored at -70°C until cell lysis. The cells were resuspended in 100-200 μ l *Leishmania* lysis buffer, incubated at 95°C for 10 min for protein denaturation and chilled on ice for 5 min.

3.3.8 Preparation of *Leishmania* S-100 lysates for *in vitro* kinase assays

1×10^9 late log-phase promastigotes were harvested at $2,050 \times g$ at 4°C for 10 min, washed with ice-cold $1 \times$ PBS and resuspended in 1.5 ml *Leishmania* lysis buffer. Cells were lysed by two freeze-thaw cycles (2 min in liquid nitrogen, 45 min on ice), and the cell debris was removed by sedimentation at $15,800 \times g$ at 4°C for 10 min followed by ultracentrifugation of the supernatant at $70,000 \times g$ at 4°C for 45 min. To remove cellular ATP the obtained S-100 lysate was subjected to gel filtration chromatography using a HiTrap Desalting column containing Sephadex G-25 (*Amersham*). The column was equilibrated with 25 ml equilibration buffer before the lysate was loaded, and proteins were eluted three times with 1.5 ml equilibration buffer.

3.3.9 Discontinuous SDS polyacrylamide gel electrophoresis (SDS-PAGE)

SDS-PAGE was performed in a *Biometra* Minigel(-Twin) system using SDS-PA gels consisting of 4% stacking gels and 8-15% resolving gels. 1/4 volume of $5 \times$ SDS-PAGE loading buffer was added to the protein samples which were subsequently incubated at 95°C for 10 min for denaturation and chilled on ice for 5 min. A maximum of 30 μ l protein sample was loaded per gel pocket. Separation of proteins was performed in $1 \times$ SDS-PAGE electrophoresis buffer at 20 mA in the stacking gel and at 30 mA in the resolving gel until the dye front reached the end of the gel. A pre-stained *NEB* protein molecular weight marker allowed an estimation of the molecular weight of the separated proteins.

3.3.10 Staining of SDS-PA gels

3.3.10.1 Coomassie staining

The resolving gel with the separated proteins was carefully agitated in Coomassie R250 staining solution for 30-60 min. The gel was subsequently incubated with agitation in

Coomassie R250 destaining solution which was occasionally changed until protein bands were clearly visible and the blue background was reduced to a minimum.

3.3.10.2 Silver staining

All steps were performed under agitation at room temperature using approximately 50 ml volumes per gel. The resolving gel with the separated proteins was carefully agitated in fixing solution for at least 10 min (0.5-3 h) followed by incubation in sensitising solution for at least 10 min (0.5-2 h, also possible overnight). Subsequently, the gel was washed three times with ddH₂O for at least 10 min (10-30 min, also possible overnight to minimise background) followed by incubation in staining solution for at least 10 min (15-60 min). To visualise the protein bands the gel was carefully agitated in developing solution until the bands reached the optimal intensities (2-8 min). To stop the reaction the gel was incubated in stopping solution for 5-10 min. The gel was immediately transferred into ddH₂O for storage.

3.3.11 Drying of SDS-PA gels

Stained gels were carefully agitated in gel drying solution for at least 30 min, and two sheets of cellophane were soaked in water. The gel was placed between the wet cellophane sheets with a few millilitres of gel drying solution using a gel drying frame (*Roth*) without trapping air-bubbles. The drying process took 24-48 h and could be reduced to 12 h if the frame was placed in a fume hood.

3.3.12 Immunoblot analysis

3.3.12.1 Electroblotting of proteins using the semi-dry method

After SDS-PAGE the separated proteins were transferred to an Immobilon-P PVDF membrane (*Millipore*) by semi-dry electroblotting using the *Biometra* Fastblot system. Before setting up the electroblot the gel was equilibrated in transfer buffer for 1 min, and six gel-size Whatman papers were soaked in transfer buffer. The membrane was incubated in methanol for 1 min and subsequently equilibrated in transfer buffer for 10 min. The electroblot was set up as illustrated in Figure 12, and the protein transfer was carried out at 4 mA/cm² of membrane surface for 30 min.

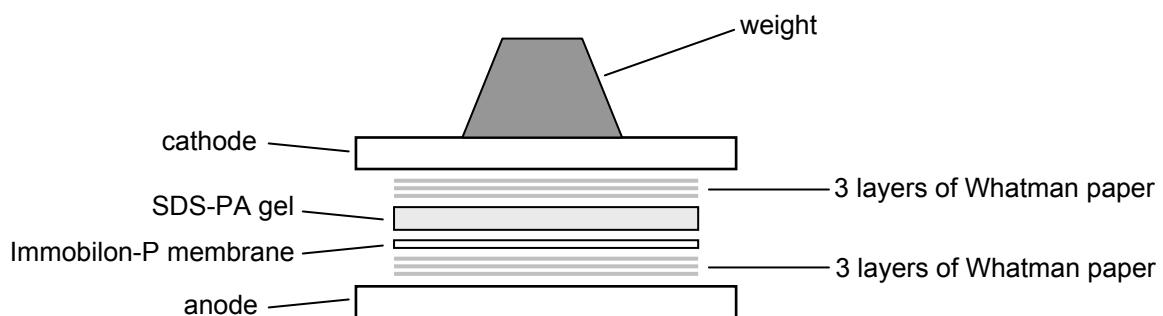


Figure 12: Schematic setup of a semi-dry electroblot

3.3.12.2 Immunological detection of proteins

The membrane was incubated in blocking solution 1 or 2 (for the detection of phosphoryl groups) at 37°C for 1 h to prevent non-specific binding of antibodies to the membrane. The membrane was subsequently incubated in blocking solution 1 or 2 containing the appropriate primary antibody at 37°C for 1 h or at 4°C overnight. It was washed four times with 1 × PBST or 1 × TBST (for the detection of phosphoryl groups) at room temperature for 5 min before the membrane was incubated in blocking solution 1 or 2 containing the appropriate HRP-conjugated secondary antibody at 37°C for 1 h. It was finally washed three times with 1 × PBST or 1 × TBST and twice with 1 × PBS or 1 × TBS at room temperature for 5 min. Both sides of the membrane were incubated in a 1:1 mix of the solutions from the respective detection kit (*Amersham* or *Pierce*). The membrane was placed in a radiographic cassette between two plastic foils, and Retina XBA X-ray films (*Fotochemische Werke*) were exposed at room temperature for 1 s to 1 h.

3.3.12.3 Stripping-off the antibodies

The immunoblot membrane was incubated in 100 mM β-mercaptoethanol, 2% (w/v) SDS, and 62.5 mM Tris-HCl pH 6.7 at 68°C in a shaking water bath for 30 min. It was washed twice with 1 × PBST or 1 × TBST (for the detection of phosphoryl groups) at room temperature for 10 min before proceeding with the blocking step.

3.4 *In vitro* kinase assays

3.4.1 Standard kinase assay with recombinant proteins

1.5–4 μg kinase and 10 μg myelin basic protein (MBP; artificial substrate) or 1–8 μg of a potential substrate protein were incubated in a total volume of 50 μl containing the appropriate 1 × kinase reaction buffer, 90 μM ATP and 5 μCi [γ -³²P]ATP (5000 Ci/mmol; *Hartmann Analytic*, Braunschweig). Reactions were performed at 27°C for 1 h and terminated by adding 12.5 μl of 5 × SDS-PAGE loading buffer followed by an incubation at 95°C for 10 min. The protein samples were chilled on ice for 5 min, and 20–25 μl sample were loaded per gel pocket and separated on an SDS-PA gel of the appropriate percentage (12% when MBP was used as a substrate). The gel was stained and dried, and Retina XBA X-ray films (*Fotochemische Werke*) were exposed in a radiographic cassette at -70°C for several hours or days.

3.4.2 *In vitro* activation of recombinant kinases

10 μg of the kinase to be activated and 1/30 amount of its activating kinase were incubated in a total volume of 20 μl containing 1 × kinase reaction buffer optimal for the activating kinase, 3 mM EGTA and 0.1 mM ATP. Reactions were performed at 27°C for 1 h before 5 μl of the

assay were used in a radioactive standard kinase assay containing 1 × kinase reaction buffer optimal for the activated kinase.

3.4.3 Kinase assays with an activated recombinant kinase on *Leishmania* S-100 lysates

Up to 4 µg activated kinase and the maximal amount of the S-100 lysate were incubated in a total volume of 100 µl containing the appropriate 1 × kinase reaction buffer, 10 µCi [γ -³²P]ATP (5000 Ci/mmol; *Hartmann Analytic*, Braunschweig), 5 mM NaF, 1 mM sodium orthovanadate and 0.1 µM okadaic acid. Reactions were performed at 27°C for 1 h and terminated by adding 25 µl of 5 × SDS-PAGE loading buffer followed by an incubation at 95°C for 10 min. The protein samples were chilled on ice for 5 min, and 20-25 µl sample were loaded per gel pocket and separated on a 12% SDS-PA gel. The gel was stained and dried, and Retina XBA X-ray films (*Fotochemische Werke*) were exposed in a radiographic cassette at -70°C for several hours or days.

3.5 Mouse foot pad infection studies

Five female 6-10 weeks old BALB/c mice were used for infection studies for each *Leishmania* clone to be tested. Late log-phase promastigotes were harvested at 5,600 × g for 20 s, washed with ice-cold 1 × PBS and resuspended in 1 × PBS to a final density of 3.3 × 10⁶ cells/ml. 30 µl of this cell suspension containing 1 × 10⁷ promastigotes were subsequently injected into the left hind foot pad of a mouse using a 0.3 mm × 13 mm needle. Using a calliper gauge the infected foot pad was measured every four weeks in comparison to the non-infected one.

3.6 Isolation of *Leishmania* amastigotes from mouse lesions

After the lesion was sterilised with 70% ethanol the tissue was cut into pieces, transferred into 10 ml of ice-cold 1 × PBS and passed through a sterile metal grid to disrupt macrophages and liberate the amastigotes. 1 × PBS was used to rinse the grid, and the cell suspension was collected in a sterile petri dish. After the cell suspension was transferred to a sterile centrifuge tube, host cells and cell debris were removed by sedimentation at 150 × g at 4°C for 10 min. The supernatant was subsequently centrifuged at 1,500 × g at 4°C for 10 min to sediment the amastigotes. The amastigotes were resuspended in 10 ml ice-cold 1 × PBS, and the cell density was determined for further experimental procedures using a Neubauer chamber.

3.7 Microscopy techniques and flagellar length determination

3.7.1 Immunofluorescence analysis

500 μ l of a log-phase *Leishmania* culture were centrifuged at $5,600 \times g$ for 20 s, and cells were washed with 1 ml ice-cold $1 \times$ PBS and subsequently resuspended in 300 μ l ice-cold $1 \times$ PBS. Meanwhile, a 10-well microscope slide was coated with poly-L-lysine by incubation with 20 μ l 0.1 mg/ml poly-L-lysine in $1 \times$ PBS per well for 15 min. Incubation steps always took place at room temperature in a petri dish with damp tissue paper at the bottom to prevent drying. Wells were washed twice with 50 μ l $1 \times$ PBS before 20 μ l cell suspension and 20 μ l 4% paraformaldehyde were added to each well. Fixation was allowed to proceed for 15 min. The wells were washed twice with 50 μ l $1 \times$ PBS before the cells were permeabilised with 50 μ l solution 1 (50 mM NH_4Cl , $1 \times$ PBS, and 0.1% (w/v) saponin) per well for 15 min. To prevent non-specific binding of antibodies to the slide, each well was incubated with 50 μ l solution 2 (2% (w/v) BSA, $1 \times$ PBS, and 0.1% (w/v) saponin) for 15 min. Subsequently, the primary antibody was added to the cells with the appropriate dilution in solution 2 and a final volume of 20 μ l per well. For each primary antibody one well was kept as a negative control which was incubated with solution 2 lacking the antibody. After 1 h wells were washed four times with 50 μ l solution 3 ($1 \times$ PBS, and 0.1% (w/v) saponin) before the secondary antibody was added with the appropriate dilution in 20 μ l solution 2 containing also DAPI in a 1:100 dilution for DNA staining. The incubation was performed in the dark for 30 min. Cells were subsequently washed three times with 50 μ l solution 3 and twice with 50 μ l $1 \times$ PBS. The cells were finally embedded in Mowiol/DABCO and covered with a cover slip without trapping air-bubbles. Cells were viewed with a Zeiss fluorescence microscope, and fluorescence images were captured by a Hamamatsu digital camera using the Openlab software v 5.0.1 (Improvision).

3.7.2 Fluorescence microscopy on living *Leishmania* promastigotes

Hoechst DNA stain was added to 500 μ l of a log-phase *Leishmania* culture in a 1:500 dilution followed by incubation at 27°C for 15 min. Promastigotes were harvested at $2,050 \times g$ at 4°C for 3 min, and cells were washed with 1 ml ice-cold $1 \times$ PBS and subsequently resuspended in 300 μ l ice-cold $1 \times$ PBS. Meanwhile, a 10-well microscope slide was coated with poly-L-lysine and washed as described in 3.7.1. Incubation steps always took place at room temperature in a petri dish with damp tissue paper at the bottom to prevent drying. 20 μ l cell suspension once again containing Hoechst DNA stain in a 1:500 dilution were added to each well, and living promastigotes were allowed to attach in the dark for 30 min. Cells were subsequently washed three times with 50 μ l $1 \times$ PBS, topped with $1 \times$ PBS and covered with a cover slip without trapping air-bubbles. The attached cells were viewed immediately with a

Zeiss fluorescence microscope. Fluorescence images were captured by a *Hamamatsu* digital camera using the Openlab software v 5.0.1 (*Improvision*) and subsequently deconvolved by means of the Openlab Volume Deconvolution module.

3.7.3 Transmission electron microscopy

10 ml of a log-phase *Leishmania* culture were centrifuged at $2,050 \times g$ at 4°C for 10 min, and cells were washed twice with ice-cold $1 \times \text{PBS}$. The following steps were carried out by Christel Schmetz (Electron Microscopy facility, BNI, Hamburg). Cells were fixed in 2% (v/v) glutardialdehyde, and 0.1 M sodium cacodylate pH 7.2, post-fixed in 1% (w/v) OsO_4 and dehydrated with graded ethanol solutions and propylene oxide. After cells were embedded in an epoxy resin (Epon), 70 nm ultrathin sections were cut (Ultra Cut E, *Reichert/Leica*, NuBlock) and counter-stained with uranyl acetate and lead citrate. Sections were viewed with a *Philips* CM 10 transmission electron microscope at an acceleration voltage of 80 kV.

3.7.4 Flagellar length determination

Fixed log-phase promastigotes were attached to a poly-L-lysine-coated 10-well microscope slide as described in 3.7.1. Wells were washed twice with $50 \mu\text{l}$ $1 \times \text{PBS}$ before the cells were embedded in Mowiol/DABCO and covered with a cover slip without trapping air-bubbles. Cells were viewed with a *Zeiss* fluorescence microscope which was equipped with a *Hamamatsu* digital camera. Flagellar lengths were measured from the cell surface to the flagellar tip exactly tracing the flagellum by using the freehand tool of the Openlab software v 5.0.1 (*Improvision*).

4 Results

4.1 The phenotype of the *LmxMPK3* null mutants and the *LmxMPK3* add back mutants

An important approach for analysing the physiological function of a certain protein is to generate a null mutant of the respective gene in the organism of investigation and to subsequently analyse the obtained phenotype. In trypanosomatids this can be achieved by replacing the gene of interest with resistance marker genes by homologous recombination.

The *LmxMPK3* null mutants already existed prior to the beginning of this work. They had been obtained by sequentially replacing both alleles of *LmxMPK3* by different resistance marker genes in two consecutive rounds of electroporation. The selected clones $\Delta LmxMPK3$ -/-HN1 and $\Delta LmxMPK3$ -/-PN6 contain selective marker genes conferring hygromycin B and neomycin resistance, and phleomycin and neomycin resistance, respectively. Both clones had been verified by Southern blot analysis (Erdmann, diploma thesis, 2004).

4.1.1 Generation of the *LmxMPK3* add back mutants

In order to prove that the phenotype of the *LmxMPK3* null mutants is actually due to the lack of *LmxMPK3*, the protein was re-expressed in the deletion background by introducing an expression vector carrying *LmxMPK3*.

Generation of the transfection construct

The phleomycin resistance marker gene of the expression plasmid pX3ELmxMPK3 was removed by cleaving the vector with *XhoI* and *NsiI*. Instead, a puromycin resistance marker gene liberated from pX63polPAC with the same restriction enzymes was ligated into the vector generating the plasmid pX7PACLmxMPK3.

Transfection

pX7PACLmxMPK3 was transfected into the independently gained *LmxMPK3* null mutants $\Delta LmxMPK3$ -/-HN1 and $\Delta LmxMPK3$ -/-PN6. Positive clones were selected using puromycin.

For each of the *LmxMPK3* null mutants an add back mutant could be obtained and was designated $\Delta LmxMPK3$ -/-HN1ab and $\Delta LmxMPK3$ -/-PN6ab.

4.1.2 *LmxMPK3* expression levels of the *LmxMPK3* mutants

Immunoblot analysis of total cell lysates from logarithmically growing promastigotes of the different *LmxMPK3* mutants was carried out using an antiserum against *LmxMPK3*. Figure 13 shows the *LmxMPK3* protein levels in the wild type compared to two independent single-allele deletion mutants, the two null mutants and the two add back mutants of

LmxMPK3. The single-allele deletion mutants $\Delta LmxMPK3^{+/-}H3$ and $\Delta LmxMPK3^{+/-}P4$ had been used to generate the null mutants $\Delta LmxMPK3^{-/-}HN1$ and $\Delta LmxMPK3^{-/-}PN6$, respectively (Erdmann, diploma thesis, 2004).

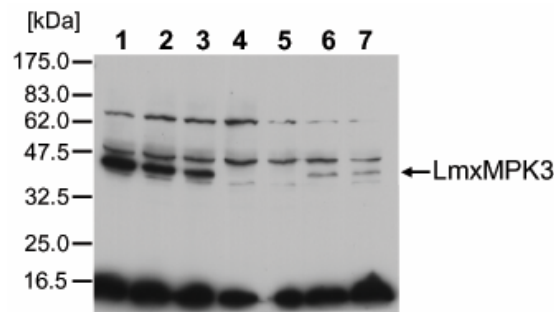


Figure 13: Immunoblot of LmxMPK3 from various *LmxMPK3* mutants

1: *LmxWT*; 2: $\Delta LmxMPK3^{+/-}H3$; 3: $\Delta LmxMPK3^{+/-}P4$; 4: $\Delta LmxMPK3^{-/-}HN1$; 5: $\Delta LmxMPK3^{-/-}PN6$; 6: $\Delta LmxMPK3^{-/-}HN1ab$; 7: $\Delta LmxMPK3^{-/-}PN6ab$.

Figure 13 states that *LmxMPK3* protein levels are slightly decreased in the single-allele deletion mutants compared to the wild type and that the protein could not be detected in the null mutants. Introduction of the gene on a plasmid into the deletion background indeed led to re-expression of the protein, however, at lower levels compared to the wild type and even to the single-allele deletion mutants.

4.1.3 Measurements of the flagellar lengths of the *LmxMPK3* mutants

Microscopic analysis already revealed that the *LmxMPK3* null mutants display flagella much shorter in length compared to the wild type (Erdmann, diploma thesis, 2004) and that the add back mutants reveal longer flagella again. To quantify those findings, the length of the flagella of *L. mexicana* wild type promastigotes, the null mutants $\Delta LmxMPK3^{-/-}HN1$ and $\Delta LmxMPK3^{-/-}PN6$, and the add back mutants $\Delta LmxMPK3^{-/-}HN1ab$ and $\Delta LmxMPK3^{-/-}PN6ab$ have been measured.

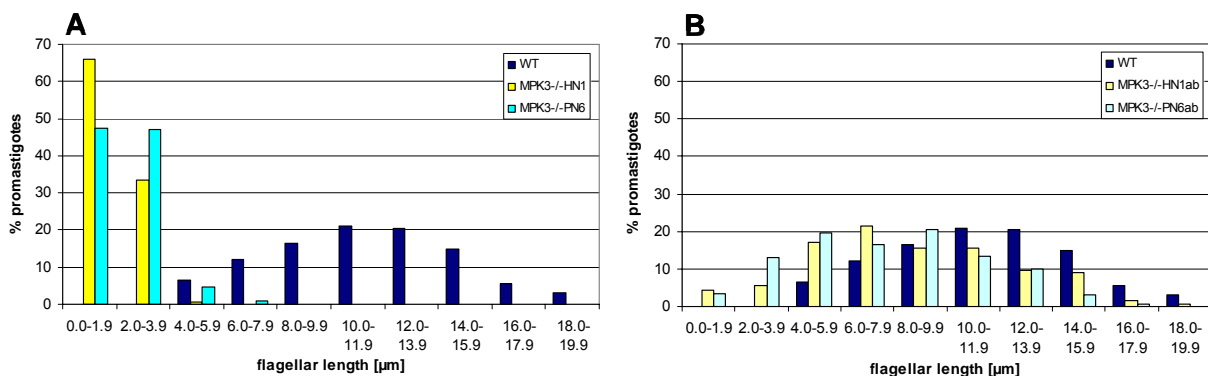


Figure 14: Histograms of flagellar lengths from *L. mexicana* wild type, *LmxMPK3* null mutants and *LmxMPK3* add back mutants

A: *LmxWT*, $\Delta LmxMPK3^{-/-}HN1$ and $\Delta LmxMPK3^{-/-}PN6$; B: *LmxWT*, $\Delta LmxMPK3^{-/-}HN1ab$ and $\Delta LmxMPK3^{-/-}PN6ab$.

	average flagellar length [μm]	standard deviation [μm]	minimum flagellar length [μm]	maximum flagellar length [μm]
WT	11.3	3.5	4.2	19.2
$\Delta\text{MPK3HN1}$	1.8	0.8	0.2	4.6
$\Delta\text{MPK3PN6}$	2.2	1.1	0.3	6.7
$\Delta\text{MPK3HN1ab}$	8.6	3.9	0.6	18.1
$\Delta\text{MPK3PN6ab}$	7.8	3.5	1.3	16.1

Table 2: Overview of average, minimum and maximum flagellar lengths from the different *LmxMPK3* mutants

Figure 14 illustrates the significant shift of flagellar lengths of the null mutants to lower values and the regeneration of wild type flagella by re-expressing *LmxMPK3* in the deletion background. Table 2 summarises the key values of the different measurements. In contrast to the wild type with an average flagellar length of 11.3 μm , the null mutants $\Delta\text{LmxMPK3-/-HN1}$ and $\Delta\text{LmxMPK3-/-PN6}$ showed mean values of only 1.8 and 2.2 μm , respectively. While the range of flagellar lengths from the wild type reached from 4.2 to 19.2 μm , *LmxMPK3-/-HN1* and $\Delta\text{LmxMPK3-/-PN6}$ displayed minimal lengths of only 0.2 and 0.3 μm and maximal lengths of 4.6 and 6.7 μm , respectively. Generally, *LmxMPK3-/-HN1* showed flagella slightly shorter than the flagella of $\Delta\text{LmxMPK3-/-PN6}$. Both add back mutants revealed a distribution of flagellar lengths fairly resembling that of the wild type. Minimal and maximal lengths were still slightly decreased and the mean values reached roughly 70-75% of the wild type value.

4.1.4 Analysis of the ultrastructure using transmission electron microscopy

Once discovered that *LmxMPK3* is involved in flagellar length regulation, it was of particular interest to analyse the ultrastructure of the *LmxMPK3* null mutants. This was achieved by using transmission electron microscopy on chemically fixed cells.

The wild type flagella showed the typical (9+2) pattern of microtubule doublets in the axoneme and the typical lattice-like structure of the paraflagellar rod (PFR) adjacent to the axoneme (Figure 15A). The flagella of the null mutants showed the same axoneme structure as the wild type, however, the assembly of the PFR seemed to be severely impaired. A broad variety in flagellar morphology could be observed. There were flagellar sections of the null mutants either showing no PFR (Figure 15D), a rudimentary PFR (Figure 15E), various amounts of undefined material around the axoneme (Figure 15F and I) or vesicles within the flagellum (Figure 15G and H). Again, the two null mutants differed from each other with $\Delta\text{LmxMPK3-/-HN1}$, the mutant with shorter flagella, displaying flagella significantly more affected (Table 3). In addition to the flagellar abnormalities, the flagellar pockets of the null mutants were often filled with membrane vesicles or fragments (Figure 15J-M). The vesicles consisted either of single, double or even multiple membrane layers and had probably been formed by budding from the flagellar pocket membrane (Figure 15K and L).

Most of the flagellar sections of the add back mutants revealed a normal architecture of the flagellum with a correctly assembled PFR, again showing that re-expression of *LmxMPK3* is indeed able to complement the null mutant phenotype. In these cells only a very small number of flagella contained a rudimentary PFR, no PFR, undefined material around the axoneme or vesicles (Table 3).

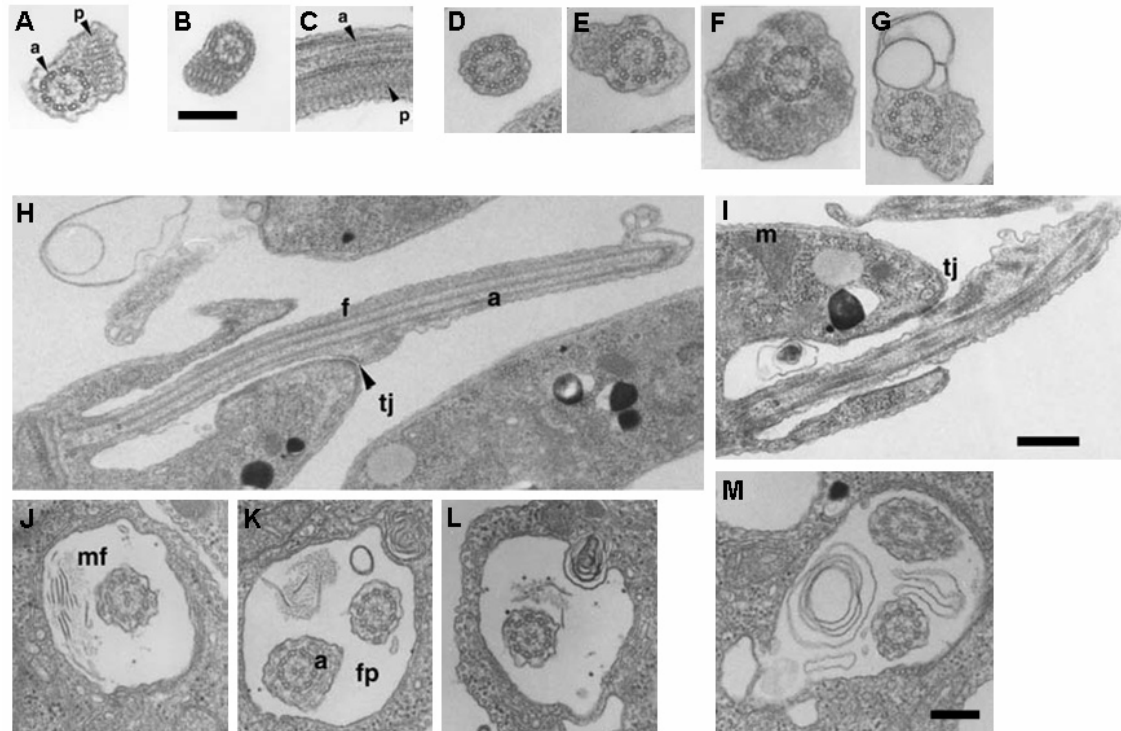


Figure 15: Transmission electron micrographs of *L. mexicana* wild type, *LmxMPK3* null mutants and *LmxMPK3* add back mutants

A: Cross section of *LmxWT* flagellum; B and C: Cross and longitudinal section of *LmxMPK3* add back mutant flagellum, respectively; D-G: Cross sections of *LmxMPK3* null mutant flagellum; H and I: Longitudinal sections of *LmxMPK3* null mutant flagellar pocket and flagellum; J-M: Cross sections of *LmxMPK3* null mutant flagellar pocket and flagellum.

a, axoneme; f, flagellum; fp, flagellar pocket; m, mitochondrion; mf, membrane fragments, tj, tight junction.

Bars, 0.25 μm (A-G and J-M), 0.5 μm (H and I).

	normal PFR	rudim. PFR	no PFR	undef. material	vesicles
$\Delta\text{MPK3HN1}$	0.0%	8.5%	29.0%	15.0%	32.0%
$\Delta\text{MPK3PN6}$	0.0%	41.0%	34.0%	7.5%	10.0%
ΔMPK3ab	70.5%	15.0%	7.5%	1.0%	6.0%

Table 3: Overview of flagellar architecture from *LmxMPK3* null mutants and *LmxMPK3* add back mutant

Interestingly, the axoneme of the add back mutant seemed to be more condensed when analysing the flagellar cross sections. Actually, its diameter is reduced to only 160 nm compared to the wild type axoneme being 180 nm in diameter. In fact, the null mutants showed the most relaxed structure with a diameter of 210 nm.

4.1.5 Quantification of PFR-2 in the *LmxMPK3* null mutants

After transmission electron microscopy had revealed that the flagella of the *LmxMPK3* null mutants contain either only residual or no PFR, it was interesting to quantify the amount of a PFR-specific protein. PFR-2 is one of the two main protein subunits of the PFR for which a monoclonal antibody against its *T. brucei* homologue PFR-A (L8C4) was available.

4.1.5.1 Immunofluorescence analysis

To determine the subcellular localisation of PFR-2 in the *LmxMPK3* null mutants in comparison to the wild type, immunofluorescence analysis was performed on fixed logarithmically growing promastigotes using the L8C4 monoclonal antibody and an Alexa Fluor 488-conjugated secondary antibody.

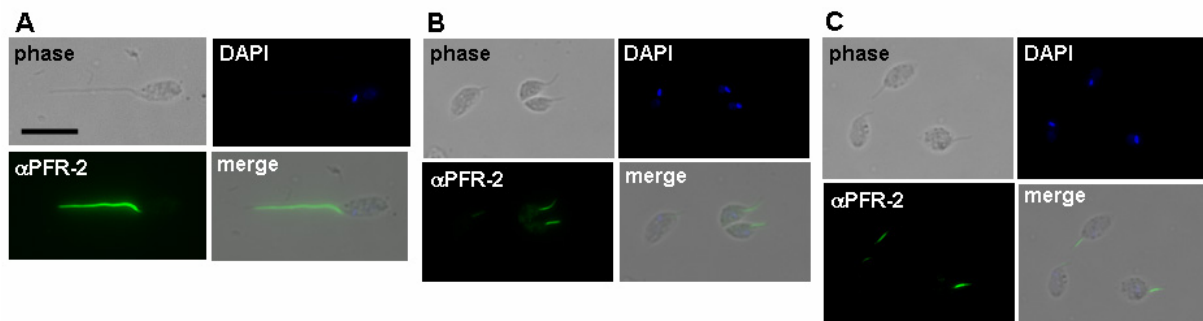


Figure 16: Immunofluorescence of PFR-2 from *L. mexicana* wild type and *LmxMPK3* null mutants

A: *LmxWT*; B: $\Delta LmxMPK3-I-HN1$; C: $\Delta LmxMPK3-I-PN6$.

Bar, 10 μ m.

	strong fluorescence	weak fluorescence	no fluorescence
WT	100%	0%	0%
$\Delta MPK3HN1$	50%	35%	15%
$\Delta MPK3PN6$	40%	45%	15%

Table 4: Fluorescence intensities in immunofluorescence analysis of PFR-2

While all flagella of the *L. mexicana* wild type showed a strong reaction with L8C4, only 50% and 40% of the flagella from $\Delta LmxMPK3-I-HN1$ and $\Delta LmxMPK3-I-PN6$ revealed a reaction of comparable intensity, respectively. The remaining flagella showed either a weak or no fluorescence (Figure 16 and Table 4). Whenever present, the antibody reaction was restricted to the flagellum in both null mutants and wild type, indicating that free or incorrectly assembled PFR subunits are also located in the flagellum.

4.1.5.2 Immunoblot analysis

In order to quantify the PFR-2 protein amounts of the *LmxMPK3* null mutants in comparison to the *L. mexicana* wild type, an immunoblot analysis was performed using L8C4 on total cell lysates from the null mutants and different numbers of wild type promastigotes.

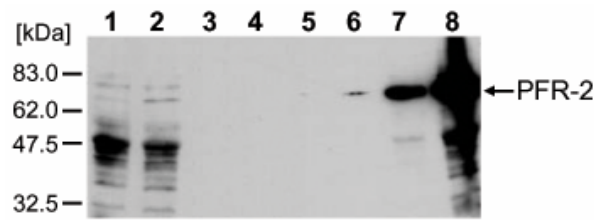


Figure 17: Immunoblot of PFR-2 from *LmxMPK3* null mutants and *L. mexicana* wild type

1: $\Delta LmxMPK3$ -I-HN1 (2×10^7 promastigotes); 2: $\Delta LmxMPK3$ -I-PN6 (2×10^7 promastigotes); 3-8: LmxWT promastigotes (3: 5×10^4 ; 4: 1×10^5 ; 5: 5×10^5 ; 6: 1×10^6 ; 7: 5×10^6 ; 8: 2×10^7).

In Figure 17 the intensity of the band corresponding to PFR-2 (68.7 kDa) in lanes 1 and 2 is approximately the same as in lane 6, suggesting that the null mutants contain roughly 20 times less PFR-2 than the wild type. A mere reduction of the flagellar length would only lead to 5 times less PFR-2, indicating that the flagellum of the null mutant contains on average roughly 4 times less PFR-2 per micrometer length than the wild type.

4.1.6 Mouse infection studies with the *LmxMPK3* mutants

To find out, whether *LmxMPK3* is important for the infectivity of *L. mexicana*, mouse infection studies have been carried out with the different *LmxMPK3* mutants. Promastigotes of the *L. mexicana* wild type, the *LmxMPK3* single-allele and null mutants as well as the add back mutants were injected into the left hind foot pad of five female BALB/c mice each. The infected foot pad was measured every four weeks in comparison to the non-infected one.

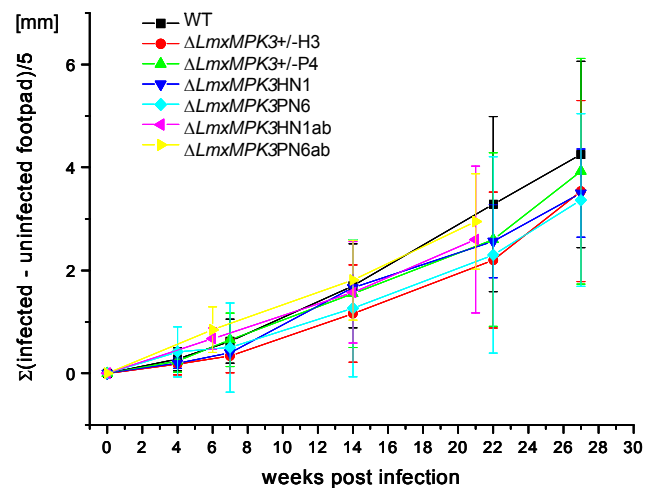


Figure 18: Foot pad swelling caused by *L. mexicana* wild type, *LmxMPK3* single-allele mutants, null mutants and add back mutants

Figure 18 shows that there was no significant difference in lesion development between the different *LmxMPK3* mutants and the wild type, concluding that *LmxMPK3* is neither required for the differentiation from promastigotes to amastigotes nor for the proliferation of the amastigotes.

4.2 The expression profile of LmxMPK3 during differentiation of *L. mexicana*

As described before, the phenotype of the *LmxMPK3* null mutant clearly points out that LmxMPK3 is involved in flagellar length regulation (Erdmann, diploma thesis, 2004). As flagellar length is affected during the differentiation from promastigotes to amastigotes and vice versa, I analysed the LmxMPK3 expression profile during differentiation of *L. mexicana*, in which the parasite and especially its flagellum undergoes profound morphological changes.

For amastigote-to-promastigote differentiation amastigotes of the *L. mexicana* wild type were isolated from the lesions of infected BALB/c mice and grown in promastigote growth medium at 27°C. Differentiation to axenic amastigotes was achieved by inoculating Schneider's *Drosophila* medium with stationary phase *L. mexicana* wild type promastigotes and incubation at 34°C with 5% CO₂. Cell samples were collected at defined intervals after initiation of differentiation and used for immunoblot analysis with an antiserum against LmxMPK3 and for DIC microscopy.

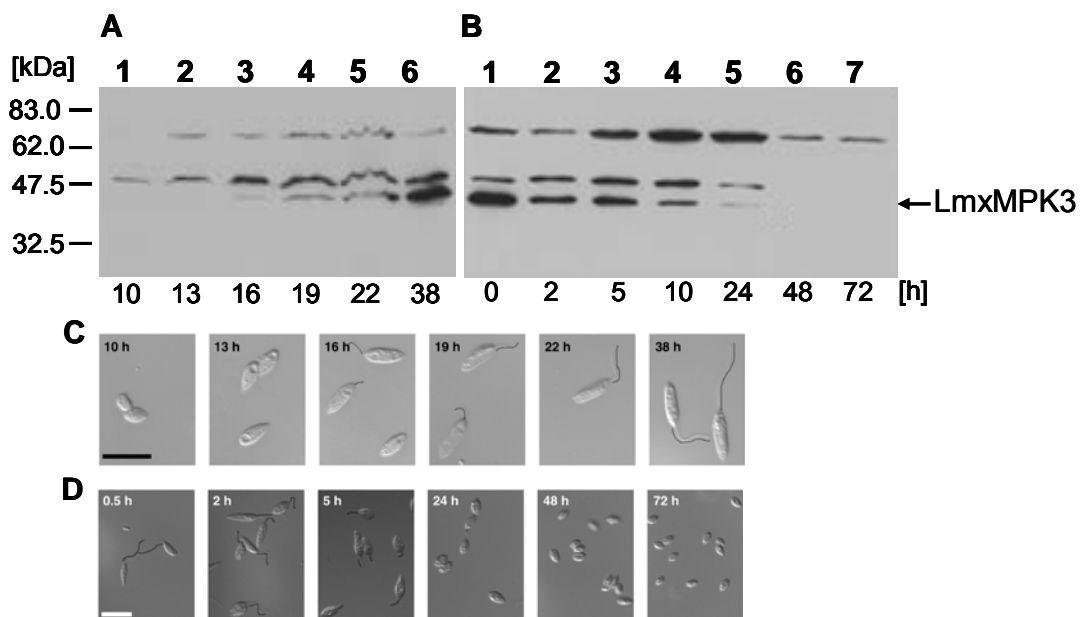


Figure 19: Immunoblots of LmxMPK3 and DIC micrographs from *L. mexicana* wild type during differentiation

A: Immunoblot of LmxMPK3 from wild type differentiating from amastigotes to promastigotes; B: Immunoblot of LmxMPK3 from wild type differentiating from promastigotes to axenic amastigotes; C: DIC micrographs of wild type differentiating to promastigotes; D: DIC micrographs of wild type differentiating to axenic amastigotes.

Hours after differentiation are indicated. For better visualization of flagella, lines were drawn along them. Bar, 10 µm.

Figure 19 shows that LmxMPK3 is detectable 16 h after initiation of differentiation to promastigotes and that LmxMPK3 protein amounts increase gradually thereafter (Figure 19A). At 16 h some of the cells displayed already a short flagellum and at 19 h most of the cells did. The typical flagellar length of wild type promastigotes was reached after 38 h

(Figure 19C). When differentiating wild type promastigotes to axenic amastigotes, the LmxMPK3 protein amounts gradually declined until being not detectable any more at 48 h after initiation of differentiation (Figure 19B). During the same time all of the cells had completely lost their flagella (Figure 19D). In summary, flagella could never be observed when LmxMPK3 was not present in the cells. As for the amastigote-to-promastigote differentiation, LmxMPK3 protein expression and the outgrowth of flagella seem to occur at the same time. Interestingly, during differentiation to axenic amastigotes the flagella seem to disappear shortly before LmxMPK3 is totally absent.

4.3 Generation and characterisation of a GFP-LmxMPK3 and a GFP-LmxMKK mutant

When studying the function of a protein, determining its subcellular localisation can give valuable hints. Both, LmxMPK3 and LmxMKK, are involved in flagellar length regulation of *L. mexicana* (Wiese *et al.*, 2003a; Erdmann, diploma thesis, 2004; Erdmann *et al.*, 2006). However, for neither of the kinases the actual function within this complex process is known. Therefore, GFP-LmxMPK3 and GFP-LmxMKK mutants were generated by introducing a copy of the *egfp*-linked kinase gene into the respective deletion mutant. The obtained GFP-LmxMPK3 mutants contain an expression vector with *egfp* linked either to the 5'- or the 3'-end of the kinase gene. The GFP-LmxMKK mutants were generated by introducing a cassette carrying *LmxMKK* linked to *egfp* at its 3'-end into the 18S rRNA locus. Subsequent analysis of the GFP mutants using fluorescence microscopy should reveal the subcellular localisation of the kinases.

4.3.1 Preparation of the different transfection constructs

In order to generate the GFP-LmxMPK3 mutants, the ORF of *LmxMPK3* was amplified from pB5upLmxMPK3ds, introducing an *MfeI* and an *HpaI* restriction site to the 5'- and the 3'-end, respectively. A PCR was performed on the plasmid using the oligonucleotides LmxMPK3GFP-Nterm and LmxMPK3GFP-Cterm. After the amplified fragment had been ligated into pCR2.1-TOPO and sequenced, it was released using *MfeI* and *HpaI* and cloned into the expression vectors pTH₆cGFPn and pTH₆nGFPc which had been linearised using the same restriction enzymes. The obtained plasmids were designated pTH1GFPLmxMPK3 and pTH1LmxMPK3GFP, respectively.

The plasmid pSSU-int-lmmkkegfp-c1-lmcpbds-pac (Wiese *et al.*, unpublished) which contains the cassette for generation of the GFP-LmxMKK mutants already existed before commencing this work and is a derivative of pSSU-int-lmmkk-lmcpbds-pac (Wiese *et al.*, 2003a). The cassette, containing *LmxMKK-egfp*, the *CPB2.8* gene intergenic region from

L. mexicana and a puromycin resistance gene, was liberated from pSSU-int-Immkkkegfp-c1-lmcpbds-pac using *PacI* and *PmeI*.

4.3.2 Transfection and verification of obtained clones

The plasmids pTH1GFPLmxMPK3 and pTH1LmxMPK3GFP were individually transfected into the null mutant $\Delta LmxMPK3$ -/-PN6. Positive clones were selected using hygromycin B. The clones bearing LmxMPK3 N-terminally linked with GFP were designated $\Delta LmxMPK3$ -/-PN6+GFP-LmxMPK3 K9, 12 and 13. The clones with LmxMPK3 C-terminally linked with GFP were named $\Delta LmxMPK3$ -/-PN6+LmxMPK3-GFP K3, 4 and 6.

In order to generate the GFP-LmxMKK mutants, the *PacI/PmeI* fragment derived from pSSU-int-Immkkkegfp-c1-lmcpbds-pac was transfected into the null mutants $\Delta LmxMKK$ -/-K3 and $\Delta LmxMKK$ -/-K4 (Wiese *et al.*, 2003a). Positive clones were selected using puromycin and were named $\Delta LmxMKK$ -/-K3+LmxMKK-GFP K1, 2, 3, 4, 5 and $\Delta LmxMKK$ -/-K4+LmxMKK-GFP K1, 2, 3, 4 and 5.

To check whether the obtained clones express the respective GFP-fusion protein, immunoblot analysis of total cell lysates from logarithmically growing promastigotes of the different GFP-LmxMPK3 and GFP-LmxMKK mutants was performed. The blots were probed with antisera against LmxMPK3, LmxMKK and GFP.

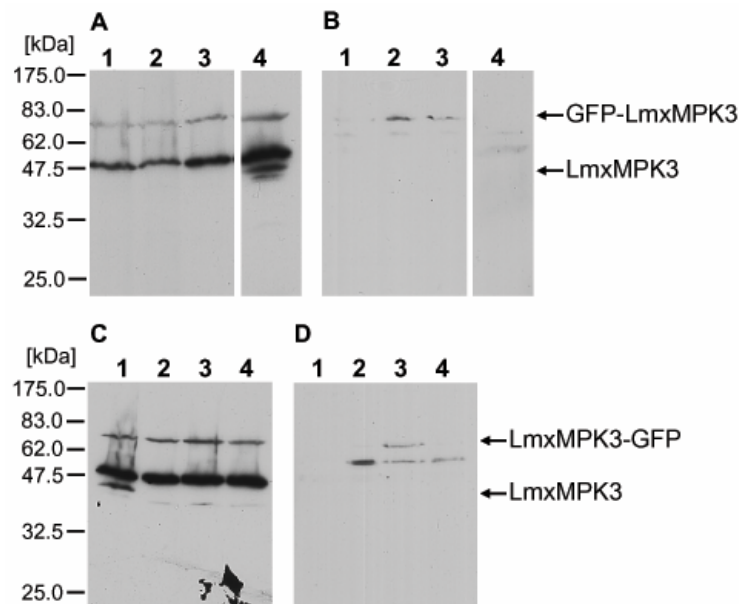


Figure 20: Immunoblots of LmxMPK3 and GFP from GFP-LmxMPK3 mutants

A and C: probed with anti-LmxMPK3 antiserum; B and D: probed with anti-GFP antiserum.

A and B: 1: $\Delta LmxMPK3$ -/-PN6+GFP-LmxMPK3 K9; 2: $\Delta LmxMPK3$ -/-PN6+GFP-LmxMPK3 K12; 3: $\Delta LmxMPK3$ -/-PN6+GFP-LmxMPK3 K13; 4: LmxWT.

C and D: 1: LmxWT; 2: $\Delta LmxMPK3$ -/-PN6+LmxMPK3-GFP K3; 3: $\Delta LmxMPK3$ -/-PN6+LmxMPK3-GFP K4; 4: $\Delta LmxMPK3$ -/-PN6+LmxMPK3-GFP K6.

The calculated molecular weight of the fusion protein for the GFP-LmxMPK3 mutants is 72.1 kDa. Unfortunately, one of the typical cross reaction bands of the anti-LmxMPK3 antiserum locates at the same position when used on *Leishmania* lysates. To clarify whether the fusion proteins were expressed, the blots were also probed with an anti-GFP antiserum (Figure 20B and D), which only produces a weak cross reaction band at a lower molecular mass and which therefore was also visible in the wild type sample (Figure 20B, lane 4). After long times of exposure a weak band of the expected molecular mass could be observed for Δ LmxMPK3/-PN6+GFP-LmxMPK3 K9, 12 and 13 and Δ LmxMPK3/-PN6+LmxMPK3-GFP K4 (Figure 20B, lanes 1, 2 and 3, and D, lane 3). For the remaining clones an expression of the fusion protein could not be verified. In 4.3.4, however, a strong GFP fluorescence is described for Δ LmxMPK3/-PN6+LmxMPK3-GFP K3 which cannot derive from GFP alone, since it could not be detected by immunoblot analysis. Additionally, all of the GFP-LmxMPK3 mutants reveal long flagella again (see 4.3.3). It is therefore very likely that the fusion protein is correctly expressed in all the different mutants, even though at very low level.

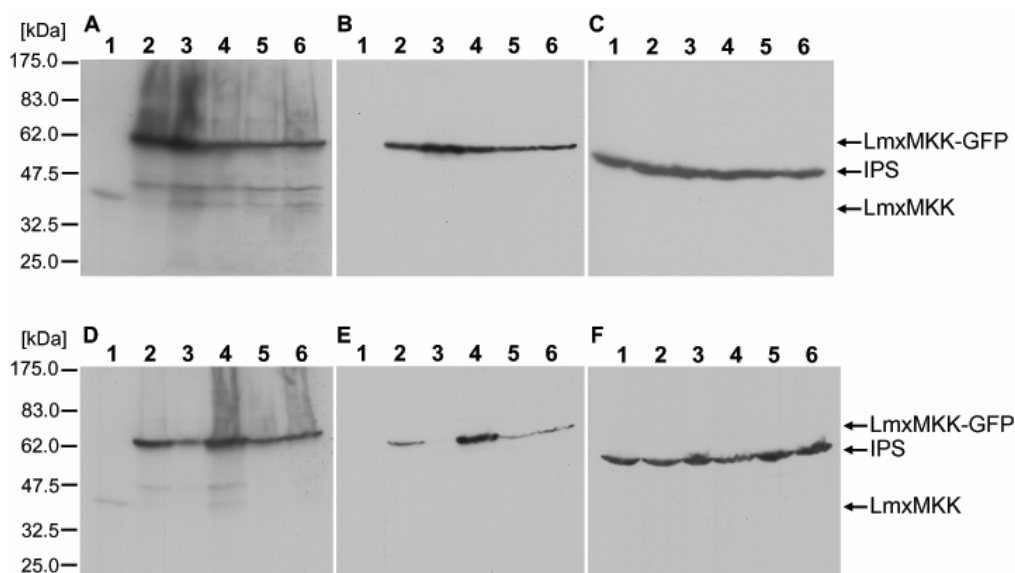


Figure 21: Immunoblots of LmxMCK and GFP from GFP-LmxMCK mutants

A and D: probed with anti-LmxMCK antiserum; B and E: probed with anti-GFP antiserum; C and F: probed with anti-IPS antiserum.

A-C: 1: LmxWT; 2: Δ LmxMCK/-K3+LmxMCK-GFP K1; 3: Δ LmxMCK/-K3+LmxMCK-GFP K2; 4: Δ LmxMCK/-K3+LmxMCK-GFP K3; 5: Δ LmxMCK/-K3+LmxMCK-GFP K4; 6: Δ LmxMCK/-K3+LmxMCK-GFP K5.

D-F: 1: LmxWT; 2: Δ LmxMCK/-K4+LmxMCK-GFP K1; 3: Δ LmxMCK/-K4+LmxMCK-GFP K2; 4: Δ LmxMCK/-K4+LmxMCK-GFP K5; 5: Δ LmxMCK/-K4+LmxMCK-GFP K4; 6: Δ LmxMCK/-K4+LmxMCK-GFP K3.

The calculated molecular weight of LmxMCK-GFP is approximately 70 kDa. Figure 21A, B, D and E, presenting the blots probed with antisera against LmxMCK and GFP, clearly show that the fusion protein is expressed in all the GFP-LmxMCK mutants. For Δ LmxMCK/-K4+LmxMCK-GFP K2, the according band was very weak in Figure 21E, lane 3, but could be

visualised clearly in Figure 21D, lane 3. The blots probed with an antiserum against *myo*-inositol-1-phosphate synthase served as loading controls (Figure 21C and F).

4.3.3 Measurements of the flagellar lengths of the GFP-LmxMPK3 and GFP-LmxMKK mutants

In order to use the generated GFP mutants for localisation studies, it was not solely important that the obtained clones express the fusion protein, but also that the kinase linked to GFP is still functional. For both kinases, LmxMPK3 and LmxMKK, this is indicated by the formation of wild type flagella in promastigotes. Each of the gained GFP-LmxMPK3 and GFP-LmxMKK mutants could restore long flagella, showing that the respective kinase was still functional. Measurements of flagellar lengths were exemplary carried out for some of the GFP mutants and were depicted in Figure 22.

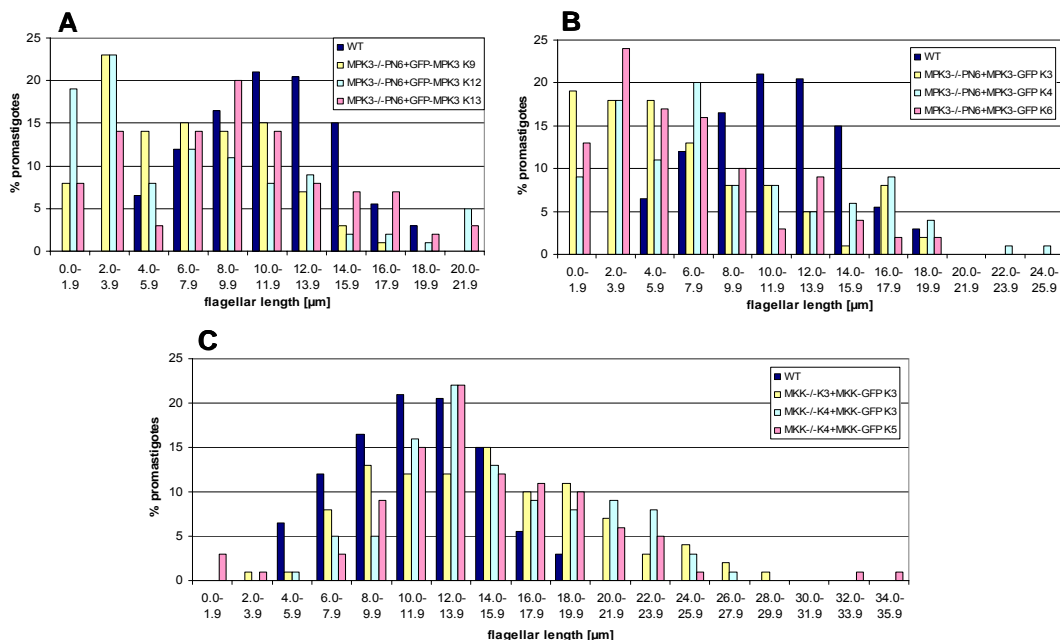


Figure 22: Histograms of flagellar lengths from *L. mexicana* wild type, GFP-LmxMPK3 and GFP-LmxMKK mutants

A: LmxWT, Δ LmxMPK3/-PN6+GFP-LmxMPK3 K9, 12 and 13; B: LmxWT, Δ LmxMPK3/-PN6+LmxMPK3-GFP K3, 4 and 6; C: LmxWT, Δ LmxMKK/-K3+LmxMKK-GFP K3, Δ LmxMKK/-K4+LmxMKK-GFP K3 and 5.

	average flagellar length [μm]	standard deviation [μm]
Δ MPK3PN6+GFP-MPK3 K9	6.9	3.9
Δ MPK3PN6+GFP-MPK3 K12	7.1	5.5
Δ MPK3PN6+GFP-MPK3 K13	9.3	5.1
Δ MPK3PN6+MPK3-GFP K3	6.8	5.0
Δ MPK3PN6+MPK3-GFP K4	8.5	5.7
Δ MPK3PN6+MPK3-GFP K6	6.6	4.6
Δ MKKK3+MKK-GFP K3	14.8	5.4
Δ MKKK4+MKK-GFP K3	15.1	4.9
Δ MKKK4+MKK-GFP K5	14.6	5.6

Table 5: Overview of average flagellar lengths from GFP-LmxMPK3 and GFP-LmxMKK mutants

As Figure 22 and Table 5 show, both the GFP-LmxMPK3 and the GFP-LmxMKK mutants clearly revealed flagella much longer than in the respective null mutants which had been used for generating the GFP mutants. As for the GFP-LmxMPK3 mutants, the average flagellar length was 6.6 to 9.3 μm , resembling that of the *LmxMPK3* add back mutants. However, the lengths of most flagella were shifted to lower values, though a small percentage of flagella reached up to 24.6 μm in length. There was no significant difference between the clones bearing GFP linked N- or C-terminally to LmxMPK3.

The GFP-LmxMKK mutants displayed much longer flagella compared to the GFP-LmxMPK3 mutants and even to the wild type, reflecting the results of the immunoblot analysis in 4.3.2. The average flagellar lengths ranged from 14.6 to 15.1 μm . When looking at the overall distribution of flagellar lengths compared to the wild type, the lengths of most flagella were shifted to higher values, even reaching up to 35.3 μm in the case of $\Delta LmxMKK$ -/-K4+LmxMKK-GFP K5.

4.3.4 Localisation studies of LmxMPK3 and LmxMKK using fluorescence microscopy on living cells

In order to use the different GFP-LmxMPK3 and GFP-LmxMKK mutants for fluorescence microscopy, living log-phase promastigotes were stained with Hoechst DNA stain in a 1:500 dilution, attached to a poly-L-lysine-coated 10-well microscope slide and viewed immediately with a Zeiss fluorescence microscope. Fluorescence images were captured by a Hamamatsu digital camera using the Openlab software v 5.0.1 (*Improvision*) and subsequently deconvolved by means of the Openlab Volume Deconvolution module.

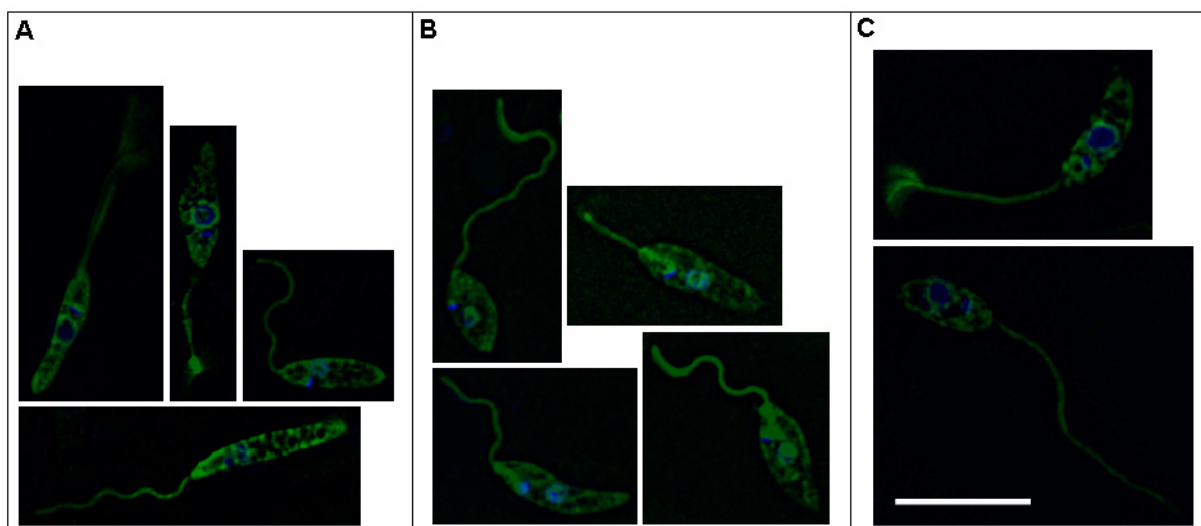


Figure 23: Deconvolved fluorescence micrographs of GFP-LmxMPK3 and GFP-LmxMKK mutants

A: $\Delta LmxMPK3$ -/-PN6+GFP-LmxMPK3 K13; B: $\Delta LmxMPK3$ -/-PN6+LmxMPK3-GFP K3; C: $\Delta LmxMKK$ -/-K3+LmxMKK-GFP K3.

Bar, 10 μm .

Figure 23 shows that the subcellular localisation of GFP-LmxMPK3 and GFP-LmxMKK looked very similar. Again, the results for the GFP-LmxMPK3 mutants did not depend on whether GFP was attached to the N- or C-terminus of the kinase. Both GFP-LmxMPK3 and GFP-LmxMKK seem to be distributed in the cytosol, but are clearly more concentrated around the nucleus, within the flagellum and at its base.

4.3.5 Determining the correlation between LmxMPK3 amount and flagellar length using fluorescence-activated cell sorting

In addition to the performed localisation studies on the GFP-LmxMPK3 mutants, it was also interesting to find out, if the fluorescence intensity of a single cell provides information about the protein amount of GFP-LmxMPK3 within this particular cell. If this was the case, the effect of the cellular LmxMPK3 amount on the flagellar length could be assessed.

First, the correlation between the fluorescence intensity and the GFP-LmxMPK3 protein amount was analysed using fluorescence-activated cell sorting (FACS) of $\Delta LmxMPK3$ -PN6+GFP-LmxMPK3 K13. Living log-phase promastigotes were separated into subpopulations (gate 5, 6 and 7) with different fluorescence intensities and subjected to immunoblot analysis using antisera against LmxMPK3 and GFP. Additionally, living cells of the different subpopulations were stained with Hoechst as described in 4.3.4 and viewed on a fluorescence microscope. Some of the cells were also fixed in order to carry out measurements of their flagella.

The splitting of $\Delta LmxMPK3$ -PN6+GFP-LmxMPK3 K13 into subpopulations with different fluorescence intensities via FACS was successful as the re-analysis of the sorted cells shows (Figure 24B-D), though the fluorescence intensities were shifted to lower values than defined by the gates in all three subpopulations.

Indeed, a strong correlation between the fluorescence intensity and the protein amount of GFP-LmxMPK3 could be figured out as depicted in Figure 24E and F. While the expected band at 72.1 kDa was very weak in the sample of the non-sorted cells (Figure 24F, lane 1), a strong enrichment of cells bearing higher GFP-LmxMPK3 protein amounts could be detected in lane 4 showing the cells of gate 7 with the highest fluorescence intensities. The cell samples of gates 5 and 6 with low and medium fluorescence intensities revealed no band and just a very weak band of the expected molecular mass, respectively. Altogether, the GFP-LmxMPK3 protein amount increased with the fluorescence intensity of the cells.

Once subpopulations of cells with different GFP-LmxMPK3 amounts had been obtained, their flagella should be analysed. The fluorescence micrographs in Figure 24G-I show that the flagellar lengths (besides the fluorescence intensities) increase from gate 5 to 7. This is also clearly pointed out by the histograms of the measured flagellar lengths (Figure 24J and K).

Thus, it can be concluded that the length of the flagellum depends on the amount of LmxMPK3 protein within the cell in a correlative manner.

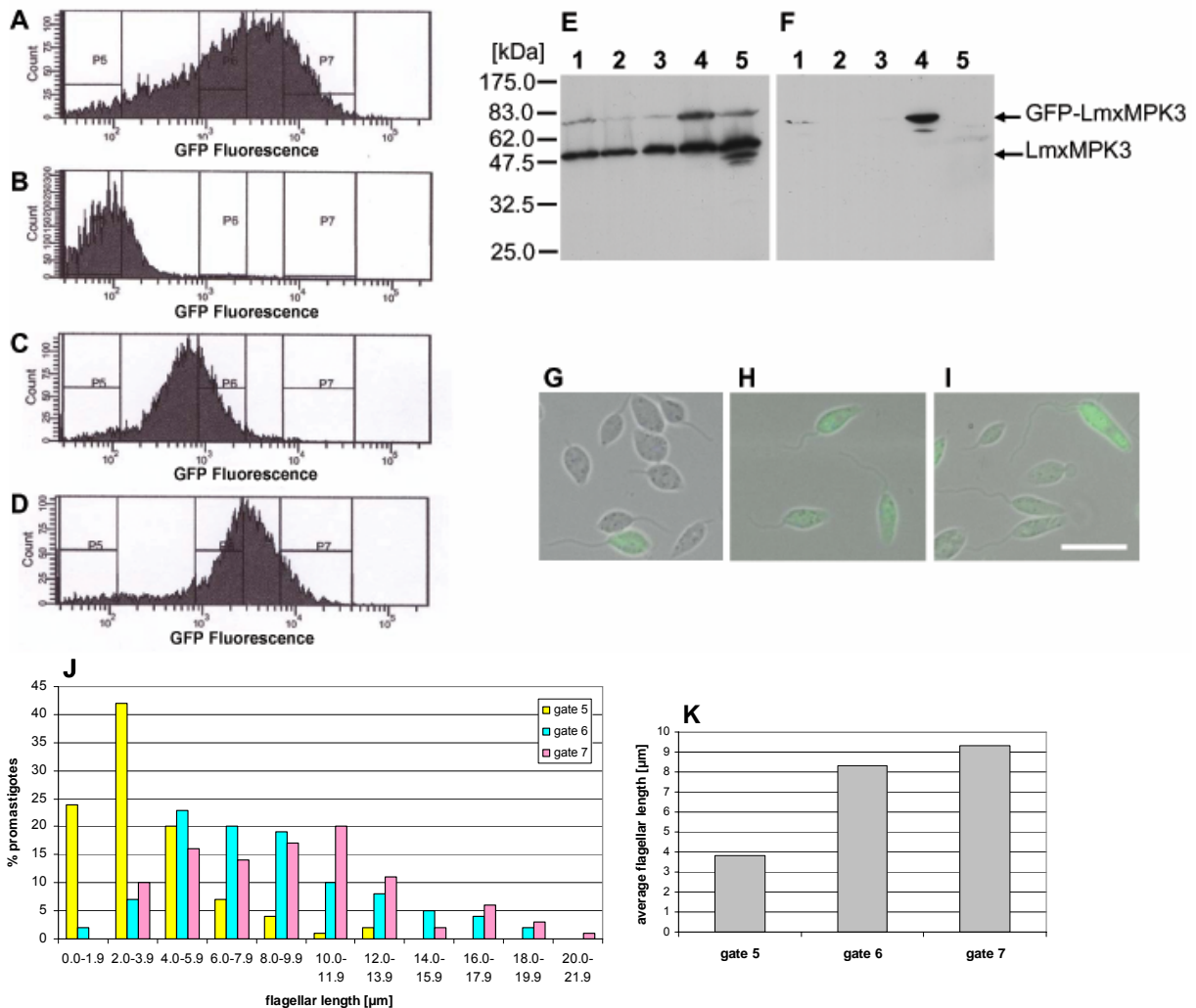


Figure 24: Correlation between fluorescence intensity, GFP-LmxMPK3 amount and flagellar length in $\Delta LmxMPK3/-PN6+GFP-LmxMPK3$ K13

A-D: Histograms of fluorescence intensities from sorted and non-sorted cells; A: non-sorted; B: gate 5; C: gate 6; D: gate 7.

E and F: Immunoblots of LmxMPK3 and GFP from sorted and non-sorted cells; E: probed with anti-LmxMPK3 antiserum; F: probed with anti-GFP antiserum; 1: non-sorted; 2: gate 5; 3: gate 6; 4: gate 7; 5: LmxWT.

G-I: Fluorescence micrographs from sorted cells; G: gate 5; H: gate 6; I: gate 7. Bar, 10 μ m.

J and K: Histograms of flagellar lengths from sorted cells; J: distribution of flagellar lengths; K: average flagellar lengths.

4.4 Generation and characterisation of an inhibitor-sensitised LmxMPK3 mutant

In 4.1 the characterisation of the *LmxMPK3* null mutants was described and served as a successful approach for analysing the function of the kinase, namely its role in flagellar length regulation. However, in order to study immediate and transient effects caused by the lack of a certain protein, an inducible system is necessary. Another advantage over gene

deletion mutants is that compensation mechanisms do not occur during the short time intervals used for inducible systems. While in trypanosomes RNA interference (RNAi) is successfully applied for induced gene-silencing, this method cannot be used in most *Leishmania* species due to the lack of some required cellular components (Robinson and Beverley, 2003).

However, Bishop *et al.* described in 2001 that a functionally silent active-site mutation can sensitise a kinase to a synthetic inhibitor which does not inhibit wild type kinases. According to this work, the so-called “gate keeper” amino acid residue (threonine 116) located in the active site of LmxMPK3 was replaced by glycine to create a small pocket in the ATP-binding site. In order to generate an inhibitor-sensitised *LmxMPK3* mutant of *L. mexicana*, a copy of the inhibitor-sensitised kinase, designated *LmxMPK3IS*, was introduced into the *LmxMPK3* null mutants on a plasmid for expression. A functioning inhibitor-sensitised system should reveal the wild type phenotype and allow a specific inhibition of only *LmxMPK3IS* by adding the appropriate inhibitor to the cells. The cellular changes triggered by the inactivation of *LmxMPK3* have subsequently been analysed.

4.4.1 Preparation of the transfection construct

Two independent PCRs were carried out on pCR2.1-23MPK3 using the oligonucleotides mpk3n.for and LmxMPK3i.rev in one reaction and LmxMPK3i.for and mpk3c.rev in the other reaction. After gel purification the amplified fragments were used as overlapping templates in a third PCR with mpk3n.for and mpk3c.rev. The product was ligated into pCR2.1-TOPO, sequenced and cleaved using *NruI* and *NdeI*. The released fragment carrying the T116→G-mutation was ligated into pX7PACLmxMPK3 which had been linearised using the same restriction enzymes. The generated plasmid was sequenced and designated pX13PACLmxMPK3IS.

4.4.2 Transfection and verification of obtained clones

pX13PACLmxMPK3IS was transfected into the *LmxMPK3* null mutants $\Delta LmxMPK3$ -/-HN1 and $\Delta LmxMPK3$ -/-PN6. Positive clones were selected using puromycin and named $\Delta LmxMPK3$ -/-HN1+LmxMPK3IS K1 and 2 and $\Delta LmxMPK3$ -/-PN6+LmxMPK3IS K1 and 3. The concentration of puromycin was subsequently raised from the standard concentration of 40 mM to 80 mM to increase the *LmxMPK3IS* expression levels. In order to verify the expression of *LmxMPK3IS*, immunoblot analysis of total cell lysates from log-phase promastigotes was performed using an antiserum against *LmxMPK3*.

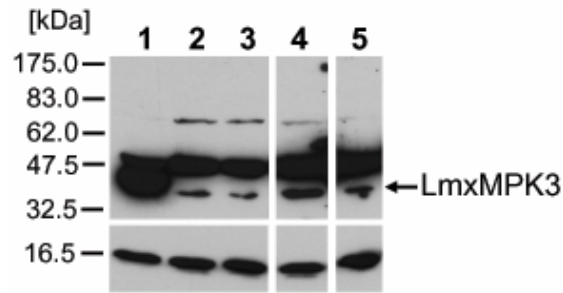


Figure 25: Immunoblot of LmxMPK3 from inhibitor-sensitised *LmxMPK3* mutants

1: *LmxWT*; 2: $\Delta LmxMPK3$ -HN1+*LmxMPK3IS* K1; 3: $\Delta LmxMPK3$ -HN1+*LmxMPK3IS* K2; 4: $\Delta LmxMPK3$ -PN6+*LmxMPK3IS* K1; 5: $\Delta LmxMPK3$ -PN6+*LmxMPK3IS* K3.

After long times of exposure a weak band of the expected molecular mass of *LmxMPK3* could be observed in the samples of the inhibitor-sensitised *LmxMPK3* mutants (Figure 25, lanes 2-5). Thus, each of the obtained clones expressed *LmxMPK3IS*, however, at very low levels compared to the wild type.

4.4.3 Measurements of the flagellar lengths of the inhibitor-sensitised *LmxMPK3* mutants

Before testing the inhibitor on the inhibitor-sensitised *LmxMPK3* mutants, it was important to secure that the expressed *LmxMPK3IS* is functional. This should be indicated by the formation of wild type flagella in the obtained mutants. Thus, measurements of flagellar lengths were carried out and displayed in Figure 26.

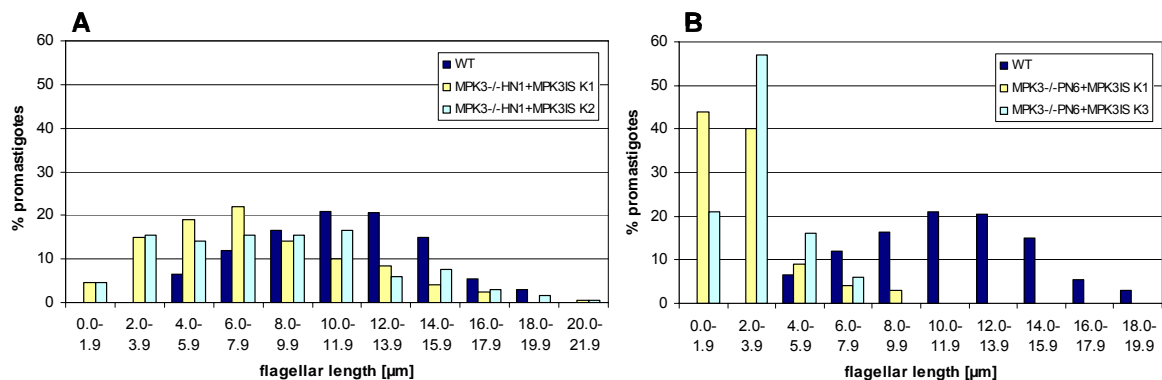


Figure 26: Histograms of flagellar lengths from *L. mexicana* wild type and inhibitor-sensitised *LmxMPK3* mutants

A: *LmxWT*, $\Delta LmxMPK3$ -HN1+*LmxMPK3IS* K1 and 2; B: *LmxWT*, $\Delta LmxMPK3$ -PN6+*LmxMPK3IS* K1 and 3.

	average flagellar length [µm]	standard deviation [µm]
$\Delta MPK3HN1+MPK3IS$ K1	7.7	4.0
$\Delta MPK3HN1+MPK3IS$ K2	8.3	4.3
$\Delta MPK3PN6+MPK3IS$ K1	2.7	1.8
$\Delta MPK3PN6+MPK3IS$ K3	3.3	1.6

Table 6: Overview of average flagellar lengths from inhibitor-sensitised *LmxMPK3* mutants

Figure 26 and Table 6 clearly reveal that the inhibitor-sensitised *LmxMPK3* mutants derived from $\Delta LmxMPK3$ -/-HN1 and $\Delta LmxMPK3$ -/-PN6 strongly differed from each other. The clones derived from $\Delta LmxMPK3$ -/-HN1 showed flagella resembling those of the *LmxMPK3* add back mutants, but with maximal lengths actually exceeding those of the wild type. In contrast, the clones which originated from $\Delta LmxMPK3$ -/-PN6 hardly differed from the null mutant, showing merely a slight shift of flagellar lengths to higher values. Since *LmxMPK3IS* is obviously functional in $\Delta LmxMPK3$ -/-HN1+*LmxMPK3IS* K1 and 2, it is very likely that *LmxMPK3IS* lost its function by additional mutations in $\Delta LmxMPK3$ -/-PN6+*LmxMPK3IS* K1 and 3 or that these clones compensated the introduction of *LmxMPK3IS*.

Some approaches had been tested to further increase the *LmxMPK3IS* expression levels and thereby generate clones with a distribution of flagellar lengths more resembling that of the wild type. Both the integration of *LmxMPK3IS* into the *LmxMPK3* gene locus and into the 18S rRNA locus indeed led to higher expression levels and thus to clones with longer flagella (Erdmann, unpublished data) compared to the clones expressing *LmxMPK3IS* from a plasmid (see above). However, the flagellar lengths of most clones were unstable and strongly decreased after several passages of the cultured promastigotes or after freezing and thawing of stabilates. Additionally, it was found that clones with long flagella apparently did not react to the inhibitor (the flagella remained long) which was probably due to additional mutations in *LmxMPK3IS* or compensation mechanisms.

Eventually, the inhibitor-sensitised *LmxMPK3* mutants $\Delta LmxMPK3$ -/-HN1+*LmxMPK3IS* K1 and 2 expressing *LmxMPK3IS* from a plasmid proved to be most suitable for establishing the inhibitor-sensitised system.

4.4.4 Inhibitor test on the inhibitor-sensitised *LmxMPK3* mutant

Once it was verified that *LmxMPK3IS* is functional *in vivo* and can fairly complement the deletion of *LmxMPK3*, its sensitivity towards the inhibitor 1-naphthyl-pyrazolo[3,4-d]pyrimidine (1-NA-PP1) was tested which had been generously provided by Kavita Shah (Purdue University, West Lafayette, USA). The specific inhibition of *LmxMPK3IS* should result in a gradual reduction of flagellar lengths until the phenotype of the *LmxMPK3* null mutant would be revealed.

For this purpose log-phase promastigotes of the *L. mexicana* wild type and $\Delta LmxMPK3$ -/-HN1+*LmxMPK3IS* K2 were diluted to 1×10^6 /ml and either incubated in the presence of 10 μ M 1-NA-PP1 (dissolved in DMSO) or DMSO alone to exclude that the observed cellular changes were triggered by the solvent. Cells were collected at defined intervals after addition of the inhibitor or the solvent and fixed to carry out measurements of flagellar lengths. In order to test if the inhibition of *LmxMPK3IS* by 1-NA-PP1 was reversible, the inhibitor was

removed from the cells after 96 h by washing them once with 1×PBS. Subsequently, the washed cells were inoculated to fresh medium at a density of approximately 1×10^6 /ml. Once again cells were collected after defined intervals after removal of the inhibitor, fixed and used for measurements of flagellar lengths.

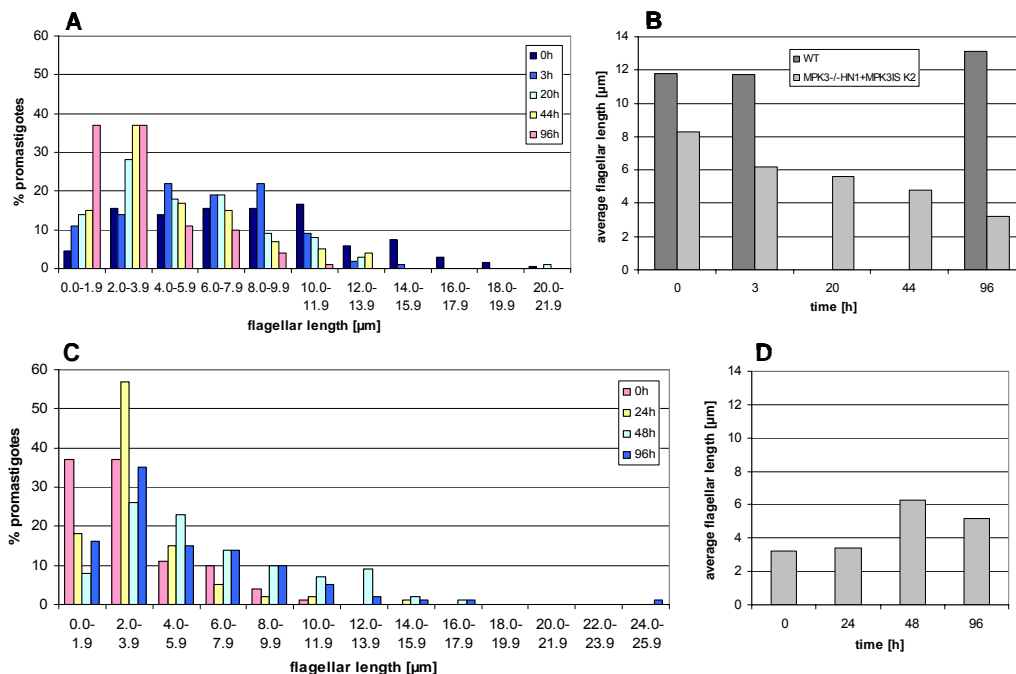


Figure 27: Inhibitor test on *L. mexicana* wild type and $\Delta LmxMPK3$ -HN1+MPK3IS K2

Histograms of flagellar lengths after adding or removing the inhibitor 1-NA-PP1; A and B: after adding 10 μ M 1-NA-PP1; C and D: after removing 1-NA-PP1; A and C: distribution of flagellar lengths; B and D: average flagellar lengths.

As depicted in Figure 27A and B, the flagellar lengths of the inhibitor-sensitised *LmxMPK3* mutant gradually declined within the observed period of 96 hours after addition of the inhibitor. While the average length was initially 8.3 μ m, it had decreased to only 3.2 μ m at 96 h (7.6 μ m in DMSO control, data not shown). After the same time interval 74% of the measured flagella were shorter than 4.0 μ m (29% in DMSO control, data not shown) compared to only 20% before the addition of the inhibitor. In contrast, the *L. mexicana* wild type did not reveal any morphological changes in response to the inhibitor. There was just a slight increase of flagellar lengths at 96 h probably due to the promastigotes reaching the metacyclic stage (Figure 27B).

When the inhibitor was removed from the inhibitor-sensitised *LmxMPK3* mutant after 96 h of incubation, the average flagellar length increased from 3.2 to 6.3 μ m within 48 h. After the same time only 34% of the flagella were still shorter than 4.0 μ m compared to 74% before the removal of the inhibitor. After 96 h a slight decrease of flagellar lengths could be observed, probably due to residual inhibitor in the medium reaching the inhibitor-sensitised kinase with a delay. The results show that the inhibition of *LmxMPK3IS* by 1-NA-PP1 is (mostly) reversible.

4.5 Biochemical characterisation of GST-LmxMPK3 and GST-LmxMPK3-KM

To use LmxMPK3 for *in vitro* studies, the kinase was recombinantly expressed in *E. coli* and affinity purified via a glutathione-S-transferase (GST)-tag. This had already been achieved for wild type LmxMPK3 (Erdmann, diploma thesis, 2004). However, when analysing a kinase in an *in vitro* kinase assay, it is important to ensure that the measured activity is not caused by a contaminating protein kinase from the expression system. Therefore, an enzymatically inactive mutant of LmxMPK3 was expressed, purified and tested in a kinase assay along with wild type LmxMPK3. The inactivation of LmxMPK3 was achieved by replacing a highly conserved lysine residue, essential for the kinase activity (Carrera *et al.*, 1993), by a methionine residue, resulting in LmxMPK3-KM.

4.5.1 Generation of the expression constructs

The plasmid pGEX-KG5aBHLmxMPK3 for the recombinant expression of a GST-fusion protein of wild type LmxMPK3 existed already before commencing this work (Erdmann, diploma thesis, 2004).

To generate an enzymatically inactive mutant of LmxMPK3, lysine 62 was mutated to methionine by site-directed mutagenesis. A PCR was performed on pGEX-KG5aBHLmxMPK3 using the oligonucleotides pGEX-KG1.for and LmxMPK3KM.rev generating a fragment of *LmxMPK3* encoding the K62→M-mutation. The fragment was cleaved with *Xba*I and *Nru*I and ligated into pGEX-KG5aBHLmxMPK3 which had been linearised using the same restriction enzymes. The resulting plasmid was sequenced and named pGEX-KG9BHLmxMPK3KM.

4.5.2 Recombinant expression and affinity purification of GST-LmxMPK3 and GST-LmxMPK3-KM

The plasmids pGEX-KG5aBHLmxMPK3 and pGEX-KG9BHLmxMPK3KM were transformed into *E. coli* XL1-Blue cells which were subsequently used to express the fusion proteins at 18°C overnight. The cells were lysed by sonication and the fusion proteins were purified on glutathione sepharose. After the eluted proteins had been quantified using the Bradford method, 2 µg of GST-LmxMPK3 and GST-LmxMPK3-KM were analysed by SDS-PAGE (Figure 28).

The recombinant expression and purification of the enzymatically inactive GST-LmxMPK3-KM was as successful as previously described for wild type GST-LmxMPK3 (Erdmann, diploma thesis, 2004). Figure 28 shows that a clear band corresponding to the GST-fusion protein could be found at the expected molecular mass (71.1 kDa). Additionally, there was a very faint double band probably corresponding to the GST-tag (27.4 kDa) caused either by cleavage of the fusion protein or by premature termination of transcription or translation.

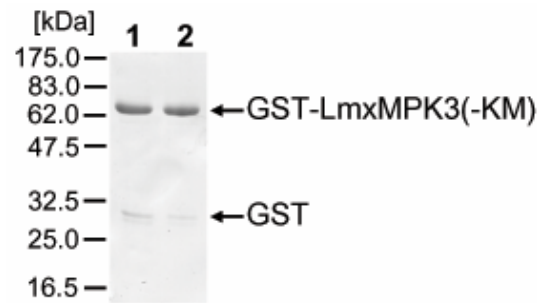


Figure 28: SDS-PAGE of affinity purified GST-LmxMPK3 and GST-LmxMPK3-KM
Coomassie-stained 12% SDS-PA gel. 1: GST-LmxMPK3; 2: GST-LmxMPK3-KM.

4.5.3 Optimisation of the kinase assay reaction conditions for GST-LmxMPK3

Although some optimisation of the reaction conditions for GST-LmxMPK3 had been carried out previously (Erdmann, diploma thesis, 2004), further improvement regarding the temperature as well as the ion concentrations and the pH value of the reaction buffer seemed reasonable. First, the pH optimum was determined using standard ion concentrations (2 mM Mn^{2+} , 10 mM Mg^{2+}) and a temperature of 27°C which is roughly the physiological temperature of promastigotes in their insect vector. Afterwards, the optimal Mn^{2+} and Mg^{2+} concentrations were assessed at the same temperature using reaction buffers with the determined pH optimum. Eventually, the optimal incubation temperature was investigated using reaction buffers with the determined optima of Mn^{2+} and Mg^{2+} concentrations and the pH optimum.

The pH optimum for maximal phosphorylation of myelin basic protein (MBP) was determined to be in a range between 6.0 and 7.0 (Figure 29B) at standard ion concentrations and 27°C. Since MBP phosphorylation seemed slightly reduced at pH 6.5, the experiment was repeated in a pH range between 5.5 and 7.2 (Figure 29D and E). Again, the strongest MBP phosphorylation was detectable at pH 6.0 to 7.0 and was not decreased at pH 6.5 this time. Using the average pH optimum of 6.5 the reaction buffer containing the highest Mn^{2+} concentration (10 mM) and lacking Mg^{2+} ions led to maximal MBP phosphorylation at 27°C (Figure 29G). Generally, manganese was preferred over magnesium which classifies LmxMPK3 as a manganese-dependent protein kinase and confirms previous results (Erdmann, diploma thesis, 2004). Increasing the incubation temperature from 25 to 40°C resulted in a gradual increase of auto- and MBP phosphorylation at pH 6.5 and 10 mM Mn^{2+} (Figure 29I). This was not expected since LmxMPK3 is a promastigote-specific MAP kinase with a physiological environmental temperature of about 27°C. All of the following kinase assays with LmxMPK3 were carried out at a physiological temperature of 27°C for which an MBP phosphorylation could also be clearly observed.

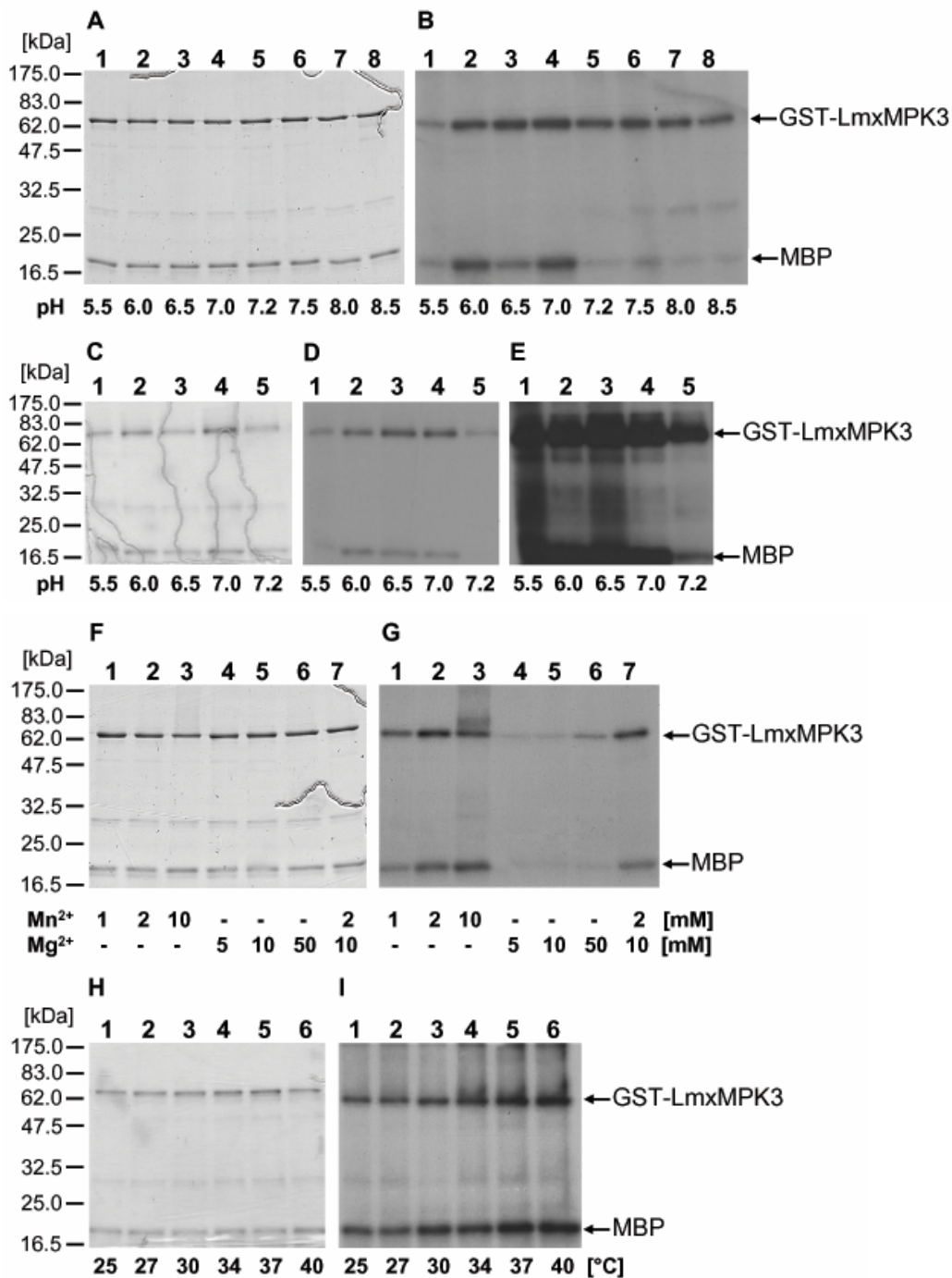


Figure 29: Kinase assays with GST-LmxMPK3 under varying conditions

A, C, F and H: Coomassie-stained 12% SDS-PAGE gels; B, G and I: Autoradiographs after 48h of exposure; D: Autoradiograph after 24h of exposure; E: Autoradiograph after 96h of exposure. pH values, ion concentrations and temperatures are indicated.

4.5.4 Kinase assays with GST-LmxMPK3 and GST-LmxMPK3-KM

Equal amounts of purified GST-LmxMPK3 and GST-LmxMPK3-KM were tested along each other in a kinase assay with MBP at 27°C using a reaction buffer with 10 mM Mn²⁺ and pH 6.5.

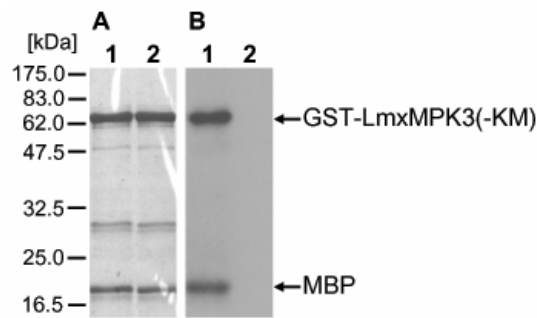


Figure 30: Kinase assays with GST-LmxMPK3 and GST-LmxMPK3-KM

A: Coomassie-stained 12% SDS-PA gel; B: Autoradiograph after 48h of exposure; 1: GST-LmxMPK3; 2: GST-LmxMPK3-KM.

Replacement of lysine 62 with methionine in LmxMPK3 entirely abolished the enzymatic activity of the kinase (Figure 30B, lane 2). This result indicates that the phosphorylation reactions in lane 1 are actually caused by GST-LmxMPK3 itself and not by a contaminating protein kinase.

4.6 Analysis and optimisation of the activation of LmxMPK3 and LmxMPK3-KM by LmxMKK-D

It had been found in our laboratory that activated LmxMKK phosphorylates and activates LmxMPK3 *in vitro* and *in vivo* (Scholz, PhD thesis, 2008; Erdmann *et al.*, 2006). Since the activator of LmxMKK is not known and thus LmxMKK cannot be activated in *in vitro* assays, a constitutively active aspartate mutant, named LmxMKK-D, was used. Therefore, several residues, including the potential phosphorylation sites of the activation loop, had been replaced by aspartate residues, thus mimicking a phosphorylation (Wiese *et al.*, 2003a). Although several kinase assays had been carried out combining equal amounts of different LmxMPK3 and LmxMKK mutant proteins (Scholz, PhD thesis, 2008; Erdmann *et al.*, 2006), the activation of LmxMPK3 was further analysed by pre-incubating the kinase with highly diluted LmxMKK-D in the presence of unlabeled ATP which should result in an *in vitro* activation of LmxMPK3. Subsequent kinase assays with the *in vitro*-activated LmxMPK3 should only reveal phosphorylations caused by LmxMPK3 and not by its activator.

4.6.1 Kinase assays with *in vitro*-activated GST-LmxMPK3 and GST-LmxMPK3-KM

Amounts of 10 µg of GST-LmxMPK3 and GST-LmxMPK3-KM were separately pre-incubated with 30 times less GST-LmxMKK-D and unlabeled ATP for *in vitro* activation. Additionally, the same assay was done solely containing the same amount of GST-LmxMKK-D, but lacking LmxMPK3. Subsequently, a quarter volume of each assay was used to carry out radioactive kinase assays with MBP as a substrate at 27°C using a reaction buffer with 10 mM Mn²⁺ and pH 6.5.

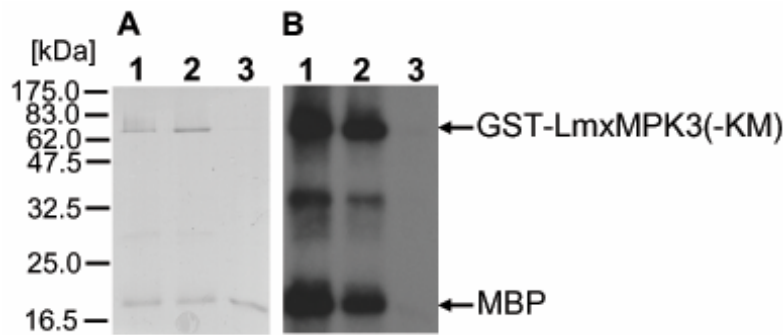


Figure 31: Kinase assays with *in vitro*-activated GST-LmxMPK3 and GST-LmxMPK3-KM

A: Coomassie-stained 12% SDS-PA gel; B: Autoradiograph after 6h of exposure; 1: GST-LmxMPK3/(GST-LmxMKK-D); 2: GST-LmxMPK3-KM/(GST-LmxMKK-D); 3: (GST-LmxMKK-D). Brackets indicate that only traces of the protein are present.

Most surprisingly, *in vitro*-activated GST-LmxMPK3-KM, which was expected to be enzymatically inactive, revealed an auto- and MBP phosphorylation which was almost as strong as for the activated wild type LmxMPK3 (Figure 31, lanes 1 and 2). This finding was confirmed by repeating the experiment and the presence of the K62→M-mutation was verified by sequencing. The observed MBP phosphorylation was definitely not caused by traces of LmxMKK-D as no signals occurred in Figure 31, lane 3 showing the kinase assay with pre-incubated LmxMKK-D lacking LmxMPK3.

4.6.2 Optimisation of the LmxMPK3 activation using an *in vivo* system

To achieve a maximal activation of LmxMPK3, the kinase and its activator LmxMKK were co-expressed in *E. coli* overnight. The long period of time in which both kinases can interact with each other *in vivo* could be beneficial for the maximal activation of LmxMPK3. Therefore, the genes of both kinases were cloned into the expression vector pJCduet which provides two multiple cloning sites (MCSs). The activator kinase, in this case LmxMKK, was cloned in one of the MCSs. The second MCS was used for the kinase to be activated, in this case LmxMPK3, and provided it with a His-tag. Thus, the activated kinase could be affinity purified separately from its activator and used in kinase assays. This is an advantage over the *in vitro* activation of a kinase in which traces of the activator can impair the results of subsequent kinase assays.

4.6.2.1 Generation of the co-expression constructs

pJCduet constructs with various combinations of different *LmxMPK3* and *LmxMKK* mutants were generated. To clone *LmxMPK3* into pJCduet, the open reading frame (ORF) of *LmxMPK3* was liberated from pCR2.1-23MPK3 using *EcoRI* and *HindIII* and cloned into pJCduet which had been linearised using the same restriction enzymes. The resulting plasmid was named pJC1MPK3. To generate the equivalent construct of the enzymatically

inactive mutant, the ORF of *LmxMPK3-KM* was amplified from pGEX-KG9BHLmxMPK3KM by performing a PCR using the oligonucleotides mpk3n.for and mpk3c.rev. After the amplified fragment had been ligated into pCR2.1-TOPO and sequenced, a 5'-end fragment carrying the K62→M-mutation was released using *EcoRI* and *SmaI*. It was cloned into pJC1MPK3 which had been linearised using the same restriction enzymes, resulting in a plasmid designated pJC2MPK3KM.

In order to also introduce *LmxMKK*, its ORF was liberated from pCR2.1lmmkk3 using *EcoRV* and *XbaI*. The sticky end caused by the cleavage with *XbaI* was filled-in using Klenow enzyme to form a blunt end. Ligation of the fragment into pJC1MPK3 which had been linearised with *EcoRV* resulted in pJC1MPK3MKK. To generate the equivalent construct of the constitutively active *LmxMKK-D*, the ORF of *LmxMKK-D* was liberated from pB41lmmkkMut2 using *EcoRV* and *XbaI* followed by treatment with Klenow enzyme. Cloning of the fragment into the *EcoRV*-linearised pJC1MPK3 resulted in pJC2MPK3MKKMut2. Additionally, the *EcoRI/SmaI*-fragment of *LmxMPK3-KM* described above was ligated into pJC2MPK3MKKMut2 which had been linearised using the same restriction enzymes. The generated plasmid was named pJC7MPK3KMMKKMut2.

Finally, a pJCduet construct solely containing *LmxMKK-D* was generated. Therefore, the Klenow-treated *EcoRV/XbaI*-fragment of *LmxMKK-D* described above was ligated into pJCduet which had been linearised with *EcoRV*, resulting in pJC20MKKMut2.

4.6.2.2 Recombinant co-expression and affinity purification of His-LmxMPK3 and His-LmxMPK3-KM

The plasmids pJC1MPK3, pJC2MPK3KM, pJC1MPK3MKK, pJC2MPK3MKKMut2, pJC7MPK3KMMKKMut2 and pJC20MKKMut2 containing various combinations of different *LmxMPK3* and *LmxMKK* mutants were transformed into *E. coli* pAPlac cells which were subsequently used to co-express both kinases at 18°C overnight. The cells were lysed by sonication and His-LmxMPK3 as well as His-LmxMPK3-KM were purified on Co²⁺ sepharose. Before the elution step, the washed sepharose beads were split into two equal parts. One part was used to elute His-LmxMPK3 and His-LmxMPK3-KM with elution buffer and the other part was taken up in ddH₂O. Using ddH₂O instead of buffer turned out to be more practical for the following experimental procedures and obviously did not harm *LmxMPK3* or impair its catalytic activity. Protein quantification of the eluates via Bradford revealed that the yield of His-LmxMPK3-KM derived from the constructs pJC2MPK3KM and pJC7MPK3KMMKKMut2 was very poor. As expected, pJC20MKKMut2 (the construct lacking *LmxMPK3*) only led to background protein detection due to the unspecific binding of contaminating proteins to the sepharose. The yield of His-LmxMPK3 expressed from pJC2MPK3MKKMut2 was just moderate, but indeed very high for pJC1MPK3 and pJC1MPK3MKK. The kept bead

suspensions carrying the non-eluted proteins were analysed by SDS-PAGE in which approximately 2 µg of His-LmxMPK3 or His-LmxMPK3-KM were loaded on each lane. As for the samples with very low protein amounts, the maximum capacity of 20 µl bead suspension was loaded (Figure 32).

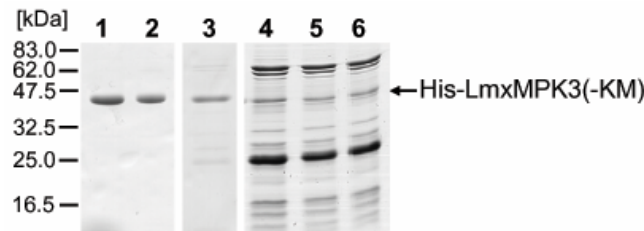


Figure 32: SDS-PAGE of affinity purified His-LmxMPK3 and His-LmxMPK3-KM on beads

Coomassie-stained 15% SDS-PA gel. 1: His-LmxMPK3; 2: His-LmxMPK3(/LmxMKK); 3: His-LmxMPK3(/LmxMKK-D); 4: His-LmxMPK3-KM; 5: His-LmxMPK3-KM(/LmxMKK-D); 6: (LmxMKK-D). Brackets indicate that the protein was only present during co-expression.

Lanes 1 to 3 of Figure 32 show a clean band of His-LmxMPK3 at the expected molecular mass (45.8 kDa). In contrast, lanes 4 to 6 revealed a lot of additional bands resulting from contaminating proteins. Though a weak band of the expected molecular mass was visible in lanes 4 and 5, it could also be observed in lane 6 which should not contain His-LmxMPK3. Hence, for kinase assays in which it was difficult to estimate if the used His-LmxMPK3 or His-LmxMPK3-KM amounts were comparable with each other, non-radioactive kinase assays had to be carried out in parallel and subjected to immunoblot analysis using an antiserum against LmxMPK3.

4.6.2.3 Optimisation of the kinase assay reaction conditions for *in vivo*-activated His-LmxMPK3

Although the reaction conditions had already been optimised for GST-LmxMPK3 (see 4.5.3), they were adjusted for *in vivo*-activated His-LmxMPK3. Therefore, the pH was tested in a range between 6.5 and 7.5 either at 10 mM Mn²⁺ or at standard ion concentrations (2 mM Mn²⁺, 10 mM Mg²⁺) at 27 °C.

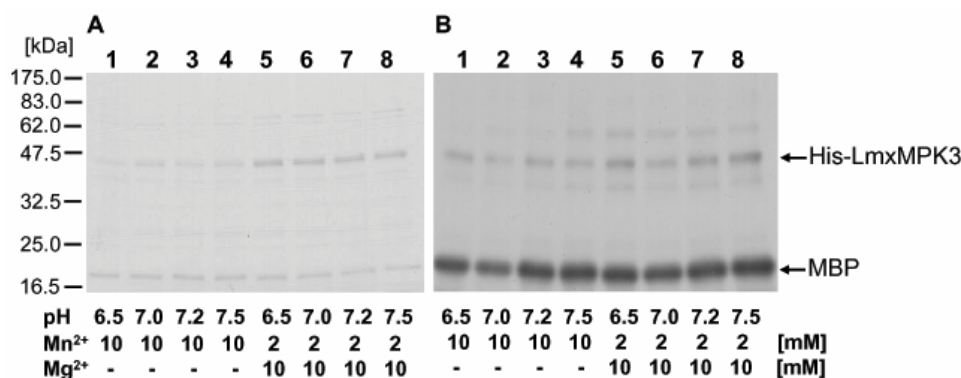


Figure 33: Kinase assays with *in vivo*-activated His-LmxMPK3 under varying conditions

A: Coomassie-stained 12% SDS-PA gel; B: Autoradiograph after 24h of exposure. pH values and ion concentrations are indicated.

Figure 33 indicates that *in vivo*-activated His-LmxMPK3 catalysed a strong MBP phosphorylation which was equally high throughout the tested pH range and the tested ion concentrations. The phosphorylation of LmxMPK3 by its activator probably triggered a conformational change which led to a high catalytic activity of the kinase tolerating a wider range of pH values and ion concentrations than the non-activated kinase. The following kinase assays were carried out using a reaction buffer with 10 mM Mn²⁺ and pH 6.5 which had previously been used for GST-LmxMPK3 (see 4.5.4 and 4.6.1).

4.6.2.4 Kinase assays with His-LmxMPK3 and His-LmxMPK3-KM derived from the different co-expressions

Approximately 2 µg of non-eluted His-LmxMPK3 and His-LmxMPK3-KM on sepharose beads (derived from the different co-expression constructs) were tested in kinase assays with MBP at 27°C using a reaction buffer with 10 mM Mn²⁺ and pH 6.5. The reason for using non-eluted proteins on beads is that otherwise high volumes would have had to be subjected to kinase assays when the protein was less abundant. The imidazole which is present in the elution buffer would have had inhibited the kinase activity, if high volumes had to be used. Since the estimation of protein amounts was very difficult for some samples, non-radioactive kinase assays were carried out in parallel and subjected to immunoblot analysis using an antiserum against LmxMPK3.

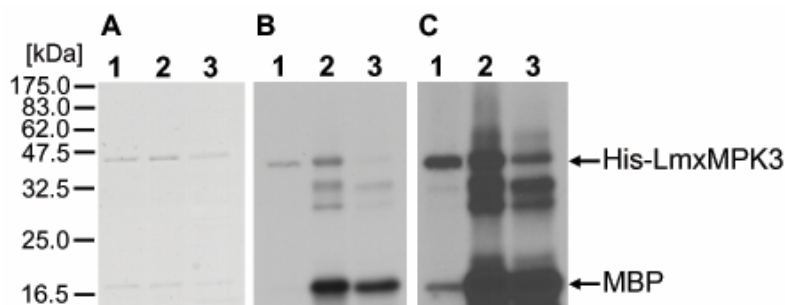


Figure 34: Kinase assays with His-LmxMPK3 derived from different co-expressions

A: Coomassie-stained 12% SDS-PA gel; B: Autoradiograph after 18h of exposure; C: Autoradiograph after 84h of exposure.

1: His-LmxMPK3; 2: His-LmxMPK3(/LmxMKK); 3: His-LmxMPK3(/LmxMKK-D).

Brackets indicate that the protein was only present during co-expression.

The co-expressions of His-LmxMPK3 with LmxMKK or LmxMKK-D both indeed led to a very strong activation of His-LmxMPK3 as shown by the strong MBP phosphorylation in Figure 34B and C, lanes 2 and 3. Considering that the His-LmxMPK3 amount loaded in lane 3 was a little lower compared to lane 2, one can conclude that the LmxMPK3 activation caused by LmxMKK and LmxMKK-D was equally strong.

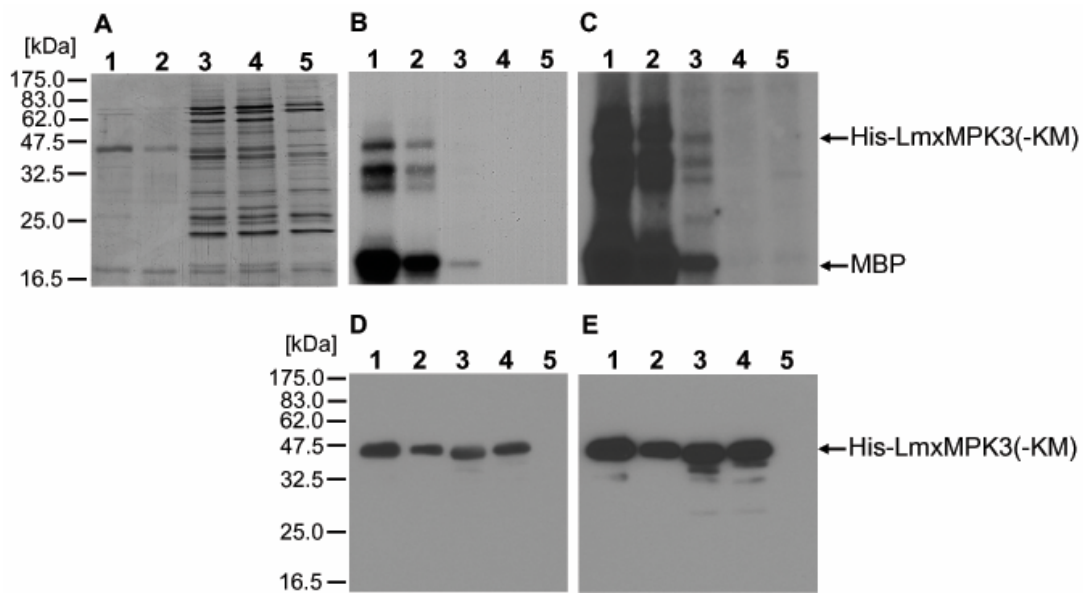


Figure 35: Kinase assays with His-LmxMPK3 and His-LmxMPK3-KM derived from different co-expressions

A: Silver-stained 12% SDS-PA gel; B: Autoradiograph after 7h of exposure; C: Autoradiograph after 48h of exposure; D: Immunoblot of LmxMPK3 after 1 s of exposure; E: Immunoblot of LmxMPK3 after 10 s of exposure.

1: His-LmxMPK3/(LmxMKK-D); 2: His-LmxMPK3/(LmxMKK-D) diluted 1:1; 3: His-LmxMPK3-KM/(LmxMKK-D); 4: His-LmxMPK3-KM; 5: (LmxMKK-D).

Brackets indicate that the protein was only present during co-expression.

The co-expression of the enzymatically inactive His-LmxMPK3-KM with LmxMKK-D also led to an activation (Figure 35B and C, lane 3), however, by far not as strong as for wild type His-LmxMPK3 (Figure 35B and C, lanes 1 and 2) for which different protein amounts had been loaded in order to get the best comparison to the other samples. Immunoblot analysis of LmxMPK3 showed that roughly the same protein amounts had been loaded in Figure 35D and E, lanes 3 and 4, and that the loaded amounts in lane 1 and 2 were only slightly higher and lower, respectively. In the control lanes containing His-LmxMPK3-KM only (lane 4) and the purified proteins from the expression of LmxMKK-D alone (lane 5) no bands could be observed on the autoradiographs (Figure 35B and C). This confirms that the observed MBP phosphorylation in Figure 35B and C, lane 3 was actually caused by the *in vivo*-activated His-LmxMPK3-KM and not by any activity of non-activated His-LmxMPK3-KM or by traces of LmxMKK-D. This finding supports the results of 4.6.1 in which a strong *in vitro* activation of GST-LmxMPK3-KM by GST-LmxMKK-D could be observed.

4.7 Analysis of the activation mechanism of LmxMPK3

The activation of a MAP kinase generally occurs by phosphorylation on amino acid residues which are located in the so-called activation loop. It has been generally anticipated that MAP kinases have to be phosphorylated on the threonine (T) and the tyrosine (Y) residue of the conserved TXY activation motif by a specific dual-specificity MAP kinase kinase for full

activation (Payne *et al.*, 1991; L'Allemain *et al.*, 1992; Wu *et al.*, 1992). Since several signalling components of higher eukaryotes could not be identified in *Leishmania* (Parsons and Ruben, 2000), it is likely that the signalling mechanisms are generally related but not completely identical. Therefore, the activation mechanism of LmxMPK3 was analysed.

The activation motif of LmxMPK3 consists of a TDY amino acid triplet. Different LmxMPK3-TDY mutants could be generated in which either threonine or tyrosine is replaced by alanine (A) or leucine (L), respectively.

On the one hand, the different LmxMPK3-TDY mutants were recombinantly co-expressed with the constitutively active version of the activating kinase, named LmxMKK-D, using the pJCduet system described in 4.6.2. Subsequently, the enzymatic activities of the affinity purified LmxMPK3-TDY mutants were assessed by *in vitro* kinase assays. Additionally, the LmxMPK3 phosphorylation state could be analysed by mass spectrometry and immunoblot analysis using a monoclonal antibody against phosphotyrosine.

On the other hand, one copy of each *LmxMPK3* mutant was introduced individually into the *LmxMPK3* null mutants $\Delta LmxMPK3$ -I-HN1 and $\Delta LmxMPK3$ -I-PN6. Flagellar lengths of the obtained clones are indicative for the function of the LmxMPK3-TDY mutants *in vivo*. The correlation between the activity of LmxMPK3 and the flagellar length had been impressively shown in 4.4.4.

4.7.1 *In vitro* studies

4.7.1.1 Generation of the co-expression constructs

Different pJCduet constructs containing either the LmxMPK3-TDL or the LmxMPK3-ADY mutant as well as the constitutively active LmxMKK-D were generated using pJC1MPK3, pJC2MPK3MKKMut2 and pJC7MPK3KMMKKMut2 as starting constructs (see 4.6.2.1).

In order to introduce the TDY mutations, two independent PCRs were carried out on pX3ELmxMPK3 using the oligonucleotides pXPHLEO2 and MPK3-TDL.rev in one reaction and pXPHLEO2 and MPK3-ADY.rev in the other reaction. A 5'-end fragment of *LmxMPK3* was amplified carrying the respective TDY mutation. After both fragments had been ligated separately into pCR2.1-TOPO and sequenced, they were released using *Bam*HI and *Acc*65I. In parallel, the receiving plasmid was prepared in a way that would also allow the introduction of the *LmxMPK3*-TDY mutants into the *LmxMPK3* gene locus (see 4.7.2). Therefore, an *Nco*I restriction site was introduced upstream to the puromycin resistance marker gene in pX63polPAC. Two independent PCRs were carried out on pX63polPAC using the oligonucleotides *Eco*RI.for and *Nco*I-PAC.rev in one reaction and *Nco*I-PAC.for and *Msc*I.rev in the other reaction. After gel purification the amplified fragments were used as overlapping templates in a third PCR with *Eco*RI.for and *Msc*I.rev. The product was ligated into pCR2.1-TOPO, sequenced and cleaved using *Eco*RI and *Msc*I. It was cloned into pX63polPAC which

had been linearised using the same restriction enzymes, resulting in pX14polNcoIPAC. Subsequently, *LmxMPK3* was cloned into pX14polNcoIPAC. Therefore, the ORF of *LmxMPK3* was liberated from pCR2.1-23MPK3 using *EcoRI* and ligated into pX14polNcoIPAC which had been linearised using *MunI*. The generated plasmid was designated pX1NcoIPACLmxMPK3.

The *BamHI/Acc65I*-fragment of *LmxMPK3* containing the different TDY mutations (see above) was ligated into pX1NcoIPACLmxMPK3 which had been linearised using the same restriction enzymes. The resulting plasmids were named pX6NcoIPACLmxMPK3(TDL) and pX6NcoIPACLmxMPK3(ADY). Those plasmids were cleaved with *NruI* and *XmaI* to generate *LmxMPK3* fragments carrying either the TDL or the ADY mutation. The obtained fragments were ligated to pJC1MPK3, pJC2MPK3MKKMut2 and pJC7MPK3KMMKKMut2 which had been linearised using the same restriction enzymes. The generated plasmids were designated pJC3MPK3(TDL), pJC3MPK3(TDL)MKKMut2, pJC3MPK3(TDL)KMMKKMut2 and pJC2MPK3(ADY), pJC3MPK3(ADY)MKKMut2 and pJC6MPK3(ADY)KMMKKMut2, respectively.

4.7.1.2 Recombinant co-expression and affinity purification of the different His-LmxMPK3-TDY mutants

The plasmids pJC3MPK3(TDL), pJC3MPK3(TDL)MKKMut2, pJC3MPK3(TDL)KMMKKMut2, pJC2MPK3(ADY), pJC3MPK3(ADY)MKKMut2 and pJC6MPK3(ADY)KMMKKMut2 containing the different *LmxMPK3-TDY* mutants and some of them also the gene for the constitutively active LmxMKK-D were transformed into *E. coli* pAPlac cells which were subsequently used to co-express the kinases at 18°C overnight. Subsequently, the cells were lysed by sonication and the different His-LmxMPK3-TDY mutants were purified on Co²⁺ sepharose. As it was already described in 4.6.2.2, the washed sepharose beads were split into two equal parts before the elution step. One part was taken up in ddH₂O and the other part was used to elute the different His-LmxMPK3-TDY mutants with elution buffer. Protein quantification of the eluates via Bradford revealed that the yields of His-LmxMPK3-TDL-KM and His-LmxMPK3-ADY-KM derived from the constructs pJC3MPK3(TDL)KMMKKMut2 and pJC6MPK3(ADY)KMMKKMut2 were very poor. In contrast, the yields of His-LmxMPK3-TDL and His-LmxMPK3-ADY expressed from pJC3MPK3(TDL), pJC3MPK3(TDL)MKKMut2, pJC2MPK3(ADY) and pJC3MPK3(ADY)MKKMut2 were indeed very high. The kept bead suspensions carrying the non-eluted proteins were analysed by SDS-PAGE in which approximately 0.1 µg of the different His-LmxMPK3-TDY mutants were loaded in each lane. As for the samples with very low protein amounts, the maximum capacity of 20 µl bead suspension was loaded (Figure 36).

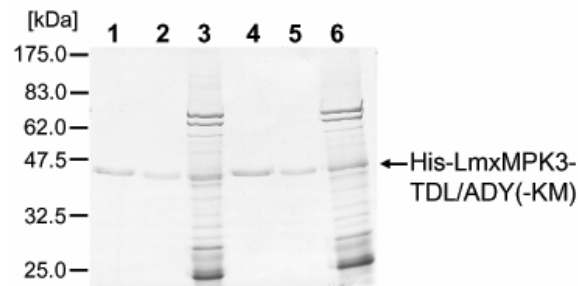


Figure 36: SDS-PAGE of different affinity purified His-LmxMPK3-TDY mutants on beads

Coomassie-stained 10% SDS-PA gel. 1: His-LmxMPK3-TDL; 2: His-LmxMPK3-TDL(/LmxMKK-D); 3: His-LmxMPK3-TDL-KM(/LmxMKK-D); 4: His-LmxMPK3-ADY; 5: His-LmxMPK3-ADY(/LmxMKK-D); 6: His-LmxMPK3-ADY-KM(/LmxMKK-D).

Brackets indicate that the protein was only present during co-expression.

Lanes 1, 2, 4 and 5 of Figure 36 show a clean band of His-LmxMPK3-TDL and His-LmxMPK3-ADY at the expected molecular mass (45.8 kDa). In contrast, lanes 3 and 6 showing His-LmxMPK3-TDL-KM and His-LmxMPK3-ADY-KM revealed a lot of additional bands resulting from contaminating proteins, as it had already been shown for His-LmxMPK3-KM (see 4.6.2.2). Hence, for kinase assays in which it was difficult to estimate, if the used amounts of the different LmxMPK3-TDY mutants were comparable with each other, non-radioactive kinase assays had to be carried out in parallel and subjected to immunoblot analysis using an antiserum against LmxMPK3 (see also 4.6.2.4).

4.7.1.3 Kinase assays and subsequent analysis of the tyrosine phosphorylation state of the different His-LmxMPK3-TDY mutants

Approximately 1.5 μg of the different non-eluted His-LmxMPK3-TDL and His-LmxMPK3-ADY mutants on sepharose beads (derived from the different co-expression constructs) were subjected to kinase assays with MBP at 27°C using a reaction buffer with 10 mM Mn^{2+} and pH 6.5. For comparison, the kinase assays were also done with His-LmxMPK3 and His-LmxMPK3-KM which contain the wild type activation motif TDY. The reason for using non-eluted proteins on beads had been commented on in 4.6.2.4. Non-radioactive kinase assays were carried out in parallel for subsequent analysis by immunoblotting using the 4G10 monoclonal antibody against phosphotyrosine. Since the estimation of protein amounts was very difficult for some samples, the immunoblot was also probed with an antiserum against LmxMPK3.

As it had already been described in 4.6.2.4, the co-expression of His-LmxMPK3 with LmxMKK-D led to a very strong activation of His-LmxMPK3 as shown by the strong MBP phosphorylation (Figure 37B and C, lane 2). In addition, a weak MBP phosphorylation catalysed by *in vivo*-activated His-LmxMPK3-KM could be observed again (Figure 37B and C, lane 3) as already shown in 4.6.2.4. The constitutively active LmxMKK-D catalysed a strong tyrosine phosphorylation of His-LmxMPK3 and His-LmxMPK3-KM (Figure 37D, lanes 2 and 3). In order to find out, if the weak tyrosine phosphorylation of the non-activated His-

LmxMPK3 (Figure 37D, lane 1) was due to autophosphorylation and not caused by *E. coli* protein kinases, immunoblot analysis of His-LmxMPK3-KM was carried out along with His-LmxMPK3 using the 4G10 monoclonal antibody against phosphotyrosine. No tyrosine phosphorylation could be observed for His-LmxMPK3-KM (Figure 38A, lane 2) showing that the non-activated wild type His-LmxMPK3 actually performs autophosphorylation on tyrosine. For His-LmxMPK3-TDL, which had been expressed on its own, neither auto- nor MBP phosphorylation could be observed (Figure 37B and C, lane 4). This finding indicates that the tyrosine of the TDY motif is the only amino acid residue on which autophosphorylation takes place when LmxMPK3 has not been activated before. Moreover, this tyrosine seems to be essential for basal substrate phosphorylation. However, when His-LmxMPK3-TDL had been co-expressed with constitutively active LmxMKK-D, the auto- and MBP phosphorylation was almost as strong as for *in vivo*-activated His-LmxMPK3 (Figure 37B and C, lane 5). This points out that the tyrosine phosphorylation of the TDY motif plays only a minor role in the activation mechanism of LmxMPK3. The total absence of tyrosine phosphorylation in His-LmxMPK3-TDL and His-LmxMPK3-TDL-KM (Figure 37D, lanes 4 to 6) reveals that the tyrosine of the TDY motif is the only tyrosine residue within the whole protein on which autophosphorylation and phosphorylation by LmxMKK-D occur. However, autophosphorylation additionally seems to take place on other amino acid residues (serine or threonine) when His-LmxMPK3-TDL had been activated, as shown by the upper band in Figure 37B and C, lane 5.

When His-LmxMPK3-ADY had been expressed on its own, the observed auto- and MBP phosphorylation was comparable to wild type His-LmxMPK3 (Figure 37B and C, lane 7) indicating that the threonine of the TDY motif is not essential for basal activity. However, when His-LmxMPK3-ADY had been co-expressed with LmxMKK-D, the enzymatic activity was increased only to a very low extend (Figure 37B and C, lane 8). The phosphorylation of threonine in the TDY motif is therefore essential for the maximal activation of LmxMPK3. Additionally, a decrease in autophosphorylation of *in vivo*-activated His-LmxMPK3-ADY could be observed. Since the protein amount loaded in lane 8 seemed to be slightly lower compared to the other lanes, the experiment was repeated several times always resulting in a decreased autophosphorylation of *in vivo*-activated His-LmxMPK3-ADY (Figure 39B, lane 2). It remains unclear, what causes the decreased autophosphorylation and on which exact residues the residual autophosphorylation takes place. Different possible explanations are discussed in chapter 5.7.2.1. The tyrosine phosphorylation of His-LmxMPK3-ADY and His-LmxMPK3-ADY-KM was not impaired as shown in Figure 37D, lanes 7 to 9.

Neither for His-LmxMPK3-TDL-KM nor for His-LmxMPK3-ADY-KM an activation was achieved when co-expressed with LmxMKK-D (Figure 37B and C, lane 6 and 9) which is unlike as in wild type His-LmxMPK3 (see above). Apparently, both threonine and tyrosine of

the TDY motif need to be phosphorylated for activation of the otherwise enzymatically inactive LmxMPK3-KM.

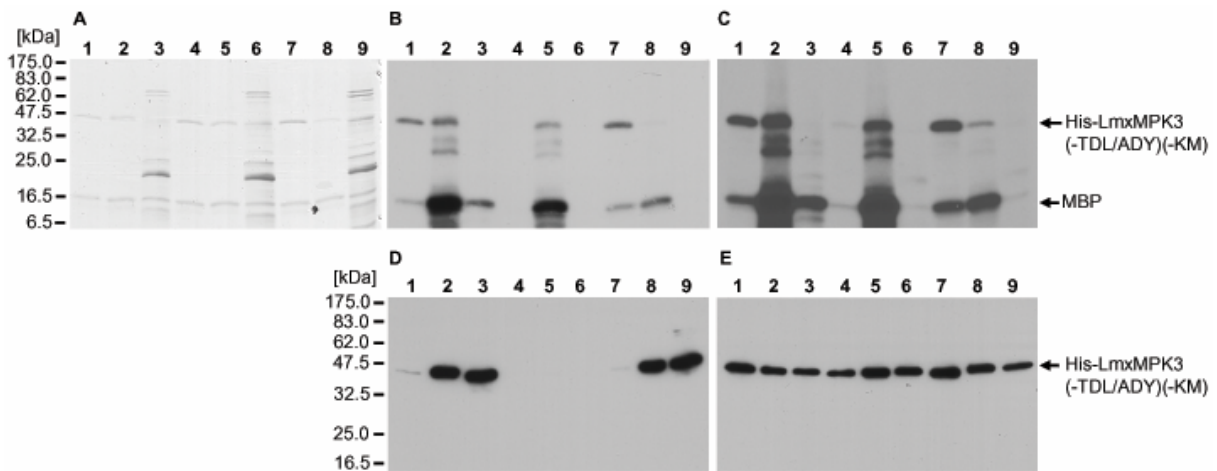


Figure 37: Kinase assays and immunoblot of phosphotyrosine from different His-LmxMPK3-TDY mutants

A: Coomassie-stained 12% SDS-PAGE gel; B: Autoradiograph after 7h of exposure; C: Autoradiograph after 15h of exposure; D: Immunoblot of phosphotyrosine; E: Immunoblot of LmxMPK3.

1: His-LmxMPK3; 2: His-LmxMPK3(/LmxMKK-D); 3: His-LmxMPK3-KM(/LmxMKK-D); 4: His-LmxMPK3-TDL; 5: His-LmxMPK3-TDL(/LmxMKK-D); 6: His-LmxMPK3-TDL-KM(/LmxMKK-D); 7: His-LmxMPK3-ADY; 8: His-LmxMPK3-ADY(/LmxMKK-D); 9: His-LmxMPK3-ADY-KM(/LmxMKK-D).

Brackets indicate that the protein was only present during co-expression.

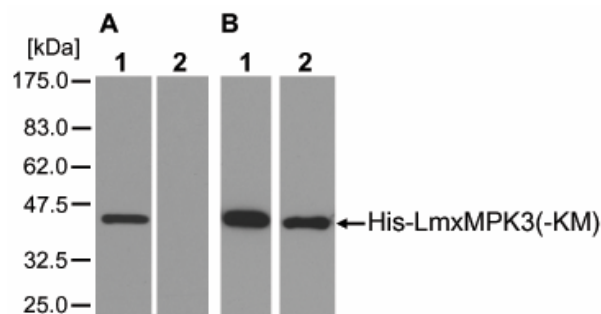


Figure 38: Immunoblot of phosphotyrosine from His-LmxMPK3 and His-LmxMPK3-KM

A: probed with anti-phosphotyrosine antiserum; B: probed with anti-LmxMPK3 antiserum.

1: His-LmxMPK3; 2: His-LmxMPK3-KM.



Figure 39: Kinase assays with His-LmxMPK3-ADY derived from different co-expressions

A: Coomassie-stained 12% SDS-PAGE gel; B: Autoradiograph after 7h of exposure.

1: His-LmxMPK3-ADY; 2: His-LmxMPK3-ADY(/LmxMKK-D).

Brackets indicate that the protein was only present during co-expression.

In summary, the autophosphorylation of non-activated LmxMPK3 only occurs on the tyrosine residue of the TDY motif. However, activated LmxMPK3 may additionally perform autophosphorylation on serine or threonine residues of the protein. Activated LmxMKK-D strongly catalyses the phosphorylation of tyrosine in the TDY motif of LmxMPK3 and of no other tyrosine residue within the whole protein. While the tyrosine of the TDY motif is only necessary for the basal activity of LmxMPK3, the threonine is indeed essential for the maximal activation of the kinase.

4.7.1.4 Analysis of the phosphorylation state of the different His-LmxMPK3-TDY mutants by mass spectrometry

Since the immunoblot analysis of the different LmxMPK3-TDY mutants carried out in 4.7.1.3 covered only the phosphorylation on tyrosine residues, a more comprehensive mapping of phosphorylation sites was performed using mass spectrometry. Therefore, the plasmids pJC1MPK3, pJC2MPK3MKKMut2, pJC3MPK3(TDL), pJC3MPK3(TDL)MKKMut2, pJC2MPK3(ADY) and pJC3MPK3(ADY)MKKMut2 containing the different *LmxMPK3-TDY* mutants and some of them also the gene for the constitutively active LmxMKK-D were transformed into *E. coli* pAPlac cells. The protein expression and purification was performed as described in 4.7.1.2. The eluates containing His-LmxMPK3 or the respective TDL and ADY mutants were separated on 8% SDS-PA gels which were subsequently stained with Coomassie. The protein bands corresponding to His-LmxMPK3 were excised using a clean scalpel, cut into roughly 1 mm³-cubes and transferred to clean 1.5 ml-tubes. The samples were further processed in the Protein Research group at the University of Southern Denmark, Odense. This included an in-gel treatment with DTT for the reduction of disulfide bonds followed by a treatment with iodoacetamide for the alkylation of cysteine residues to prevent the re-formation of disulfide bonds. Subsequently, an in-gel digest with trypsin was performed which was followed by an extraction of the generated peptides. Phosphopeptides were then enriched on C8-TiO₂ micro-columns. The flow through containing the non-phosphorylated peptides was collected for identification purposes. Both the non-phosphorylated peptide fractions as well as the TiO₂-purified phosphopeptides were desalted before MALDI-TOF MS was carried out on a Bruker Ultraflex TOF-TOF instrument (Bruker Daltronics, Bremen, Germany). Tandem MS analysis was subsequently performed on peaks of interest. Data analysis was conducted using FlexAnalysis, version 2.4 and BioTools, version 3.0. Database searches were carried out using the Mascot search engine (www.matrixscience.com). The different MALDI-TOF MS and MS/MS spectra of the phosphopeptide eluates are shown in 8.3.

MALDI-TOF MS analysis of the different flow throughs could identify LmxMPK3 with a sequence coverage of 39-63%. Analysis was then focused on the TiO₂-purified

phosphopeptides. The MALDI-TOF MS spectrum of His-LmxMPK3 derived from pJC1MPK3 showed a clear peak at m/z 1936.849 which matches the mass of the TDY-containing peptide in a singly-phosphorylated state. MS/MS analysis of this peptide produced only peaks of very low intensity, but could yet identify the tyrosine of the TDY motif as the phosphorylation site. In MALDI-TOF MS analysis of His-LmxMPK3 which had been co-expressed with LmxMKK-D two peaks of very high intensities at m/z 1936.764 and 2016.711 dominated the spectrum. They match the singly- and doubly-phosphorylated TDY-containing peptide, respectively. MS/MS analysis of the singly-phosphorylated peptide actually identified a mixture of peptides with the phosphoryl group situated either on the threonine or the tyrosine residue of the TDY motif. The doubly-phosphorylated peptide contained phosphothreonine and phosphotyrosine in the TDY motif as revealed by MS/MS analysis. For His-LmxMPK3-TDL derived from pJC3MPK3(TDL) no peak corresponding to any phosphorylated LmxMPK3 peptide could be observed. However, when His-LmxMPK3-TDL had been co-expressed with LmxMKK-D a peak of very high intensity appeared at m/z 1886.700 corresponding to the TDL-containing peptide in a singly-phosphorylated state. Subsequent MS/MS analysis confirmed a phosphorylation on the threonine residue of the TDL motif. As for His-LmxMPK3-ADY, a peak of low intensity at m/z 1906.727 was displayed by the MALDI-TOF MS spectrum which matches the mass of the ADY-containing peptide in a singly-phosphorylated state. Indeed, MS/MS analysis could identify the tyrosine of the ADY motif as the phosphorylated residue. When His-LmxMPK3-ADY had been co-expressed with LmxMKK-D the respective peak (at m/z 1906.662) appeared with much higher intensity. Again, the phosphorylation could be clearly located on the tyrosine of the ADY motif by MS/MS analysis.

To summarise, His-LmxMPK3 and the respective ADY mutant performed a weak autophosphorylation on the tyrosine of the TDY motif. Co-expression of His-LmxMPK3 with the constitutively active LmxMKK-D led to a very strong phosphorylation on the threonine and/or the tyrosine of the TDY motif. This result was supported by the MS/MS analysis of the LmxMPK3-TDL and -ADY mutants co-expressed with LmxMKK-D which revealed a strong threonine and a strong tyrosine phosphorylation in the activation motif, respectively.

4.7.2 *In vivo* studies

4.7.2.1 Generation of the different transfection constructs

While *in vitro* studies of the LmxMPK3 activation mechanism had been carried out on LmxMPK3-TDL and LmxMPK3-ADY, *in vivo* studies also included an LmxMPK3-ADL double mutant. Therefore, a PCR was performed on pX3ELmxMPK3 using the oligonucleotides pXPHLEO2 and MPK3-ADL.rev. The produced 5'-end fragment of *LmxMPK3* carrying the ADL mutation was ligated into pCR2.1-TOPO and sequenced. The respective 5'-end

fragments of the LmxMPK3-TDL and -ADY mutants had been generated previously (see 4.7.1.1). An *NruI/Acc65I*-fragment of *LmxMPK3* containing the respective TDY mutation was liberated for each LmxMPK3-TDY mutant.

In parallel, the receiving plasmid was prepared by cloning the ORF of *LmxMPK3* into pX14polNcoIPAC. The plasmid pX1NcoIPACLmxMPK3 which had been generated in 4.7.1.1 should not be used for *in vivo* experiments, since an introduction of a *BspLU11I* restriction site had caused a mutation of the second amino acid residue of LmxMPK3 (H2→Y) (Erdmann *et al.*, 2006) which did not impair the *in vitro* activity of the kinase (Erdmann, diploma thesis, 2004) but might affect its function *in vivo*. Thus, the entire ORF of *LmxMPK3* was amplified from pB5upLmxMPK3ds by performing a PCR with the oligonucleotides mpk3nClaI.for and mpk3cXbaI.rev. After the amplified fragment had been ligated into pCR2.1-TOPO and sequenced, the ORF of *LmxMPK3* was liberated using *EcoRI* and ligated into pX14polNcoIPAC which had been linearised using *MunI*. The obtained plasmid was named pX1bNcoIPACLmxMPK3.

The *NruI/Acc65I*-fragment of *LmxMPK3* containing the different TDY mutations (see above) was ligated into pX1bNcoIPACLmxMPK3 which had been linearised using the same restriction enzymes. The resulting plasmids were named pX3NcoIPACLmxMPK3(TDL), pX4NcoIPACLmxMPK3(ADY) and pX3NcoIPACLmxMPK3(ADL). Those plasmids were cleaved with *NcoI* and *EcoRV* to obtain a cassette which comprised the puromycin resistance marker gene followed by the intergenic region of the *DHFR-TS* gene locus and the ORF of the different *LmxMPK3-TDY* mutants. For control reasons, the transfection should also be carried out with wild type *LmxMPK3*. Therefore, the corresponding *NcoI/EcoRV*-fragment was liberated directly from pX1bNcoIPACLmxMPK3 thus generating the construct with wild type *LmxMPK3*.

Meanwhile, pBE2upds(MPK3) containing the 5'- and 3'-UTR of *LmxMPK3* was linearised using *NheI* and subsequently treated with Klenow enzyme in order to form blunt ends. Afterwards, the linearised plasmid was cleaved with *BspLU11I* and separately ligated with the different cassettes described above. The resulting plasmids contain the respective cassette flanked by the 5'- and 3'-UTR of *LmxMPK3*. The plasmids containing the different LmxMPK3-TDY mutations were named pB4upPACMPK3(TDL)ds, pB2upPACMPK3(ADY)ds, pB8upPACMPK3(ADL)ds and pB2upPACMPK3ds. All plasmids were cleaved with *EcoRV* to generate linear transfection constructs composed of the puromycin resistance marker gene, the *DHFR-TS* intergenic region and the ORF of the different *LmxMPK3-TDY* mutants, all flanked by the 5'- and 3'-UTR of *LmxMPK3*.

4.7.2.2 Transfection and verification of obtained clones

To generate the different LmxMPK3-TDY mutants of *L. mexicana*, the *EcoRV*-fragments derived from pB4upPACMPK3(TDL)ds, pB2upPACMPK3(ADY)ds, pB8upPACMPK3(ADL)ds and pB2upPACMPK3ds were individually transfected into the null mutants $\Delta LmxMPK3$ -/-HN1 and $\Delta LmxMPK3$ -/-PN6. The construct should subsequently replace one of the two different resistance marker genes in the *LmxMPK3* gene locus. This process would occur by the mechanism of homologous recombination supported by the flanking regions of the *LmxMPK3* gene locus. Positive clones were selected using puromycin.

The obtained LmxMPK3-TDL mutants were designated $\Delta LmxMPK3$ -/-HN1+LmxMPK3-TDL K1, 2, 3 and $\Delta LmxMPK3$ -/-PN6+LmxMPK3-TDL K1, 2 and 3. The respective LmxMPK3-ADY mutants were named $\Delta LmxMPK3$ -/-HN1+LmxMPK3-ADY K1, 2, 3 and $\Delta LmxMPK3$ -/-PN6+LmxMPK3-ADY K1, 2 and 3. The generated LmxMPK3-ADL mutants were named $\Delta LmxMPK3$ -/-HN1+LmxMPK3-ADL K1, 2, 3 and $\Delta LmxMPK3$ -/-PN6+LmxMPK3-ADL K1, 2 and 3. Eventually, the obtained wild type controls were designated $\Delta LmxMPK3$ -/-HN1+LmxMPK3-TDY K1 and $\Delta LmxMPK3$ -/-PN6+LmxMPK3-TDY K1, 2 and 3.

Southern blot and immunoblot analysis was carried out in order to verify the generated LmxMPK3-TDY mutants of *L. mexicana*.

Southern blot analysis

The genomic DNA from late log-phase promastigotes of the *L. mexicana* wild type, the null mutants $\Delta LmxMPK3$ -/-HN1 and $\Delta LmxMPK3$ -/-PN6, and the different LmxMPK3-TDY mutants was isolated, cleaved with *HincII* and precipitated. After the cleaved DNA had been separated on an agarose gel and transferred to a nylon membrane, it was probed using a DIG-labelled hybridisation probe which binds within the 3'-UTR of *LmxMPK3* (Erdmann, diploma thesis, 2004). Figure 40 gives a schematic overview of *LmxMPK3*, the different resistance marker genes and the cassette, containing the puromycin resistance marker gene and the different *LmxMPK3*-TDY mutants, in the *LmxMPK3* gene locus.

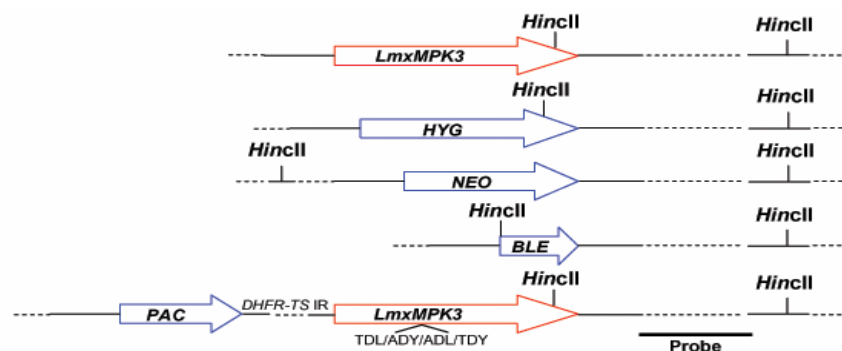


Figure 40: Schematic illustration of *LmxMPK3*, different resistance marker genes and *LmxMPK3*-TDY mutants in *LmxMPK3* gene locus

HYG, hygromycin B resistance marker gene; *NEO*, neomycin resistance marker gene; *BLE*, bleomycin resistance marker gene; *PAC*, puromycin resistance marker gene; IR, intergenic region. The hybridisation site of the probe is indicated.

The band sizes of the Southern blot were expected at about 1.8 kb for *LmxMPK3* or the different *LmxMPK3-TDY* mutants, roughly 1.9 kb for the hygromycin B resistance marker gene (*HYG*), around 3.8 kb for the neomycin resistance marker gene (*NEO*) and about 2.1 kb for the phleomycin resistance marker gene (*BLE*). The calculations were based on sequence informations of the different genes as wells as on previous Southern blot results in which a gene-internal hybridisation probe had been used on *HincII*-cleaved *L. mexicana* wild type genomic DNA (Erdmann, diploma thesis, 2004).

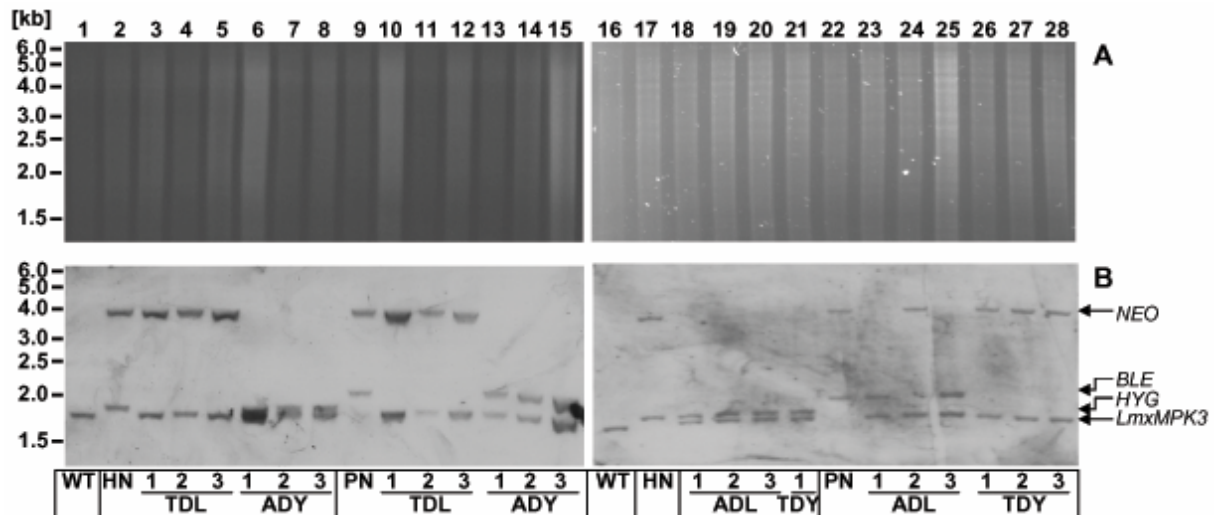


Figure 41: Southern blot of *HincII*-cleaved gDNA from *LmxMPK3-TDY* mutants

A: 0.7% agarose gels; B: Southern blots; 1: *LmxWT*; 2: Δ *LmxMPK3-I-HN1*; 3-5: Δ *LmxMPK3-I-HN1*+*LmxMPK3-TDL* K1-3; 6-8: Δ *LmxMPK3-I-HN1*+*LmxMPK3-ADY* K1-3; 9: Δ *LmxMPK3-I-PN6*; 10-12: Δ *LmxMPK3-I-PN6*+*LmxMPK3-TDL* K1-3; 13-15: Δ *LmxMPK3-I-PN6*+*LmxMPK3-ADY* K1-3; 16: *LmxWT*; 17: Δ *LmxMPK3-I-HN1*; 18-20: Δ *LmxMPK3-I-HN1*+*LmxMPK3-ADL* K1-3; 21: Δ *LmxMPK3-I-HN1*+*LmxMPK3-TDY* K1; 22: Δ *LmxMPK3-I-PN6*; 23-25: Δ *LmxMPK3-I-PN6*+*LmxMPK3-ADL* K1-3; 26-28: Δ *LmxMPK3-I-PN6*+*LmxMPK3-TDY* K1-3.

Figure 41 shows that in each of the tested clones one resistance marker gene had been successfully replaced by the cassette construct containing the different *LmxMPK3-TDY* mutants. This was indicated by the respective band at approximately 1.8 kb. Moreover, the band pattern revealed which of the resistance marker genes had been replaced. While all Δ *LmxMPK3-I-HN1*+*LmxMPK3-TDL* clones had lost *HYG* (lanes 3 to 5), all of the Δ *LmxMPK3-I-HN1*+*LmxMPK3-ADY*, -*ADL* and -*TDY* clones had lost *NEO* (lanes 6 to 8 and 18 to 21). All of the obtained Δ *LmxMPK3-I-PN6*+*LmxMPK3-TDL* and -*TDY* clones had lost *BLE* (lanes 10 to 12 and 26 to 28), whereas the Δ *LmxMPK3-I-PN6*+*LmxMPK3-ADY* clones had lost *NEO* (lanes 13 to 15). As for Δ *LmxMPK3-I-PN6*+*LmxMPK3-ADL*, clones 1 and 3 had lost *NEO* (lanes 23 and 25), whereas clone 2 had lost *BLE* (lane 24).

Immunoblot analysis

To check whether the different LmxMPK3-TDY mutants of *L. mexicana* actually re-express the mutated kinase, immunoblot analysis of total cell lysates from log-phase promastigotes of the different LmxMPK3-TDY mutants was performed using an antiserum against LmxMPK3.

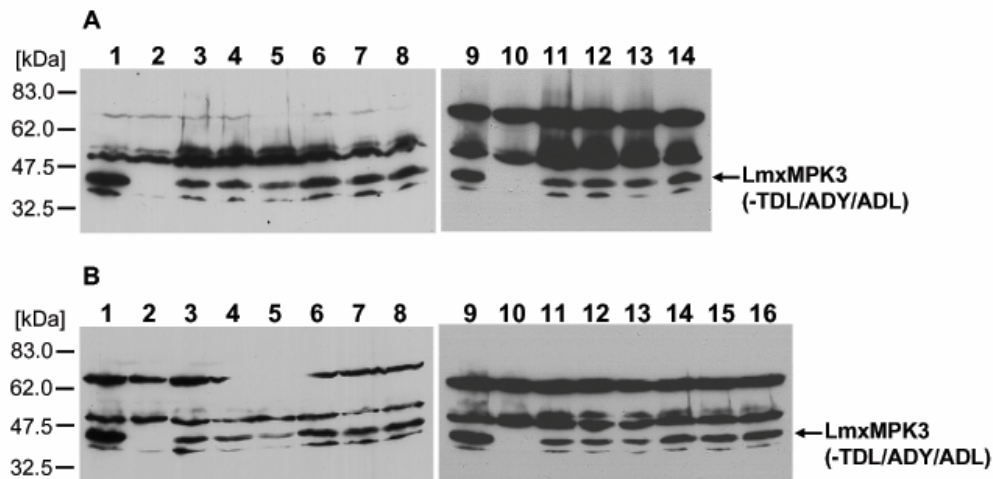


Figure 42: Immunoblots of LmxMPK3 from LmxMPK3-TDY mutants

A: LmxMPK3-TDY mutants derived from $\Delta LmxMPK3-I-HN1$; B: LmxMPK3-TDY mutants derived from $\Delta LmxMPK3-I-PN6$.

A: 1: LmxWT; 2: $\Delta LmxMPK3-I-HN1$; 3-5: $\Delta LmxMPK3-I-HN1$ +LmxMPK3-TDL K1-3; 6-8: $\Delta LmxMPK3-I-HN1$ +LmxMPK3-ADY K1-3; 9: LmxWT; 10: $\Delta LmxMPK3-I-HN1$; 11-13: $\Delta LmxMPK3-I-HN1$ +LmxMPK3-ADL K1-3; 14: $\Delta LmxMPK3-I-HN1$ +LmxMPK3-TDY K1

B: 1: LmxWT; 2: $\Delta LmxMPK3-I-PN6$; 3-5: $\Delta LmxMPK3-I-PN6$ +LmxMPK3-TDL K1-3; 6-8: $\Delta LmxMPK3-I-PN6$ +LmxMPK3-ADY K1-3; 9: LmxWT; 10: $\Delta LmxMPK3-I-PN6$; 11-13: $\Delta LmxMPK3-I-PN6$ +LmxMPK3-ADL K1-3; 14-16: $\Delta LmxMPK3-I-PN6$ +LmxMPK3-TDY K1-3.

Indeed, all of the generated LmxMPK3-TDY mutants of *L. mexicana* successfully re-expressed the mutated kinase as shown in Figure 42A and B. The intensities of the cross reaction bands depended on how often the antiserum had been used before. Each of the immunoblots in Figure 42 displays a sample from the *L. mexicana* wild type for comparison. For all tested clones the protein levels of the LmxMPK3-TDY mutants were lower compared to the LmxMPK3 protein level of the wild type, mostly reaching the levels of the *LmxMPK3* single-allele deletion mutants (see 4.1.2). It was of even greater importance that the protein levels of the different LmxMPK3-TDY mutants were fairly similar in the different clones. Especially clone 3 of the $\Delta LmxMPK3-I-PN6$ +LmxMPK3-TDL mutants displayed a weaker LmxMPK3 band (Figure X42, lane 5). However, also the intensity of the respective cross reaction bands was lower indicating that a smaller amount of cell lysate had been loaded. Hence, the requirements were fulfilled for a comparative analysis of the obtained phenotypes.

4.7.2.3 Measurements of the flagellar lengths of the LmxMPK3-TDY mutants

In 4.4.4 it was shown that the LmxMPK3 activity correlates with the flagellar length of the parasite. Thus, measurements of flagellar lengths were carried out for the generated LmxMPK3-TDY mutants in order to elucidate which of the potential phosphorylation sites in the TDY motif are essential for the activation of LmxMPK3 *in vivo*.

	average flagellar length [μm]	standard deviation [μm]
$\Delta\text{MPK3HN1+MPK3-TDL K1}$	1.8	0.7
$\Delta\text{MPK3HN1+MPK3-TDL K2}$	1.7	0.6
$\Delta\text{MPK3HN1+MPK3-TDL K3}$	1.8	0.7
$\Delta\text{MPK3HN1+MPK3-ADY K1}$	2.5	0.9
$\Delta\text{MPK3HN1+MPK3-ADY K2}$	2.4	1.1
$\Delta\text{MPK3HN1+MPK3-ADY K3}$	2.6	1.0
$\Delta\text{MPK3HN1+MPK3-ADL K1}$	1.1	0.5
$\Delta\text{MPK3HN1+MPK3-ADL K2}$	1.1	0.6
$\Delta\text{MPK3HN1+MPK3-ADL K3}$	1.1	0.7
$\Delta\text{MPK3HN1+MPK3-TDY K1}$	7.7	6.0
$\Delta\text{MPK3PN6+MPK3-TDL K1}$	2.4	0.8
$\Delta\text{MPK3PN6+MPK3-TDL K2}$	2.6	1.0
$\Delta\text{MPK3PN6+MPK3-TDL K3}$	2.6	0.9
$\Delta\text{MPK3PN6+MPK3-ADY K1}$	2.3	0.8
$\Delta\text{MPK3PN6+MPK3-ADY K2}$	2.1	0.7
$\Delta\text{MPK3PN6+MPK3-ADY K3}$	2.7	0.8
$\Delta\text{MPK3PN6+MPK3-ADL K1}$	2.5	0.9
$\Delta\text{MPK3PN6+MPK3-ADL K2}$	2.3	0.9
$\Delta\text{MPK3PN6+MPK3-ADL K3}$	2.2	0.7
$\Delta\text{MPK3PN6+MPK3-TDY K1}$	10.9	4.1
$\Delta\text{MPK3PN6+MPK3-TDY K2}$	10.5	3.7
$\Delta\text{MPK3PN6+MPK3-TDY K3}$	11.3	3.6

Table 7: Overview of average flagellar lengths from LmxMPK3-TDY mutants

As Table 7 and Figure 43 show, only LmxMPK3 containing the TDY wild type activation motif could restore long flagella in the *LmxMPK3* null mutants. The LmxMPK3-TDL, -ADY and -ADL mutants derived from $\Delta\text{LmxMPK3-I-HN1}$ and $\Delta\text{LmxMPK3-I-PN6}$ displayed flagella still resembling those of the null mutants as depicted by the mean values (Table 7) and the distribution of flagellar lengths (Figure 43A and E). Differences between those LmxMPK3-TDL, -ADY and -ADL mutants were insignificant. In contrast, $\Delta\text{LmxMPK3-I-PN6+LmxMPK3-TDY K1, 2}$ and 3 could indeed regenerate flagella of wild type length. The respective mean values of 10.5 to 11.3 μm (Table 7) as well as the distribution of flagellar lengths (Figure 43F) are consistent with the wild type. For $\Delta\text{LmxMPK3-I-HN1+LmxMPK3-TDY K1}$ the mean value of 7.7 μm resembled more that of the *LmxMPK3* add back mutants, though the overall distribution of flagellar lengths was much broader compared to the *LmxMPK3* add back mutants. Additionally, 39% of measured flagella actually did not exceed 4.0 μm in length. However, it has to be mentioned that this measurement was carried out after the clone had been frozen as a stablate and thawed again for culturing. The decrease in flagella lengths after freezing and thawing of stabilates has already been described in 4.4.3. Nevertheless,

the lengths of most flagella from $\Delta LmxMPK3$ -/-HN1+LmxMPK3-TDY K1 clearly exceeded those of the respective LmxMPK3-TDL, -ADY and -ADL mutants. In conclusion, only LmxMPK3 containing the TDY wild type activation motif could restore long flagella.

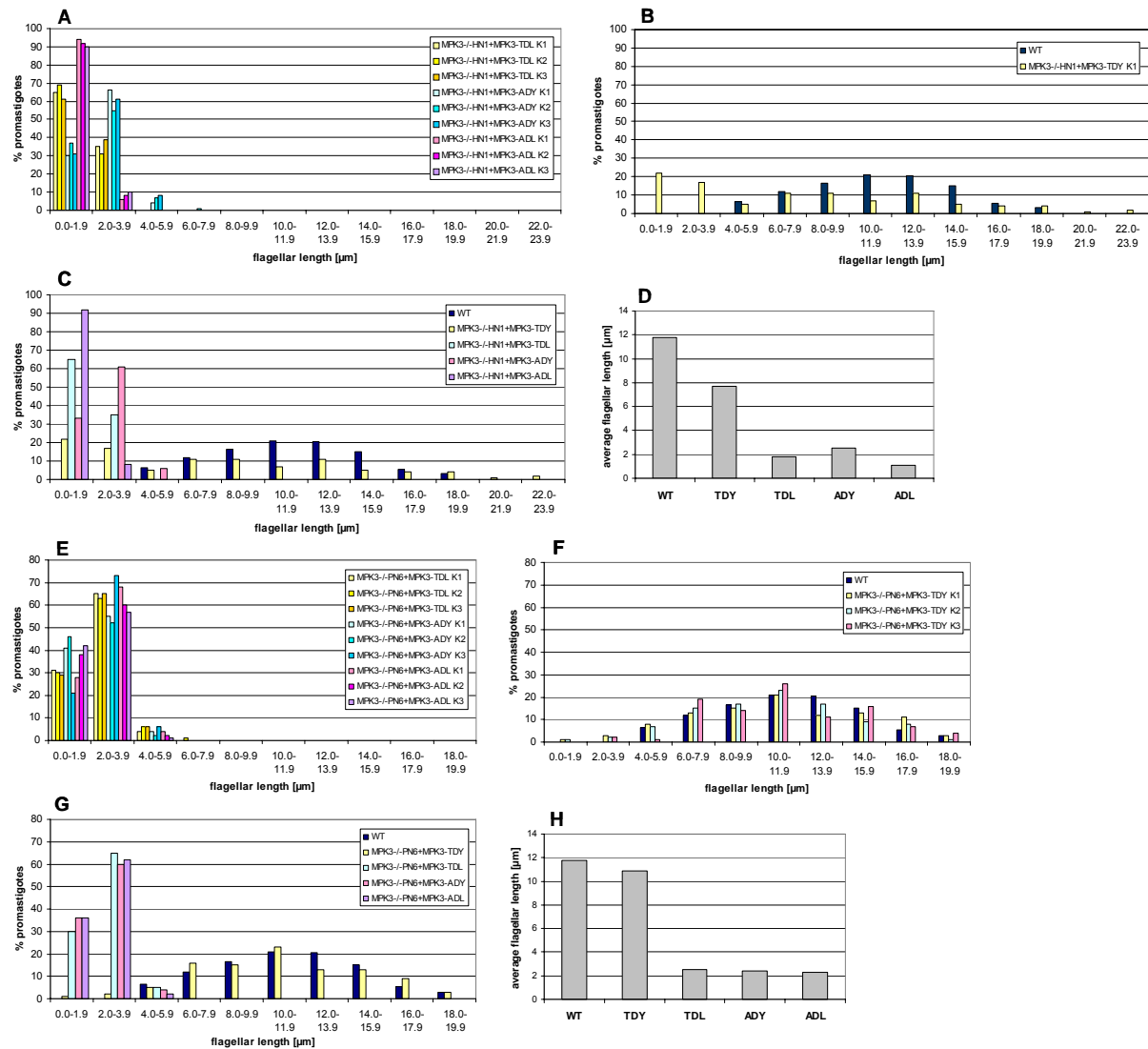


Figure 43: Histograms of flagellar lengths from *L. mexicana* wild type and LmxMPK3-TDY mutants

A, B, E and F: distribution of flagellar lengths; C and G: average distribution of flagellar lengths; D and H: average flagellar lengths.

A: $\Delta LmxMPK3$ -/-HN1+LmxMPK3-TDL K1-3, $\Delta LmxMPK3$ -/-HN1+LmxMPK3-ADY K1-3 and $\Delta LmxMPK3$ -/-HN1+LmxMPK3-ADL K1-3; B: LmxWT and $\Delta LmxMPK3$ -/-HN1+LmxMPK3-TDY K1; C and D: LmxWT, $\Delta LmxMPK3$ -/-HN1+LmxMPK3-TDY, -TDL, -ADY and -ADL; E: $\Delta LmxMPK3$ -/-PN6+LmxMPK3-TDL K1-3, $\Delta LmxMPK3$ -/-PN6+LmxMPK3-ADY K1-3 and $\Delta LmxMPK3$ -/-PN6+LmxMPK3-ADL K1-3; F: LmxWT and $\Delta LmxMPK3$ -/-PN6+LmxMPK3-TDY K1-3; G and H: LmxWT, $\Delta LmxMPK3$ -/-PN6+LmxMPK3-TDY, -TDL, -ADY and -ADL.

4.8 Substrate search for LmxMPK3

The LmxMKK/LmxMPK3-pair revealed the first protein interaction of a signalling cascade which had been described for *Leishmania* (Erdmann *et al.*, 2006). Having identified LmxMKK as the activator of LmxMPK3 it was now of further interest to search for LmxMPK3 substrates which would elucidate the physiological role of LmxMPK3 and the signalling pathway in which it is involved.

Most of the MAP kinase cascades in higher eukaryotes typically culminate in the activation of transcription factors which directly regulate gene expression on the transcriptional level. Such factors have not been identified in *Leishmania* and it is therefore assumed that gene expression is regulated on the posttranscriptional level. This could possibly be mediated by molecules influencing the transport, processing, modification or turnover of RNA as well as the translation, modification, transport or turnover of the respective protein. Besides transcription factors also cytosolic protein kinases and other cytosolic enzymes could be identified as MAP kinase substrates in higher eukaryotes. In addition, the association of some MAP kinases of higher eukaryotes with microtubules suggests also a role in the reorganisation of the cytoskeleton. Hence, there is actually a wide variety of molecules which can be considered as potential MAP kinase substrates in *Leishmania*.

Taking into account that LmxMPK3 is essential for the outgrowth of the flagellum, the maintenance of its length and the correct assembly of the PFR, it is likely that the LmxMPK3 substrate either regulates the gene expression of components which are involved in these processes or that it is a flagellar protein itself. The latter could either be a structural flagellar subunit or a component which is involved in the interaction, transport or modification of other flagellar subunits. For instance, the substrate could either support the anterograde or inhibit the retrograde intraflagellar transport (IFT) of flagellar subunits.

In order to identify substrates of LmxMPK3 two generally different approaches were used. On the one hand, likely candidates were tested either by using available antisera against the respective proteins in immunoblot analyses or by testing the respective affinity purified candidate proteins in kinase assays. Each of those assays was focused solely on one single candidate protein. The criteria for being a likely candidate were a predicted flagellar localisation, the presence of potential phosphorylation sites within the protein and ideally a hypothetical role in flagellar assembly. On the other hand, the entire proteome should be screened either by subjecting *Leishmania* lysates to kinase assays or by using the computer programme PREDIKIN (Brinkworth *et al.*, 2003) for an *in silico* substrate search. Subsequently, identified candidates would be verified by subjecting the recombinantly expressed proteins to kinase assays with activated LmxMPK3.

4.8.1 PFR-2 as a potential LmxMPK3 substrate

Analysis of the *LmxMPK3* null mutant phenotype had revealed a severely impaired assembly of the PFR. The observed flagella contained either only residual PFR or no PFR next to the axoneme (see 4.1.4). Immunoblot analysis using an antiserum recognising PFR-2, one of the two main protein subunits of the PFR, showed that the null mutants contained roughly 4 times less PFR-2 per micrometer of flagellar length compared to the wild type (see 4.1.5.2). Those findings bear the possibility that PFR-2 is a substrate of LmxMPK3. Phosphorylation of PFR-2 by LmxMPK3 could therefore regulate its transport, assembly or turnover.

The *PFR-2* gene of *L. mexicana* had been isolated and extensively characterized by Moore *et al.* in 1996. It is arranged in the genome as a tandem array of three identical genes designated *PFR-2A*, *PFR-2B* and *PFR-2C*. Although there is no typical MAP kinase phosphorylation motif (SP or TP) present in the PFR-2 amino acid sequence, its substrate function was tested, since it is not known to date, if phosphorylations carried out by MAP kinases are actually restricted to those motifs in *Leishmania*. The PFR-2C amino acid sequence can be viewed in 8.1.2.

4.8.1.1 Immunoblot analysis of PFR-2 in *L. mexicana* phosphoprotein fractions

Phosphoproteins were purified from approximately 2×10^9 logarithmically growing promastigotes of the *L. mexicana* wild type and the null mutant $\Delta LmxMPK3$ -/-HN1 using the PhosphoProtein Purification Kit (Qiagen). Subsequently, the soluble fractions of the cell lysates (unphosphorylated and phosphorylated proteins), the flow throughs (unphosphorylated proteins) and the phosphoprotein eluates were subjected to immunoblot analysis using the L8C4 monoclonal antibody recognising PFR-2 (see also 4.1.5).

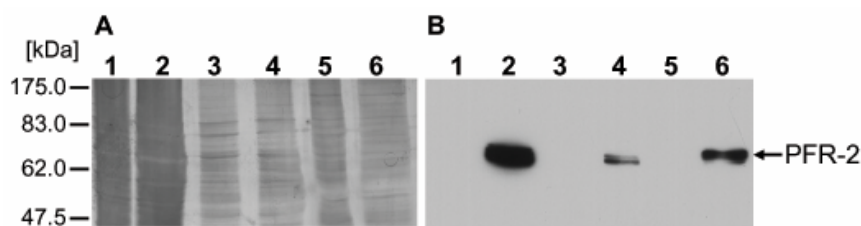


Figure 44: Immunoblot of PFR-2 in unphosphorylated and phosphorylated protein fractions from *L. mexicana* wild type and *LmxMPK3* null mutant

A: Silver-stained 10% SDS-PA gel; B: Immunoblot of PFR-2; 1: $\Delta LmxMPK3$ -/-HN1 cell lysate; 2: LmxWT cell lysate; 3: $\Delta LmxMPK3$ -/-HN1 flow through; 4: LmxWT flow through; 5: $\Delta LmxMPK3$ -/-HN1 phosphoprotein eluate; 6: LmxWT phosphoprotein eluate.

The immunoblot in Figure 44B clearly shows that a fraction of PFR-2 is phosphorylated in the wild type (lane 6). In contrast, there is no band visible in lane 5 showing the phosphoprotein eluate of the *LmxMPK3* null mutant. However, PFR-2 is not even detectable in the cell lysate of the null mutant (lane 1) which contains the highest protein concentration compared to the flow through and the eluate. This reflects the results of chapter 4.1.5 in which it had been

shown that PFR-2 is much less abundant in the *LmxMPK3* null mutants. Although this approach could not reveal the phosphorylation state of PFR-2 in the *LmxMPK3* null mutant, it could yet identify PFR-2 as a phosphorylated protein in the wild type.

4.8.2 A PFR-2 mRNA regulating protein as a potential *LmxMPK3* substrate

As it had been described in chapter 4.1.5.2, promastigotes of the *LmxMPK3* null mutants contain roughly 20 times less PFR-2 than the wild type. A mere reduction of the flagellar length would only lead to 5 times less PFR-2. This down-regulation of the PFR-2 expression could either take place on the mRNA level or the protein level of PFR-2.

Interestingly, an AU-rich *cis*-regulatory element of 10 nucleotides had been identified in the 3'-UTR of all *PFR* genes in *L. mexicana* strongly resembling the AU-rich elements (AREs) of higher eukaryotes. It had been shown that this element leads to a 10-fold down-regulation of the *PFR* mRNA amounts in amastigotes by inducing mRNA degradation (Mishra *et al.*, 2003). It is therefore possible that this process is mediated by an RNA binding protein which is constitutively expressed but only available for binding in amastigotes. The selective binding properties could be mediated by phosphorylation of the protein and *LmxMPK3* could be the responsible kinase.

4.8.2.1 RT-PCR analysis of *PFR-2* mRNA in *LmxMPK3* null mutants

RT-PCRs were carried out on total RNA isolates of the *LmxMPK3* null mutants $\Delta LmxMPK3$ -I-HN1 and $\Delta LmxMPK3$ -I-PN6 using the *PFR-2C*-specific oligonucleotides PFR2C_1.for and PFR2C_1.rev in order to quantify the *PFR-2* mRNA amounts (see 8.1.2 for the *PFR-2C* nucleotide sequence). In parallel, RT-PCRs were performed in the same way using total RNA isolates of the *L. mexicana* wild type and the *LmxMKK* null mutants $\Delta LmxMKK$ -I-K3 and $\Delta LmxMKK$ -I-K4. All reactions were also carried out using the glutamine synthetase (GS)-specific oligonucleotides gln6.sense and gln9.rev to serve as quantity controls.

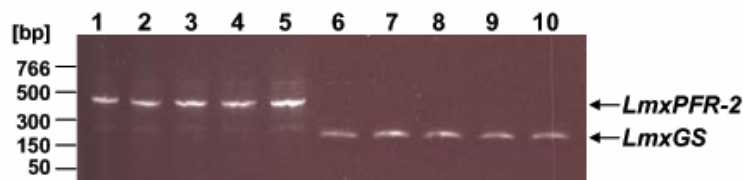


Figure 45: Quantification of *PFR-2* mRNA in *L. mexicana* wild type, *LmxMPK3* null mutants and *LmxMKK* null mutants

1-5: RT-PCR with *PFR-2C*-specific oligonucleotides; 6-10: RT-PCR with GS-specific oligonucleotides; 1 and 6: *LmxWT*; 2 and 7: $\Delta LmxMPK3$ -I-HN1; 3 and 8: $\Delta LmxMPK3$ -I-PN6; 4 and 9: $\Delta LmxMKK$ -I-K3; 5 and 10: $\Delta LmxMKK$ -I-K4.

Lanes 6 to 10 of Figure 45 clearly show that equal RNA amounts had been used in the different RT-PCRs. However, also the band corresponding to the *PFR-2* amplicate appears

equally strong in lanes 1 to 5 which indicates that the *PFR-2* mRNA amounts in the *LmxMPK3* and *LmxMKK* null mutants do not differ from that of the wild type. Thus, neither *LmxMPK3* nor *LmxMKK* are involved in the regulation of *PFR-2* mRNA stability or in the transcription of the *PFR-2* genes. Obviously, the down-regulation of the *PFR-2* expression takes place on the protein level and could be due to an impaired translation, modification, turnover or transport of *PFR-2*.

Therefore, the next chapter describes the analysis of an OSM3-like kinesin which has a potential role in transporting flagellar subunits from the cell body into the flagellum.

4.8.3 An OSM3-like kinesin as a potential *LmxMPK3* substrate

Since the regulation of flagellar length is impaired in the *LmxMPK3* null mutants, it is possible that the substrate of *LmxMPK3* is directly involved in the intraflagellar transport (IFT) of flagellar proteins. IFT has been shown to be the mechanism responsible for flagellar length regulation (Rosenbaum and Witman, 2002; Rosenbaum, 2003). The ubiquitous motor proteins driving the anterograde IFT are kinesins which belong to the kinesin-2 family (Rosenbaum and Witman, 2002). Analysis of the IFT in the chemosensory cilia of *Caenorhabditis elegans* revealed that besides kinesin-II a second kinesin-2 family member called OSM-3 drives the anterograde IFT as a homodimeric complex (Signor *et al.*, 1999; Snow *et al.*, 2004).

The *L. major* genome DB (Ivens *et al.*, 2005) reveals two putative OSM-3-like kinesins, LmjF17.0800 and LmjF32.0680. They contain an N-terminal motor, an internal stalk and a short C-terminal tail domain. Dimerisation occurs most likely by forming homo- or heterodimeric coiled coils between the stalk regions as it had been revealed for kinesin holoenzymes in other organisms (Rashid *et al.*, 1995). Kinesins have been shown to be regulated via specific phosphorylation events (Wordeman, 2005) and indeed, both *L. major* OSM-3-like kinesins contain potential MAP kinase phosphorylation sites in their motor and stalk domains.

To test an OSM-3-like kinesin as a potential substrate candidate of *LmxMPK3*, the motor domain of the *L. mexicana* homologue of LmjF32.0680, designated *LmxKin32*, was cloned for recombinant expression as a GST-fusion protein (see 8.1.3 for the nucleotide and amino acid sequence of the *LmxKin32* motor domain). The cloned domain contains a PSSP and an SP motif with the potential phosphorylation site at S232 and S293, respectively. The fusion protein was subsequently tested in kinase assays with *in vitro*-activated GST-*LmxMPK3*.

4.8.3.1 Generation of the expression construct

To generate a construct for recombinant expression of the GST-tagged LmxKin32 motor domain, a PCR was performed on genomic DNA of the *L. mexicana* wild type using the oligonucleotides Kin320680_1.for and Kin320680_1.rev which were based on the LmjF32.0680 nucleotide sequence. The amplified 1049 bp-fragment was ligated into pCR2.1-TOPO and three clones were sequenced yielding a 100% identical nucleotide sequence which was 96% identical to the respective *L. major* sequence. Moreover, the translated sequences of the LmxKin32 and LmjF32.0680 motor domains are 100% identical to each other. The amplified fragment was liberated using *Nco*I and *Hind*III and cloned into pGEX-KG(-P) which had been linearised using the same restriction enzymes. pGEX-KG(-P) is a derivative of the expression vector pGEX-KG in which three nucleotides had been removed to delete the proline residue of an SP motif which is situated directly C-terminally to the thrombin cleavage site of the GST fusion protein (John von Freyend, unpublished). This avoids the serine being recognised as a MAP kinase phosphorylation site which would make the interpretation of kinase assays very difficult. The only other SP motif in the GST-tag is located N-terminally to the thrombin cleavage site and thus can be removed together with the GST-tag by cleavage with thrombin. The resulting expression vector containing the 5'-end fragment of *LmxKin32* was named pGEX-KG(-P)1LmxKin32.

4.8.3.2 Recombinant expression and affinity purification of GST-LmxKin32

The plasmid pGEX-KG(-P)1LmxKin32 was transformed into *E. coli* XL1-Blue cells which were subsequently used to express the fusion protein at 18°C overnight. The cells were lysed by sonication and the fusion protein was purified on glutathione sepharose. After the eluted protein had been quantified using the Bradford method, 2 µg of GST-LmxKin32 were analysed by SDS-PAGE (Figure 46).

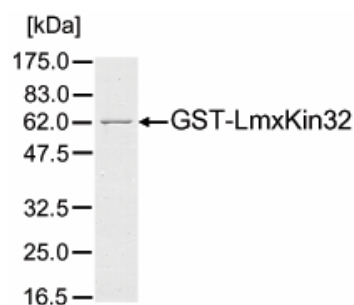


Figure 46: SDS-PAGE of affinity purified GST-LmxKin32
Coomassie-stained 12% SDS-PA gel.

Figure 46 shows a clear band corresponding to GST-LmxKin32 at the expected molecular mass (65.5 kDa) indicating that the recombinant expression and affinity purification of the fusion protein was successful.

4.8.3.3 Kinase assays with GST-LmxKin32 and *in vitro*-activated GST-LmxMPK3

To test whether the motor domain of LmxKin32 is phosphorylated by activated LmxMPK3, kinase assays were carried out with GST-LmxKin32 and *in vitro*-activated GST-LmxMPK3. The GST-tag was cleaved from LmxKin32 using thrombin to remove the potential MAP kinase phosphorylation motif located N-terminally to the thrombin cleavage site (see 4.8.3.1). Moreover, the LmxKin32 motor domain lacking the GST-tag (with a remaining molecular mass of 38.1 kDa) separates more efficiently from GST-LmxMPK3 in SDS-PAGE. Since it had been observed that the motor domain of LmxKin32 retains a high ATPase activity and leads to an extensive cleavage of ATP (Erdmann, unpublished data), the kinesin was heat-inactivated at 65°C for 20 min. Subsequently, 2 µg of thrombin-cleaved and heat-inactivated GST-LmxKin32 were tested in a kinase assay with 2 µg of *in vitro*-activated GST-LmxMPK3 at 27°C using a reaction buffer with 10 mM Mn²⁺ and pH 6.5. The non-radioactive pre-incubation of GST-LmxMPK3 with GST-LmxMCK-D for the *in vitro* activation of LmxMPK3 was carried out as described in 4.6.1 and also included a control assay lacking GST-LmxMCK-D. The radioactive kinase assays were additionally performed with MBP to test whether the *in vitro* activation was successful.

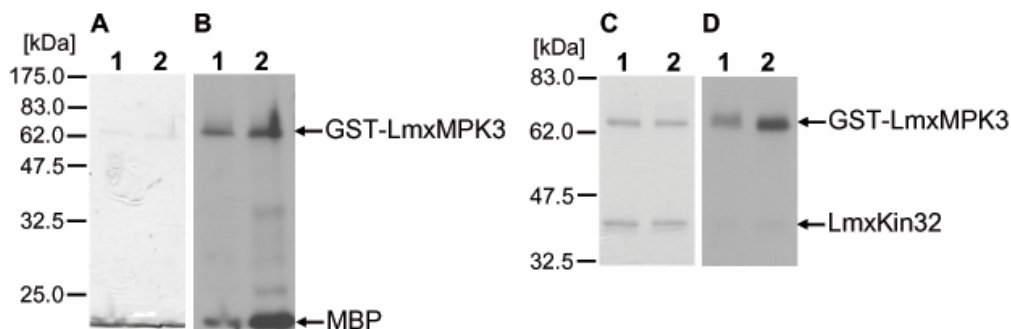


Figure 47: Kinase assays with GST-LmxKin32 and *in vitro*-activated GST-LmxMPK3

A: Coomassie-stained 12% SDS-PAGE gel; C: Coomassie-stained 10% SDS-PAGE gel; B and D: Autoradiographs after 66h of exposure.

A and B: 1: GST-LmxMPK3 + MBP; 2: GST-LmxMPK3/(GST-LmxMCK-D) + MBP.

C and D: 1: GST-LmxMPK3 + LmxKin32; 2: GST-LmxMPK3/(GST-LmxMCK-D) + LmxKin32.

Brackets indicate that only traces of the protein are present.

Figure 47B shows that the MBP phosphorylation is much stronger in lane 2 compared to lane 1 and thus indicates that the *in vitro* activation of GST-LmxMPK3 by GST-LmxMCK-D was successful. However, there was only a very faint and hardly visible signal corresponding to LmxKin32 in Figure 47D, lane 2 which was insignificant compared to the MBP phosphorylation. As a result, the OSM-3-like kinesin LmxKin32 is most likely no substrate of LmxMPK3.

4.8.4 The outer dynein arm docking complex (ODA-DC) subunit DC2 as a potential LmxMPK3 substrate

In 2005, Harder *et al.* generated an *L. donovani* null mutant lacking the gene of the 70 kDa subunit of the outer dynein arm docking complex (ODA-DC) termed LdDC2. Interestingly, the phenotype of the *LdDC2* null mutant strongly resembled that of the *LmxMPK3* null mutant. Likewise the *LmxMPK3* null mutant, the promastigotes of the *LdDC2* null mutant displayed flagella severely reduced in length and cell bodies which were oval-shaped and smaller compared to the wild type suggesting that LmxDC2 could be a substrate of LmxMPK3. Indeed, the *L. donovani* as well as the 100% identical *L. major* homologue CAB55364 (Ivens *et al.*, 2005) and the 94% identical *L. mexicana* homologue (*Leishmania mexicana* genome project) contain three potential MAP kinase SP phosphorylation motifs in the C-terminal part of the protein with the potential phosphorylation sites at S493, S515 and S532. An alignment of the LmjDC2 and LmxDC2 amino acid sequences can be viewed in 8.1.4.

The *Chlamydomonas reinhardtii* homologue of LdDC2, termed CrDC2, had been characterised as part of the ODA-DC by Takada *et al.* in 2002. This complex was shown to consist of three subunits (DC1, DC2 and DC3) and to be responsible for binding of outer arm dynein to the A-tubules of the axonemal outer microtubule doublets.

4.8.4.1 Immunoblot analysis of LmxDC2 in *L. mexicana* phosphoprotein fractions

The fractions of the phosphoprotein purification from the *L. mexicana* wild type and the null mutant Δ *LmxMPK3*-I-HN1 promastigotes described in 4.8.1.1 were subjected to immunoblot analysis using an antiserum against LdDC2.

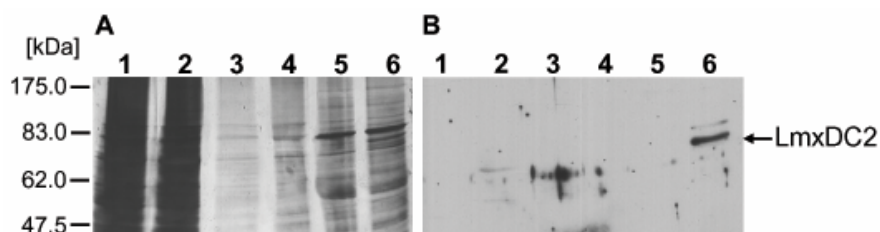


Figure 48: Immunoblot of LmxDC2 in unphosphorylated and phosphorylated protein fractions from *L. mexicana* wild type and *LmxMPK3* null mutant

A: Silver-stained 10% SDS-PA gel; B: Immunoblot of LmxDC2; 1: Δ *LmxMPK3*-I-HN1 cell lysate; 2: LmxWT cell lysate; 3: Δ *LmxMPK3*-I-HN1 flow through; 4: LmxWT flow through; 5: Δ *LmxMPK3*-I-HN1 phosphoprotein eluate; 6: LmxWT phosphoprotein eluate.

The immunoblot in Figure 48B clearly shows that LmxDC2 is phosphorylated in the wild type (lane 6). In contrast, no band can be observed in lane 5 showing the phosphoprotein eluate of the *LmxMPK3* null mutant. To interpret this result the ratio of LmxDC2 protein amounts in the cell lysates of the *LmxMPK3* null mutant and the wild type should be considered. Like PFR-2, LmxDC2 is a flagellar component and therefore could be much less abundant in the short-flagellated *LmxMPK3* null mutants. Unfortunately, LmxDC2 was neither detectable in

the cell lysates nor in the flow throughs which only showed some weak cross reaction bands. Although the phosphorylation state of LmxDC2 could not be assessed in the *LmxMPK3* null mutant, LmxDC2 was found to be extensively phosphorylated in the wild type.

4.8.4.2 Kinase assays with His-LdDC2 and *in vivo*-activated His-LmxMPK3

To test whether DC2 is phosphorylated by LmxMPK3, kinase assays were carried out with His-LdDC2 and *in vivo*-activated His-LmxMPK3. The reason for using the *L. donovani* homologue of DC2 was that it had already been cloned into the expression vector pJC45 (Harder, PhD thesis, 2005). Moreover, LdDC2 and LmxDC2 reveal a high percentage of amino acid identities (94%) in which the potential MAP kinase SP phosphorylation motifs are conserved (see 8.1.4). The high percentage of amino acid identities is also reflected by the fact that an antiserum against LdDC2 also recognised the *L. mexicana* homologue (see 4.8.4.1).

To purify His-LdDC2 the expression vector pJC45LdDC2 was transformed into *E. coli* pAPlac cells which were subsequently used to express the protein at 37°C for 2h. The cells were lysed by sonication and His-LdDC2 was purified on Co²⁺ sepharose.

Subsequently, approximately 1 µg His-LdDC2 was tested in a kinase assay with 2 µg of *in vivo*-activated His-LmxMPK3 at 27°C using a reaction buffer with 10 mM Mn²⁺ and pH 6.5. In parallel, the same kinase assays were carried out either using non-activated LmxMPK3 or lacking LmxMPK3. The kinase assays were additionally performed with MBP to test whether the *in vivo* activation of LmxMPK3 was successful.

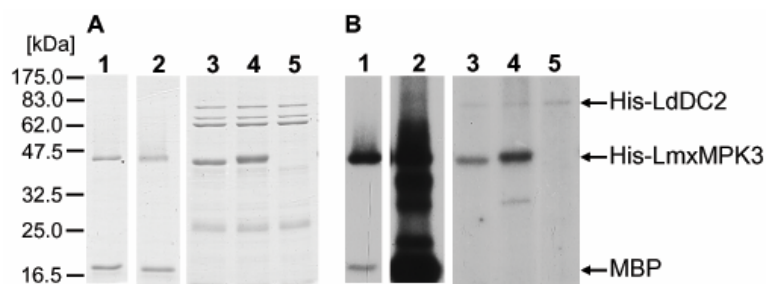


Figure 49: Kinase assays with His-LdDC2 and *in vivo*-activated His-LmxMPK3

A: Coomassie-stained 12% SDS-PA gel; B: Autoradiograph after 66h of exposure.

1: His-LmxMPK3 + MBP; 2: His-LmxMPK3(LmxMKK-D) + MBP; 3: His-LmxMPK3 + His-LdDC2; 4: His-LmxMPK3(LmxMKK-D) + His-LdDC2; 5: His-LdDC2.

Brackets indicate that the protein was only present during co-expression.

Figure 49B shows that the MBP phosphorylation is much stronger in lane 2 compared to lane 1 and thus indicates that the *in vivo* activation of His-LmxMPK3 by LmxMKK-D was successful. The slight reduction of autophosphorylation of LmxMPK3 in Figure 49B, lanes 3 and 4 results from higher concentrations of imidazole, since high volumes of the His-LdDC2 eluate had been used in those assays. This issue had been commented on in 4.6.2.4. There is a very faint signal corresponding to His-LdDC2 at the expected molecular mass (ca.

73 kDa) in Figure 49B, lanes 3 to 5. The fact that this signal is equally strong regardless of the presence or absence of (activated) LmxMPK3 indicates that the weak phosphorylation of HisLdDC2 does not originate from LmxMPK3. In conclusion, the ODA-DC subunit LmxDC2 is most likely no substrate of LmxMPK3.

4.8.5 Glutamine synthetase as a potential LmxMPK3 substrate

Wagner *et al.* analysed the phosphoproteome of *Chlamydomonas reinhardtii* in 2006 and could identify 32 flagellar phosphoproteins by a comparative analysis with the already known subproteome from the flagellum of *C. reinhardtii* (Pazour *et al.*, 2005). The cytosolic isoform of glutamine synthetase (GS1) could be identified among the flagellar phosphoproteome. In *C. reinhardtii* this enzyme is known to be involved in ammonium assimilation, the regulation of nitrate assimilation (Cullimore and Sims, 1981) and glutamine production. It had been shown that *C. reinhardtii* GS1 is phosphorylated by a Ca^{2+} - and calmodulin-dependent protein kinase and that it binds to 14-3-3 proteins which are highly conserved among eukaryotes and participate in protein-protein interaction processes and signal transduction cascades (Fertl, 1996; Finnie *et al.*, 1999). However, neither phosphorylation nor 14-3-3 binding led to a change in GS catalytic activity (Pozuelo *et al.*, 2000). Indeed, the canonical 14-3-3-binding motif RSXS*X(P) (in which S* is the potential phosphorylation site) is present in the *C. reinhardtii* GS1 amino acid sequence. However, the phosphopeptide identified by Wagner *et al.* did not contain this 14-3-3-binding motif. Instead, T326 and S328 could be identified as phosphorylation sites within the analysed phosphopeptide.

The respective threonine residue can also be found in the glutamine synthetase of *L. mexicana* (Wiese *et al.*, unpublished data) and *L. major* (Ivens *et al.*, 2005) whereas the respective serine residue is absent in both proteins. The 14-3-3-binding motif is altered to RSKDR in both *Leishmania* species and thus lacks the conserved phosphorylation site. However, there are three conserved typical MAP kinase S/TP phosphorylation motifs in the *L. mexicana* and *L. major* protein at T197, T359 and S366. The amino acid numbering was adjusted to *L. mexicana* GS since alignment of *L. major* GS with the *C. reinhardtii* and *L. mexicana* amino acid sequences strongly suggests that annotation of the ORF in the *L. major* genome DB was incorrect. The actual start codon seems to be the sixth ATG triplet downstream and in frame with the reported one. An alignment of the *L. mexicana*, *L. major* and *C. reinhardtii* GS amino acid sequences can be viewed in 8.1.5.

4.8.5.1 Immunoblot analysis of LmxGS in *L. mexicana* phosphoprotein fractions

To test LmxGS as an LmxMPK3 substrate the fractions of the phosphoprotein purification from the *L. mexicana* wild type and the null mutant $\Delta\text{LmxMPK3}/\text{-HN1}$ promastigotes

described in 4.8.1.1 were subjected to immunoblot analysis using an antiserum against LmxGS.

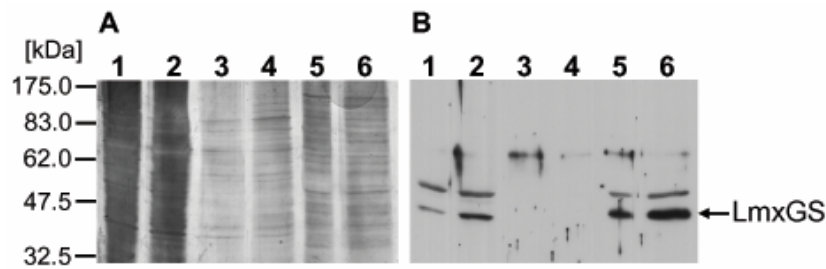


Figure 50: Immunoblot of LmxGS in unphosphorylated and phosphorylated protein fractions from *L. mexicana* wild type and *LmxMPK3* null mutant

A: Silver-stained 10% SDS-PAGE gel; B: Immunoblot of LmxGS; 1: $\Delta LmxMPK3$ -HN1 cell lysate; 2: LmxWT cell lysate; 3: $\Delta LmxMPK3$ -HN1 flow through; 4: LmxWT flow through; 5: $\Delta LmxMPK3$ -HN1 phosphoprotein eluate; 6: LmxWT phosphoprotein eluate.

The immunoblot in Figure 50B shows that LmxGS is phosphorylated in the wild type (lane 6) as well as in the *LmxMPK3* null mutant (lane 5). The signal for the null mutant seems to be slightly weaker compared to the wild type. However, the band corresponding to LmxGS also appears with lower intensity in the cell lysates of the *LmxMPK3* null mutant (lane 1) compared to the wild type (lane 2). The slight reduction of the LmxGS protein amount in the short-flagellated null mutant could be due to its partially flagellar localisation. In conclusion, LmxGS does not seem to be solely located in the flagellum but also to a great extent in the cytoplasm of the cell body. Moreover, LmxGS is strongly phosphorylated in the wild type. Since the level of phosphorylation did not decrease in the absence of LmxMPK3, it is likely that LmxGS is not a substrate of LmxMPK3.

4.8.6 Kinase assays with *in vitro*-activated GST-LmxMPK3 on *Leishmania* lysates

A direct approach for identifying protein kinase substrates is the incubation of cell lysates from the organism of interest with the respective recombinantly expressed and purified protein kinase in the presence of radioactively labelled ATP (Knebel *et al.*, 2001). After separation of the samples via SDS-PAGE phosphorylated proteins can be visualised by exposing X-ray films to the dried gels.

To screen the *Leishmania* proteome for LmxMPK3 substrates, *Leishmania* lysates were obtained from 1×10^9 promastigotes of the *L. mexicana* wild type and the null mutant $\Delta LmxMPK3$ -HN1. The lysates were subjected to gel filtration chromatography to remove cellular ATP, ADP and other small molecules. Radioactive kinase assays were subsequently carried out with 120 μ g of the desalted cell extracts and 4 μ g of *in vitro*-activated GST-LmxMPK3. The non-radioactive pre-incubation of GST-LmxMPK3 with GST-LmxMCK-D for the *in vitro* activation of LmxMPK3 was carried out as described in 4.6.1. A radioactive control assay was performed with MBP to test whether the *in vitro* activation of GST-

LmxMPK3 was successful. The radioactive kinase assays containing the cell extracts were carried out in the presence and absence of LmxMPK3 to identify which signals of phosphorylation reactions were caused by LmxMPK3 and which by cellular protein kinases in the lysates. The reason for testing not only lysates of the wild type but also of the *LmxMPK3* null mutant is the assumption that the LmxMPK3 substrate is not - or at least less - phosphorylated in cells lacking LmxMPK3 and thus allows a stronger incorporation of radioactively labelled phosphate.

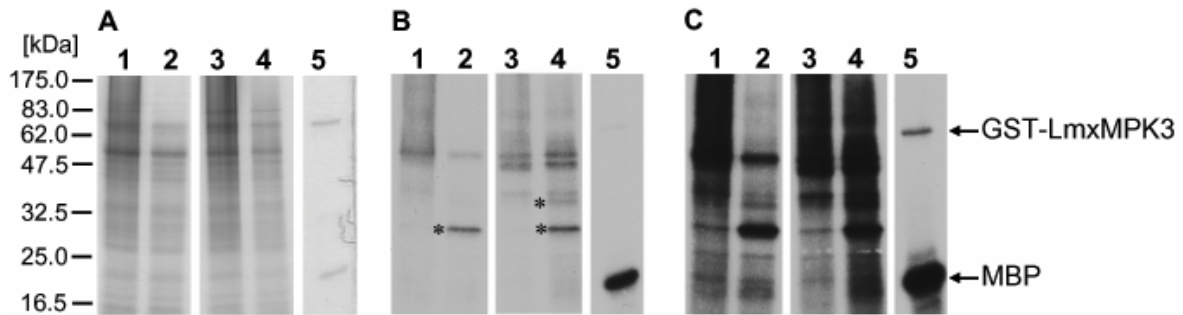


Figure 51: Kinase assays with *in vitro*-activated GST-LmxMPK3 and cell lysates of *L. mexicana* wild type and *LmxMPK3* null mutant

A: Coomassie-stained 12% SDS-PA gel; B: Autoradiograph after 5min of exposure; C: Autoradiograph after 20min of exposure; 1: LmxWT lysate + GST-LmxMPK3(/GST-LmxMKK-D); 2: LmxWT lysate; 3: Δ *LmxMPK3*-/-HN1 lysate + GST-LmxMPK3(/GST-LmxMKK-D); 4: Δ *LmxMPK3*-/-HN1 lysate; 5: MBP + GST-LmxMPK3(/GST-LmxMKK-D).

Brackets indicate that only traces of the protein are present. Asterisks indicate bands of interest.

Figure 51B and C, lane 5 shows that the *in vitro* activation of GST-LmxMPK3 was successful. A potential LmxMPK3 substrate should be indicated on the autoradiograph by a band which is present when the different lysates had been incubated with LmxMPK3 and which is absent when the assay had been performed without LmxMPK3. A very faint band can be observed at ca. 40 kDa in Figure 51B, lane 1 showing the wild type lysates which had been incubated with LmxMPK3. This band is obviously missing in lane 2 showing the same lysate without LmxMPK3. However, this band can also be found in both lane 3 and lane 4 presenting the null mutant lysates with and without LmxMPK3, respectively, which indicates that this band does not correspond to a substrate of LmxMPK3. Interestingly, the only further differences in band patterns were represented by two bands which emerged when the lysates had been incubated without LmxMPK3 and which have been marked by asterisks in Figure 51B. The band at ca. 30 kDa is present in the wild type lysate (lane 2) as well as in the lysate of the null mutant (lane 4) indicating that the primary phosphorylation state of the corresponding protein hardly differs in wild type and null mutant. In contrast, the band at ca. 38 kDa is only visible in the lysate of the null mutant (lane 4) suggesting that the respective protein is less phosphorylated in the null mutant and is able to incorporate more radioactively labelled ATP. Further analysis of the additional bands using mass spectrometry was not possible due to the poor resolution of the protein bands in the gel.

4.8.7 *In silico* substrate search for LmxMPK3 using PREDIKIN

In 2003, Brinkworth *et al.* developed a set of rules for the prediction of the substrate specificity of serine/threonine protein kinases based on the primary sequence of their catalytic domain and implemented them in the web-interfaced programme PREDIKIN. The rules for the prediction of a heptapeptide substrate motif surrounding the phosphorylation site (positions -3 to +3) were derived from available crystal structures, sequence analysis of kinases and substrates and oriented peptide library experiments. PREDIKIN identifies the substrate-determining residues (SDRs) in the primary sequence of the submitted protein kinase which had been defined in relation to conserved kinase motifs and which make contact with the side chains of the residues surrounding the phosphorylation site in the substrate (see Figure 52). It is generally anticipated that the SDRs are predominantly complimentary with the substrate regarding size, polarity, charge and hydrogen-bonding potential. Brinkworth *et al.* could finally show that the accuracy of PREDIKIN predictions is comparable to that of systematic large-scale experimental approaches.

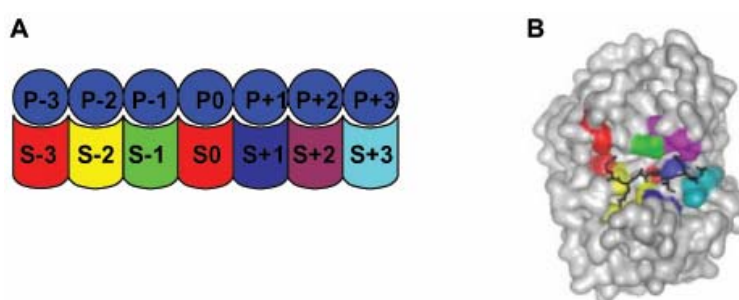


Figure 52: Specific interaction of protein kinase with heptapeptide substrate

A: Schematic representation of the heptapeptide substrate (P-3 to P+3) binding to the SDR-containing subsites (S-3 to S+3) of the protein kinase; B: Surface representation of protein kinase A with subsites (coloured as in A) binding to the heptapeptide region of the substrate. (modified from <http://predikin.biosci.uq.edu.au/pkr/>, 2008)

Since experimental approaches for identifying substrates of LmxMPK3 had not been successful, PREDIKIN was used to generate a consensus sequence of a heptapeptide substrate for LmxMPK3. The output substrate scoring matrices for LmxMPK3 provided the consensus [APQ]P[LQ][ST]P[CTSV][ASY] which was used for a motif search in the *L. major* genome DB (Ivens *et al.*, 2005). A total of 19 hits could be obtained (see Table 8) comprising 16 proteins of unknown function and three proteins with the following putative functions: an endonuclease/exonuclease/phosphatase (LmjF36.1150), a CPSF-domain protein (LmjF30.3710) and the splicing factor 3A (LmjF30.1830). From those three proteins the putative endonuclease/exonuclease/phosphatase LmjF36.1150, designated LmjHS (HS for hypothetical substrate), revealed the highest substrate score being 92.49 (maximum is 100) which is a parameter for the likelihood of a sequence to present a real substrate motif.

potential LmxMPK3 substrate	position of potential phosphorylation site	heptapeptide substrate	substrate score
LmjF02.0490	469	APLSPCA	97.61
LmjF31.1700	91	APLSPVA	93.09
LmjF36.1150	120	PPLTPTA	92.49
LmjF26.1510	543	PPLTPTA	92.49
LmjF06.0690	2166	APLSPSA	91.47
LmjF25.0970	1001	APLTPVS	91.38
LmjF01.0560	150	APQTPSA	90.20
LmjF03.0360	1609	APQSPSA	89.98
LmjF22.1310	801	PPLSPSA	89.66
LmjF22.0600	311	PPLTPVS	89.57
LmjF30.1830	175	APLSPSS	89.55
LmjF34.0620	2007	APLSPSS	89.55
LmjF10.0900	977	QPQSPTA	89.21
LmjF26.1850	101	PPQSPVS	87.87
LmjF15.0530	227	PPLSPSS	87.74
LmjF35.0490	1187	PPLSPSS	87.74
LmjF30.3710	693	PPLSPSS	87.74
LmjF25.1590	471	QPQTPSA	86.82
LmjF09.0190	105	PPQSPSS	86.25

Table 8: Overview of potential LmxMPK3 substrates with potential phosphorylation site position, heptapeptide substrate and predicted substrate score.

The heptapeptide sequence in LmjHS is PPLTPTA with the central threonine being the potential phosphorylation site. Moreover, located immediately N-terminally to the substrate phosphorylation motif there is a sequence motif resembling the so-called docking domains (D-domains) which are typically present in MAP kinase substrates and support the selective interaction with the MAP kinase (Enslin *et al.*, 2000). Whereas the D-domain consensus is (K/R)₂-X₂₋₆-I/L/V-X-I/L/V which sometimes is C-terminally extended by another X-I/L/V motif, the respective domain in LmjHS is represented by KDPSGGLPLLRV starting only with one basic residue and lacking the residue between the two I/L/V-X-I/L/V motifs. Glycine and proline are typical residues in the spacer region between the basic and hydrophobic residues and directly C-terminal to the consensus sequence and can indeed be found in LmjHS. The LmjHS amino acid sequence can be viewed in 8.1.6 (see 4.8.7.1 for the adjusted annotation).

The promising substrate score as well as the sequence features typical for MAP kinase substrates suggested to clone parts of *LmjHS* and its *L. mexicana* homologue, designated *LmxHS*, for recombinant expression. Subsequent kinase assays would clarify, if the predicted substrate sequence motif is phosphorylated by *in vivo*-activated LmxMPK3 *in vitro*.

4.8.7.1 Features of LmjHS and its homologues

The *L. major* genome DB (Ivens *et al.*, 2005) annotates *LmjHS* as a gene consisting of 3069 bp and encoding a protein of 1022 aa with a molecular mass of 110.8 kDa. However, alignment with the *L. infantum* and *L. braziliensis* homologues strongly suggests that the actual start codon is the next ATG triplet downstream and in frame with the reported one.

This results in a gene of 2790 bp encoding a protein of 929 aa with a molecular mass of 100.8 kDa. The latter will be regarded as the correctly annotated gene/protein and the amino acid numbering has been adjusted accordingly. LmjHS was identified as a putative member of the endonuclease/exonuclease/phosphatase family by the Pfam protein families database (amino acids 378-920). This family includes magnesium-dependent endonucleases and a large number of phosphatases involved in intracellular signalling. Indeed, the SMART tool identified sequence homologies to an inositol polyphosphate related phosphatase mostly overlapping with the endonuclease/exonuclease/phosphatase family domain (amino acids 665-928). The amino acid sequence of LmjHS is 85% identical to its homologue in *L. infantum* and only 54% identical to the *L. braziliensis* sequence. There are orthologues in *T. cruzi* and *T. brucei* which are only 39% and 37% identical to LmjHS and lack the first 190 and 151 residues, respectively. Moreover, there are several sequence deletions and insertions compared to LmjHS. No significant similarities could be found to proteins of other organisms. An alignment of LmjHS and its homologues can be viewed in 8.1.6.

4.8.7.2 Testing the predicted LmjHS peptide as an LmxMPK3 substrate *in vitro*

Before cloning larger parts of LmjHS and LmxHS, a construct was generated containing the nucleotide sequence encoding the predicted LmjHS heptapeptide and some amino acid residues located N-terminally to the heptapeptide including part of the putative D-domain. The resulting peptide LRVGNSAPPPLTPTA, designated LmjHSpep, was subsequently affinity purified as a GST-fusion protein and subjected to kinase assays together with *in vivo*-activated LmxMPK3. To assess the specificity of the phosphorylation reaction, the assay was also performed with activated LmxMPK13, the only other MAP kinase in our laboratory for which the activating MAP kinase kinase - here LmxPK4 - could be identified (Scholz, PhD thesis, 2008). PREDIKIN classifies LmxMPK13 as a RAGE-1 kinase (CDC2/MAP kinase-related). The PREDIKIN-predicted consensus sequence of the heptapeptide substrate for LmxMPK13 is M[ARY][AFKLNRS][ST]X[MV][NS] (Scholz, PhD thesis, 2008), lacking the proline residues at positions -2 and +1 which are otherwise highly conserved in MAP kinase substrates. Therefore, the consensus heptapeptide substrate sequences for LmxMPK3 (see 4.8.7) and LmxMPK13 strongly differ from each other. LmjHSpep reveals a substrate score of only 61.1 for LmxMPK13.

Generation of the expression construct

To generate a DNA-fragment encoding the peptide LRVGNSAPPPLTPTA, the overlapping 5'-phosphorylated oligonucleotides LmjF36pep1 and LmjF36pep2 were annealed resulting in a DNA double-strand with a sticky *Bsp*LU111- and *Hind*III-site at the 5'- and 3'-end, respectively. The fragment was subsequently ligated into pGEX-KG(-P) which had been

linearised using *Nco*I and *Hind*III generating pGEX-KG(-P)2LmjHSpep. The integrity of the construct was verified by sequencing.

Recombinant expression and affinity purification of GST-LmjHSpep

The plasmid pGEX-KG(-P)2LmjHSpep was transformed into *E. coli* XL1-Blue cells which were subsequently used to express the fusion protein at 18°C overnight. The cells were lysed by sonication and the fusion protein was purified on glutathione sepharose. After the eluted protein had been quantified using the Bradford method, 2 µg of GST-LmjHSpep were analysed by SDS-PAGE (Figure 53A). In addition, 1 µg of the fusion protein was loaded next to the GST-tag lacking the peptide derived from pGEX-KG(-P) in order to visualise the band shift (Figure 53B).

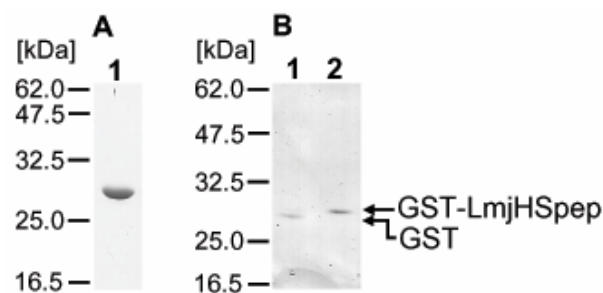


Figure 53: SDS-PAGE of affinity purified GST-LmjHSpep

A: Coomassie-stained 15% SDS-PA gel; B: Coomassie-stained 12% SDS-PA gel.

A: 1: GST-LmjHSpep.

B: 1: GST; 2: GST-LmjHSpep.

Figure 53A, lane 1 and Figure 53B, lane 2 show a clear band corresponding to GST-LmjHSpep at the expected molecular mass (28.9 kDa) indicating that the recombinant expression and affinity purification of the fusion protein was successful. Moreover, the band shift compared to the GST-tag is visible in Figure 53B confirming that the purified protein actually contains the substrate peptide.

Kinase assays with GST-LmjHSpep and *in vivo*-activated His-LmxMPK3

To test whether the predicted substrate peptide is phosphorylated by activated LmxMPK3, kinase assays were carried out with GST-LmjHSpep and *in vivo*-activated His-LmxMPK3. In order to assess the specificity of the phosphorylation reaction, the assay was also performed with activated LmxMPK13, the only other MAP kinase in our laboratory for which the activating MAP kinase kinase - here LmxPK4 - could be identified (Scholz, PhD thesis, 2008). As for LmxMPK3, the co-expression system for an *in vivo* activation of LmxMPK13 had been established successfully (Scholz, PhD thesis, 2008). The expression and purification of His-LmxMPK13 was performed as described for His-LmxMPK3. Subsequently, approximately 4 µg GST-LmjHSpep were tested in a kinase assay with 4 µg of non-activated or activated His-LmxMPK3 at 27°C using a reaction buffer with 10 mM Mn²⁺ and pH 6.5. In parallel, the same assays were also performed with non-activated or activated His-

LmxMPK13 using the standard reaction buffer which had been found to be optimal for the LmxMPK13 catalytic activity (Scholz, PhD thesis, 2008). It is assumed that the highest protein band in the different LmxMPK13 eluates in SDS-PAGE represents the full length protein which is in addition phosphorylated to the maximum degree when the MAP kinase has been co-expressed with LmxPK4 (Scholz, PhD thesis, 2008). Thus, protein amounts were estimated according to the highest protein band, respectively. Kinase assays using non-activated or activated LmxMPK3 and LmxMPK13 together with MBP served as positive controls.

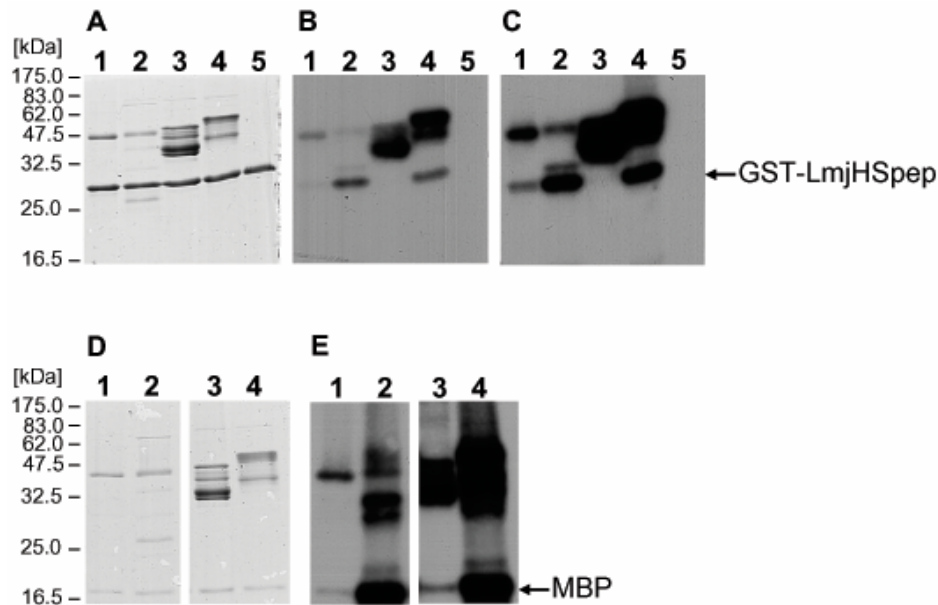


Figure 54: Kinase assays with GST-LmjHSpep and *in vivo*-activated His-LmxMPK3 and His-LmxMPK13

A: Coomassie-stained 15% SDS-PA gel; B: Autoradiograph after 2.5h of exposure; C: Autoradiograph after 16h of exposure; D: Coomassie-stained 12% SDS-PA gel; E: Autoradiograph after 16h of exposure.

A-C: 1: GST-LmjHSpep + His-LmxMPK3; 2: GST-LmjHSpep + His-LmxMPK3/(LmxMKK-D); 3: GST-LmjHSpep + His-LmxMPK13; 4: GST-LmjHSpep + His-LmxMPK13/(LmxPK4); 5: GST-LmjHSpep.

D and E: 1: MBP + His-LmxMPK3; 2: MBP + His-LmxMPK3/(LmxMKK-D); 3: MBP + His-LmxMPK13; 4: MBP + His-LmxMPK13/(LmxPK4).

Brackets indicate that the protein was only present during co-expression.

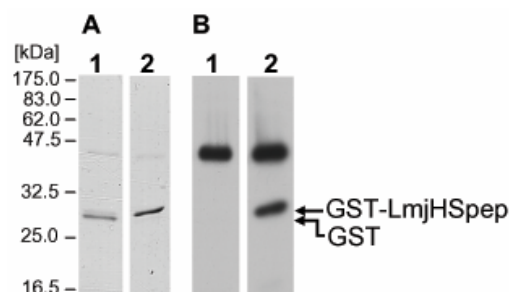


Figure 55: Kinase assays with GST and GST-LmjHSpep together with *in vivo*-activated His-LmxMPK3

A: Coomassie-stained 12% SDS-PA gel; B: Autoradiograph after 48h of exposure; 1: GST + His-LmxMPK3/(LmxMKK-D); 2: GST-LmjHSpep + His-LmxMPK3/(LmxMKK-D).

Brackets indicate that the protein was only present during co-expression.

The MBP phosphorylation in Figure 54E lane 2 and 4 is much stronger compared to lane 1 and 3, respectively, showing that the *in vivo* activation of His-LmxMPK3 and His-LmxMPK13 was successful. While GST-LmjHSep alone showed no unspecific incorporation of radioactively labelled phosphate (Figure 54B and C, lane 5), a slight phosphorylation was detectable when it had been incubated with non-activated LmxMPK3 (lane 1). However, non-activated LmxMPK13 did not catalyse a phosphorylation of the fusion protein (lane 3). In contrast, when GST-LmjHSep had been incubated with activated LmxMPK3 or LmxMPK13 a strong phosphorylation could be observed (lane 2 and 4). Figure 55B confirms that the radioactively labelled phosphate had exclusively been incorporated into the substrate peptide and not into the GST-tag which yet contains one SP motif as a potential MAP kinase phosphorylation site. Phosphorylation site mapping of the phosphorylated GST-LmjHSep using mass spectrometry was not successful. In summary, activated LmxMPK3 recognises the predicted substrate peptide as a substrate *in vitro*. However, the peptide seems to be a rather unspecific substrate as the reaction was catalysed equally strong by activated LmxMPK13. Nevertheless, a larger part of LmjHS was cloned for recombinant expression and tested for substrate function (see next chapter).

4.8.7.3 Testing an N-terminal part of LmjHS as a LmxMPK3 substrate *in vitro*

In 4.8.7.2 it has been shown that the phosphorylation of the predicted substrate peptide by activated LmxMPK3 is rather unspecific. However, it seems possible that a larger part of the amino acid environment which determines the protein conformation influences the specificity of the phosphorylation reaction. Therefore, an N-terminal part of LmjHS including the predicted phosphorylation site was cloned for recombinant expression.

Generation of the expression construct

To generate a construct for recombinant expression of the GST-tagged LmjHS N-terminus, a PCR was performed on genomic DNA of *L. major* wild type using the oligonucleotides LmjF36_2.for and LmjF36_2.rev. After the amplified 527 bp-fragment had been ligated into pCR2.1-TOPO and sequenced, it was released using *Bsp*HI and *Hind*III and cloned into pGEX-KG(-P) which had been linearised using *Nco*I and *Hind*III generating pGEX-KG(-P)2LmjHS.

Recombinant expression and affinity purification of GST-LmjHS

The plasmid pGEX-KG(-P)2LmjHS was transformed into *E. coli* XL1-Blue cells which were used to express the fusion protein at 18°C overnight. The cells were lysed by sonication and the fusion protein was purified on glutathione sepharose. 1 µg of GST-LmjHS was analysed by SDS-PAGE (Figure 56).

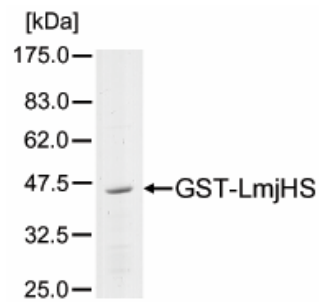


Figure 56: SDS-PAGE of affinity purified GST-LmjHS
Coomassie-stained 10% SDS-PA gel.

The clear band at the expected molecular mass (45.0 kDa) in Figure 56 corresponds to GST-LmjHS indicating that the recombinant expression and affinity purification of the fusion protein was successful.

Kinase assays with GST-LmjHS and *in vivo*-activated His-LmxMPK3

To test whether also a larger part of LmjHS including the predicted phosphorylation site is phosphorylated by activated LmxMPK3, kinase assays were carried out with GST-LmjHS and *in vivo*-activated His-LmxMPK3. It was of special interest to assess whether the amino acid environment alters the specificity of the phosphorylation reaction. Therefore, the same assay was again performed with *in vivo*-activated His-LmxMPK13 as already described in 4.8.7.2. Since the eluates of non-activated and activated His-LmxMPK13 show several protein bands approximately at the same molecular mass as GST-LmjHS in SDS-PAGE, the kinase assays were carried out with non-eluted LmxMPK13 on beads. Thereafter, beads (washed twice with reaction buffer) and supernatants were loaded on separate lanes for subsequent SDS-PAGE to visualise LmxMPK13 autophosphorylation and GST-LmjHS substrate phosphorylation, respectively. Kinase assays lacking GST-LmjHS served as negative controls. Approximately 4 μg GST-LmjHS were incubated with 4 μg of non-activated or activated His-LmxMPK3 on beads at 27°C using a reaction buffer with 10 mM Mn^{2+} and pH 6.5. Likewise, the kinase assays were performed with 4 μg of non-activated or activated His-LmxMPK13 on beads and standard reaction buffer. Kinase assays using non-activated and activated LmxMPK3 together with MBP served as positive controls.

Figure 57D shows that the MBP phosphorylation is much stronger in lane 2 compared to lane 1 and thus indicates that the *in vivo* activation of His-LmxMPK3 was successful. Activated LmxMPK13 can be recognised by the significant shift of protein bands to higher molecular masses in SDS-PAGE caused by the strong phosphorylation of the kinase (Figure 57E, lane 6 and 8). A faint band is visible in Figure 57B, lane 2 corresponding to GST-LmjHS alone which shows a weak unspecific incorporation of radioactively labelled phosphate. The phosphorylation was slightly increased when GST-LmjHS had been incubated with non-activated LmxMPK3 (lane 3) and was indeed significantly increased after incubation with activated LmxMPK3 (lane 4). The strong signal was definitely not caused by

autophosphorylation of activated LmxMPK3 as indicated by lane 1 which contains activated LmxMPK3 alone. Figure 57F, lane 1 shows that non-activated LmxMPK13 did not catalyse a phosphorylation of GST-LmjHS. When the fusion protein had been incubated with activated LmxMPK13 a weak phosphorylation could be observed (lane 5). The weak signal definitely corresponds to GST-LmjHS and not to a contaminating protein since it is not visible in control lane 7 showing the supernatant of the kinase assay lacking GST-LmjHS. However, the phosphorylation of GST-LmjHS by activated LmxMPK13 is much weaker compared to the phosphorylation caused by activated LmxMPK3. Phosphorylation site mapping of the phosphorylated GST-LmjHS using mass spectrometry was not successful. In summary, activated LmxMPK3 specifically recognises LmjHS as a substrate *in vitro*.

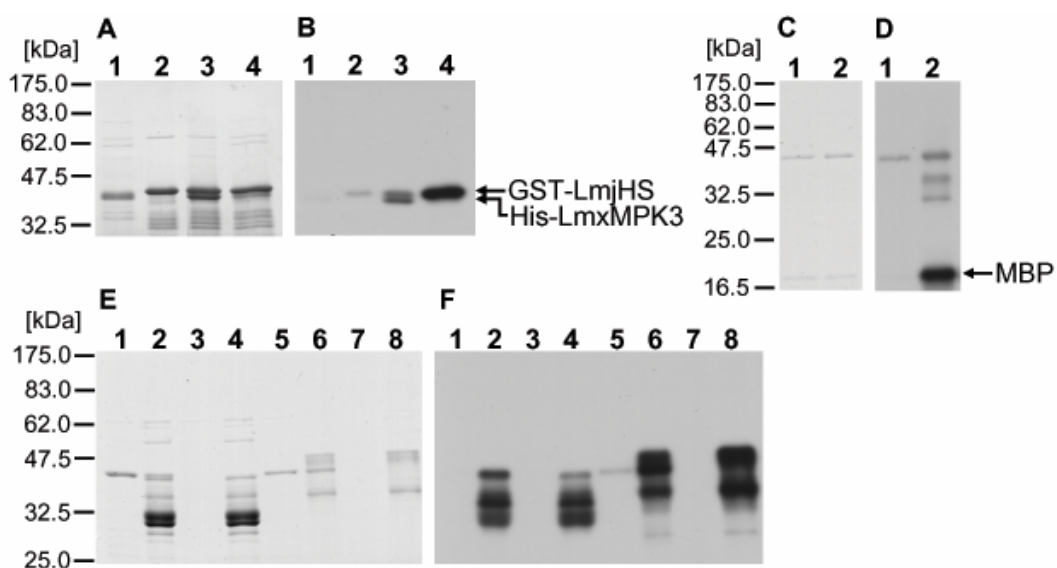


Figure 57: Kinase assays with GST-LmjHS and *in vivo*-activated His-LmxMPK3 and His-LmxMPK13

A: Silver-stained 10% SDS-PA gel; B: Autoradiograph after 18h of exposure; C: Coomassie-stained 12% SDS-PA gel; D: Autoradiograph after 18h of exposure; E: Coomassie-stained 10% SDS-PA gel; F: Autoradiograph after 18h of exposure.

A and B: 1: His-LmxMPK3(/LmxMKK-D); 2: GST-LmjHS; 3: GST-LmjHS + His-LmxMPK3; 4: GST-LmjHS + His-LmxMPK3(/LmxMKK-D).

C and D: 1: MBP + His-LmxMPK13; 2: MBP + His-LmxMPK13(/LmxMKK-D).

E and F: 1 and 2: GST-LmjHS + His-LmxMPK13 (1: supernatant; 2: beads); 3 and 4: His-LmxMPK13 (3: supernatant; 4: beads); 5 and 6: GST-LmjHS + His-LmxMPK13(/LmxPK4) (5: supernatant; 6: beads); 7 and 8: His-LmxMPK13(/LmxPK4) (7: supernatant; 8: beads).

Brackets indicate that the protein was only present during co-expression.

4.8.7.4 Testing an N-terminal part of LmxHS as a LmxMPK3 substrate *in vitro*

Chapter 4.8.7.2 and 4.8.7.3 described that the predicted LmjHS peptide as well as an N-terminal part of LmjHS are actually phosphorylated by *in vivo*-activated LmxMPK3 *in vitro*. However, to identify a real *in vivo* substrate of LmxMPK3 it obviously has to be an *L. mexicana* protein. Thus, the equivalent N-terminal part of the *L. mexicana* homologue, designated LmxHS, was cloned for recombinant expression. An alignment of the LmjHS and LmxHS N-termini can be viewed in 8.1.6.

Generation of the expression construct

To generate a construct for recombinant expression of the GST-tagged LmxHS N-terminus, a PCR was performed on genomic DNA of the *L. mexicana* wild type using the oligonucleotides LmjF36_2.for and LmjF36_2.rev which were based on the *L. major* nucleotide sequence. The amplified 527 bp-fragment was ligated into pCR2.1-TOPO and three clones were sequenced yielding a 100% identical nucleotide sequence which was 78% identical to the respective *L. major* sequence excluding the oligonucleotide sequences (see 8.1.6 for the *LmxHS* 5'-end nucleotide sequence). The translated sequences of the LmxHS and LmjHS N-termini are 60% identical to each other. It is important to mention that the respective *L. mexicana* heptapeptide sequence is SPLTSTA and thus unfortunately lacking the proline residue at position +1 which is otherwise highly conserved in MAP kinase substrates. Consequently, the substrate score for the heptapeptide is reduced to only 60.15 and 69.12 for LmxMPK3 and LmxMPK13, respectively, and other heptapeptide sequences within LmxHS actually reveal higher scores. The amplified fragment was liberated using *Bsp*HI and *Hind*III and cloned into pGEX-KG(-P) which had been linearised using *Nco*I and *Hind*III generating pGEX-KG(-P)1LmxHS.

Recombinant expression and affinity purification of GST-LmxHS

The plasmid pGEX-KG(-P)1LmxHS was transformed into *E. coli* XL1-Blue cells which were subsequently used to express the fusion protein at 18°C overnight. The cells were lysed by sonication and the fusion protein was purified on glutathione sepharose. 1 µg of GST-LmxHS was analysed by SDS-PAGE (Figure 58).

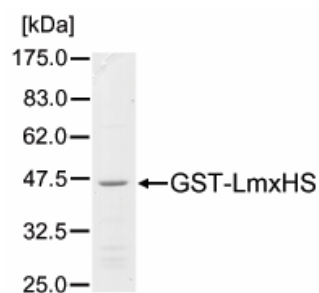


Figure 58: SDS-PAGE of affinity purified GST-LmxHS
Coomassie-stained 10% SDS-PA gel.

Figure 58 shows a clear band corresponding to GST-LmxHS at the expected molecular mass (45.0 kDa) indicating that the recombinant expression and affinity purification of the fusion protein was successful.

Kinase assays with GST-LmxHS and *in vivo*-activated His-LmxMPK3

To test whether also the N-terminus of the *L. mexicana* homologue is phosphorylated by activated LmxMPK3, kinase assays were carried out with GST-LmxHS and *in vivo*-activated His-LmxMPK3. Again, the specificity of the substrate phosphorylation was assessed by

performing the same assays with *in vivo*-activated His-LmxMPK13 as already described in 4.8.7.2 and 4.8.7.3. Likewise, the kinase assays were carried out with non-eluted LmxMPK13 on beads followed by SDS-PAGE in which beads and supernatants were separated individually (see 4.8.7.3). Approximately 8 μ g GST-LmxHS were incubated with 4 μ g of non-activated or activated His-LmxMPK3 at 27°C using a reaction buffer with 10 mM Mn^{2+} and pH 6.5. The same kinase assays were performed with 4 μ g GST-LmxHS and 4 μ g of non-activated or activated His-LmxMPK13 on beads using the standard reaction buffer. Kinase assays using non-activated and activated LmxMPK3 together with MBP served as positive controls.

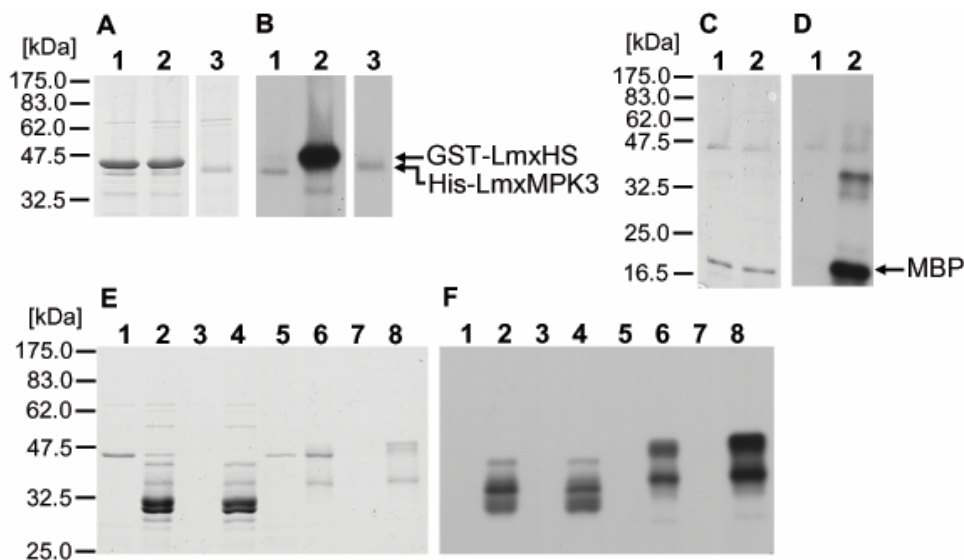


Figure 59: Kinase assays with GST-LmxHS and *in vivo*-activated His-LmxMPK3 and His-LmxMPK13

A: Coomassie-stained 12% SDS-PA gel; B: Autoradiograph after 3.5h of exposure; C: Coomassie-stained 12% SDS-PA gel; D: Autoradiograph after 3.5h of exposure; E: Coomassie-stained 10% SDS-PA gel; F: Autoradiograph after 18h of exposure.

A and B: 1: GST-LmxHS + His-LmxMPK3; 2: GST-LmxHS + His-LmxMPK3(/LmxMKK-D); 3: His-LmxMPK3(/LmxMKK-D).

C and D: 1: MBP + His-LmxMPK3; 2: MBP + His-LmxMPK3(/LmxMKK-D).

E and F: 1 and 2: GST-LmxHS + His-LmxMPK13 (1: supernatant; 2: beads); 3 and 4: His-LmxMPK13 (3: supernatant; 4: beads); 5 and 6: GST-LmxHS + His-LmxMPK13(/LmxPK4) (5: supernatant; 6: beads); 7 and 8: His-LmxMPK13(/LmxPK4) (7: supernatant; 8: beads).

Brackets indicate that the protein was only present during co-expression.

The MBP phosphorylation in Figure 59D, lane 2 is much stronger compared to lane 1 showing that the *in vivo* activation of His-LmxMPK3 was successful. Activated LmxMPK13 can be recognised by the significant shift of protein bands to higher molecular masses in SDS-PAGE caused by the strong phosphorylation of the kinase (Figure 59E, lane 6 and 8). GST-LmxHS was phosphorylated to a very low degree by non-activated LmxMPK3 indicated by a band hardly visible above the band corresponding to LmxMPK3 (Figure 59B, lane 1). However, the phosphorylation of the fusion protein was indeed strongly increased when it had been incubated with *in vivo*-activated LmxMPK3 (lane 2). The strong signal was definitely not caused by autophosphorylation of activated LmxMPK3 as indicated by lane 3

which contains activated LmxMPK3 alone. The experiment was repeated again showing an increased phosphorylation of GST-LmxHS by activated LmxMPK3, however, the phosphorylation was not as strong as in Figure 59B, lane 2. No signal can be observed in Figure 59F, lane 1 and 5 indicating that neither non-activated nor activated LmxMPK13 phosphorylates GST-LmxHS. Phosphorylation site mapping of GST-LmxHS phosphorylated by activated LmxMPK3 using mass spectrometry was not successful. In summary, activated LmxMPK3 specifically recognises LmxHS as a substrate *in vitro*.

5 Discussion

5.1 The phenotype of the *LmxMPK3* null mutants and the *LmxMPK3* add back mutants

To analyse the physiological function of *LmxMPK3*, two independent *LmxMPK3* null mutants, termed $\Delta LmxMPK3$ -I-HN1 and $\Delta LmxMPK3$ -I-PN6, had been generated prior to the beginning of this work (Erdmann, diploma thesis, 2004). Microscopic analysis had already revealed that the *LmxMPK3* null mutants display flagella significantly reduced in length compared to the wild type and suggested a role of the MAP (mitogen-activated protein) kinase in flagellar length regulation. Here, several strategies have been successfully applied to investigate the function of *LmxMPK3* in more detail.

In this work *LmxMPK3* add back mutants were generated for both *LmxMPK3* null mutants in order to prove that the phenotype of the null mutants is actually due to the lack of *LmxMPK3* and can be reversed by its re-expression. *LmxMPK3* re-expression in both add back mutants could be verified by immunoblot analysis (see 4.1.2). To get a general overview of the *LmxMPK3* protein levels in the different *LmxMPK3* mutants, also the wild type, two independent single-allele deletion mutants and the two null mutants of *LmxMPK3* had been included in this analysis. *LmxMPK3* protein levels are slightly decreased in the single-allele deletion mutants compared to the wild type and the MAP kinase is not detectable in the null mutants. The add back mutants revealed *LmxMPK3* protein levels which were lower compared to the wild type and even to the single-allele deletion mutants. Nevertheless, the *LmxMPK3* add back mutants were able to restore the wild type phenotype which is included in the following chapter.

5.1.1 The morphology and structure of the flagellum

Measurements of the flagellar lengths revealed that the absence of *LmxMPK3* leads to the generation of flagella reduced to an average of only 1.8 and 2.2 μm in the different deletion mutants (see 4.1.3) which is contrasting to the average length of 11.3 μm in the wild type. This quantification strongly underscores the hypothesis that *LmxMPK3* is critically involved in flagellar length regulation. The fact that re-expression of *LmxMPK3* in the deletion background leads to the restoration of flagella with average lengths between 7.8 and 8.6 μm (roughly 70-75% of the wild type value) proves that flagellar shortening is actually an effect caused by the lack of *LmxMPK3*. The observation that flagellar lengths of the add back mutants do not quite reach the wild type values matches with the fact that the *LmxMPK3* protein levels in the add back mutants are lower than in the wild type.

Ultrastructural analysis using transmission electron microscopy (TEM) showed that the flagella of the *LmxMPK3* null mutants possess a correctly assembled “9+2” axoneme,

however, neither of the flagellar sections revealed a normally assembled paraflagellar rod (PFR) (see 4.1.4). Actually, there was no PFR visible in 29 and 34% of flagellar sections of the different deletion mutants while most of the remaining flagella contained either a rudimentary PFR, various amounts of undefined material around the axoneme or vesicles. This finding clearly points out that the lack of *LmxMPK3* strongly affects the assembly of the PFR. The fact that most of the flagella (70.5%) of the add back mutants were able to restore a correctly assembled PFR proves that disruption of the PFR is indeed due to the lack of *LmxMPK3*.

Immunofluorescence analysis using the monoclonal antibody L8C4 recognising PFR-2, one of the two main protein subunits of the PFR, revealed only 15% of the null mutant flagella showing no reaction with L8C4 (see 4.1.5.1). The remaining flagella showed either a weak (35-45%) or even a strong (40-50%) fluorescence which was always restricted to the flagellum.

Taking the observations of the TEM and the immunofluorescence analysis together, approximately one half of the flagella showing no PFR in TEM analysis probably contain free PFR subunits within the flagellum. Generally, the strong fluorescence observed in roughly one half of the null mutant flagella which never showed a correctly assembled PFR in TEM analysis indeed suggests high amounts of unassembled PFR subunits within the flagella possibly also explaining the undefined material observed in TEM analysis.

Immunoblot analysis using the same antibody showed that the *LmxMPK3* null mutants contain approximately 20 times less PFR-2 than the wild type (see 4.1.5.2). Since a mere reduction of the flagellar length would only lead to 5 times less PFR-2, the flagella of the null mutants contain on average roughly 4 times less PFR-2 per micrometer length than the wild type.

Thus, there are several possible explanations for the formation of the *LmxMPK3* null mutant phenotype. *LmxMPK3* could regulate the expression of PFR-2 by modulating the function of proteins involved in processes such as transport, processing, modification or turnover of the *PFR-2* mRNA as well as the translation or turnover of the PFR-2 protein. Interestingly, an AU-rich *cis*-regulatory element of 10 nucleotides had been identified in the 3'-UTR of all *PFR* genes in *L. mexicana* which leads to a 10-fold down-regulation of the *PFR* mRNA amounts in amastigotes by inducing mRNA degradation (Mishra *et al.*, 2003). The degradation process could be mediated by an RNA binding protein which is constitutively expressed but only available for binding in amastigotes. The ability to bind to the mRNA regulatory element could be abolished by phosphorylation of the protein in promastigotes, and *LmxMPK3* could be the responsible kinase. However, RT-PCR analysis revealed that *PFR-2* mRNA amounts in the *LmxMPK3* null mutants do not differ from that of the wild type (see 4.8.2.1) indicating that *LmxMPK3* is neither involved in the regulation of *PFR-2* mRNA

stability or in the transcription of the *PFR-2* genes (see 5.8.1.1). Thus, the down-regulation of the PFR-2 expression takes place on the protein level, probably by affecting translation or protein degradation. Lack of LmxMPK3 could therefore lead to a down-regulation in the amounts of PFR proteins which, however, would still be selectively transported into the flagellum. One could assume that the mere limitation of PFR subunits would eventually stop a further outgrowth of the flagellum possibly using a feed back mechanism. However, this assumption is not consistent with the phenotypes of the *T. brucei snl-1* mutant in which PFR-A expression was ablated (Bastin *et al.*, 1998) and the *L. mexicana* null mutants for *PFR-1* (Maga *et al.*, 1999), *PFR-2* (Santrich *et al.*, 1997) or both of these genes (Maga *et al.*, 1999). PFR assembly was severely impaired (or the PFR was absent in case of the *PFR-1/PFR-2* double deletion), however, axonemal assembly and flagellar length were not affected.

Moreover, the hypothesis of decreased amounts of PFR proteins restricting flagellar outgrowth would not explain why the PFR subunits present within the majority of the null mutant flagella do not form a normal PFR structure. A possible explanation could be that PFR subunits need to be phosphorylated by LmxMPK3 to be correctly assembled, thus being direct substrates of the MAP kinase. Otherwise, a different substrate protein could mediate PFR assembly either being a structural component of the PFR itself or a subunit of the IFT (intraflagellar transport) machinery. The observed decrease in PFR-2 protein amounts might be a consequence of the accumulation of flagellar proteins in the cell body which can not reach their final destination and are therefore degraded. Actually, in case of the *PFR-1* and *PFR-2* null mutants of *L. mexicana* the PFR-2 and PFR-1 protein levels were also lower compared to the wild type, respectively, while the respective mRNA levels were unchanged in the null mutants (Santrich *et al.*, 1997; Maga *et al.*, 1999). It was therefore suggested that the rate of PFR-1 and PFR-2 degradation is increased when these proteins are not incorporated into a native PFR.

IFT is the motor-dependent bidirectional movement of IFT particles along the length of eukaryotic flagella and cilia and is essential for the construction and maintenance of those organelles. Flagellar length has been proposed to be regulated by shifting the ratio between the rates of assembly and disassembly (Marshall and Rosenbaum, 2001). Indeed, morphologically similar particles have been found in the flagella of trypanosomatids (Sherwin and Gull, 1989), and homologues of several proteins involved in IFT have been identified in trypanosomatids. Based on RNAi (RNA interference) studies it has been strongly suggested that IFT is functional in trypanosomes (Kohl *et al.*, 2003).

Numerous different proteins are involved in IFT. The IFT complexes A and B are composed of at least 17 protein subunits which are conserved among green algae, nematodes and vertebrates. However, many proteins involved in IFT have yet to be identified (Haycraft *et al.*,

2003). Using an *in silico* approach twelve of the conserved IFT complex subunits could be identified in *Leishmania* (Gouveia *et al.*, 2007). Moreover, different motor proteins are required for functional IFT. While retrograde movement of IFT complex A is driven by the cytoplasmic motor protein complex dynein 1b (Pazour *et al.*, 1999; Porter *et al.*, 1999; Signor *et al.*, 1999), anterograde movement of IFT complex B is mainly driven by heterotrimeric kinesin-2 (Cole, 1999). However, there are multiple kinesins (Fox *et al.*, 1994) which can modulate IFT or even take over the function of heterotrimeric kinesin-2 (Scholey, 2008). In *Leishmania* a putative Unc104-like kinesin, a kinesin-2 subunit (Gouveia *et al.*, 2007) and two putative OSM-3-like kinesins (Ivens *et al.*, 2005) have been identified. Moreover, the *Leishmania* genome contains two distinct cytoplasmic dynein-2 heavy chain (DHC2) genes (Adhiambo *et al.*, 2005). The large number of components functionally involved in IFT underlines the variety of proteins qualified as potential substrates of LmxMPK3.

Furthermore, IFT motors seem to be regulated at several control points (Pedersen *et al.*, 2006; Scholey, 2008). Initially, the motor and cargo proteins have to be transported from the site of synthesis to the base of the flagellum where the IFT machinery is assembled. Subsequently, the motor and cargo proteins have to enter the flagellum where the motors dock onto the IFT particles and move along the axoneme. Motor switching and turnaround is required at the axonemal tip. Cargo loading and unloading has to be controlled at both the base and the tip of the flagellum. Therefore, a lot of additional proteins besides the standard complement of the IFT machinery are likely to be involved in those processes. For instance, the tetratricopeptide repeat (TPR) protein DYF-1 probably activates OSM-3 by docking it onto IFT particles and relieving its autoinhibition, whereas a complex of Bardet-Biedl syndrome proteins (the BBSome; Nachury *et al.*, 2007) is supposed to contribute to the cooperation of kinesin-II and OSM-3 by maintaining the association of the IFT complexes A and B (Ou *et al.*, 2005). As the *L. major* genome reveals genes for both kinesins, similar regulation mechanisms might be used in this parasite. Although the flagellum in *Leishmania* cannot be subdivided into different segments with clearly differing axonemal structures as in chemosensory cilia of *Caenorhabditis elegans*, it is yet thinkable that flagellar assembly is the result of the coordinated action of kinesin-II and OSM-3. A potential role of LmxMPK3 in regulating this cooperation might explain why the flagella of the *LmxMPK3* null mutants still reach a defined length and are not completely resorbed into the cell. It is important to note that ablation of IFT complex B proteins (mediating anterograde IFT of cargo proteins) completely blocked axoneme construction and thus flagellar outgrowth in *T. brucei* (Absalon *et al.*, 2008). This was due to the fact that no IFT particles could enter the flagellum. *T. brucei* mutants for IFT complex A proteins or the dynein heavy chain (DHC1b) (responsible for retrograde IFT of cargo proteins) displayed short flagella with large dilations caused by an

accumulation of IFT particles in the flagellum (Absalon *et al.*, 2008). This observation was explained by the fact that heterotrimeric kinesin-2 and other IFT components could not be recycled back to the base of the flagellum. Similar results have been obtained for the respective IFT mutants of *Chlamydomonas reinhardtii* (Cole, 2003). However, in *L. mexicana* disruption of the dynein heavy chain gene *LmxDHC2.2* resulted in promastigotes with flagella barely extending beyond the flagellar pocket, showing disorganised axonemes and lacking the PFR (Adhiambo *et al.*, 2005). Since an accumulation of IFT particles could not be found in this mutant, *LmxDHC2.2* was supposed to affect IFT only indirectly. The *LmxMPK3* null mutant phenotype does not match any of those phenotypes exactly, as the flagella are short but not bulging although some undefined material is distributed around the axoneme. Altogether, the flagellar morphology in the *LmxMPK3* null mutants suggests that the lack of *LmxMPK3* either leads only to a moderate impairment of the key IFT motors or to a misregulation of sensing molecules or regulators controlling IFT and flagellar length. For instance, IFT57 is an IFT complex B protein with an exceptional function in flagellar length control as *C. reinhardtii* IFT57 mutants are able to assemble short flagella with a correctly assembled axoneme (Cole, 2003). Interestingly, the IFT57 homologues in *L. mexicana* (*Leishmania mexicana* genome project), *L. major*, *L. infantum* and *L. braziliensis* (GeneDB) each reveal a PXTTP and a TP motif as typical MAP kinase phosphorylation sites (Erdmann, unpublished results), and IFT57 could thus be an interesting substrate candidate for *LmxMPK3*. The corresponding TP motif is also present in the IFT57 homologues of *C. reinhardtii*, *Trypanosoma brucei* and *Trypanosoma cruzi* (GeneDB). An alignment of different IFT57 homologues can be viewed in 8.1.7. Moreover, the microtubule-depolymerising kinesin-13 is supposed to cooperate with the IFT machinery at the flagellar tip to control the length of the flagellum in *Leishmania* (Blaineau *et al.*, 2007). There are also several examples of protein kinases apart from *LmxMPK3* and its activator *LmxMKK* which have a role in flagellar length control (see 1.2.2), however, deletion or RNAi studies revealed only very few examples with similarities to the *LmxMPK3* null mutant phenotype (e.g. glycogen synthase kinase GSK3 β in *C. reinhardtii*; Wilson and Lefebvre, 2004).

Noteworthy, the axoneme in the *LmxMPK3* null mutant flagella has a relaxed structure with a diameter of 210 nm compared to 180 nm in the wild type (see 4.1.4) indicating that axonemal components possibly connecting the axonemal microtubules might be absent or incorrectly assembled. The presence of at least 250 different proteins in the axoneme of *Chlamydomonas* species (Piperno *et al.*, 1977) points out that a variety of proteins could be affected. Again, those components could be direct substrates of *LmxMPK3* or the MAP kinase could control either their expression or their IFT. Finally, the mere absence of a correctly assembled PFR might affect the axonemal structure, since the PFR is usually connected to the axonemal microtubule doublets 4 to 7 by fibres. Moreover, IFT particles are

preferentially transported along the axonemal microtubule doublets 3 and 4, or 7 and 8, and thus along both sides of the PFR (Absalon *et al.*, 2008). It is possible that the lack of PFR impairs IFT of specific axonemal proteins.

TEM also revealed that the flagellar pockets of the *LmxMPK3* null mutants were often filled with membrane vesicles or fragments (see 4.1.4) which could be due to an overproduction of membrane components which cannot be hosted by the short flagella. It has actually been shown that flagellar membrane elongation (and the formation of vesicles emerging from the flagellar pocket) can take place in the absence of IFT (Absalon *et al.*, 2008).

It is important to mention that deletion studies for *LmxMCK*, the physiological activator of *LmxMPK3*, produced a very similar phenotype, however, flagellar assembly was even more affected. Indeed, 78.5% of the flagella, which were also reduced to roughly one-fifth of the wild type length, did not display a PFR in TEM analysis, and the remaining 21.5% contained a rudimentary PFR. Moreover, 11% of the flagellar “9+2” axonemes of the *LmxMCK* null mutant lacked the central pair of microtubule singlets. Likewise for the *LmxMPK3* null mutants, immunoblot analysis indicated that PFR-2 protein amounts are strongly reduced. Indeed, most of the *LmxMCK* null mutant promastigotes showed no PFR-2 in immunofluorescence analysis while the fluorescence intensity in the remaining cells was weak. Furthermore, membrane fragments could also be found in the flagellar pocket of the *LmxMCK* null mutant. It has thus been suggested that *LmxMCK* represents a branch point in the regulation of flagellar morphogenesis and has other substrates in addition to *LmxMPK3* (Erdmann *et al.*, 2006). It is likely that those substrates additionally contribute either to the expression of PFR subunits or to the IFT and assembly of PFR and axonemal components. This hypothesis would explain why the amounts of PFR subunits are more reduced and flagellar assembly is even more affected in the *LmxMCK* null mutant than in the *LmxMPK3* null mutants.

5.1.2 The ability to complete the life cycle

Mouse infection studies showed that there was no significant difference in lesion development between the *LmxMPK3* null mutants and the wild type or add back mutants (see 4.1.6), suggesting that *LmxMPK3* is neither required for the differentiation from promastigotes to amastigotes nor for the proliferation of amastigotes.

This result reflects the tight down-regulation of *LmxMPK3* mRNA and *LmxMPK3* protein levels in amastigotes (Wiese *et al.*, 2003b; Erdmann *et al.*, 2006). It is tempting to speculate if the down-regulation of *LmxMPK3* is obligatory for the differentiation from promastigotes to amastigotes and for the maintenance of the amastigote stage. *LmxMPK3* was not detectable in amastigotes of the *LmxMPK3* add back mutants using immunoblot analysis (Erdmann,

unpublished results). Since *LmxMPK3* mRNA levels of the add back mutants should be controlled by the *DHFR-TS* intergenic region included in the plasmid construct and conferring constitutive gene expression, it is likely that LmxMPK3 protein levels are decreased in amastigotes of the add back mutants. Whether this is an active down-regulation in order to maintain the amastigote stage or the degradation of abundant protein which cannot be used remains unclear. Thus, the question about LmxMPK3 impairing the differentiation to amastigotes and their physiology cannot be answered at the moment.

However, LmxMPK3 has been shown to be essential for passing through the insect stage of the life cycle. Transmission studies using the *LmxMPK3* null mutant Δ *LmxMPK3*-I-HN1 for the infection of sand flies of the species *Lutzomyia longipalpis* showed that the null mutant is not able to produce late-stage infections (6 days post infection) as parasites were completely expelled during defecation (Volf, Charles University, Prague, Czechia, personal communication). This is most likely a result of the decreased flagella length and motility which might impede both attachment of the parasite to the gut epithelium and migration of the parasite towards the anterior midgut and the stomodeal valve. By day 6 post infection wild type parasites would already have developed into leptomonad forms causing a massive infection and a “blocked fly” by producing the promastigote secretory gel (PSG). This stage is obligatory for developing infectious metacyclic promastigotes and for the eventual transmission of the parasite to the mammalian host. In conclusion, *LmxMPK3* null mutants are not able to complete their life cycle by failing to establish sand fly infection.

5.2 The expression profile of LmxMPK3 during differentiation of *L. mexicana*

Having the knowledge that LmxMPK3 has a critical role in flagellar length regulation and is only expressed in the promastigote stage of the parasite (Erdmann, diploma thesis, 2004; Erdmann *et al.*, 2006), differentiation studies were performed for *L. mexicana* in order to identify a possible correlation between the LmxMPK3 expression pattern and flagellar outgrowth and resorption (see 4.2).

Both LmxMPK3 expression as well as flagellar outgrowth were first detectable 16 h after initiation of differentiation to promastigotes and gradually increased thereafter. Thus, flagellar assembly might be directly coupled with LmxMPK3 expression. This would imply that the MAP kinase had already been activated at that time which is actually possible as its physiological activator LmxMKK was already detectable at 10 h. However, neither the phosphorylation pattern nor the enzymatic activity of LmxMPK3 and LmxMKK have been assessed during differentiation.

Both LmxMPK3 expression as well as flagellar length declined during differentiation to axenic amastigotes. However, the flagella had been completely resorbed before LmxMPK3 was completely absent at 48 h. Again, nothing is known about the phosphorylation state or the activity of the MAP kinase during differentiation which makes an interpretation of this observation difficult.

It can be summarised that flagella protruding from the flagellar pocket can only be found in cells expressing LmxMPK3. Nevertheless, it has to be kept in mind that *LmxMPK3* null mutants can grow a flagellum to a certain extent - however lacking a normal PFR - and can also completely resorb the flagellum during differentiation to amastigotes. It is therefore very likely that additional regulator proteins control the early events in flagellar outgrowth and the late events in flagellar resorption during differentiation.

5.3 The subcellular localisation of LmxMPK3 and its activator LmxMKK

Both LmxMPK3 and its activator LmxMKK are involved in flagellar length regulation (Wiese *et al.*, 2003a; Erdmann, diploma thesis, 2004; Erdmann *et al.*, 2006), however, the precise function of both kinases in this complex mechanism is unknown. This question was approached by the successful generation of *L. mexicana* GFP-LmxMPK3 and GFP-LmxMKK mutants and subsequent localisation studies using fluorescence microscopy (see 4.3).

The expression of the different GFP-fusion proteins in the respective deletion background could be verified for most of the GFP-LmxMPK3 mutants and for all GFP-LmxMKK mutants by immunoblot analysis (see 4.3.2). Actually, all GFP mutants are able to restore long flagella (see 4.3.3). This also includes the GFP-LmxMPK3 clones for which immunoblot analysis had failed indicating that the fusion protein is correctly expressed in all the different mutants.

The GFP-LmxMPK3 mutants and the GFP-LmxMKK mutants differ from each other in terms of the expression levels of the fusion proteins and flagellar lengths which is probably due to the different expression strategies used. The GFP-LmxMPK3 mutants contain an extrachromosomal copy of the GFP-fusion protein on an expression vector constructed by Dubessay *et al.* in 2006 in which gene expression is controlled by the *DHFR-TS* intergenic region. In contrast, the GFP-LmxMKK mutants have been generated by introducing a cassette with the *LmxMKK-egfp* gene and the *L. mexicana CPB2.8* gene intergenic region into the 18S rRNA locus. The cassette construct was created by Misslitz *et al.* in 2000 for uniform and high level expression of transgenes in *Leishmania*. Extrachromosomal expression of GFP-LmxMPK3 is weaker than LmxMPK3 expression in the *L. mexicana* wild type which is reflected by the shift of flagellar lengths to lower values compared to the wild type. GFP-LmxMKK expression under control of the 18S rRNA promoter and the *CPB2.8*

gene intergenic region is higher than LmxMKK expression in the wild type matching the shift of flagellar lengths to higher values compared to the wild type.

Despite the differences in expression levels of the GFP-fusion proteins in the GFP-LmxMPK3 and GFP-LmxMKK mutants, the subcellular localisation of the different kinases looks very similar (see 4.3.4). This reflects that LmxMPK3 and LmxMKK are interaction partners in the same MAP kinase signalling pathway. Both kinases are localised in the cytosol, but are clearly more concentrated around the nucleus, within the flagellum and at its base. Since GFP alone had never been detected in immunoblot analysis, the fluorescence clearly derived from the respective GFP-fusion protein. Furthermore, mutants with GFP linked either N- or C-terminally to LmxMPK3 reveal no difference in the subcellular localisation of the kinase indicating that GFP is unlikely to interfere with the physiological function of LmxMPK3.

Taking together the subcellular localisation of LmxMPK3 and the phenotype of the *LmxMPK3* null mutants, there are again several putative physiological roles of the MAP kinase as already elucidated in 5.1.1. A localisation around the nucleus indicates that LmxMPK3 could either be involved in the export of mRNA from the nucleus, regulation of mRNA stability or translation initiation which is closely linked to the nuclear export of mRNAs. However, the MAP kinase does not seem to be involved in splicing events or the modification of premature RNA which occurs within the nucleus. The respective mRNAs would probably encode proteins which are involved in flagellar assembly or intraflagellar transport (IFT). LmxMPK3 could also be localised to the ER and thus have an indirect role in the targeting of lysosomal, secretory or membrane proteins.

The flagellar localisation of LmxMPK3 dovetails nicely with its role in flagellar assembly and length regulation. As the fluorescence along the whole length of the flagellum is stronger than in the cytoplasm, the MAP kinase is suggested to be actively transported into the flagellum, most likely by IFT. There, it might phosphorylate components of the IFT machinery including accessory kinesins and thereby regulate IFT. LmxMPK3 might also be constantly moved in and out of the flagellum by IFT and serve as a molecular sensor of the outside environment or the state of the flagellum. A change in the phosphorylation state and thus in the enzymatic activity of LmxMPK3 returning to the flagellar base or to the cell body would provide the cell with the relevant information. It has actually been shown that the aurora protein kinase CALK is targeted into the flagellum and is involved in a sensing system regulating flagellar assembly (Pan and Snell, 2000; Pan and Snell, 2003; Pan *et al.*, 2004). It is also very interesting to find LmxMPK3 concentrated at the base of the flagellum as this is the area where IFT particle assembly takes place and cargo proteins are selected for targeting into the flagellum (Cole, 2003). Indeed, several IFT complex proteins localise around the area of the basal body (Cole *et al.*, 1998; Deane *et al.*, 2001; Pedersen *et al.*,

2005; Absalon *et al.*, 2008). LmxMPK3 could therefore control IFT particle formation or cargo selection and thereby regulate flagellar assembly.

5.4 Characterisation of an inhibitor-sensitised LmxMPK3 mutant - an inducible system for selective kinase silencing

Although the generation of the *LmxMPK3* null mutants and the subsequent phenotype analysis provided a lot of information about the physiological function of LmxMPK3, an inducible system for the specific silencing of LmxMPK3 *in vivo* was additionally established (see 4.4). A main advantage of an inducible system over the knock-out strategy is that the examined cells lack the time to compensate for the missing activity of the target protein. Instead, immediate and transient effects caused by the induced silencing of the target protein can be studied. The inducible system used in this work was described by Bishop *et al.* (2001) and works through the specific inhibition of an inhibitor-sensitised protein kinase by a cell-permeable synthetic inhibitor. Kinase sensitisation was described to be achieved by replacing the so-called “gate keeper” residue - an amino acid which carries a bulky side chain - by glycine or alanine, thereby engineering a pocket in the ATP-binding site. The inhibitor reveals a corresponding bump fitting into the created pocket of the kinase. A main requirement is that the introduced mutation of the kinase is functionally silent and does not alter the subcellular localisation, protein-protein binding interactions or substrate specificity. In addition, the inhibitor must not act on any wild type kinases.

The “gate keeper” residue of LmxMPK3 (threonine 116) had been replaced by glycine as confirmed by sequencing of the generated expression vector containing one copy of the inhibitor-sensitised kinase gene *LmxMPK3IS*. The expression of LmxMPK3IS in the *LmxMPK3* deletion background of *L. mexicana* could be verified by immunoblot analysis (see 4.4.2). Expression levels are, however, significantly decreased as compared to LmxMPK3 levels in the wild type. Strangely, the *LmxMPK3IS* mutants derived from the two independent null mutants $\Delta LmxMPK3-I-HN1$ and $\Delta LmxMPK3-I-PN6$ strongly differ from each other in flagellar lengths (see 4.4.3). The clones derived from $\Delta LmxMPK3-I-HN1$ are clearly able to restore long flagella with a distribution of lengths resembling those of the *LmxMPK3* add back mutants, but with maximal lengths even exceeding those of the wild type. The observation that most flagella do not quite reach the wild type values reflects the fact that LmxMPK3IS protein levels in these mutants are lower than LmxMPK3 levels in the wild type. The ability of the mutant to restore long flagella indicates that it is very likely that the sensitising mutation in LmxMPK3 is functionally silent. Obviously, LmxMPK3IS can carry out all physiological functions relevant for a proper regulation of flagellar length. In contrast, the clones which originated from $\Delta LmxMPK3-I-PN6$ are not able to restore wild type flagella

displaying flagellar lengths hardly exceeding those of the null mutants. The fact that the same vector construct has been used as for the $\Delta LmxMPK3$ -HN1-derived clones and that LmxMPK3IS protein amounts are equally high in the mutants originating from $\Delta LmxMPK3$ -HN1- and $\Delta LmxMPK3$ -PN6 leads to the conclusion that the expressed protein in the $\Delta LmxMPK3$ -PN6-derived clones is not functional.

An inhibitor test on the inhibitor-sensitised mutant $\Delta LmxMPK3$ -HN1+LmxMPK3IS K2 (see 4.4.4) showed that the inhibitor 1-naphthyl-pyrazolo[3,4d]pyrimidine (1-NA-PP1) selectively inhibits LmxMPK3IS and does not affect the activity of LmxMPK3. This was indicated by the gradual flagellar shortening in the inhibitor-sensitised mutant after addition of the inhibitor which could not be observed in the *L. mexicana* wild type. This observation also suggests that 1-NA-PP1 does not inhibit any other protein kinase in *Leishmania* at the concentration used. At least, the observed drug effect of flagellar shortening is undoubtedly specific to the inhibitor-sensitised *LmxMPK3* mutant. Effects caused by the solvent of inhibitor are insignificant. Moreover, the inhibition of LmxMPK3IS by 1-NA-PP1 is (mostly) reversible as flagella of the inhibitor-sensitised mutant elongated after removal of the inhibitor by washing of the cells. A complete removal of the inhibitor might have been achieved by performing additional washing steps.

In summary, the sensitisation strategy could be successfully applied to LmxMPK3 as all requirements of the system have been met. Furthermore, the performed inhibitor test confirmed the role of LmxMPK3 in flagellar length control and thus supports the results of the *LmxMPK3* deletion studies. The system had also been successfully established for LmxMPK1 and actually revealed its role in controlling promastigote proliferation which had not been identified by the knock-out approach (Melzer, PhD thesis, 2007). It is especially interesting to apply this strategy to essential kinases for which functional analysis using the knock-out strategy completely fails.

Moreover, the kinase sensitisation strategy represents a tool for identifying protein kinase substrates. This could be achieved by a comparison of mRNA levels or the (phospho)proteome of the respective inhibitor-sensitised mutant before and after inhibitor treatment. It has also been shown that inhibitor-sensitised kinases accept structurally modified ATP analogues such as N⁶(benzyl)ATP which are again poorly accepted by wild type kinases (Shah *et al.*, 1997; Liu *et al.*, 1998a; Liu *et al.*, 1998b). Using [γ -³²P]ATP analogues the direct kinase substrates are specifically labelled in the presence of other kinases. This approach has already been successfully applied for the identification of several kinase substrates (Habelhah *et al.*, 2001; Shah and Shokat, 2002; Eblen *et al.*, 2003).

5.5 The correlation between LmxMPK3 amount and activity, and flagella length

Before commencing this work it was already known that the lack of LmxMPK3 in *L. mexicana* leads to flagella which are reduced to roughly one-fifth of the wild type length (Erdmann, diploma thesis, 2004). However, it was not clear whether flagellar length depends on the amount of LmxMPK3 protein in a gradual manner or immediately assumes its maximal value once the amount of the MAP kinase exceeds a specific threshold level. Moreover, nothing was known about the correlation between the enzymatic activity of LmxMPK3 and flagellar length. In this work two key experiments have been carried out to approach this question. First, fluorescence-activated cell sorting (FACS) was performed using an *L. mexicana* GFP-LmxMPK3 mutant (see 4.3 and 5.3), and second, an inhibitor test was carried out on an inhibitor-sensitised *LmxMPK3* mutant which has already been discussed in 5.4.

Sorting of the GFP-LmxMPK3 promastigotes into subpopulations with different fluorescence intensities was successful, and immunoblot analysis revealed that fluorescence intensity directly correlates with the GFP-LmxMPK3 protein amount of a single cell (see 4.3.5). The latter was rather expected, as neither GFP nor LmxMPK3 alone had been detected in immunoblot analysis of the GFP-LmxMPK3 mutant (see 4.3.2 and 5.3). Measurements of flagella lengths in the different subpopulations (see 4.3.5) eventually elucidated that the length of the flagellum depends on the LmxMPK3 protein amount in a gradual manner.

Some other results in this work are actually in accordance with this finding. The *LmxMPK3* add back mutants re-express the MAP kinase at lower protein levels compared to the wild type, and consistently the flagella of the add back mutants reach only 70-75% of the wild type value on average (see 4.1.2, 4.1.3 and 5.1.1). Furthermore, up- and down-regulation of LmxMPK3 protein levels during *L. mexicana* wild type differentiation is tightly linked with flagellar elongation and shortening (see 4.2 and 5.2). However, numerous other proteins are up- or down-regulated during differentiation from amastigotes to promastigotes and vice versa. Thus, this observation does not allow a direct conclusion about a correlation between LmxMPK3 amounts and flagellar lengths but is yet in accordance with this hypothesis.

The FACS experiment using the GFP-LmxMPK3 mutant did not consider the phosphorylation state or the activity of the MAP kinase. Although it might seem evident that protein kinases exclusively act through their enzymatic activity, it is not uncommon for them to also function via protein-protein interactions. This is most clearly reflected by examples where the expression of a kinase-deficient form of a protein kinase generates a phenotype that is distinct from the knock-out (Bishop *et al.*, 2001). For instance, the MAP kinases Fus3 and Kss1 have been shown to reveal kinase-independent functions in *Saccharomyces cerevisiae* (Madhani *et al.*, 1997).

To investigate the correlation between the enzymatic activity of LmxMPK3 and flagellar length, an inhibitor test was carried out on an inhibitor-sensitised *LmxMPK3* mutant (see 4.4.4) which has already been discussed in 5.4. It turned out that the length of the flagellum in *L. mexicana* correlates with the activity of LmxMPK3.

In summary, it can be concluded that flagellar length correlates with the intracellular amount of activated LmxMPK3. This is most likely only a very small fraction of the total LmxMPK3 protein amount within the cell. Generally, the ratio of the phosphorylated to non-phosphorylated form of a protein can be very low, especially for signalling proteins. For instance, a certain serine residue of the transcription factor p53 is only phosphorylated in 5% of all molecules in *C. reinhardtii* (Wagner *et al.*, 2006).

5.6 Biochemical characterisation of LmxMPK3 and LmxMPK3-KM

For the biochemical characterisation of LmxMPK3 recombinant expression of the wild type kinase in *E. coli* and subsequent affinity purification via a glutathione-S-transferase (GST)-tag had already been established (Erdmann, diploma thesis, 2004). In this work optimisation of the reaction conditions for GST-LmxMPK3 regarding temperature, ion concentrations and the pH value for *in vitro* kinase assays was further improved (see 4.5.3). Maximal substrate phosphorylation takes place at a pH between 6.0 and 7.0. Optima around a neutral pH have been found for all *Leishmania* MAP kinases investigated to date (Wiese *et al.*, unpublished) which is in accordance with the cytosolic pH of *Leishmania* which is strictly kept between 6.5 and 7.4 (Zilberstein and Shapira, 1994). LmxMPK3 prefers manganese over magnesium as maximal substrate phosphorylation occurred at the highest Mn^{2+} concentration (10 mM) in the absence of Mg^{2+} ions. This classifies LmxMPK3 as a manganese-dependent protein kinase and confirms previous results (Erdmann, diploma thesis, 2004). The divalent metal cations are essential for the proper coordination of the phosphoryl groups of ATP for catalysis. One ion is chelated by an asparagine residue situated in the catalytic loop and the other is chelated by the aspartate residue of the conserved DFG motif at the base of the activation loop. Between two and four water molecules contribute to the coordination sphere of one cation (Matte *et al.*, 1998). The crystal structure of phosphoenolpyruvate carboxykinase which requires one Mg^{2+} and one Mn^{2+} ion for enzymatic activity revealed that the cations are specific for their respective binding site probably due to their Lewis acidity and ionic radii (Tari *et al.*, 1997). Accordingly, non-activated LmxMPK3 might only allow binding of Mn^{2+} . Alternatively, both Mg^{2+} and Mn^{2+} might be able to bind to the kinase, however, only Mn^{2+} might be in a position which allows a proper coordination of the phosphoryl groups of ATP. A preference for Mn^{2+} over Mg^{2+} has been found for most MAP kinases investigated in *L. mexicana* (Wiese *et al.*, unpublished) and also for several plant

protein kinases (Mayrose *et al.*, 2004). However, it has to be kept in mind that activated LmxMPK3 might show a different preference for divalent cations which is elucidated in 5.7.1. Furthermore, Mg^{2+} is much more abundant in cells than Mn^{2+} with a ratio of approximately 1000:1 (Bolton *et al.*, 2002). Auto- and substrate phosphorylation of LmxMPK3 gradual increase from 25 to 40°C which does not reflect the exclusive function of the MAP kinase in the promastigote stage with an environmental temperature of roughly 27°C. However, similar results have been obtained for other MAP kinases of *L. mexicana* such as LmxMPK1 which also contributes to specific functions in promastigotes (Melzer, PhD thesis, 2007).

In this work an enzymatically inactive mutant of LmxMPK3 was generated as a negative control by replacing the highly conserved lysine residue of subdomain II (K62), essential for the kinase activity (Carrera *et al.*, 1993), by a methionine residue. In active kinases the invariant lysine forms an ionic bond with a conserved glutamate residue in the α C-helix which is an important mediator of conformational changes taking place within the catalytic centre. Moreover, the lysine residue positions the α - and β -phosphoryl groups of ATP for catalysis. The lysine residue is essential for the phosphoryl transfer reaction. The recombinant expression and subsequent purification of the enzymatically inactive GST-LmxMPK3-KM was successful (see 4.5.2). As expected, replacement of lysine 62 entirely abolishes the enzymatic activity of the MAP kinase as proven by an *in vitro* kinase assay which has been carried out along with wild type LmxMPK3 (see 4.5.4). Phosphorylation reactions in assays using the wild type kinase are therefore caused by LmxMPK3 itself and not by a contaminating protein kinase. Thus, the requirement was met to proceed with the analysis of the activation of LmxMPK3 by its physiological activator LmxMCK.

5.7 The activation of LmxMPK3 and its molecular mechanism

5.7.1 Phosphorylation and activation of LmxMPK3 and LmxMPK3-KM

Activated LmxMCK has been found to phosphorylate and activate LmxMPK3 *in vitro* and *in vivo* (Scholz, PhD thesis, 2008; Erdmann *et al.*, 2006). Since the physiological activator of LmxMCK is not known, *in vitro* assays are generally performed with a constitutively active aspartate mutant of the MAP kinase kinase (MAPKK), named LmxMCK-D. Several residues, including the potential phosphorylation sites of the activation loop, have been replaced by aspartate residues, thus mimicking a phosphorylation (Wiese *et al.*, 2003a). Several kinase assays have already been carried out to assess the interaction between LmxMPK3 and LmxMCK-D and the activation of LmxMPK3 (Scholz, PhD thesis, 2008; Erdmann *et al.*, 2006). However, the combination of equal amounts of the different LmxMPK3 and LmxMCK

mutant proteins made it difficult to ascribe the observed phosphorylation of the artificial substrate MBP (myelin basic protein) to one of those kinases.

Here, the activation of LmxMPK3 was further analysed by pre-incubating the MAP kinase with highly diluted LmxMKK-D in the presence of unlabeled ATP for an *in vitro* activation of LmxMPK3 (see 4.6.1). Subsequent radioactive kinase assays using pre-incubated GST-LmxMPK3 or GST-LmxMPK3-KM with MBP revealed something very interesting. The *in vitro*-activated LmxMPK3-KM, which was expected to be enzymatically inactive, revealed an auto- and substrate phosphorylation which was almost as strong as for the activated wild type MAP kinase (see Figure 31). A control assay containing only the pre-incubated activator in the absence of LmxMPK3 and showing no phosphorylation proved that the observed substrate phosphorylation was not caused by traces of LmxMKK-D.

Obviously, replacement of the invariant lysine 62 in LmxMPK3 can only eliminate the basic enzymatic activity of the MAP kinase. Once LmxMPK3 is phosphorylated by its activator the kinase is most likely forced into a conformation that leads to a high catalytic activity which is not dependent on the presence of the otherwise essential lysine residue. There are two possible explanations for this finding. On the one side, the conformation of the catalytic centre as well as the orientation of other important residues and of the divalent cations after activation of LmxMPK3 might be sufficient to catalyse the phosphoryl transfer reaction in the absence of lysine 62 or any substituting residue. Indeed, K52R ERK2 lacking the invariant lysine retains 5% basal activity and 5-7% maximal activity after phosphorylation by ERK activator compared to the wild type kinase (Robbins *et al.*, 1993). However, structural analysis of this mutant kinase showed that arginine in this position can interact with ATP (Robinson *et al.*, 1996). It is very unlikely that methionine, which was used to replace lysine 62 in LmxMPK3, can function in the same way as it is not positively charged. Accordingly, K52A ERK2 retains only 1% of wild type activity (Robinson *et al.*, 1993). Thus, the other possibility is that a different lysine residue might compensate for the loss of lysine 62 in the active state of LmxMPK3. The kinase indeed contains an adjacent lysine in position 63 which might take up this role. This adjacent lysine is also found in LmxMPK13, however, an enzymatically inactive mutant of this MAP kinase does not recover activity after phosphorylation by its activator LmxPK4 (Scholz, PhD thesis, 2008). Interestingly, the serine/threonine protein kinase WNK (with no lysine (K)) 1 lacks the otherwise invariant lysine in subdomain II and uses a lysine residue in subdomain I to carry out the phosphoryl transfer reaction (Xu *et al.*, 2000). LmxMPK3, however, does not contain any positively charged residues in subdomain I. To clarify the situation for this MAP kinase, site-directed mutagenesis of lysine and arginine residues of subdomain II could be performed. Furthermore, determination of the crystal structure of phosphorylated LmxMPK3-KM with ATP and Mg²⁺ or Mn²⁺ could identify the residues approaching the α - and β -phosphoryl

groups of ATP or the conserved glutamate residue in the α C-helix. It would also be very interesting to test whether LmxMPK3-KM is able to complement the *LmxMPK3* null mutant phenotype. Respective mutants of Src, CDKs, protein kinase C, MAP/ERK kinase and other protein kinases, however, have been shown to be non-functional *in vivo* (Robinson *et al.*, 1996).

In this work a co-expression system was successfully established (see 4.6.2) which allows an *in vivo* activation of LmxMPK3 by its activator LmxMKK within *Escherichia coli* cells overnight. As only the MAP kinase to be activated is provided with a His-tag, it can be affinity purified separately from its activator. The main advantages of this system over the *in vitro* activation described above are the long period of time in which both kinases can interact with each other supporting a maximal activation and the absence of the activator in the eluate containing activated LmxMPK3. The cloning of various combinations of the different kinase mutants into the co-expression vector pJCduet allowed an extensive analysis of the activation mechanism of LmxMPK3.

The recombinant expression and affinity purification of His-LmxMPK3 and enzymatically inactive His-LmxMPK3-KM derived from the different co-expression constructs was successful although the yield of the purified kinase differed significantly (see 4.6.2.2). The yield of His-LmxMPK3 expressed on its own or co-expressed with wild type LmxMKK was very high. In contrast, the yield of His-LmxMPK3 was just moderate upon co-expression with constitutively active LmxMKK-D, and the yield of His-LmxMPK3-KM was generally very poor. This was not due to the affinity purification as immunoblot analysis detected only low protein amounts of the MAP kinase in the cell lysates (Erdmann, unpublished results). Therefore, it is assumed that His-LmxMPK3-KM is rapidly turned over in *E. coli*.

His-LmxMPK3 is activated upon co-expression with constitutively active LmxMKK-D as verified by a strong MBP phosphorylation in *in vitro* kinase assays (see 4.6.2.4, Figure 34). The kinase activity is indeed equally high in a pH range between 6.5 and 7.5, and at 10 mM Mn^{2+} and standard ion concentrations (2 mM Mn^{2+} , 10 mM Mg^{2+}) (see 4.6.2.3). This result reflects that the phosphorylation of LmxMPK3 by its activator probably triggers a conformational change which leads to a high catalytic activity of the kinase tolerating a wider range of pH values and ion concentrations than the non-activated kinase. Nevertheless, kinase assays were always performed at 10 mM Mn^{2+} and pH 6.5 which had previously been used for GST-LmxMPK3. Interestingly, LmxMPK3 activation caused by wild type LmxMKK and LmxMKK-D is equally strong as shown by the MBP phosphorylation in kinase assays (see 4.6.2.4, Figure 34). This finding was rather unexpected, since it had previously been shown that recombinant wild type LmxMKK has neither autophosphorylation (Wiese *et al.*, 2003a) nor MBP phosphorylation activity (Scholz, unpublished data). Obviously, LmxMKK strongly prefers its physiological substrate LmxMPK3 over MBP, the artificial substrate. The

physiological substrate might initiate an “induced fit” (Koshland, 1958) and thereby optimise enzyme conformation for the phosphoryl transfer reaction. It is also very interesting that once the physiological substrate is offered, LmxMCK catalyses its phosphorylation no matter if LmxMCK itself is activated by a mimicked phosphorylation in the activation loop. It is generally anticipated that the activation of MAPKKs requires the phosphorylation of two conserved serine or threonine residues in their activation loops, however, either phosphorylation alone leads already to a strong increase of kinase activity (Alessi *et al.*, 1994; Zheng and Guan, 1994). It is yet possible that the long period of time in which both kinases interact with each other in the *E. coli* cells supports the phosphorylation and thus activation of LmxMPK3 by non-activated LmxMCK. Second, non-activated LmxMPK3 reveals basal substrate phosphorylation activity and has been shown to phosphorylate enzymatically inactive LmxMCK-KM-D (Scholz, PhD thesis, 2008). However, it is not known whether wild type LmxMCK is also phosphorylated by LmxMPK3 and if phosphorylation occurs also on the two conserved residues in the activation loop critical for kinase activation.

Moreover, it was observed that co-expression of the enzymatically inactive His-LmxMPK3-KM with LmxMCK-D also leads to an activation of the MAP kinase, however, not as strong as observed for wild type His-LmxMPK3 (see Figure 35). Control assays using His-LmxMPK3-KM only as well as the purified proteins from the expression of LmxMCK-D alone confirmed that the observed MBP phosphorylation was indeed caused by the *in vivo*-activated His-LmxMPK3-KM. Thus, this finding is in accordance with the *in vitro* activation of GST-LmxMPK3-KM by GST-LmxMCK-D discussed above. However, the activation of His-LmxMPK3-KM using the co-expression system is not as strong as that for GST-LmxMPK3-KM upon *in vitro* activation. It is possible that the *in vivo* activation system, providing an extensive phosphorylation over a long period of time, additionally leads to deactivating phosphorylations. On the other side, contaminating proteins were most abundant in the assays using His-LmxMPK3-KM which had always been carried out with high bead volumes. Those contaminations might have impaired the catalytic reaction in *in vitro* kinase assays.

5.7.2 Phosphorylation and activation of different LmxMPK3-TDY mutants

MAP kinases are generally activated by phosphorylation on the threonine (T) and the tyrosine (Y) residue of the conserved TXY activation motif located in the activation loop. This is typically carried out by a specific dual-specificity MAP kinase kinase (Payne *et al.*, 1991; L'Allemain *et al.*, 1992; Wu *et al.*, 1992). The respective motif in LmxMPK3 is represented by the triplet TDY.

To elucidate whether *Leishmania* MAP kinases, and in particular LmxMPK3, are activated by an equivalent mechanism, different LmxMPK3-TDY mutants were generated in which either T or Y is replaced by alanine (A) or leucine (L), respectively.

5.7.2.1 *In vitro* studies

The different His-LmxMPK3-TDY mutants and the respective catalytically inactive mutants were recombinantly co-expressed with constitutively active LmxMKK-D, using the *in vivo* activation system described in 5.7.1. While the yield of the affinity purified His-LmxMPK3-TDY mutants expressed on their own or co-expressed with LmxMKK-D was very high, the yield of the respective catalytically inactive His-LmxMPK3-TDY-KM mutants which had been co-expressed with LmxMKK-D was very low (see 4.7.1.2). The latter is consistent with the poor yield of His-LmxMPK3-KM which has been ascribed to a rapid turn over of this kinase mutant in *E. coli* (see 5.7.1).

The different His-LmxMPK3-TDY mutants and the respective catalytically inactive mutants from the different co-expressions were subjected to *in vitro* kinase assays along with wild type His-LmxMPK3 and His-LmxMPK3-KM. The extent of tyrosine phosphorylation of LmxMPK3 was traced by immunoblotting of equivalent non-radioactive kinase assays using a monoclonal antibody against phosphotyrosine (see 4.7.1.3, Figure 37).

Non-activated His-LmxMPK3 performs a weak autophosphorylation on tyrosine. The lack of phosphorylated tyrosine residues in the catalytically inactive His-LmxMPK3-KM expressed on its own proves that the tyrosine phosphorylation in His-LmxMPK3 was not caused by any *E. coli* protein kinases (see Figure 38). The constitutively active LmxMKK-D catalyses a strong phosphorylation on tyrosine in both His-LmxMPK3 and His-LmxMPK3-KM.

His-LmxMPK3-TDL expressed on its own lost its ability to perform auto- and substrate phosphorylation indicating that the TDY-tyrosine is the only amino acid residue on which autophosphorylation takes place in non-activated LmxMPK3. Furthermore, this tyrosine seems to be essential for basal substrate phosphorylation activity. Similar results have recently been obtained for a TDF mutant of LmxMPK1 (Melzer, PhD thesis, 2007; Melzer, unpublished results). However, upon activation by LmxMKK-D the auto- and substrate phosphorylation activity of His-LmxMPK3-TDL is almost as strong as that of activated His-LmxMPK3. Thus, tyrosine phosphorylation in the TDY activation motif seems to play a minor role in the activation of LmxMPK3. In other words, phosphorylation of the TDY-threonine is sufficient for the activation of the MAP kinase. This is contrary to TEF mutants of ERK1 and ERK2 which reveal no substrate phosphorylation activity *in vitro* after phosphorylation by their activator (Robbins et al., 1993). Nevertheless, it is anticipated that phosphothreonine in the activation loop occupies a central coordinating position forming critical contacts to the α C-helix thereby promoting closure of the N- and C-terminal lobes of the kinase essential for activation (Canagarajah *et al.*, 1997). Indeed, *in vivo* analysis of the LmxMPK1 activation mechanism revealed that phosphorylation of the TDY-threonine is sufficient for the full activation of the kinase (Melzer, PhD thesis, 2007). The total absence of tyrosine phosphorylation in His-LmxMPK3-TDL and His-LmxMPK3-TDL-KM reveals that the TDY-

tyrosine is the only tyrosine residue within the whole protein on which autophosphorylation and phosphorylation by the activator occur. However, activated His-LmxMPK3-TDL performs autophosphorylation on other residues (serine or threonine) as an autophosphorylation signal appears in the kinase assay which is discussed below.

The auto- and substrate phosphorylation activity of His-LmxMPK3-ADY expressed on its own is comparable to that of wild type His-LmxMPK3 indicating that the TDY-threonine is not essential for basal activity. In contrast, basal substrate phosphorylation activity in an ERK1-AEY mutant is decreased by 90% (Robbins *et al.*, 1993). Similar results have been obtained for an ADY mutant of LmxMPK1 (Melzer, PhD thesis, 2007). However, upon co-expression with LmxMKK-D the substrate phosphorylation activity of His-LmxMPK3-ADY is only increased to a very low extent. Thus, the phosphorylation of the TDY-threonine is essential for the maximal activation of the MAP kinase as it has already been shown for ERK 1/2 (Robbins *et al.*, 1993). In accordance, phosphorylation of the TDY-threonine is indeed necessary for the full activation of LmxMPK1 *in vivo* (Melzer, PhD thesis, 2007). The autophosphorylation is decreased in activated His-LmxMPK3-ADY. Taking also into account that activated His-LmxMPK3-TDL can still perform autophosphorylation (on serine or threonine), the TDY-threonine could be used as an additional autophosphorylation site after kinase activation. This would imply an intermolecular mechanism of autophosphorylation as the threonine of activated His-LmxMPK3-TDL has already been phosphorylated by the activator. A different hypothesis would suggest the additional autophosphorylation site (serine or threonine) of the activated kinase to be located outside of the TDY activation motif. In this case, the decreased autophosphorylation of activated His-LmxMPK3-ADY might be due to the low activation rate. The extent of tyrosine phosphorylation of His-LmxMPK3-ADY and His-LmxMPK3-ADY-KM by LmxMKK-D is comparable to that of His-LmxMPK3 and His-LmxMPK3-KM reflecting that phosphorylation of the TDY-tyrosine - the only tyrosine residue within LmxMPK3 which is phosphorylated by the activator - is not affected in the ADY mutant.

Unlike His-LmxMPK3-KM, neither His-LmxMPK3-TDL-KM nor His-LmxMPK3-ADY-KM reveal enzymatic activity upon phosphorylation by LmxMKK-D. Apparently, both threonine and tyrosine of the TDY motif need to be phosphorylated for activation of LmxMPK3-KM.

As only tyrosine phosphorylation of the His-LmxMPK3-TDY mutants had been considered in the immunoblot analysis, a more comprehensive mapping of phosphorylation sites was performed using tandem mass spectrometry on enriched phosphopeptides of the different purified His-LmxMPK3-TDY mutants which had been expressed on their own or co-expressed with LmxMKK-D (see 4.7.1.4 and 8.3).

The TDY-tyrosine was identified as the only phosphorylation site in non-activated His-LmxMPK3 and His-LmxMPK3-ADY, whereas His-LmxMPK3-TDL expressed on its own does

not reveal any phosphorylation. These results are consistent with the previous finding that autophosphorylation of non-activated LmxMPK3 only occurs on the TDY-tyrosine. Moreover, low peak intensities propose that autophosphorylation occurs only in a small fraction of kinase molecules which matches with the weak signal in immunoblot analysis tracing phosphotyrosine (see above).

In contrast, high peak intensities for activated His-LmxMPK3 suggest that a much higher percentage of kinase molecules is phosphorylated compared to the mere autophosphorylation occurring in non-activated His-LmxMPK3. Actually, activated His-LmxMPK3 exists in three different phosphorylation states. Either the threonine or the tyrosine alone is phosphorylated in the TDY activation motif, or both of those residues carry a phosphoryl group. Obviously, there is no defined order concerning which residue has to be phosphorylated first. This is contrary to the finding that ERK 1/2 is phosphorylated on the tyrosine before the threonine is phosphorylated *in vitro* and *in vivo* (Robbins and Cobb, 1992; Ferrell and Bhatt, 1997). This mechanism usually assures that non-active tyrosine-phosphorylated MAP kinases reach a defined accumulation threshold before threonine phosphorylation rapidly converts them to the active state (Ferrell, 1997; Ferrell, 1999). At least *in vitro* the situation seems to be different for LmxMPK3. Nevertheless, LmxMCK could indeed be characterised as a dual-specificity MAP kinase kinase (MAPKK). This was also confirmed by MS/MS analysis of the His-LmxMPK3-TDL and -ADY mutants after co-expression with LmxMCK-D, since a strong threonine and a strong tyrosine phosphorylation in the activation motif could be observed, respectively.

Therefore, the results gained by mass spectrometry could support as well as complement the results of the kinase assays and the immunoblot analysis discussed above. It still has to be pointed out that not all LmxMPK3 peptides were captured by mass spectrometry as not all of them could be successfully ionised and subsequently pass the mass analyser and the detector. It therefore cannot be totally excluded that there are additional threonine (or serine) phosphorylation sites in LmxMPK3.

Altogether, the fact that LmxMCK is a dual-specificity MAPKK which phosphorylates LmxMPK3 on both the threonine and the tyrosine of the TDY activation motif is consistent with the situation in higher eukaryotes (Payne *et al.*, 1991; L'Allemain *et al.*, 1992; Wu *et al.*, 1992). However, the finding that phosphorylation of the TDY-threonine is sufficient for the maximal activation of LmxMPK3 is contrary to what is usually found for MAP kinases in higher eukaryotes (Anderson *et al.*, 1990; Ahn *et al.*, 1991; Boulton and Cobb, 1991).

5.7.2.2 *In vivo* studies

The activation mechanism of LmxMPK3 was also investigated *in vivo* (see 4.7.2). The situation *in vivo* can differ significantly from that *in vitro* regarding ion concentrations and pH values. Moreover, in a cell MAP kinase signalling pathways are usually embedded into a complex network with other signalling pathways (Pawson and Saxton, 1999) and regulatory proteins such as scaffold proteins (Elion, 1998; Garrington and Johnson, 1999; Burack and Shaw, 2000). Furthermore, the *Leishmania* cell bears the physiological substrate of LmxMPK3.

Besides LmxMPK3-TDL and LmxMPK3-ADY, *in vivo* studies also included an LmxMPK3-ADL double mutant. The *L. mexicana* LmxMPK3-TDY mutants were generated by the introduction of the different *LmxMPK3-TDY* constructs - including a wild type control - into the null mutants $\Delta LmxMPK3-I-HN1$ and $\Delta LmxMPK3-I-PN6$. The constructs, also containing the 5'- and 3'-UTR of *LmxMPK3*, subsequently replaced one of the two different resistance marker genes in the *LmxMPK3* gene locus as verified by Southern blot analysis (see 4.7.2.2, Figure 41).

Flagellar lengths of the obtained clones are indicative for the activation state of the LmxMPK3-TDY mutants *in vivo*. The correlation between the activity of LmxMPK3 and the flagellar length has been discussed in 5.4 and 5.5. A comparative analysis of the mutant phenotypes, however, requires that the protein levels of the different LmxMPK3-TDY mutants are fairly similar in the different clones as flagellar length also depends on the LmxMPK3 protein amount (see 5.5). Immunoblot analysis confirmed a re-expression of the mutated kinase for all *L. mexicana* LmxMPK3-TDY mutants (see 4.7.2.2, Figure 42). The protein amounts of the different LmxMPK3-TDY mutants do not reach wild type LmxMPK3 levels, however, they are rather comparable to the LmxMPK3 protein levels in the *LmxMPK3* single-allele deletion mutants. This is consistent with the fact that one *LmxMPK3* allele in the *LmxMPK3* null mutants has been successfully reconstructed by the introduction of an *LmxMPK3-TDY* mutant gene copy. More importantly, the protein levels of the different LmxMPK3-TDY mutants were fairly similar in the different clones thus meeting the requirement for a comparative analysis of the mutant phenotypes.

Measurements of flagellar lengths were carried out for the different *L. mexicana* LmxMPK3-TDY mutants to elucidate which of the potential phosphorylation sites in the TDY motif are essential for the activation of LmxMPK3 *in vivo* (see 4.7.2.3). Actually, only LmxMPK3 containing the TDY wild type activation motif is able to restore long flagella in the *LmxMPK3* null mutants. In contrast, the *L. mexicana* LmxMPK3-TDL, -ADY and -ADL mutants display short flagella still resembling those of the null mutants.

The results clearly indicate that both the threonine and the tyrosine of the TDY activation motif of LmxMPK3 are essential for the full activation of LmxMPK3 *in vivo*. Moreover, it is most likely that both residues have to be phosphorylated by LmxMKK to achieve an activation of LmxMPK3 *in vivo* as the *LmxMKK* null mutants display short flagella although LmxMPK3 is present (Wiese *et al.*, 2003a). It had also been shown by immunoblot analysis of purified phosphoproteins that LmxMPK3 is only phosphorylated in *L. mexicana* wild type promastigotes but not in the *LmxMKK* null mutant (Scholz, PhD thesis, 2008; Erdmann *et al.*, 2006). The *in vivo* results are therefore contrary to the *in vitro* results which proclaimed that the phosphorylation of the threonine in the TDY motif is sufficient for the full activation of LmxMPK3 (see 5.7.2.1). This once again demonstrates that *in vitro* assays can never exactly mimic the *in vivo* situation. Neither the provided substrate nor the microenvironment including interacting proteins and ion concentrations are consistent with conditions in *Leishmania* promastigotes. It is therefore very likely that the LmxMPK3 activation mechanism is actually corresponding to that of MAP kinases in higher eukaryotes which require phosphorylation on both threonine and tyrosine in the conserved TXY activation motif for maximal activation which is usually catalysed by a dual-specificity MAP kinase kinase (Anderson *et al.*, 1990; Ahn *et al.*, 1991; Boulton and Cobb, 1991; Payne *et al.*, 1991; L'Allemain *et al.*, 1992; Wu *et al.*, 1992).

ERK 1/2 is phosphorylated on the tyrosine of the TXY activation motif before the threonine is phosphorylated *in vitro* and *in vivo* (Robbins and Cobb, 1992; Ferrell and Bhatt, 1997). Only as the non-active tyrosine-phosphorylated MAP kinases reach a defined accumulation threshold, threonine phosphorylation rapidly converts them to the active state (Ferrell, 1997; Ferrell, 1999). This mechanism enhances the cooperativity of MAP kinase activation (Pearson *et al.*, 2001) leading to an “ultrasensitive” and strictly regulated response to an input stimulus (Ferrell, 1999). Bearing in mind that LmxMPK3 is critically involved in the regulation of flagellar length, which varies strongly in the different morphological forms of promastigotes in the insect gut (see 1.1.4, Table 1), it is very likely that also LmxMPK3 requires a strict regulation. Thus, LmxMPK3 phosphorylation probably occurs in the same non-progressive manner as described for ERK 1/2. Only a strict regulation of LmxMPK3 would allow a close adaptation of flagellar lengths to the physiological function of the different forms of promastigotes. This includes, for instance, the ability of the long-flagellated nectomonads to attach to the midgut epithelium and to migrate towards the anterior midgut or the haptomonads in which the mostly short flagellum with an expanded tip mediates attachment to the cuticle-lined surface of the stomodeal valve (see 1.1.4).

5.8 Substrate search for LmxMPK3

Having identified LmxMKK as the activator of LmxMPK3 (Scholz, PhD thesis, 2008; Erdmann *et al.*, 2006) it was of further interest to search for LmxMPK3 substrates to elucidate the physiological role of LmxMPK3 and the downstream events of its signalling pathway. The opportunity to activate recombinantly expressed LmxMPK3 using its physiological activator set the stage for an effective *in vitro* substrate search.

Transcription factors are typical MAPK substrates in higher eukaryotes, and thus MAP kinase signalling often culminates in an altered gene transcription. As transcription factors are absent in *Leishmania* and gene expression is assumed to be regulated on the posttranscriptional level, *Leishmania* MAP kinase substrates might be involved in processes such as mRNA processing, transport, turnover or translation as well as modification, transport or turnover of proteins (Clayton and Shapira, 2007; Haile and Papadopoulou, 2007). Besides transcription factors also cytosolic protein kinases such as MAPKAPKs (MAPK-activated protein kinases) and other cytosolic proteins could be identified as MAP kinase substrates in higher eukaryotes. The association of some MAP kinases of higher eukaryotes with microtubules suggests also a role in the reorganisation of the cytoskeleton. Also bearing in mind that MAP kinases are known to be involved in numerous different processes such as cell proliferation, differentiation, stress response and apoptosis, there is actually a wide variety of molecules which can be considered as potential MAP kinase substrates in *Leishmania*.

Taking into account that LmxMPK3 is essential for flagellar assembly and flagellar length regulation, it is likely that the LmxMPK3 substrate either regulates gene expression of components involved in processes such as intraflagellar transport (IFT) or that it is a flagellar protein itself. The latter could either be a structural flagellar subunit or a component which is involved in the IFT, interaction or modification of other flagellar subunits.

Several primary sequence determinants have been found to be characteristic for MAPK substrates. The phosphorylation site (serine or threonine) defined as position 0 is usually followed by a proline residue in position +1 (Pearson *et al.*, 2001). Especially ERK 1/2 substrates often possess another proline residue in position -2 thus revealing the phosphorylation motif PXS/TP (Pearson *et al.*, 2001). Moreover, MAPK substrates often contain docking domains (D-domains) supporting the selective interaction with MAP kinases (Yang *et al.*, 1998; Enslin *et al.*, 2000). The D-domain consensus is (K/R)₂-X₂₋₆-I/L/V-X-I/L/V with at least two basic residues separated by 2-6 residues from a "hydrophobic-X-hydrophobic" sequence, where the hydrophobic residues are either leucine, isoleucine or valine. Occasionally, the sequence is C-terminally extended by another X-I/L/V motif. The FXFP motif is a different docking site specifically mediating the interaction with ERK 1/2 (Jacobs *et al.*, 1999).

Several unsuccessful approaches had already been made to identify substrates of LmxMPK3. These included the screening of a λ phage cDNA expression library by radioactive solid-phase phosphorylation using activated purified LmxMPK3 according to Fukunaga and Hunter (1997). In addition, phosphoproteins had been purified from promastigotes of the *L. mexicana* wild type and the *LmxMPK3* null mutant using the PhosphoProtein Purification Kit (Qiagen), and the obtained phosphoprotein eluates were separated by SDS-PAGE. The SDS-PAGE gel was silver-stained and screened for bands lacking in the eluate of the null mutant. There was, however, no visible difference in the band pattern of the wild type and the null mutant.

Here, two generally different approaches were used to identify LmxMPK3 substrates. On the one hand, single candidate proteins were tested which have a predicted flagellar localisation, exhibit potential MAP kinase phosphorylation sites and ideally have a hypothetical role in flagellar assembly. On the other hand, the entire proteome was screened by subjecting *Leishmania* lysates to kinase assays and by using the web-based computer programme PREDIKIN (Brinkworth *et al.*, 2003) for an *in silico* substrate search.

5.8.1 Testing potential candidate proteins for LmxMPK3 substrate function

5.8.1.1 PFR-2 and a PFR-2 mRNA regulating protein

It has been shown that the PFR assembly is strongly impaired in the *LmxMPK3* null mutants with flagella containing either only residual PFR or no PFR next to the axoneme. Immunoblot analysis additionally revealed that the null mutants contain roughly 4 times less PFR-2 per micrometer of flagellar length compared to the wild type. Therefore, PFR-2 could be a direct substrate of LmxMPK3, and phosphorylation of PFR-2 by LmxMPK3 might regulate its transport, assembly and/or turnover. PFR-2 does not contain a typical MAP kinase phosphorylation motif (SP or TP) (see 8.1.2), however, it is not known to date whether phosphorylations carried out by *Leishmania* MAP kinases are restricted to those motifs.

Immunoblot analysis of different fractions of phosphoprotein purifications from *L. mexicana* wild type and *LmxMPK3* null mutant promastigotes revealed that a fraction of PFR-2 is indeed phosphorylated in the wild type (see 4.8.1.1). However, the phosphorylation state of PFR-2 in the *LmxMPK3* null mutant could not be assessed as the protein was not detectable in any of the different fractions. This once more reflects the relative paucity of PFR-2 in the *LmxMPK3* null mutant (see 5.1.1). Consequently, the LmxMPK3 substrate function of PFR-2 could not be determined.

To improve the method, flagellar protein levels of the wild type and *LmxMPK3* null mutant could be adjusted using a fivefold excess of the null mutant, as flagellar lengths in the null mutant are reduced to approximately one-fifth of the wild type length. A flagellar protein

whose amount per micrometer of flagellar length is unchanged in the *LmxMPK3* null mutant - preferentially an axonemal protein - could serve as an internal loading control by probing the blot with a corresponding antiserum. The phosphorylation state of potential *LmxMPK3* substrate proteins in the wild type and the null mutant could then be directly compared. In the case of PFR-2, however, a roughly 20-fold excess of the null mutant fractions would have to be used to adjust PFR-2 levels (see 5.1.1).

The observed down-regulation of the PFR-2 expression in the *LmxMPK3* null mutants could alternatively take place on the mRNA level. Indeed, an AU-rich *cis*-regulatory element of 10 nucleotides had been found in the 3'-UTR of all *PFR* genes in *L. mexicana* strongly resembling the AU-rich elements (AREs) of higher eukaryotes. It had been shown that this element triggers a 10-fold down-regulation of the *PFR* mRNA amounts in amastigotes by inducing mRNA degradation (Mishra *et al.*, 2003). The latter could be mediated by an RNA binding protein which is constitutively expressed but only available for binding in amastigotes. The ability to bind to the mRNA regulatory element could be abolished by phosphorylation of the protein in promastigotes, and *LmxMPK3* could be the responsible kinase.

The *PFR-2* gene of *L. mexicana* had been isolated and characterised by Moore *et al.* in 1996. It is arranged in the genome as a tandem array of three identical genes designated *PFR-2A*, *PFR-2B* and *PFR-2C*. In this work RT-PCRs were performed on total RNA isolates of the *L. mexicana* wild type, the *LmxMPK3* null mutants and the *LmxMKK* null mutants using *PFR-2C*-specific oligonucleotides to assess whether the *PFR-2* mRNA amounts in the null mutants differ from that of the wild type (see 4.8.2.1). Actually, the *PFR-2* mRNA levels are equally high in the different null mutants and the wild type. In conclusion, neither *LmxMPK3* nor *LmxMKK* are involved in the regulation of *PFR-2* mRNA stability or in the transcription of the *PFR-2* genes. Instead, the down-regulation of the PFR-2 expression seems to take place on the protein level and could be due to a decreased translation rate or an impaired transport or assembly of PFR-2. The latter would eventually lead to an accumulation of the protein followed by its degradation which has already been discussed in 5.1.1.

5.8.1.2 The OSM3-like kinesin *LmxKin32*

As the *LmxMPK3* null mutants reveal flagella reduced to roughly one-fifth of the wild type length, it has been suggested that *LmxMPK3* is critically involved in flagellar length regulation (Erdmann, diploma thesis, 2004; see 5.1.1).

Intraflagellar transport (IFT) is the motor-dependent bidirectional movement of IFT particles along the length of eukaryotic flagella which is essential for the construction and maintenance of those organelles. Flagellar length has been suggested to be regulated by

shifting the ratio between the rates of assembly and disassembly (Marshall and Rosenbaum, 2001). Anterograde IFT (from base to tip) is mainly driven by heterotrimeric kinesin-2 (Cole, 1999), however, multiple kinesins (Fox *et al.*, 1994) can modulate IFT or even take over the function of heterotrimeric kinesin-2 (Scholey, 2008). Actually, in chemosensory cilia of *C. elegans* anterograde IFT is driven by heterotrimeric kinesin-2, termed kinesin-II, and a second kinesin-2 family member, known as OSM-3, which forms a homodimeric complex (Signor *et al.*, 1999; Snow *et al.*, 2004). While both kinesins function together to assemble the middle segment of the axoneme composed of microtubule doublets (with each motor being able to work in the absence of the other motor), OSM-3 alone extends the distal end consisting of microtubule singlets. However, OSM-3 only extends distal singlets in some ciliary types (Scholey, 2008).

The *L. major* genome reveals genes for two putative OSM-3-like kinesins, LmjF17.0800 and LmjF32.0680, and thus a similar mechanism for flagellar assembly might be used in this parasite. Kinesins have been shown to be regulated through phosphorylation (Wordeman, 2005). Indeed, both *L. major* OSM-3-like kinesins contain potential MAP kinase phosphorylation sites. Assuming that an OSM-3-like kinesin is a direct substrate of LmxMPK3, absence of the MAP kinase in the null mutants might abolish OSM-3 activity and thus the coordinated action of kinesin-II and OSM-3. The residual activity of kinesin-II might explain why null mutant flagella still reach a defined length.

In this work the *L. mexicana* homologue of LmjF32.0680 was tested as a potential substrate candidate of LmxMPK3 (see 4.8.3). The respective motor domain, designated LmxKin32, which is 100% identical to the *L. major* protein, was cloned and recombinantly expressed as a GST-fusion protein. LmxKin32 contains a PSSP and an SP motif with the potential phosphorylation site at S232 and S293, respectively. The former motif is flanked by two amino acid stretches resembling D-domains (see 8.1.3).

However, *in vitro* kinase assays did not reveal any phosphorylation of LmxKin32 by *in vitro*-activated GST-LmxMPK3 indicating that the OSM-3-like kinesin LmxKin32 is most likely no substrate of LmxMPK3 (see 4.8.3.3). As the kinesin motor domain had to be heat-inactivated before use, because it retained a high ATPase activity and led to an extensive cleavage of ATP (Erdmann, unpublished data), it cannot be totally excluded that recognition of the kinesin as a substrate was impeded by its loss of tertiary and secondary structure. Thus, generation and use of an enzymatically inactive mutant of LmxKin32 might help to clarify if the kinesin is a substrate of LmxMPK3. Klumpp *et al.* showed in 2003 that a switch I R210K mutant of *Drosophila melanogaster* kinesin is unable to hydrolyse ATP while microtubule functions are unaffected. A corresponding mutation could be introduced to the switch I element - with the consensus NXXSSRSH - of LmxKin32 which is partially overlapping with one of the potential D-domains.

5.8.1.3 The outer dynein arm docking complex (ODA-DC) subunit DC2

In the flagella of *Chlamydomonas reinhardtii* a protein complex called “outer dynein arm docking complex” (ODA-DC) was shown to consist of three subunits (DC1, DC2 and DC3) and to be responsible for binding of outer arm dynein to the A-tubules of the axonemal outer microtubule doublets (Takada *et al.*, 2002). Deletion studies for the subunit LdDC2 in *L. donovani* revealed a phenotype strongly resembling that of the *LmxMPK3* null mutant with promastigotes displaying flagella significantly reduced in length and cell bodies which were oval-shaped and smaller compared to the wild type (Harder, PhD thesis, 2005).

This observation suggested that the *L. mexicana* homologue (*Leishmania mexicana* genome project), designated LmxDC2, might be a direct substrate of LmxMPK3. Indeed, LdDC2 as well as the 100% identical *L. major* homologue CAB55364 (Ivens *et al.*, 2005) and the 94% identical LmxDC2 contain three potential MAP kinase SP phosphorylation motifs in the C-terminal part of the protein with the potential phosphorylation sites at S493, S515 and S532 (see 8.1.4).

Immunoblot analysis of different fractions of phosphoprotein purifications from *L. mexicana* wild type and *LmxMPK3* null mutant promastigotes proved that LmxDC2 is indeed phosphorylated in the wild type (see 4.8.4.1). As for PFR-2 (see above), the phosphorylation state of LmxDC2 in the *LmxMPK3* null mutant could not be determined as the protein was not detectable in any of the different fractions. Like PFR-2, LmxDC2 is a flagellar component and therefore could be much less abundant in the short-flagellated *LmxMPK3* null mutants.

As described above for PFR-2, the method could be improved by using a roughly fivefold excess of the null mutant fractions (accounting for the fivefold reduction in flagellar length) to adjust flagellar protein levels of the wild type and *LmxMPK3* null mutant. The exact ratio of LmxDC2 protein amounts in the cell lysates of the *LmxMPK3* null mutant and the wild type would have to be determined to exactly adjust LmxDC2 protein levels to those of the wild type.

In vitro kinase assays were also carried out using *in vivo*-activated LmxMPK3 and LdDC2 (see 4.8.4.2) which was already available for expression (Harder, PhD thesis, 2005) and shares a high percentage of amino acid identities (94%) with LmxDC2 including all of the potential MAP kinase SP phosphorylation motifs. As no increase in the phosphorylation of LdDC2 was detectable upon incubation with activated LmxMPK3, the ODA-DC subunit LmxDC2 is most likely no substrate of LmxMPK3.

5.8.1.4 Glutamine synthetase

In 2006, Wagner *et al.* identified 32 flagellar phosphoproteins in *Chlamydomonas reinhardtii* among which is the cytosolic isoform of glutamine synthetase named GS1. In *C. reinhardtii*

this enzyme is involved in ammonium assimilation, the regulation of nitrate assimilation (Cullimore and Sims, 1981) and glutamine production. Moreover, it is known to be phosphorylated by a Ca^{2+} - and calmodulin-dependent protein kinase and to bind to 14-3-3 proteins which participate in protein-protein interaction processes and signal transduction cascades in all eukaryotes (Ferl, 1996; Finnie *et al.*, 1999). The canonical 14-3-3-binding motif RSXS*X(P) (in which S* is the potential phosphorylation site) could indeed be identified in *C. reinhardtii* GS1 (see 8.1.5), however, it was not presented by any of the phosphopeptides detected by Wagner *et al.* (2006). Instead, T326 and S328 were identified as phosphorylation sites.

The corresponding threonine residue is also present in the glutamine synthetase of *L. mexicana* (Wiese *et al.*, unpublished data), designated LmxGS, and *L. major* (Ivens *et al.*, 2005) while the respective serine residue is absent in both proteins. Furthermore, the 14-3-3-binding motif is altered to RSKDR in both *Leishmania* species thus lacking the conserved phosphorylation site. However, both *Leishmania* proteins contain three conserved typical MAP kinase S/TP phosphorylation motifs at T197, T359 and S366 (see 8.1.5).

To test LmxGS as an LmxMPK3 substrate immunoblot analysis was performed on different fractions of phosphoprotein purifications from *L. mexicana* wild type and *LmxMPK3* null mutant promastigotes using an antiserum against LmxGS (see 4.8.5.1). It was discovered that LmxGS is phosphorylated to the same extent in the wild type and in the *LmxMPK3* null mutant indicating that LmxGS is most likely no substrate of LmxMPK3. The overall LmxGS protein amounts are slightly lower in the short-flagellated null mutant which could be due to a partially flagellar localisation. However, LmxGS also seems to be located mainly in the cytoplasm of the cell body. Immunofluorescence analysis using the same antiserum against LmxGS could be performed to confirm this assumption.

5.8.2 Screening the entire *Leishmania* proteome for LmxMPK3 substrates

5.8.2.1 *In vitro* kinase assays with activated LmxMPK3 on *Leishmania* lysates

A direct approach for identifying protein kinase substrates is the incubation of cell lysates from the organism of interest with the respective recombinantly expressed and purified protein kinase in the presence of radioactively labelled ATP followed by analysis of the phosphorylated proteins. However, this approach has rarely been applied as the cell lysates contain numerous other protein kinases and their respective substrates leading to a high background phosphorylation. In 2001, Knebel *et al.* introduced some modifications to this method which strongly reduced the background signals. First, the lysates should be subjected to gel filtration chromatography before analysis in order to remove cellular ATP. Second, the reaction buffer should contain Mn^{2+} instead of Mg^{2+} greatly reducing background

noise as found out empirically by Knebel *et al.* (2001). In addition, the method requires an active purified protein kinase.

Thus, to screen the *Leishmania* proteome for LmxMPK3 substrates, *Leishmania* lysates derived from *L. mexicana* wild type and *LmxMPK3* null mutant promastigotes were initially subjected to gel filtration chromatography to remove cellular ATP. The desalted cell extracts were subsequently subjected to radioactive kinase assays with activated LmxMPK3 using 10 mM Mn^{2+} in the absence of Mg^{2+} . The assays were carried out in the presence and absence of activated LmxMPK3 to distinguish phosphorylations catalysed by LmxMPK3 from those caused by cellular protein kinases from the lysates. A potential LmxMPK3 substrate is indicated by a band on the autoradiograph which is present when the lysates had been incubated with activated LmxMPK3 and absent when the assay had been performed without the MAP kinase. The reason for testing not only lysates of the wild type but also of the null mutant is that the LmxMPK3 substrate is most likely not - or at least less - phosphorylated in cells lacking LmxMPK3 and thus allows a stronger incorporation of radioactively labelled phosphate.

Interestingly, the autoradiograph showed two bands at approximately 30 and 38 kDa which were only detectable when the lysates had been incubated without activated recombinant LmxMPK3 (see 4.8.6). A possible interpretation of this result is that the LmxMPK3 substrate is either a protein kinase or phosphatase which is inactivated or activated by LmxMPK3, respectively. In this case, the two additional bands would correspond to substrates of the LmxMPK3 substrate. The LmxMPK3 substrate phosphorylation itself was obviously beyond the detection limit indicating that it is either a low-abundance protein or phosphorylated to a very low extent. Further analysis of the two additional bands using mass spectrometry was not possible due to the poor resolution of the protein bands in the gel. Knebel *et al.* (2001) suggested to subject the cell extracts to ion-exchange chromatography prior analysis to reduce background phosphorylation and also the number of different proteins in one gel lane.

5.8.2.2 *In silico* substrate search for LmxMPK3 using PREDIKIN

As experimental approaches had failed to identify substrates of LmxMPK3, an indirect computer-based method using the programme PREDIKIN (Brinkworth *et al.*, 2003) was applied to predict the consensus sequence of a heptapeptide substrate motif for LmxMPK3.

The programme is based on a set of rules for the prediction of the substrate specificity of serine/threonine protein kinases deduced from the primary sequence of their catalytic domain. The rules for the prediction of a heptapeptide substrate motif surrounding the phosphorylation site (positions -3 to +3) were developed from available crystal structures, sequence analysis of kinases and substrates and oriented peptide library experiments. 20 "substrate-determining residues" (SDRs) making contact with the side chains of six

residues surrounding the phosphorylation site in the substrate have been defined in relation to conserved kinase motifs. The SDRs are predominantly complimentary with the residues of the substrate regarding size, polarity, charge and hydrogen-bonding potential. The accuracy of PREDIKIN predictions has been shown to be comparable to that of systematic large-scale experimental approaches such as oriented peptide library experiments. Actually, for some protein kinases such as SIK1, Chk2 and CK1 PREDIKIN predictions can resemble real substrates even better (Brinkworth *et al.*, 2003).

For LmxMPK3 PREDIKIN predicted the substrate consensus [APQ]P[LQ][ST]P[CTSV][ASY]. A motif search in the *L. major* genome DB (Ivens *et al.*, 2005) using this consensus sequence yielded a total of 19 hits (see 4.8.7, Table 8) comprising 16 proteins of unknown function and three proteins with the following putative functions: an endonuclease/exonuclease/phosphatase (LmjF36.1150), a CPSF-domain protein (LmjF30.3710) and the splicing factor 3A (LmjF30.1830). As already discussed in 5.1.1, there is a wide variety of proteins qualified as potential LmxMPK3 substrates judging from the large number of components functionally involved in gene regulation and IFT. Thus, the choice of a test candidate out of those potential substrate proteins was not based on the predicted physiological function but on the substrate score, a parameter for the likelihood of a sequence to present a real substrate motif.

The putative endonuclease/exonuclease/phosphatase LmjF36.1150, designated LmjHS (HS for hypothetical substrate), containing the heptapeptide substrate motif PPLTPTA - with the central threonine being the potential phosphorylation site - revealed the highest substrate score of 92.49 (maximum is 100). Moreover, LmjHS contains the sequence motif KDPSGGLPLLRV resembling a D-domain typically supporting the selective interaction with MAP kinases (see above) which is located immediately N-terminally to the substrate phosphorylation motif (see 8.1.6). In this work the actual start codon of LmjHS has been defined as the next ATG triplet downstream and in frame with the one reported in the *L. major* genome DB (Ivens *et al.*, 2005) based on sequence alignments with the *L. infantum* and *L. braziliensis* homologues. Consequently, *LmjHS* is a gene of 2790 bp encoding a protein of 929 aa with a molecular mass of 100.8 kDa. LmjHS is 85% identical to its *L. infantum* homologue and only 54% identical to the *L. braziliensis* sequence. The orthologous proteins in *T. cruzi* and *T. brucei* are only 39% and 37% identical to LmjHS. In addition, they lack the first 190 and 151 amino acid residues, respectively, and display several sequence deletions and insertions compared to LmjHS (see 8.1.6). No significant similarities could be found to proteins of other organisms.

The Pfam protein families database classified LmjHS as a putative member of the endonuclease/exonuclease/phosphatase family which comprises magnesium-dependent

endonucleases and a large number of phosphatases involved in intracellular signalling. Indeed, sequence homologies to an inositol polyphosphate related phosphatase have been identified by the SMART tool. Interestingly, Dlakić (2000) discovered that different functionally unrelated signalling proteins contain a fold similar to Mg²⁺-dependent endonucleases. This fold is formed by a four-layered α/β sandwich motif which can cleave phosphoester bonds on different substrates. Proteins with sequence or structural similarities to AP (apurinic/aprimidinic) endonucleases include LINE-1 retrotransposons (Feng *et al.*, 1996), sphingomyelinases (Matsuo *et al.*, 1996), inositol polyphosphate 5-phosphatases, yeast cell cycle-regulating protein Ccr4p and the vertebrate circadian-clock-regulated protein nocturnin which is most likely involved in the posttranscriptional regulation of genes necessary for nutrient uptake, metabolism and storage (Green *et al.*, 2007). While the core of the different enzymes was preserved due to the common catalytic mechanism, variations were introduced to the loops connecting core β -strands and α -helices (Mol *et al.*, 1995; Gorman *et al.*, 1997) for the recognition of various substrates such as nucleic acids, phospholipids and possibly proteins.

Initially, only a small part of LmjHS was cloned encoding the peptide LRVGNSAPPPLTPA, designated LmjHSpep, which contains the predicted substrate heptapeptide and some adjacent amino acid residues including part of the putative D-domain. A GST-fusion protein of LmjHSpep was subjected to *in vitro* kinase assays with non-activated and activated LmxMPK3 (see 4.8.7.2, Figure 54). It was found that, while the non-activated MAP kinase phosphorylates LmjHSpep only to a very low extent, activated LmxMPK3 indeed catalyses a strong phosphorylation of the peptide. A control assay using the GST-tag alone confirmed that the phosphorylation had occurred exclusively on the substrate peptide (see Figure 55). This result indicates that activated LmxMPK3 actually recognises the PREDIKIN-predicted substrate peptide as a substrate *in vitro*. As phosphorylation site mapping of the phosphorylated peptide using mass spectrometry had not been successful, it is not known for sure that phosphorylation actually occurred on the threonine residue predicted by PREDIKIN. This is, however, very likely as it presents the only typical MAP kinase phosphorylation motif (PXS/TP) within the peptide. To assess the specificity of the phosphorylation reaction, the assays had also been performed with non-activated and activated LmxMPK13 (see Figure 54), the only other MAP kinase in our laboratory for which the activating MAP kinase kinase - in this case LmxPK4 - had been identified (Scholz, PhD thesis, 2008). Non-activated LmxMPK13 does not phosphorylate LmjHSpep showing that the peptide phosphorylation catalysed by non-activated LmxMPK3 is indeed specific. However, activated LmxMPK13 phosphorylates LmjHSpep roughly as strong as activated LmxMPK3. Again, it is not known on which exact residue the observed phosphorylation took place. Nevertheless, this result

indicates that the peptide is a rather unspecific substrate towards activated MAP kinases or at least towards the MAP kinases tested here.

Curiously, the PREDIKIN-predicted substrate consensus sequences for LmxMPK13 being M[ARY][AFKLNRS][ST]X[MV][NS] (Scholz, PhD thesis, 2008) and for LmxMPK3 which is [APQ]P[LQ][ST]P[CTSV][ASY] strongly differ from each other. Consequently, the LmjHS substrate motif PPLTPTA does not match the LmxMPK13 substrate consensus and reveals a substrate score of only 61.1 for this MAP kinase. Thus, the experimental data are not consistent with the predictions made by PREDIKIN. However, the LmjHS substrate motif contains mainly small residues often making few, if any, contacts with the enzyme (Brinkworth *et al.*, 2003) which might explain the low specificity.

The specificity of some protein kinases depends on other subsites than those considered above. Moreover, the substrate sequence has to be accessible to the kinase and adopt an extended conformation (Brinkworth *et al.*, 2003). It thus seems possible that a larger part of the amino acid environment of the substrate peptide, contributing to the protein conformation, influences the specificity of the phosphorylation reaction. Therefore, a 172 aa long N-terminal part of LmjHS including the predicted phosphorylation site was cloned for recombinant expression as a GST-fusion protein. *In vitro* kinase assays showed that non-activated LmxMPK3 performs a weak phosphorylation on LmjHS, whereas the activated MAP kinase catalyses indeed a strong phosphorylation of the hypothetical substrate (see 4.8.7.3, Figure 57). In conclusion, activated LmxMPK3 actually recognises LmjHS - whose selection was based on the PREDIKIN-predicted substrate motif - as a substrate *in vitro*. Since phosphorylation site mapping of the phosphorylated fusion protein using mass spectrometry had not been successful, it is not known if the phosphorylation actually occurred on the threonine residue predicted by PREDIKIN as there is also an SP phosphorylation motif located C-terminally to the predicted phosphorylation site. This time, however, the phosphorylation of LmjHS by LmxMPK3 was found to be specific as incubation with non-activated and activated LmxMPK13 led to no phosphorylation and only a very weak phosphorylation of LmjHS, respectively. Apparently, the protein conformation and/or additional subsites in the amino acid environment of the substrate are perfectly adjusted to those of LmxMPK3 resulting in a specific MAP kinase-substrate recognition.

A real substrate of LmxMPK3 certainly has to be a protein from *L. mexicana*. However, at the time the PREDIKIN-based LmxMPK3 substrate search was performed the *Leishmania mexicana* genome project had not yet been completed. Thus, an indirect way had to be chosen in which the heptapeptide motif search was initially carried out in the *L. major* genome DB, and the *L. mexicana* homologue could subsequently be accessed by homology-based PCR. Therefore, an equivalent N-terminal part of the *L. mexicana* homologue,

designated LmxHS, was cloned by PCR using *L. major*-based oligonucleotides. The *L. mexicana* 5'-end nucleotide sequence is 78% identical to the *L. major* sequence, and also the corresponding N-terminal amino acid sequences of LmxHS and LmjHS are only 60% identical to each other. Meanwhile, the entire amino acid sequence of LmxHS is accessible (*Leishmania mexicana* genome project) showing a total of 77% identical amino acid residues with LmjHS. Unfortunately, the heptapeptide substrate motif in LmxHS is altered to SPLTSTA lacking the proline residue at position +1 which is otherwise highly conserved in phosphorylation motifs of MAP kinase substrates (see 8.1.6). Consequently, the substrate score for the *L. mexicana* heptapeptide is reduced to only 60.15 and 69.12 for LmxMPK3 and LmxMPK13, respectively, with other heptapeptide sequences within LmxHS actually revealing higher scores. Indeed, the cloned N-terminal part of LmxHS contains one TP motif and three SP motifs, one of which is located within the altered heptapeptide sequence and reveals the highest substrate score (75.38) for LmxMPK3. *In vitro* kinase assays showed that LmxHS is phosphorylated to a very low degree by non-activated LmxMPK3, but indeed to a high extent by the activated MAP kinase (see 4.8.7.4, Figure 59). Again, phosphorylation site mapping of the phosphorylated fusion protein using mass spectrometry was not successful, and thus it remains unclear on which exact residue(s) the observed phosphorylation occurred. It is, however, very likely that one or more of the above mentioned S/TP motifs have been involved. Strikingly, neither non-activated nor activated LmxMPK13 are able to catalyse a phosphorylation of LmxHS indicating that the *L. mexicana* protein is specifically recognised and phosphorylated by LmxMPK3 *in vitro*. Here, a specific *in vitro* substrate of LmxMPK3 has been identified, although it does not contain the initial substrate motif predicted by PREDIKIN.

The classification of the substrate as a putative member of the endonuclease/exonuclease/phosphatase family including a large number of phosphatases is consistent with the interpretation of the direct screening assay on *Leishmania* lysates (see 5.8.2.1) which as well suggested that the LmxMPK3 substrate is a phosphatase. LmxHS could thus be involved in intracellular signalling either regulating gene expression of components involved in processes such as IFT or directly modifying the function of those components. The direct substrates of LmxHS might actually be identified by analysis of the critical protein bands of the direct screening assay on *Leishmania* lysates mentioned above (see also 5.8.2.1) which would, however, require a higher resolution of protein bands.

Nevertheless, the function of LmxHS as an *in vivo* substrate remains to be proven. Thus, the phosphorylation state of the hypothetical substrate in the *L. mexicana* wild type and the *LmxMPK3* null mutant will have to be compared. The generation of a specific antibody against LmxHS would allow immunoprecipitation of the hypothetical substrate protein with subsequent analysis of its phosphorylation state via specific antibodies (directed against

phosphoserine and -threonine) or (tandem) mass spectrometry. Alternatively, a tagged version of LmxHS could be introduced into the parasite and subsequent enrichment of the hypothetical substrate would be achieved using commercial antibodies directed against the tag used.

5.9 LmxMPK3 as a target for blocking leishmanial transmission to the insect vector

As shown in sand fly transmission studies, LmxMPK3 is essential for the *Leishmania* parasite to pass through the insect stage of its life cycle, since *LmxMPK3* null mutants fail to establish sand fly infection (see 5.1.2). LmxMPK3 might thus be a good target for blocking parasite transmission to the insect vector.

Especially in malaria research the development of drugs and vaccines with a strong transmission-blocking potential has become increasingly important as programmes for the elimination of the disease are strongly supported by several influential organisations (Greenwood, 2008; Targett and Greenwood, 2008). While malaria control describes the reduction in cases of clinical malaria and mortality (with the parasite still persisting in the community as asymptomatic infections), malaria elimination aims at stopping transmission completely within a defined region. The latter can only be achieved by killing all of the parasites within the target population. The concept of transmission-blocking vaccines (TBVs) is the induction of antibodies against sexual-stage/zygote-specific surface molecules of the malaria parasite which are passively transferred to blood-feeding mosquitoes where they block further parasite development. There is also an enhanced research priority for transmission-blocking drugs that could be used safely for mass drug administration (MDA) which describes the administration of drugs to the whole of a population at risk whether or not individuals are infected. This chemopreventive method had successfully contributed to the elimination of malaria from the island Aneityum in Vanuatu (Kaneko *et al.*, 2000).

Likewise, modern trends in *Leishmania* vaccine development aim at transmission-blocking activities (Tabbara, 2006). Indeed, LPG has been found to be a promising TBV candidate against CL (Tonui *et al.*, 2001a; Tonui *et al.*, 2001b). Moreover, the FML (fucose mannose ligand) vaccine Leishmune[®] is a TBV against zoonotic VL which has been shown to inhibit the binding of procyclic promastigotes to the insect midgut (Saraiva *et al.*, 2006). It has been suggested that the decrease in dog infectivity to the insect vector by prophylactic vaccination reduces human infections (Dye, 1996).

As LmxMPK3 is an intracellular molecule it is qualified rather as a transmission-blocking drug target than as a TBV candidate. As it has already been discussed in 5.4, a cell-permeable synthetic inhibitor selectively inhibits an inhibitor-sensitised version of LmxMPK3 in the

LmxMPK3 deletion background and thus induces flagellar shortening which eventually leads to parasites revealing the *LmxMPK3* null mutant phenotype. Referring to this observation, a selective inhibitor for wild type *LmxMPK3* which must not interfere with mammalian MAP kinases could be used as a transmission-blocking drug. Preventive administration of such an inhibitor to a target population might contribute to the elimination of CL - and possibly also other forms of leishmaniasis - in this population. The inhibitor would either enter the parasite in the mammalian host or would be passively transferred to the blood-feeding sand fly and reach the parasite there. However, this approach requires the development of a cell-permeable inhibitor which is highly specific for *LmxMPK3* and extremely safe as the majority of individuals to whom it would be administered will not be infected.

The inhibitor might also be applied as a spray alternatively to the chemical insecticides used for spraying of houses as a vector control intervention for reducing and interrupting parasite transmission (WHO, 2006). It is uncertain if such an inhibitor spray would induce a rapid and effective response before the sand fly would feed on the next host. Moreover, promastigotes would have to be attacked in early developmental insect stages to interrupt their life cycle. Nevertheless, a main advantage of a highly specific inhibitor over chemical insecticides is a less harmful effect on the environment and on human health.

5.10 *LmxMPK3* mutants as model systems to study human ciliopathies

It has been shown that lack of *LmxMPK3* in *L. mexicana* leads to short-flagellated parasites (Erdmann, diploma thesis, 2004; see 5.1.1) which lost ability to establish sand fly infection and thus to complete its life cycle (see 5.1.2). As pointed out in 5.1.1, the MAP kinase is likely to be critically involved in intraflagellar transport (IFT), a process essential for the construction and maintenance of flagella and cilia.

A loss of the physiological function of cells/tissues following cilia defects is also reflected by numerous different human ciliopathies. Cilia are actually present in a number of organs (kidneys, liver, pancreas, lungs, thyroid gland) and cells (endothelial cells, photoreceptors in the retina, sperm cells, myocardium, odontoblasts, cortical and hypothalamic neurons) of the human body (Badano *et al.*, 2006). Those cilia confer the motility of sperm cells, the transport of fluids over epithelial cells and also sensory perception (Pazour and Rosenbaum, 2002b). Depending on the mutant protein the resulting disorders range from organ-specific to pleiotropic phenotypes. It can be distinguished between motile and sensory cilia dysfunctions. The former affect motile cilia with a "9+2" axonemal organisation of microtubule pairs (see 1.2.1), while the latter refer to primary, non-motile cilia with a "9+0" axonemal construction. This classification is, however, strongly simplified as examples of motile primary cilia (e.g. in the renal epithelium; Ong and Wagner, 2005) as well as motile cilia with sensory

roles exist. The latter include cilia in the female reproductive tract containing TRP channels (cation channels) which have been suggested to relay physiochemical changes in the oviduct (Teilmann *et al.*, 2005). Several human ciliopathies have been mainly ascribed to mutations in IFT components including the IFT motor proteins.

The laterality abnormality *situs inversus* is caused by the paralysis of the otherwise motile primary cilia on the embryonic node which normally generate a leftward flow of extraembryonic fluid by which the left-right axis of symmetry is established. It has been shown that targeted knock-outs of KIF3A and KIF3B, subunits of the heterotrimeric kinesin complex, and Tg737, the mouse orthologue of IFT complex B protein IFT88, indeed prevent assembly of nodal cilia and produce *situs inversus* in 50% of mouse embryos (Nonaka *et al.*, 1998; Marszalek *et al.*, 1999; Murcia *et al.*, 2000).

In addition, Tg737 mutations are responsible for the development of polycystic kidney disease (PKD) - characterised by cystic, enlarged kidneys - and hepatic fibrosis (Moyer *et al.*, 1994). The primary cilia of kidney epithelial cells project into the lumen of the ducts/tubules of the nephrons and might have a role in detecting fluid flow through the nephrons. Polycystins, membrane proteins which have been suggested to form cation channels, might be involved in Ca²⁺ signalling which detects the state of the epithelium and regulates its proliferation and differentiation (Somlo and Ehrlich, 2001). PKD can thus result from a defect in the polycystins themselves, in their IFT or in the cilium where those membrane proteins are localised.

Furthermore, retinal degeneration - leading to retinitis pigmentosa (RP) and blindness - can develop as a result of defects in the IFT machinery. Vertebrate photoreceptor rods and cones are polarised sensory neurons in which the outer segments are formed from primary cilia. The synthesis of proteins and lipids required for the assembly and maintenance of the outer segment occurs in the inner segment. Consequently, IFT is required for moving the cargo through the connecting cilium, the only direct link between the inner and the outer segment. Indeed, studies of a KIF3A knock-out in photoreceptor cells (Marszalek *et al.*, 2000) and Tg737 mutant mice (Pazour *et al.*, 2002) revealed accumulations of opsin in the inner segments, degenerated outer segments and also apoptotic photoreceptor cells, an indicator of RP.

It has been realised that several human pleiotropic disorders are also caused by ciliary dysfunctions. Those include not only kidney and retinal defects, but also affect other tissues such as the limb and nervous system, as is the case in Bardet-Biedl syndrome (BBS) (Badano *et al.*, 2006). Indeed, the orthologue of the BBS protein BBS3 in *C. elegans* has been shown to be involved in IFT (Fan *et al.*, 2004) and moreover, loss of BBS7 and BBS8 resulted in the formation of short cilia (Blacque *et al.*, 2004).

To fully understand the molecular background of those different ciliopathies, the exact mechanisms by which IFT controls ciliary assembly and maintenance will have to be elucidated. Moreover, the role of individual IFT components within this mechanism will have to be analysed. Badano *et al.* (2006) therefore claimed that *in vivo* models that allow the specific blocking and unblocking of ciliogenesis are invaluable. *LmxMPK3* mutants of *L. mexicana*, in particular the inhibitor-sensitised *LmxMPK3* mutant, could provide such an *in vivo* model as the reversible inhibition of the MAP kinase results in a reversible disassembly of the flagellum (see 4.4.4 and 5.4).

6 Summary

MAP (mitogen-activated protein) kinases play a central role in regulating proliferation, differentiation and apoptosis of eukaryotic cells. At least four of 15 MAP kinase homologues identified in *Leishmania mexicana* are involved in flagellar length regulation of the parasite which displays a long flagellum in the insect stage promastigotes. Once transferred to the mammalian host, the parasite differentiates to the amastigote form melting down its flagellum until it is almost buried in the flagellar pocket. LmxMPK3 is the only MAP kinase so far whose absence in *L. mexicana* leads to a reduction of flagellar length and is the subject of this work.

Prior to the beginning of this work, some information was already available about the biochemical characteristics of LmxMPK3 and its possible *in vivo* functions. *LmxMPK3* mRNA levels are high in promastigotes, but indeed tightly down-regulated in amastigotes (Wiese *et al.*, 2003b). Consistently, the LmxMPK3 protein is only present in the promastigote stage (Erdmann *et al.*, 2006). I have shown before that recombinantly expressed LmxMPK3 reveals auto- and substrate phosphorylation activity *in vitro* and is a manganese-dependent protein kinase. Moreover, I generated *LmxMPK3* null mutants which displayed flagella strongly reduced in length. Those findings led to the conclusion that LmxMPK3 is involved in flagellar length regulation probably by controlling the intraflagellar transport (IFT). Furthermore, the MAP kinase kinase LmxMCK - showing a null mutant phenotype similar to that of LmxMPK3 - was identified as the activator of LmxMPK3 *in vitro* and *in vivo* (Scholz, PhD thesis, 2008; Erdmann *et al.*, 2006).

In this work, the average flagellar length of the *LmxMPK3* null mutants was determined to be roughly one-fifth of the wild type length. TEM analysis revealed that LmxMPK3 is essential for the assembly of the paraflagellar rod (PFR) as roughly 30% of the null mutants lack this structure while the remaining cells contain either a rudimentary PFR or an amorphous structure around the axoneme. Immunofluorescence analysis detected the PFR protein PFR-2 in 80% of the *LmxMPK3* null mutant flagella, and immunoblot analysis revealed that the null mutants contain roughly 20 times less PFR-2 than the wild type which corresponds to roughly 4 times less PFR-2 per micrometer length. A possible role of LmxMPK3 in controlling PFR-2 expression was investigated. RT-PCR analysis revealed that *PFR-2* mRNA amounts in the *LmxMPK3* null mutants do not differ from that of the wild type and thus left the possibility that LmxMPK3 regulates PFR-2 expression on the protein level. However, as *L. mexicana PFR-1/2* null mutants retain long flagella (Maga *et al.*, 1999), LmxMPK3 has most likely a role in directly controlling IFT.

Mouse infection studies using the *LmxMPK3* null mutants showed that the MAP kinase is not required for the parasite to establish mammalian infections. However, transmission studies in the sand fly proved that LmxMPK3 is essential for the parasite to pass through the insect

stage of its life cycle as null mutants were expelled before they could establish sand fly infection (Volf, personal communication). LmxMPK3 could thus be a good target for blocking parasite transmission to the insect vector.

Fluorescence microscopy using *L. mexicana* GFP-LmxMPK3 and GFP-LmxMKK mutants localised both kinases to the cytosol with a higher concentration around the nucleus, within the flagellum and at its base. The flagellar localisation of both kinases reflects their participation in the same signalling pathway involved in flagellar length regulation. FACS analysis of the GFP-LmxMPK3 mutant revealed that flagellar length correlates with the amount of LmxMPK3.

An inhibitor-sensitised LmxMPK3 mutant of *L. mexicana* was generated which displayed wild type flagella as the introduced mutation is functionally silent. Addition of a small molecule inhibitor induced reversible flagellar shortening while the flagella of the wild type remained unaffected indicating the specificity of the inhibitor. The sensitisation strategy could thus be successfully applied to LmxMPK3 and revealed that flagellar length depends on the activity of LmxMPK3. Furthermore, the inhibitor-sensitised LmxMPK3 mutant might provide an inducible *in vivo* model system to study the molecular mechanisms underlying different human ciliopathies.

Furthermore, the activation mechanism of LmxMPK3 was investigated *in vitro*. Strikingly, constitutively active LmxMKK-D leads to a strong activation not only of wild type LmxMPK3, but also of LmxMPK3-KM in which the invariant lysine - otherwise essential for kinase activity - had been replaced by methionine. It was also interesting to find that non-activated wild type LmxMKK activates LmxMPK3 *in vitro* to the same extent as LmxMKK-D. This observation, however, is likely to differ from the *in vivo* situation where a strict regulation of the signalling components via phosphorylation events is required. MAP kinase activation generally occurs by a dual phosphorylation on a threonine (T) and a tyrosine (Y) residue in a conserved TXY activation motif. *In vitro* kinase assays using different LmxMPK3 TXY mutants and tandem mass spectrometry analyses revealed that the TXY-tyrosine is the only residue on which non-activated LmxMPK3 performs autophosphorylation and that this tyrosine is essential for basal activity. Contrary, phosphorylation of the TXY-threonine is essential and sufficient for the maximal activation of LmxMPK3 *in vitro*. Indeed, LmxMKK was identified as a dual-specificity MAP kinase kinase. The activation mechanism of LmxMPK3 was also examined *in vivo* by generating different LmxMPK3-TXY mutants of *L. mexicana* using flagellar length as an indicator for the LmxMPK3 activation state. As only wild type LmxMPK3 was able to complement the null mutant phenotype, it can be concluded that both the threonine and the tyrosine of the activation motif are essential for maximal LmxMPK3 activation. The *in vivo* results are therefore consistent with the common MAP kinase activation mechanism of higher eukaryotes.

Finally, the web-based computer programme PREDIKIN was applied for an *in silico* LmxMPK3 substrate search. The predicted heptapeptide consensus sequence was used for a motif search in the *L. major* genome DB. From 19 hits the endonuclease/exonuclease/phosphatase LmjF36.1150, designated LmjHS, was cloned and tested as an LmxMPK3 substrate using *in vitro* kinase assays. While the phosphorylation of an LmjHS peptide by activated LmxMPK3 turned out to be unspecific (as it was also phosphorylated by activated LmxMPK13), larger N-terminal parts of LmjHS and its *L. mexicana* homologue LmxHS indeed present specific *in vitro* substrates of LmxMPK3. The role of LmxHS as an *in vivo* substrate of LmxMPK3 remains to be demonstrated.

7 References

- Aboagye-Kwarteng T, Ole-MoiYoi OK, Lonsdale-Eccles JD (1991) Phosphorylation differences among proteins of bloodstream developmental stages of *Trypanosoma brucei brucei*. *Biochem J* **275**:7-14.
- Absalon S, Blisnick T, Kohl L, Toutirais G, Doré G, Julkowska D, Tavenet A, Bastin P (2008) Intraflagellar transport and functional analysis of genes required for flagellum formation in trypanosomes. *Mol Biol Cell* **19**:929-44.
- Adhiambo C, Forney JD, Asai DJ, LeBowitz JH (2005) The two cytoplasmic dynein-2 isoforms in *Leishmania mexicana* perform separate functions. *Mol Biochem Parasitol* **143**:216-25.
- Agron PG, Reed SL, Engel JN (2005) An essential, putative MEK kinase of *Leishmania major*. *Mol Biochem Parasitol* **142**:121-5.
- Ahn NG, Seger R, Bratlien RL, Diltz CD, Tonks NK, Krebs EG (1991) Multiple components in an epidermal growth factor-stimulated protein kinase cascade. *In vitro* activation of a myelin basic protein/microtubule-associated protein 2 kinase. *J Biol Chem* **266**:4220-7.
- Al-Chalabi KA, Ziz LA, Al-Khayat B (1989) Presence and properties of cAMP phosphodiesterase from promastigote forms of *Leishmania tropica* and *Leishmania donovani*. *Comp Biochem Physiol B* **93**:789-92.
- Alessi DR, Saito Y, Campbell DG, Cohen P, Sithanandam G, Rapp U, Ashworth A, Marshall CJ, Cowley S (1994) Identification of the sites in MAP kinase kinase-1 phosphorylated by p74raf-1. *EMBO J* **13**:1610-9.
- Alonso G, Guevara P, Ramirez JL (1992) *Trypanosomatidae* codon usage and GC distribution. *Mem Inst Oswaldo Cruz* **87**(4):517-23.
- Anderson NG, Maller JL, Tonks NK, Sturgill TW (1990) Requirement for integration of signals from two distinct phosphorylation pathways for activation of MAP kinase. *Nature* **343**:651-3.
- Antoine JC, Prina E, Lang T, Courret N (1998) The biogenesis and properties of the parasitophorous vacuoles that harbour *Leishmania* in murine macrophages. *Trends Microbiol.* **6**:392-401.
- Badano JL, Mitsuma N, Beales PL, Katsanis N (2006) The ciliopathies: an emerging class of human genetic disorders. *Annu Rev Genomics Hum Genet* **7**:125-48.
- Bakalara N, Seyfang A, Baltz T, Davis C (1995) *Trypanosoma brucei* and *Trypanosoma cruzi*: life cycle-regulated protein tyrosine phosphatase activity. *Exp Parasitol* **81**:302-12.
- Bandyopadhyay G, Sajan MP, Kanoh Y, Standaert ML, Burke TR Jr, Quon MJ, Reed BC, Dikic I, Noel LE, Newgard CB, Farese R (2000) Glucose activates mitogen-activated protein kinase (extracellular signal-regulated kinase) through proline-rich tyrosine kinase-2 and the Glut1 glucose transporter. *J Biol Chem* **275**:40817-26.
- Barcinski MA, Schechtman D, Quintao LG, Costa Dde A, Soares LR, Moreira ME, Charlab R (1992) Granulocyte-macrophage colony-stimulating factor increases the infectivity of *Leishmania amazonensis* by protecting promastigotes from heat-induced death. *Infect Immun* **60**:3523-7.
- Bastin P, MacRae TH, Francis SB, Matthews KR, Gull K (1999b) Flagellar morphogenesis: protein targeting and assembly in the paraflagellar rod of trypanosomes. *Mol Cell Biol* **19**:8191-200.
- Bastin P, Pullen TJ, Moreira-Leite FF, Gull K (2000) Inside and outside of the trypanosome flagellum: a multifunctional organelle. *Microbes Infect* **2**:1865-74.
- Bastin P, Pullen TJ, Sherwin T, Gull K (1999a) Protein transport and flagellum assembly dynamics revealed by analysis of the paralysed trypanosome mutant *snl-1*. *J Cell Sci* **112**:3769-77.
- Bastin P, Sherwin T, Gull K (1998) Paraflagellar rod is vital for trypanosome motility. *Nature* **391**:548.

- Bates PA, Robertson CD, Tetley L, Coombs GH (1992) Axenic cultivation and characterization of *Leishmania mexicana* amastigote-like forms. *Parasitology* **105**:193-202.
- Bengs F, Scholz A, Kuhn D, Wiese M (2005) LmxMPK9, a mitogen-activated protein kinase homologue affects flagellar length in *Leishmania mexicana*. *Mol Microbiol* **55**:1606-15.
- Berman SA, Wilson NF, Haas NA, Lefebvre PA (2003) A novel MAP kinase regulates flagellar length in *Chlamydomonas*. *Curr Biol* **13**:1145-9.
- Beverley SM (1991) Gene amplification in *Leishmania*. *Annu Rev Microbiol* **45**:417-44.
- Bishop AC, Buzko O, Shokat KM (2001) Magic bullets for protein kinases. *Trends Cell Biol* **11**:167-72.
- Blacque OE, Reardon MJ, Li C, McCarthy J, Mahjoub MR, Ansley SJ, Badano JL, Mah AK, Beales PL, Davidson WS, Johnsen RC, Audeh M, Plasterk RH, Baillie DL, Katsanis N, Quarmby LM, Wicks SR, Leroux MR (2004) Loss of *C. elegans* BBS-7 and BBS-8 protein function results in cilia defects and compromised intraflagellar transport. *Genes Dev* **18**:1630-42.
- Blaineau C, Tessier M, Dubessay P, Tasse L, Crobu L, Pagès M, Bastien P (2007) A novel microtubule-depolymerizing kinesin involved in length control of a eukaryotic flagellum. *Curr Biol* **17**:778-82.
- Bogdan C, Donhauser N, Döring R, Röllinghoff M, Diefenbach A, Rittig MG (2000) Fibroblasts as host cells in latent leishmaniosis. *J Exp Med* **191**:2121-30.
- Bolton EC, Mildvan AS, Boeke JD (2002) Inhibition of reverse transcription *in vivo* by elevated manganese ion concentration. *Mol Cell* **9**:879-89.
- Boulton TG, Cobb MH (1991) Identification of multiple extracellular signal-regulated kinases (ERKs) with antipeptide antibodies. *Cell Regul* **2**:357-71.
- Bradley BA, Quarmby LM (2005) A NIMA-related kinase, Cnk2p, regulates both flagellar length and cell size in *Chlamydomonas*. *J Cell Sci* **118**:3317-26.
- Brandau S, Dresel A, Clos J (1995) High constitutive levels of heat-shock proteins in human-pathogenic parasites of the genus *Leishmania*. *Biochem J* **310**:225-32.
- Briggs LJ, Davidge JA, Wickstead B, Ginger ML, Gull K (2004) More than one way to build a flagellum: comparative genomics of parasitic protozoa. *Curr Biol* **14**:R611-2.
- Bringaud F, Vedrenne C, Cuvillier A, Parzy D, Baltz D, Tetaud E, Pays E, Venegas J, Merlin G, Baltz T (1998) Conserved organization of genes in trypanosomatids. *Mol Biochem Parasitol* **94**:249-64.
- Brinkworth RI, Breinl RA, Kobe B (2003) Structural basis and prediction of substrate specificity in protein serine/threonine kinases. *Proc Natl Acad Sci U S A* **100**:74-9.
- Brittingham A, Morrison CJ, McMaster WR, McGwire BS, Chang KP, Mosser DM (1995) Role of the *Leishmania* surface protease gp63 in complement fixation, cell adhesion, and resistance to complement-mediated lysis. *J Immunol* **155**:3102-11.
- Britto C, Ravel C, Bastien P, Blaineau C, Pagès M, Dedet JP, Wincker P (1998) Conserved linkage groups associated with large-scale chromosomal rearrangements between Old World and New World *Leishmania* genomes. *Gene* **222**:107-17.
- Brumlik MJ, Wei S, Finstad K, Nesbit J, Hyman LE, Lacey M, Burow ME, Curiel TJ (2004) Identification of a novel mitogen-activated protein kinase in *Toxoplasma gondii*. *Int J Parasitol* **34**:1245-54.
- Brun R, Schönenberger M (1979) Cultivation and *in vitro* cloning of procyclic culture forms of *Trypanosoma brucei* in a semi-defined medium. *Acta Trop* **36**:289-92.

- Burack WR, Shaw AS (2000) Signal transduction: hanging on a scaffold. *Curr Opin Cell Biol* **12**:211-6.
- Burghoorn J, Dekkers MP, Rademakers S, de Jong T, Willemsen R, Jansen G (2007) Mutation of the MAP kinase DYF-5 affects docking and undocking of kinesin-2 motors and reduces their speed in the cilia of *Caenorhabditis elegans*. *Proc Natl Acad Sci U S A* **104**:7157-62.
- Calvert PD, Klenchin VA, Bownds MD (1995) Rhodopsin kinase inhibition by recoverin. Function of recoverin myristoylation. *J Biol Chem* **270**:24127-9.
- Camps M, Nichols A, Arkinstall S (2000) Dual specificity phosphatases: a gene family for control of MAP kinase function. *FASEB J* **14**:6-16.
- Canagarajah BJ, Khokhlatchev A, Cobb MH, Goldsmith EJ (1997) Activation mechanism of the MAP kinase ERK2 by dual phosphorylation. *Cell* **90**:859-69.
- Carrera AC, Alexandrov K, Roberts TM (1993) The conserved lysine of the catalytic domain of protein kinases is actively involved in the phosphotransfer reaction and not required for anchoring ATP. *Proc Natl Acad Sci U S A* **90**:442-6.
- Caux C, Liu YJ, Banchereau J (1995) Recent advances in the study of dendritic cells and follicular dendritic cells. *Immunol Today* **16**:2-4.
- Clayton C, Shapira M (2007) Post-transcriptional regulation of gene expression in trypanosomes and leishmaniasis. *Mol Biochem Parasitol* **156**:93-101.
- Clayton CE (1999) Genetic manipulation of kinetoplastida. *Parasitol Today* **15**:372-8.
- Clayton CE (2002) Life without transcriptional control? From fly to man and back again. *EMBO J* **21**:1881-8.
- Cole DG (1999) Kinesin-II, the heteromeric kinesin. *Cell Mol Life Sci* **56**:217-26.
- Cole DG (2003) The intraflagellar transport machinery of *Chlamydomonas reinhardtii*. *Traffic* **4**:435-42.
- Cole DG, Chinn SW, Wedaman KP, Hall K, Vuong T, Scholey JM (1993) Novel heterotrimeric kinesin-related protein purified from sea urchin eggs. *Nature* **366**:268-70.
- Cole DG, Diener DR, Himelblau AL, Beech PL, Fuster JC, Rosenbaum JL (1998) *Chlamydomonas* kinesin-II-dependent intraflagellar transport (IFT): IFT particles contain proteins required for ciliary assembly in *Caenorhabditis elegans* sensory neurons. *J Cell Biol* **141**:993-1008.
- Croft SL, Coombs GH (2003) Leishmaniasis--current chemotherapy and recent advances in the search for novel drugs. *Trends Parasitol* **19**:502-8.
- Croft SL, Sundar S, Fairlamb AH (2006) Drug resistance in leishmaniasis. *Clin Microbiol Rev* **19**:111-26.
- Cruz A, Coburn CM, Beverley SM (1991) Double targeted gene replacement for creating null mutants. *Proc Natl Acad Sci U S A* **88**:7170-4.
- Cullimore JV, Sims AP (1981) Glutamine synthetase of *Chlamydomonas*: its role in the control of nitrate assimilation. *Planta* **153**:18-24.
- Dawson SC, Sagolla MS, Mancuso JJ, Woessner DJ, House SA, Fritz-Laylin L, Cande WZ (2007) Kinesin-13 regulates flagellar, interphase, and mitotic microtubule dynamics in *Giardia intestinalis*. *Eukaryot Cell* **6**:2354-64.
- De Castro SL, Luz MR (1993) The second messenger cyclic 3',5'-adenosine monophosphate in pathogenic microorganisms with special reference to protozoa. *Can J Microbiol* **39**:473-9.

- Deane JA, Cole DG, Seeley ES, Diener DR, Rosenbaum JL (2001) Localization of intraflagellar transport protein IFT52 identifies basal body transitional fibers as the docking site for IFT particles. *Curr Biol* **11**:1586-90.
- Dell KR, Engel JN (1994) Stage-specific regulation of protein phosphorylation in *Leishmania major*. *Mol Biochem Parasitol* **64**:283-92.
- Dizhoor AM, Ray S, Kumar S, Niemi G, Spencer M, Brolley D, Walsh KA, Philipov PP, Hurley JB, Stryer L (1991) Recoverin: a calcium sensitive activator of retinal rod guanylate cyclase. *Science* **251**:915-8.
- Dlakić M (2000) Functionally unrelated signalling proteins contain a fold similar to Mg²⁺-dependent endonucleases. *Trends Biochem Sci* **25**:272-3.
- Docampo R, Moreno SN (1996) The role of Ca²⁺ in the process of cell invasion by intracellular parasites. *Parasitol Today* **12**:61-5.
- Docampo R, Moreno SN (1999) Acidocalcisome: A novel Ca²⁺ storage compartment in trypanosomatids and apicomplexan parasites. *Parasitol Today* **15**:443-8.
- Docampo R, Pignataro OP (1991) The inositol phosphate/diacylglycerol signalling pathway in *Trypanosoma cruzi*. *Biochem J* **275**:407-11.
- Domenicali Pfister D, Burkard G, Morand S, Renggli CK, Roditi I, Vassella E (2006) A Mitogen-activated protein kinase controls differentiation of bloodstream forms of *Trypanosoma brucei*. *Eukaryot Cell* **5**:1126-35.
- Dubessay P, Blaineau C, Bastien P, Tasse L, Van Dijk J, Crobu L, Pagès M (2006) Cell cycle-dependent expression regulation by the proteasome pathway and characterization of the nuclear targeting signal of a *Leishmania major* Kin-13 kinesin. *Mol Microbiol* **59**:1162-74.
- Dye C (1996) The logic of visceral leishmaniasis control. *Am J Trop Med Hyg* **55**:125-30.
- Eblen ST, Kumar NV, Shah K, Henderson MJ, Watts CK, Shokat KM, Weber MJ (2003) Identification of novel ERK2 substrates through use of an engineered kinase and ATP analogs. *J Biol Chem* **278**:14926-35.
- Elion EA (1998) Routing MAP kinase cascades. *Science* **281**:1625-6.
- Ellis J, Sarkar M, Hendriks E, Matthews K (2004) A novel ERK-like, CRK-like protein kinase that modulates growth in *Trypanosoma brucei* via an autoregulatory C-terminal extension. *Mol Microbiol* **53**:1487-99.
- Engman DM, Krause KH, Blumin JH, Kim KS, Kirchhoff LV, Donelson JE (1989) A novel flagellar Ca²⁺-binding protein in trypanosomes. *J Biol Chem* **264**:18627-31.
- Enslin H, Brancho DM, Davis RJ (2000) Molecular determinants that mediate selective activation of p38 MAP kinase isoforms. *EMBO J* **19**:1301-11.
- Erdmann M (2004) Molecular analysis of LmxMPK3, a mitogen-activated protein kinase from *Leishmania mexicana*. Diploma thesis, Biochemistry/Molecular Biology, University of Hamburg.
- Erdmann M, Scholz A, Melzer IM, Schmetz C, Wiese M (2006) Interacting protein kinases involved in the regulation of flagellar length. *Mol Biol Cell* **17**:2035-45.
- Fan Y, Esmail MA, Ansley SJ, Blacque OE, Borojevich K, Ross AJ, Moore SJ, Badano JL, May-Simera H, Compton DS, Green JS, Lewis RA, van Haelst MM, Parfrey PS, Baillie DL, Beales PL, Katsanis N, Davidson WS, Leroux MR (2004) Mutations in a member of the Ras superfamily of small GTP-binding proteins causes Bardet-Biedl syndrome. *Nat Genet* **36**:989-93.
- Feng Q, Moran JV, Kazazian HH Jr, Boeke JD (1996) Human L1 retrotransposon encodes a conserved endonuclease required for retrotransposition. *Cell* **87**:905-16.

- Ferl RJ (1996) 14-3-3 proteins and signal transduction. *Annu Rev Plant Physiol Plant Mol Biol* **47**:49-73.
- Ferrell JE Jr (1997) How responses get more switch-like as you move down a protein kinase cascade. *Trends Biochem Sci* **22**:288-9.
- Ferrell JE Jr (1999) Building a cellular switch: more lessons from a good egg. *Bioessays* **21**:866-70.
- Ferrell JE Jr, Bhatt RR (1997) Mechanistic studies of the dual phosphorylation of mitogen-activated protein kinase. *J Biol Chem* **272**:19008-16.
- Finnie C, Borch J, Collinge DB (1999) 14-3-3 proteins: eukaryotic regulatory proteins with many functions. *Plant Mol Biol* **40**:545-54.
- Flawiá MM, Téllez-Iñón MT, Torres HN (1997) Signal transduction mechanisms in *Trypanosoma cruzi*. *Parasitol Today* **13**:30-3.
- Fox LA, Sawin KE, Sale WS (1994) Kinesin-related proteins in eukaryotic flagella. *J Cell Sci* **107**:1545-50.
- Frost JA, Steen H, Shapiro P, Lewis T, Ahn N, Shaw PE, Cobb MH (1997) Cross-cascade activation of ERKs and ternary complex factors by Rho family proteins. *EMBO J* **16**:6426-38.
- Fukunaga R, Hunter T (1997) MNK1, a new MAP kinase-activated protein kinase, isolated by a novel expression screening method for identifying protein kinase substrates. *EMBO J* **16**:1921-33.
- Ganiatsas S, Kwee L, Fujiwara Y, Perkins A, Ikeda T, Labow MA, Zon LI (1998) SEK1 deficiency reveals mitogen-activated protein kinase cascade crossregulation and leads to abnormal hepatogenesis. *Proc Natl Acad Sci U S A* **95**:6881-6.
- Garrington TP, Johnson GL (1999) Organization and regulation of mitogen-activated protein kinase signaling pathways. *Curr Opin Cell Biol* **11**:211-8.
- Gaskins C, Maeda M, Firtel RA (1994) Identification and functional analysis of a developmentally regulated extracellular signal-regulated kinase gene in *Dictyostelium discoideum*. *Mol Cell Biol* **14**:6996-7012.
- Gbenle GO (1990) *Trypanosoma brucei*: calcium-dependent endoribonuclease is associated with inhibitor protein. *Exp Parasitol* **71**:432-8.
- Gibson W, Stevens J (1999) Genetic exchange in the *trypanosomatidae*. *Adv Parasitol* **43**:1-46.
- Ginger ML, Ngazoa ES, Pereira CA, Pullen TJ, Kabiri M, Becker K, Gull K, Steverding D (2005) Intracellular positioning of isoforms explains an unusually large adenylate kinase gene family in the parasite *Trypanosoma brucei*. *J Biol Chem* **280**:11781-9.
- Gorman MA, Morera S, Rothwell DG, de La Fortelle E, Mol CD, Tainer JA, Hickson ID, Freemont PS (1997) The crystal structure of the human DNA repair endonuclease HAP1 suggests the recognition of extra-helical deoxyribose at DNA abasic sites. *EMBO J* **16**:6548-58.
- Gouveia JJ, Vasconcelos EJ, Pacheco AC, Araújo-Filho R, Maia AR, Kamimura MT, Costa MP, Viana DA, Costa RB, Maggioni R, Oliveira DM (2007) Intraflagellar transport complex in *Leishmania* spp. *In silico* genome-wide screening and annotation of gene function. *Genet Mol Res* **6**:766-98.
- Green CB, Douris N, Kojima S, Strayer CA, Fogerty J, Lourim D, Keller SR, Besharse JC (2007) Loss of Nocturnin, a circadian deadenylase, confers resistance to hepatic steatosis and diet-induced obesity. *Proc Natl Acad Sci U S A* **104**:9888-93.
- Greenwood BM (2008) Control to elimination: implications for malaria research. *Trends Parasitol* **24**:449-54.

- Grondin K, Roy G, Ouellette M (1996) Formation of extrachromosomal circular amplicons with direct or inverted duplications in drug-resistant *Leishmania tarentolae*. *Mol Cell Biol* **16**:3587-95.
- Gull K (1999) The cytoskeleton of trypanosomatid parasites. *Annu Rev Microbiol* **53**:629-55.
- Habelhah H, Shah K, Huang L, Burlingame AL, Shokat KM, Ronai Z (2001) Identification of new JNK substrate using ATP pocket mutant JNK and a corresponding ATP analogue. *J Biol Chem* **276**:18090-5.
- Haile S, Papadopoulou B (2007) Developmental regulation of gene expression in trypanosomatid parasitic protozoa. *Curr Opin Microbiol* **10**:569-77.
- Hanahan D (1983) Studies on transformation of *Escherichia coli* with plasmids. *J Mol Biol* **166**:557-80.
- Hanks SK, Quinn AM, Hunter T (1988) The protein kinase family: conserved features and deduced phylogeny of the catalytic domains. *Science* **241**:42-52.
- Harder S (2005) Characterisation of two stage-specific proteins of the protozoan parasite *Leishmania donovani* [Ross, 1903]. PhD thesis, Department of Biology, University of Hamburg.
- Hassan P, Fergusson D, Grant KM, Mottram JC (2001) The CRK3 protein kinase is essential for cell cycle progression of *Leishmania mexicana*. *Mol Biochem Parasitol* **113**:189-98.
- Haycraft CJ, Schafer JC, Zhang Q, Taulman PD, Yoder BK (2003) Identification of CHE-13, a novel intraflagellar transport protein required for cilia formation. *Exp Cell Res* **284**:251-63.
- Hendrickson N, Sifri CD, Henderson DM, Allen T, Wirth DF, Ullman B (1993) Molecular characterization of the *ldmdr1* multidrug resistance gene from *Leishmania donovani*. *Mol Biochem Parasitol* **60**:53-64.
- Hermoso T, Fishelson Z, Becker SI, Hirschberg K, Jaffe CL (1991) Leishmanial protein kinases phosphorylate components of the complement system. *EMBO J* **10**:4061-7.
- Hide G, Gray A, Harrison CM, Tait A (1989) Identification of an epidermal growth factor receptor homologue in trypanosomes. *Mol Biochem Parasitol* **36**:51-9.
- Hua SB, Wang CC (1997) Interferon-gamma activation of mitogen-activated protein kinase, KFR1, in the bloodstream form of *Trypanosoma brucei*. *J Biol Chem* **272**:10797-803.
- Huang H, Werner C, Weiss LM, Wittner M, Orr GA (2002) Molecular cloning and expression of the catalytic subunit of protein kinase A from *Trypanosoma cruzi*. *Int J Parasitol* **32**:1107-15.
- Hubbard MJ, Cohen P (1993) On target with a new mechanism for the regulation of protein phosphorylation. *Trends Biochem Sci* **18**:172-7.
- Hubbard SR (1997) Crystal structure of the activated insulin receptor tyrosine kinase in complex with peptide substrate and ATP analog. *EMBO J* **16**:5572-81.
- Hübel A, Brandau S, Dresel A, Clos J (1995) A member of the ClpB family of stress proteins is expressed during heat shock in *Leishmania* spp. *Mol Biochem Parasitol* **70**(1-2):107-18.
- Huse M, Kuriyan J (2002) The conformational plasticity of protein kinases. *Cell* **109**:275-82.
- Ilg T (2002) Generation of *myo*-inositol-auxotrophic *Leishmania mexicana* mutants by targeted replacement of the *myo*-inositol-1-phosphate synthase gene. *Mol Biochem Parasitol* **120**:151-6.
- Ivens AC, Peacock CS, Worthey EA, Murphy L, Aggarwal G, Berriman M, Sisk E, Rajandream MA, Adlem E, Aert R, Anupama A, Apostolou Z, Attipoe P, Bason N, Bauser C, Beck A, Beverley SM, Bianchetti G, Borzym K, Bothe G, Bruschi CV, Collins M, Cadag E, Ciarloni L, Clayton C, Coulson RM, Cronin A, Cruz AK, Davies RM, De Gaudenzi J, Dobson DE, Duesterhoeft A, Fazelina G, Fosker N, Frasch AC, Fraser A, Fuchs M, Gabel C, Goble A, Goffeau A, Harris D, Hertz-Fowler C, Hilbert H, Horn D, Huang Y, Klages S, Knights A, Kube M, Larke N, Litvin L, Lord A, Louie T, Marra M, Masuy D, Matthews K, Michaeli S, Mottram JC, Müller-Auer S, Munden H, Nelson S, Norbertczak H, Oliver K,

- O'neil S, Pentony M, Pohl TM, Price C, Purnelle B, Quail MA, Rabbinowitsch E, Reinhardt R, Rieger M, Rinta J, Robben J, Robertson L, Ruiz JC, Rutter S, Saunders D, Schäfer M, Schein J, Schwartz DC, Seeger K, Seyler A, Sharp S, Shin H, Sivam D, Squares R, Squares S, Tosato V, Vogt C, Volckaert G, Wambutt R, Warren T, Wedler H, Woodward J, Zhou S, Zimmermann W, Smith DF, Blackwell JM, Stuart KD, Barrell B, Myler PJ (2005) The genome of the kinetoplastid parasite, *Leishmania major*. *Science* **309**:436-42.
- Jacobs D, Glossip D, Xing H, Muslin AJ, Kornfeld K (1999) Multiple docking sites on substrate proteins form a modular system that mediates recognition by ERK MAP kinase. *Genes Dev* **13**:163-75.
- Jenkins PM, Hurd TW, Zhang L, McEwen DP, Brown RL, Margolis B, Verhey KJ, Martens JR (2006) Ciliary targeting of olfactory CNG channels requires the CNGB1b subunit and the kinesin-2 motor protein, KIF17. *Curr Biol* **16**:1211-6.
- Johnson KA, Rosenbaum JL (1992) Polarity of flagellar assembly in *Chlamydomonas*. *J Cell Biol* **119**:1605-11.
- Junghae M, Raynes JG (2002) Activation of p38 mitogen-activated protein kinase attenuates *Leishmania donovani* infection in macrophages. *Infect Immun* **70**:5026-35.
- Kane MM, Mosser DM (2000) *Leishmania* parasites and their ploys to disrupt macrophage activation. *Curr Opin Hematol*. **7**:26-31.
- Kaneko A, Taleo G, Kalkoa M, Yamar S, Kobayakawa T, Björkman A (2000) Malaria eradication on islands. *Lancet* **356**:1560-4.
- Klumpp LM, Mackey AT, Farrell CM, Rosenberg JM, Gilbert SP (2003) A kinesin switch I arginine to lysine mutation rescues microtubule function. *J Biol Chem* **278**:39059-67.
- Knebel A, Morrice N, Cohen P (2001) A novel method to identify protein kinase substrates: eEF2 kinase is phosphorylated and inhibited by SAPK4/p38delta. *EMBO J* **20**:4360-9.
- Kohl L, Robinson D, Bastin P (2003) Novel roles for the flagellum in cell morphogenesis and cytokinesis of trypanosomes. *EMBO J* **22**:5336-46.
- Koshland DE (1958) Application of a Theory of Enzyme Specificity to Protein Synthesis. *Proc Natl Acad Sci U S A* **2**:98-104.
- Krupa A, Preethi G, Srinivasan N (2004) Structural modes of stabilization of permissive phosphorylation sites in protein kinases: distinct strategies in Ser/Thr and Tyr kinases. *J Mol Biol* **339**:1025-39.
- Kuhn D (2004) *In vitro* and *in vivo* analysis of LmxPK4, a MAP kinase kinase from *Leishmania mexicana*. PhD thesis, Department of Chemistry, University of Hamburg.
- Kuhn D, Wiese M (2005) LmxPK4, a mitogen-activated protein kinase kinase homologue of *Leishmania mexicana* with a potential role in parasite differentiation. *Mol Microbiol* **56**:1169-82.
- L'Allemain G, Her JH, Wu J, Sturgill TW, Weber MJ (1992) Growth factor-induced activation of a kinase activity which causes regulatory phosphorylation of p42/microtubule-associated protein kinase. *Mol Cell Biol* **12**:2222-9.
- Landfear SM, Ignatushchenko M (2001) The flagellum and flagellar pocket of trypanosomatids. *Mol Biochem Parasitol* **115**:1-17.
- Laskay T, van Zandbergen G, Solbach W (2003) Neutrophil granulocytes--Trojan horses for *Leishmania major* and other intracellular microbes? *Trends Microbiol* **11**:210-4.
- Laufs H, Müller K, Fleischer J, Reiling N, Jahnke N, Jensenius JC, Solbach W, Laskay T (2002) Intracellular survival of *Leishmania major* in neutrophil granulocytes after uptake in the absence of heat-labile serum factors. *Infect Immun* **70**:826-35.

- Lee K, Du C, Horn M, Rabinow L (1996) Activity and autophosphorylation of LAMMER protein kinases. *J Biol Chem* **271**:27299-303.
- Lee SA, Hasbun R (2003) Therapy of cutaneous leishmaniasis. *Int J Infect Dis* **7**:86-93.
- Liu S, Lu W, Obara T, Kuida S, Lehoczky J, Dewar K, Drummond IA, Beier DR (2002) A defect in a novel Nek-family kinase causes cystic kidney disease in the mouse and in zebrafish. *Development* **129**:5839-46.
- Liu Y, Shah K, Yang F, Witucki L, Shokat KM (1998a) A molecular gate which controls unnatural ATP analogue recognition by the tyrosine kinase v-Src. *Bioorg Med Chem* **6**:1219-26.
- Liu Y, Shah K, Yang F, Witucki L, Shokat KM (1998b) Engineering Src family protein kinases with unnatural nucleotide specificity. *Chem Biol* **5**:91-101.
- Madhani HD, Styles CA, Fink GR (1997) MAP kinases with distinct inhibitory functions impart signaling specificity during yeast differentiation. *Cell* **91**:673-84.
- Maga JA, Sherwin T, Francis S, Gull K, LeBowitz JH (1999) Genetic dissection of the *Leishmania* paraflagellar rod, a unique flagellar cytoskeleton structure. *J Cell Sci* **112**:2753-63.
- Mahjoub MR, Qasim Rasi M, Quarmby LM (2004) A NIMA-related kinase, Fa2p, localizes to a novel site in the proximal cilia of *Chlamydomonas* and mouse kidney cells. *Mol Biol Cell* **15**:5172-86.
- Marcus S, Polverino A, Barr M, Wigler M (1994) Complexes between STE5 and components of the pheromone-responsive mitogen-activated protein kinase module. *Proc Natl Acad Sci U S A* **91**:7762-6.
- Marshall WF, Rosenbaum JL (2001) Intraflagellar transport balances continuous turnover of outer doublet microtubules: implications for flagellar length control. *J Cell Biol* **155**:405-14.
- Marszalek JR, Liu X, Roberts EA, Chui D, Marth JD, Williams DS, Goldstein LS (2000) Genetic evidence for selective transport of opsin and arrestin by kinesin-II in mammalian photoreceptors. *Cell* **102**:175-87.
- Marszalek JR, Ruiz-Lozano P, Roberts E, Chien KR, Goldstein LS (1999) Situs inversus and embryonic ciliary morphogenesis defects in mouse mutants lacking the KIF3A subunit of kinesin-II. *Proc Natl Acad Sci U S A* **96**:5043-8.
- Martiny A, Meyer-Fernandes JR, de Souza W, Vannier-Santos MA (1999) Altered tyrosine phosphorylation of ERK1 MAP kinase and other macrophage molecules caused by *Leishmania* amastigotes. *Mol Biochem Parasitol* **102**:1-12.
- Matsuo Y, Yamada A, Tsukamoto K, Tamura H, Ikezawa H, Nakamura H, Nishikawa K (1996) A distant evolutionary relationship between bacterial sphingomyelinase and mammalian DNase I. *Protein Sci* **5**:2459-67.
- Matte A, Tari LW, Delbaere LT (1998) How do kinases transfer phosphoryl groups? *Structure* **6**:413-9.
- Mayrose M, Bonshtien A, Sessa G (2004) LeMPK3 is a mitogen-activated protein kinase with dual specificity induced during tomato defense and wounding responses. *J Biol Chem* **279**:14819-27.
- Medina-Acosta E, Cross GA (1993) Rapid isolation of DNA from trypanosomatid protozoa using a simple 'mini-prep' procedure. *Mol Biochem Parasitol* **59**:327-9.
- Melzer IM (2007) Biochemical characterisation of LmxMPK1, an essential MAP kinase from *Leishmania mexicana*. PhD thesis, Department of Chemistry, University of Hamburg.
- Mishra KK, Holzer TR, Moore LL, LeBowitz JH (2003) A negative regulatory element controls mRNA abundance of the *Leishmania mexicana* paraflagellar rod gene *PFR2*. *Eukaryot Cell* **2**:1009-17.

- Misslitz A, Mottram JC, Overath P, Aebischer T (2000) Targeted integration into a rRNA locus results in uniform and high level expression of transgenes in *Leishmania* amastigotes. *Mol Biochem Parasitol* **107**:251-61.
- Mol CD, Kuo CF, Thayer MM, Cunningham RP, Tainer JA (1995) Structure and function of the multifunctional DNA-repair enzyme exonuclease III. *Nature* **374**:381-6.
- Moore LL, Santrich C, LeBowitz JH (1996) Stage-specific expression of the *Leishmania mexicana* paraflagellar rod protein PFR-2. *Mol Biochem Parasitol* **80**:125-35.
- Moreno SN, Vercesi AE, Pignataro OP, Docampo R (1992) Calcium homeostasis in *Trypanosoma cruzi* amastigotes: presence of inositol phosphates and lack of an inositol 1,4,5-trisphosphate-sensitive calcium pool. *Mol Biochem Parasitol* **52**:251-61.
- Mottram JC (1994) cdc2-related protein kinases and cell cycle control in trypanosomatids. *Parasitol Today* **10**:253-7.
- Mottram JC, McCready BP, Brown KG, Grant KM (1996) Gene disruptions indicate an essential function for the LmmCRK1 cdc2-related kinase of *Leishmania mexicana*. *Mol Microbiol* **22**:573-83.
- Moyer JH, Lee-Tischler MJ, Kwon HY, Schrick JJ, Avner ED, Sweeney WE, Godfrey VL, Cacheiro NL, Wilkinson JE, Woychik RP (1994) Candidate gene associated with a mutation causing recessive polycystic kidney disease in mice. *Science* **264**:1329-33.
- Müller IB, Domenicali-Pfister D, Roditi I, Vassella E (2002) Stage-specific requirement of a mitogen-activated protein kinase by *Trypanosoma brucei*. *Mol Biol Cell* **13**:3787-99.
- Murcia NS, Richards WG, Yoder BK, Mucenski ML, Dunlap JR, Woychik RP (2000) The Oak Ridge Polycystic Kidney (orpk) disease gene is required for left-right axis determination. *Development* **127**:2347-55.
- Myler PJ, Audleman L, deVos T, Hixson G, Kiser P, Lemley C, Magness C, Rickel E, Sisk E, Sunkin S, Swartzell S, Westlake T, Bastien P, Fu G, Ivens A, Stuart K (1999) *Leishmania major* Friedlin chromosome 1 has an unusual distribution of protein-coding genes. *Proc Natl Acad Sci U S A* **96**:2902-6.
- Nachury MV, Loktev AV, Zhang Q, Westlake CJ, Peränen J, Merdes A, Slusarski DC, Scheller RH, Bazan JF, Sheffield VC, Jackson PK (2007) A core complex of BBS proteins cooperates with the GTPase Rab8 to promote ciliary membrane biogenesis. *Cell* **129**:1201-13.
- Nolan DP, Reverlard P, Pays E (1994) Overexpression and characterization of a gene for a Ca²⁺-ATPase of the endoplasmic reticulum in *Trypanosoma brucei*. *J Biol Chem* **269**:26045-51.
- Nonaka S, Tanaka Y, Okada Y, Takeda S, Harada A, Kanai Y, Kido M, Hirokawa N (1998) Randomization of left-right asymmetry due to loss of nodal cilia generating leftward flow of extraembryonic fluid in mice lacking KIF3B motor protein. *Cell* **95**:829-37.
- Nozaki T, Toh-e A, Fujii M, Yagisawa H, Nakazawa M, Takeuchi T (1999) Cloning and characterization of a gene encoding phosphatidyl inositol-specific phospholipase C from *Trypanosoma cruzi*. *Mol Biochem Parasitol* **102**:283-95.
- Oberholzer M, Marti G, Baresic M, Kunz S, Hemphill A, Seebeck T (2007) The *Trypanosoma brucei* cAMP phosphodiesterases TbrPDEB1 and TbrPDEB2: flagellar enzymes that are essential for parasite virulence. *FASEB J* **21**:720-31.
- O'Connell MJ, Krien MJ, Hunter T (2003) Never say never. The NIMA-related protein kinases in mitotic control. *Trends Cell Biol* **13**:221-8.
- Olmo A, Arrebola R, Bernier V, González-Pacanowska D, Ruiz-Pérez LM (1995) Co-existence of circular and multiple linear amplicons in methotrexate-resistant *Leishmania*. *Nucleic Acids Res* **23**:2856-64.

- Ong AC, Wagner B (2005) Detection of proximal tubular motile cilia in a patient with renal sarcoidosis associated with hypercalcemia. *Am J Kidney Dis* **45**:1096-9.
- Ou G, Blacque OE, Snow JJ, Leroux MR, Scholey JM (2005) Functional coordination of intraflagellar transport motors. *Nature* **436**:583-7.
- Overath P, Stierhof YD, Wiese M (1997) Endocytosis and secretion in trypanosomatid parasites - Tumultuous traffic in a pocket. *Trends Cell Biol* **7**:27-33.
- Ozcan S, Dover J, Rosenwald AG, Wöfl S, Johnston M (1996) Two glucose transporters in *Saccharomyces cerevisiae* are glucose sensors that generate a signal for induction of gene expression. *Proc Natl Acad Sci U S A* **93**:12428-32.
- Paindavoine P, Rolin S, Van Assel S, Geuskens M, Jauniaux JC, Dinsart C, Huet G, Pays E (1992) A gene from the variant surface glycoprotein expression site encodes one of several transmembrane adenylate cyclases located on the flagellum of *Trypanosoma brucei*. *Mol Cell Biol* **12**:1218-25.
- Pan J, Snell WJ (2000) Regulated targeting of a protein kinase into an intact flagellum. An aurora/lpl1p-like protein kinase translocates from the cell body into the flagella during gamete activation in *Chlamydomonas*. *J Biol Chem* **275**:24106-14.
- Pan J, Snell WJ (2003) Kinesin II and regulated intraflagellar transport of *Chlamydomonas aurora* protein kinase. *J Cell Sci* **116**:2179-86.
- Pan J, Wang Q, Snell WJ (2004) An aurora kinase is essential for flagellar disassembly in *Chlamydomonas*. *Dev Cell* **6**:445-51.
- Panton LJ, Tesh RB, Nadeau KC, Beverley SM (1991) A test for genetic exchange in mixed infections of *Leishmania major* in the sand fly *Phlebotomus papatasi*. *J Protozool* **38**:224-8.
- Parsons M, Carter V, Muthiani A, Murphy N (1995) *Trypanosoma congolense*: developmental regulation of protein kinases and tyrosine phosphorylation during the life cycle. *Exp Parasitol* **80**:507-14.
- Parsons M, Ledbetter JA, Schieven GL, Nel AE, Kanner SB (1994) Developmental regulation of pp44/46, tyrosine-phosphorylated proteins associated with tyrosine/serine kinase activity in *Trypanosoma brucei*. *Mol Biochem Parasitol* **63**:69-78.
- Parsons M, Ruben L (2000) Pathways involved in environmental sensing in trypanosomatids. *Parasitol Today* **16**:56-62.
- Parsons M, Valentine M, Carter V (1993) Protein kinases in divergent eukaryotes: identification of protein kinase activities regulated during trypanosome development. *Proc Natl Acad Sci U S A* **90**:2656-60.
- Parsons M, Valentine M, Deans J, Schieven GL, Ledbetter JA (1990) Distinct patterns of tyrosine phosphorylation during the life cycle of *Trypanosoma brucei*. *Mol Biochem Parasitol* **45**:241-8.
- Parsons M, Worthey EA, Ward PN, Mottram JC (2005) Comparative analysis of the kinomes of three pathogenic trypanosomatids: *Leishmania major*, *Trypanosoma brucei* and *Trypanosoma cruzi*. *BMC Genomics* **6**:127.
- Pawson T, Saxton TM (1999) Signaling networks--do all roads lead to the same genes? *Cell* **97**:675-8.
- Payne DM, Rossomando AJ, Martino P, Erickson AK, Her JH, Shabanowitz J, Hunt DF, Weber MJ, Sturgill TW (1991) Identification of the regulatory phosphorylation sites in pp42/mitogen-activated protein kinase (MAP kinase). *EMBO J* **10**:885-92.
- Pazour GJ, Agrin N, Leszyk J, Witman GB (2005) Proteomic analysis of a eukaryotic cilium. *J Cell Biol* **170**:103-13.

- Pazour GJ, Baker SA, Deane JA, Cole DG, Dickert BL, Rosenbaum JL, Witman GB, Besharse JC (2002) The intraflagellar transport protein, IFT88, is essential for vertebrate photoreceptor assembly and maintenance. *J Cell Biol* **157**:103-13.
- Pazour GJ, Dickert BL, Witman GB (1999) The DHC1b (DHC2) isoform of cytoplasmic dynein is required for flagellar assembly. *J Cell Biol* **144**:473-81.
- Pazour GJ, Rosenbaum JL (2002a) The vertebrate primary cilium is a sensory organelle. *TICB* **12**:551-5.
- Pazour GJ, Rosenbaum JL (2002b) Intraflagellar transport and cilia-dependent diseases. *Trends Cell Biol* **12**:551-5.
- Peacock CS, Seeger K, Harris D, Murphy L, Ruiz JC, Quail MA, Peters N, Adlem E, Tivey A, Aslett M, Kerhornou A, Ivens A, Fraser A, Rajandream MA, Carver T, Norbertczak H, Chillingworth T, Hance Z, Jagels K, Moule S, Ormond D, Rutter S, Squares R, Whitehead S, Rabbinowitsch E, Arrowsmith C, White B, Thurston S, Bringaud F, Baldauf SL, Faulconbridge A, Jeffares D, Depledge DP, Oyola SO, Hilley JD, Brito LO, Tosi LR, Barrell B, Cruz AK, Mottram JC, Smith DF, Berriman M (2007) Comparative genomic analysis of three *Leishmania* species that cause diverse human disease. *Nat Genet.* **39**:839-47.
- Pearson G, Robinson F, Beers Gibson T, Xu BE, Karandikar M, Berman K, Cobb MH (2001) Mitogen-activated protein (MAP) kinase pathways: regulation and physiological functions. *Endocr Rev* **22**:153-83.
- Peden EM, Barr MM (2005) The KLP-6 kinesin is required for male mating behaviors and polycystin localization in *Caenorhabditis elegans*. *Curr Biol* **15**:394-404.
- Pedersen LB, Geimer S, Rosenbaum JL (2006) Dissecting the molecular mechanisms of intraflagellar transport in *Chlamydomonas*. *Curr Biol* **16**:450-9.
- Pedersen LB, Miller MS, Geimer S, Leitch JM, Rosenbaum JL, Cole DG (2005) *Chlamydomonas* IFT172 is encoded by *FLA11*, interacts with CrEB1, and regulates IFT at the flagellar tip. *Curr Biol* **15**:262-6.
- Perrone CA, Tritschler D, Taulman P, Bower R, Yoder BK, Porter ME (2003) A novel dynein light intermediate chain colocalizes with the retrograde motor for intraflagellar transport at sites of axoneme assembly in *Chlamydomonas* and mammalian cells. *Mol Biol Cell* **14**:2041-56.
- Pimenta PF, Modi GB, Pereira ST, Shahabuddin M, Sacks DL (1997) A novel role for the peritrophic matrix in protecting *Leishmania* from the hydrolytic activities of the sand fly midgut. *Parasitology* **115**:359-69.
- Piper RC, Xu X, Russell DG, Little BM, Landfear SM (1995) Differential targeting of two glucose transporters from *Leishmania enriettii* is mediated by an NH₂-terminal domain. *J Cell Biol* **128**:499-508.
- Piperno G, Huang B, Luck DJ (1977) Two-dimensional analysis of flagellar proteins from wild-type and paralyzed mutants of *Chlamydomonas reinhardtii*. *Proc Natl Acad Sci U S A* **74**:1600-4.
- Porter ME, Bower R, Knott JA, Byrd P, Dentler W (1999) Cytoplasmic dynein heavy chain 1b is required for flagellar assembly in *Chlamydomonas*. *Mol Biol Cell* **10**:693-712.
- Pozuelo M, MacKintosh C, Galván A, Fernández E (2001) Cytosolic glutamine synthetase and not nitrate reductase from the green alga *Chlamydomonas reinhardtii* is phosphorylated and binds 14-3-3 proteins. *Planta* **212**:264-9.
- Pradel LC, Bonhivers M, Landrein N, Robinson DR (2006) NIMA-related kinase TbNRKC is involved in basal body separation in *Trypanosoma brucei*. *J Cell Sci* **119**:1852-63.

- Privé C, Descoteaux A (2000) *Leishmania donovani* promastigotes evade the activation of mitogen-activated protein kinases p38, c-Jun N-terminal kinase, and extracellular signal-regulated kinase-1/2 during infection of naive macrophages. *Eur J Immunol* **30**:2235-44.
- Proudfoot L, O'Donnell CA, Liew FY (1995) Glycoinositolphospholipids of *Leishmania major* inhibit nitric oxide synthesis and reduce leishmanicidal activity in murine macrophages. *Eur J Immunol* **25**:745-50.
- Puentes SM, Da Silva RP, Sacks DL, Hammer CH, Joiner KA (1990) Serum resistance of metacyclic stage *Leishmania major* promastigotes is due to release of C5b-9. *J Immunol* **145**:4311-6.
- Pullen TJ, Ginger ML, Gaskell SJ, Gull K (2004) Protein targeting of an unusual, evolutionarily conserved adenylate kinase to a eukaryotic flagellum. *Mol Biol Cell* **15**:3257-65.
- Qin H, Burnette DT, Bae YK, Forscher P, Barr MM, Rosenbaum JL (2005) Intraflagellar transport is required for the vectorial movement of TRPV channels in the ciliary membrane. *Curr Biol* **15**:1695-9.
- Ralston KS, Hill KL (2008) The flagellum of *Trypanosoma brucei*: new tricks from an old dog. *Int J Parasitol* **38**:869-84.
- Rashid DJ, Wedaman KP, Scholey JM (1995) Heterodimerization of the two motor subunits of the heterotrimeric kinesin, KRP85/95. *J Mol Biol* **252**:157-62.
- Ridgley E, Webster P, Patton C, Ruben L (2000) Calmodulin-binding properties of the paraflagellar rod complex from *Trypanosoma brucei*. *Mol Biochem Parasitol* **109**:195-201.
- Robbins DJ, Cobb MH (1992) Extracellular signal-regulated kinases 2 autophosphorylates on a subset of peptides phosphorylated in intact cells in response to insulin and nerve growth factor: analysis by peptide mapping. *Mol Biol Cell* **3**:299-308.
- Robbins DJ, Zhen E, Owaki H, Vanderbilt CA, Ebert D, Geppert TD, Cobb MH (1993) Regulation and properties of extracellular signal-regulated protein kinases 1 and 2 *in vitro*. *J Biol Chem* **268**:5097-106.
- Robinson KA, Beverley SM (2003) Improvements in transfection efficiency and tests of RNA interference (RNAi) approaches in the protozoan parasite *Leishmania*. *Mol Biochem Parasitol* **128**:217-28.
- Robinson MJ, Harkins PC, Zhang J, Baer R, Haycock JW, Cobb MH, Goldsmith EJ (1996) Mutation of position 52 in ERK2 creates a nonproductive binding mode for adenosine 5'-triphosphate. *Biochemistry* **35**:5641-6.
- Rogers ME, Chance ML, Bates PA (2002) The role of promastigote secretory gel in the origin and transmission of the infective stage of *Leishmania mexicana* by the sandfly *Lutzomyia longipalpis*. *Parasitology* **124**:495-507.
- Rolin S, Paindavoine P, Hanocq-Quertier J, Hanocq F, Claes Y, Le Ray D, Overath P, Pays E (1993) Transient adenylate cyclase activation accompanies differentiation of *Trypanosoma brucei* from bloodstream to procyclic forms. *Mol Biochem Parasitol* **61**:115-25.
- Rosenbaum JL (2003) Organelle size regulation: length matters. *Curr Biol* **13**:R506-7.
- Rosenbaum JL, Witman GB (2002) Intraflagellar transport. *Nat Rev Mol Cell Biol* **3**:813-25.
- Rosenthal LA, Sutterwala FS, Kehrl ME, Mosser DM (1996) *Leishmania major*-human macrophage interactions: cooperation between Mac-1 (CD11b/CD18) and complement receptor type 1 (CD35) in promastigote adhesion. *Infect Immun* **64**:2206-15.
- Ross DT, Raibaud A, Florent IC, Sather S, Gross MK, Storm DR, Eisen H (1991) The trypanosome VSG expression site encodes adenylate cyclase and a leucine-rich putative regulatory gene. *EMBO J* **10**:2047-53.

- Ruben L, Patton CL (1985) Comparative structural analysis of calmodulins from *Trypanosoma brucei*, *T. congolense*, *T. vivax*, *Tetrahymena thermophila* and bovine brain. *Mol Biochem Parasitol* **17**:331-41.
- Saito RM, Elgort MG, Campbell DA (1994) A conserved upstream element is essential for transcription of the *Leishmania tarentolae* mini-exon gene. *EMBO J* **13**:5460-9.
- Sanchez MA, Zeoli D, Klamo EM, Kavanaugh MP, Landfear SM (1995) A family of putative receptor-adenylate cyclases from *Leishmania donovani*. *J Biol Chem* **270**:17551-8.
- Santrich C, Moore L, Sherwin T, Bastin P, Brokaw C, Gull K, LeBowitz JH (1997) A motility function for the paraflagellar rod of *Leishmania* parasites revealed by *PFR-2* gene knockouts. *Mol Biochem Parasitol* **90**:95-109.
- Saraiva EM, de Figueiredo Barbosa A, Santos FN, Borja-Cabrera GP, Nico D, Souza LO, de Oliveira Mendes-Aguiar C, de Souza EP, Fampa P, Parra LE, Menz I, Dias JG Jr, de Oliveira SM, Palatnik-de-Sousa CB (2006) The FML-vaccine (Leishmune) against canine visceral leishmaniasis: a transmission blocking vaccine. *Vaccine* **24**:2423-31.
- Schlein Y, Jacobson RL, Shlomai J (1991) Chitinase secreted by *Leishmania* functions in the sandfly vector. *Proc Biol Sci* **245**:121-6.
- Scholey JM (2008) Intraflagellar transport motors in cilia: moving along the cell's antenna. *J Cell Biol* **180**:23-9.
- Scholz A (2008) Interacting protein kinases in *Leishmania mexicana* which are involved in the regulation of flagellar length. PhD thesis, Department of Chemistry, University of Hamburg.
- Segovia M (1994) *Leishmania* gene amplification: a mechanism of drug resistance. *Ann Trop Med Parasitol* **88**:123-30.
- Shah K, Liu Y, Deirmengian C, Shokat KM (1997) Engineering unnatural nucleotide specificity for Rous sarcoma virus tyrosine kinase to uniquely label its direct substrates. *Proc Natl Acad Sci U S A* **94**:3565-70.
- Shah K, Shokat KM (2002) A chemical genetic screen for direct v-Src substrates reveals ordered assembly of a retrograde signaling pathway. *Chem Biol* **9**:35-47.
- Shapira M, McEwen JG, Jaffe CL (1988) Temperature effects on molecular processes which lead to stage differentiation in *Leishmania*. *EMBO J* **7**:2895-901.
- Shaw G (1996) The pleckstrin homology domain: an intriguing multifunctional protein module. *Bioessays* **18**:35-46.
- Sherwin T, Gull K (1989) The cell division cycle of *Trypanosoma brucei brucei*: timing of event markers and cytoskeletal modulations. *Philos Trans R Soc Lond B Biol Sci* **323**:573-88.
- Shiu SH, Blecker AB (2001) Plant receptor-like kinase gene family: diversity, function, and signaling. *Sci STKE* **2001**:RE22.
- Signor D, Wedaman KP, Orozco JT, Dwyer ND, Bargmann CI, Rose LS, Scholey JM (1999) Role of a class DHC1b dynein in retrograde transport of IFT motors and IFT raft particles along cilia, but not dendrites, in chemosensory neurons of living *Caenorhabditis elegans*. *J Cell Biol* **147**:519-30.
- Sloboda RD (2005) Intraflagellar transport and the flagellar tip complex. *J Cell Biochem* **94**:266-72.
- Snow JJ, Ou G, Gunnarson AL, Walker MR, Zhou HM, Brust-Mascher I, Scholey JM (2004) Two anterograde intraflagellar transport motors cooperate to build sensory cilia on *C. elegans* neurons. *Nat Cell Biol* **6**:1109-13.
- Somlo S, Ehrlich B (2001) Human disease: calcium signaling in polycystic kidney disease. *Curr Biol* **11**:R356-60.

- Song L, Dentler WL (2001) Flagellar protein dynamics in *Chlamydomonas*. *J Biol Chem* **276**:29754-63.
- Sørensen AL, Hey AS, Kharazmi A (1994) *Leishmania major* surface protease Gp63 interferes with the function of human monocytes and neutrophils *in vitro*. *APMIS* **102**:265-71.
- Stephens RE (1997) Synthesis and turnover of embryonic sea urchin ciliary proteins during selective inhibition of tubulin synthesis and assembly. *Mol Biol Cell* **8**:2187-98.
- Stiles JK, Hicock PI, Shah PH, Meade JC (1999) Genomic organization, transcription, splicing and gene regulation in *Leishmania*. *Ann Trop Med Parasitol* **93**:781-807.
- Stojdl DF, Clarke MW (1996) *Trypanosoma brucei*: analysis of cytoplasmic Ca²⁺ during differentiation of bloodstream stages *in vitro*. *Exp Parasitol* **83**:134-46.
- Sundar S (2003) Indian kala-azar--better tools needed for diagnosis and treatment. *J Postgrad Med* **49**:29-30.
- Sundaram MV (2006) RTK/Ras/MAPK signaling. *WormBook* **11**:1-19.
- Tabbara KS (2006) Progress towards a *Leishmania* vaccine. *Saudi Med J* **27**:942-50.
- Takada S, Wilkerson CG, Wakabayashi K, Kamiya R, Witman GB (2002) The outer dynein arm-docking complex: composition and characterization of a subunit (oda1) necessary for outer arm assembly. *Mol Biol Cell* **13**:1015-29.
- Tam LW, Wilson NF, Lefebvre PA (2007) A CDK-related kinase regulates the length and assembly of flagella in *Chlamydomonas*. *J Cell Biol* **176**:819-29.
- Tanoue T, Nishida E (2003) Molecular recognitions in the MAP kinase cascades. *Cell Signal* **15**:455-62.
- Targett GA, Greenwood BM (2008) Malaria vaccines and their potential role in the elimination of malaria. *Malar J* **7** Suppl 1:S10.
- Tari LW, Matte A, Goldie H, Delbaere LT (1997) Mg²⁺-Mn²⁺ clusters in enzyme-catalyzed phosphoryl-transfer reactions. *Nat Struct Biol* **4**:990-4.
- Teilmann SC, Byskov AG, Pedersen PA, Wheatley DN, Pazour GJ, Christensen ST (2005) Localization of transient receptor potential ion channels in primary and motile cilia of the female murine reproductive organs. *Mol Reprod Dev* **71**:444-52.
- Tonui WK, Mbatia PA, Anjili CO, Orago AS, Turco SJ, Githure JI, Koech DK (2001a) Transmission blocking vaccine studies in leishmaniasis: I. Lipophosphoglycan is a promising transmission blocking vaccine molecule against cutaneous leishmaniasis. *East Afr Med J* **78**:84-9.
- Tonui WK, Mbatia PA, Anjili CO, Orago AS, Turco SJ, Githure JI, Koech DK (2001b) Transmission blocking vaccine studies in leishmaniasis: II. Effect of immunisation using *Leishmania major* derived 63 kilodalton glycoprotein, lipophosphoglycan and whole parasite antigens on the course of *L. major* infection in BALB/c mice. *East Afr Med J* **78**:90-2.
- Tuxhorn J, Daise T, Dentler WL (1998) Regulation of flagellar length in *Chlamydomonas*. *Cell Motil Cytoskeleton* **40**:133-46.
- Ullu E, Matthews KR, Tschudi C (1993) Temporal order of RNA-processing reactions in trypanosomes: rapid trans-splicing precedes polyadenylation of newly synthesized tubulin transcripts. *Mol Cell Biol* **13**:720-5.
- Wagner V, Gessner G, Heiland I, Kaminski M, Hawat S, Scheffler K, Mittag M (2006) Analysis of the phosphoproteome of *Chlamydomonas reinhardtii* provides new insights into various cellular pathways. *Eukaryot Cell* **5**:457-68.

- Wanders P (2004) *In vitro* and *in vivo* characterisation of an *LmxMPK5* deletion mutant in *Leishmania mexicana*. MD thesis, University of Veterinary Medicine Hannover.
- Wang Q, Melzer IM, Kruse M, Sander-Juelch C, Wiese M (2005) *LmxMPK4*, a mitogen-activated protein (MAP) kinase homologue essential for promastigotes and amastigotes of *Leishmania mexicana*. *Kinetoplastid Biol Dis* **4**:6.
- Wedaman KP, Meyer DW, Rashid DJ, Cole DG, Scholey JM (1996) Sequence and submolecular localization of the 115-kD accessory subunit of the heterotrimeric kinesin-II (KRP85/95) complex. *J Cell Biol* **132**:371-80.
- Wiese M (1998) A mitogen-activated protein (MAP) kinase homologue of *Leishmania mexicana* is essential for parasite survival in the infected host. *EMBO J* **17**:2619-28.
- Wiese M (2007) *Leishmania* MAP kinases--familiar proteins in an unusual context. *Int J Parasitol* **37**:1053-62.
- Wiese M, Kuhn D, Grünfelder CG (2003a) Protein kinase involved in flagellar-length control. *Eukaryot Cell* **2**:769-77.
- Wiese M, Wang Q, Görcke I (2003b) Identification of mitogen-activated protein kinase homologues from *Leishmania mexicana*. *Int J Parasitol* **33**:1577-87.
- Wilson NF, Lefebvre PA (2004) Regulation of flagellar assembly by glycogen synthase kinase 3 in *Chlamydomonas reinhardtii*. *Eukaryot Cell* **3**:1307-19.
- Windelberg M (2007) Molecular characterisation of the mitogen-activated protein kinases *LmxMPK11* and *LmxMPK12* from *Leishmania mexicana*. MD thesis, University of Hamburg.
- Wordeman L (2005) Microtubule-depolymerizing kinesins. *Curr Opin Cell Biol* **17**:82-8.
- World Health Organisation (2006) Indoor Residual Spraying. Use of indoor residual spraying for scaling up global malaria control and elimination. World Health Organisation, Geneva.
- Wu J, Rossomando AJ, Horng-Her J, Weber MJ, Sturgill TW (1992) Apparent sufficiency of a dual-specificity tyrosine/threonine kinase for activation of MAP kinase poses new questions for the dual-phosphorylation mechanism. *Biochem Soc Trans* **20**:675-7.
- Wu Y, Deford J, Benjamin R, Lee MG, Ruben L (1994) The gene family of EF-hand calcium-binding proteins from the flagellum of *Trypanosoma brucei*. *Biochem J* **304**:833-41.
- Xiong ZH, Ruben L (1998) *Trypanosoma brucei*: the dynamics of calcium movement between the cytosol, nucleus, and mitochondrion of intact cells. *Exp Parasitol* **88**:231-9.
- Xu B, English JM, Wilsbacher JL, Stippec S, Goldsmith EJ, Cobb MH (2000) WNK1, a novel mammalian serine/threonine protein kinase lacking the catalytic lysine in subdomain II. *J Biol Chem* **275**:16795-801.
- Yang SH, Yates PR, Whitmarsh AJ, Davis RJ, Sharrocks AD (1998) The Elk-1 ETS-domain transcription factor contains a mitogen-activated protein kinase targeting motif. *Mol Cell Biol* **18**:710-20.
- Zheng CF, Guan K (1994) Cytoplasmic localisation of the mitogen-activated protein kinase activator MEK. *J Biol Chem* **269**:19947-52.
- Zhou C, Yang Y, Jong AY (1990) Mini-prep in ten minutes. *Biotechniques* **8**:172-3.
- Zilberstein D (1993) Transport of nutrients and ions across membranes of trypanosomatid parasites. *Adv Parasitol* **32**:261-91.
- Zilberstein D, Blumenfeld N, Liveanu V, Gepstein A, Jaffe CL (1991) Growth at acidic pH induces an amastigote stage-specific protein in *Leishmania* promastigotes. *Mol Biochem Parasitol* **45**:175-8.

Zilberstein D, Shapira M (1994) The role of pH and temperature in the development of *Leishmania* parasites. *Annu Rev Microbiol* **48**:449-70.

Zoraghi R, Seebeck T (2002) The cAMP-specific phosphodiesterase TbPDE2C is an essential enzyme in bloodstream form *Trypanosoma brucei*. *Proc Natl Acad Sci U S A* **99**:4343-8.

8 Appendix

8.1 Nucleotide and amino acid sequences

8.1.1 LmxMPK3

LmxMPK3 ORF and flanking regions, LmxMPK3 translated sequence

```

1  CCCCCCCCCACGTCCCCCCCCCTCTGCCGAACAAGGCGTCTTATAATTCACGCTTCCGT 60
61  GTGCATCCGCGCCTTCTCTCTTTTTTTTTTTTTGTTTGTTCCTGTACGCTACTCACTTCA 120
121 CTGTTGCGCGTGTCTGCGTGTGCCTCTGCCACCGCCGGCTCTTCGATCCCAAATCACCG 180
181 CGAGCACAGAGACGGAGGCGACGCGTGCACGGACAAACGACACGGCGATCCAGAACACG 240
241 GGAGACGGAAACTCAGACAGGCAACGAAACGCATCGTGCGTACCGCCGTTCAAAGGAACG 300
301 GACGGAGACACACACACGGACACACAAACGGGGGACGCATTCTATTTTTAATGGTTCGAGA 360
361 AGGGCACACGTGTCATTGGTATTGTGGGAAATACATACATAGCTCTATAGTGCTCTGTGC 420
421 TCGTTGTGTTGCGCTCGTCTGCGGCTGGTCTCATTTTTTTTTCTTGGGCTCGTGTAGGGCG 480
481 TCATTCCCCCCCCCCGCCTTCTCTCCCCCTCTCTCCCCCTCTCTCCCCCTTCCCCTCCCT 540
541 CTCTTCGAGTTGTTGTTCTTTCGCGTTGTTGCGCTTTTTTCACTCTCCTAACGGGCTCATC 600
601 CTCGCCGTTGCTGTGTGTGTGCGTGTGCGTCTGTGTCTATGCCGGCGTCCGGATAGTCAA 660
661 GGCAACGTACGTTGCACGTCTGGCCCTCGTCGCTCCTCTGCTGGTGGTGGTGGTCTGCC 720
721 ATTGTACTGCCGTATCCTCTTCTCGGCTGTGCGCGTGTGAACGCTGCTCCGTTTATTTTC 780
781 GCCGTGTCTCTCCGTGTGTGTGTGTGTATATATATATATATACAGCAGCGCCACCCAT 840
841 ACCCGGCGCACTCTTTTTTTTTTCTTCGCTCGCTCGCTTGGGCTCTCTCGTTGGCGTGTC 900
901 TTCCACGTGGCGAGGCGGCGGTTGGGACGGTGCCGAAGCGAGTGAAAAGAGGCCCAATT 960
961 TTTTTTTGTTGTTTTCGTTGGCTCAGAGCGCCAAAGAGAGCAGCTGTACGCGCCGCTCCT 1020
1021 CATCCGCCCTCTGTCTGTGTCTGTGTGTGTGTGTGTGTGTGTGCTGCCTGCCTGCCTC 1080
1081 CCACCCACCCCTCTACCCTTCTCTTCTGTTGTTTGAACACTACGCGTACATCCCGTTCTTCT 1140
1141 TTCGGAGGAAGGGGGGTTGTCGAACCTCTATCTGGCTAGTCAGCTATCCATCTCTCTGTC 1200
1201 CCTCTCTTGACCGTGACTACCACCGCCGTCGCTGGCCTTGTATCTTCTCGGCTCTTCTT 1260
1261 GTCTCTCCTCCTCCTCCCTACCTTCCCTCCCTTTGTTTGGATCACATCCACGAGCGCT 1320
1321 CATATCACCGGCCCCACCGGGCCACCTGCCACAGGCTTCCCTCCCCCTCTCCCCCTC 1380
1381 CCCCTCTCTCACTTTCACTTTCACTACCGCCCTCGCCATCTTCTCAGTCTCTTTTTTTA 1440
1441 TTTCTGTACCCGCAGTAGCCACACCAGCCAGTTGTGCAGCGGTGCGCAGGCACGATAG 1500
1501 CACACAGAGTAGCCAAAATGCACAAGAGCAACCAGGAGCTGAGCGTGCCCAAGGTTGTGG 1560
      M H K S N Q E L S V P K V V G

1561 GGGACTTCAAGGTGTACAACGTAAGCGGCTCCCCATTCGAGGTTCCGTTCCAAGTACACGC 1620
      D F K V Y N V S G S P F E V P S K Y T L

1621 TGCTCAAGATCCTTGGCATGGGTGCCTACGGTATCGCGTGCAGCTGCTTGGATGGCGACA 1680
      L K I L G M G A Y G I A C S C L D G D T

1681 CTGGCGAGAAGGTGTCCATCAAGAAGTGTGCGGACGTGTTCCGCGATGTCGAGGATGGCA 1740
      G E K V S I K K C R D V F R D V E D G K

1741 AGCGAGTGCTGCGCGAGATCGACATGATGCGCTTCTTCCACCACGAAAACCTGCTCAATG 1800
      R V L R E I D M M R F F H H E N L L N V

1801 TGGTGAACATTTTGCCTCCGCTGAAGTGCGAATACCACAGCTTCGAAGACGTGTACGTCG 1860
      V N I L P P L K C E Y H S F E D V Y V V

1920 TCACTCCGCTCATGGACGTAGACATGAATGTGCTACTGCGCTCTCGACAGGTGCTGGAGG 1920
      T P L M D V D M N V V L R S R Q V L E E

1921 AGTCGCACATGCAGTACTTTGTCTACCAGATTCTGCGGGGCTCAAGTACCTGCACAGCG 1980
      S H M Q Y F V Y Q I L R G L K Y L H S A

1981 CGAACGTGCCCCACCGAGACTTGAAGCCAGCCAACCTTGTACAAAACATCTCTTGTGAGC 2040
      N V A H R D L K P A N L V T N I S C E L

2041 TCAAGATTATAGACTTCGGGCTGAGCCGACGCTCGATGTGCCGTA CTGGAGCTTACGG 2100

```

K I I D F G L S R S V D V P Y S E L T D

2101 ATTACGTCATCACGCGCTGGTACCGCCCGCCGGAGCTGCTTCTGGAGAACACGAACTATT 2160
Y V I T R W Y R P P E L L L E N T N Y S

2161 CCACCGCAGTCGACATATGGTCTGTTGGCTGCATCTTTGCTGAGATGTACAACCGTAAGC 2220
T A V D I W S V G C I F A E M Y N R K P

2221 CCGTTTTCCAGGTTCGAAATACGATGGACCAGCTGCGCATGATCGCGCAGCACATTGGCA 2280
V F P G R N T M D Q L R M I A Q H I G K

2281 AGCCGCCGGCCAGCATCGTCGAGCACCGCGAGGCGCTGGAGAAGCTGAATGAGCTGCCGG 2340
P P A S I V E H R E A L E K L N E L P G

2341 GCGGGTGCCTCAACATTCCTAAACTCGTCCCCGGGCTGGCTGGCAACACGGAGGGCATAG 2400
G S L N I P K L V P G L A G N T E G I D

2401 ACTTTCTCTCCAAGATGTGGACGCTAGACCCGAGCAAGCGTCCGACCGCGGCTGACATGC 2460
F L S K M W T L D P S K R P T A A D M L

2461 TCGCGCACCCATACCTGGCCACCTGCACGACGAGGAAGATGAGCCGGCCTGCCCTGCC 2520
A H P Y L A H L H D E E D E P A C P C P

2521 CCTTCTGTGGGCACATGAGAGCACCCCGATGGGCGTCTCGGAGCTTCGTGCGCCTTCT 2580
F L W A H E S T P M G V S E L R R A F W

2581 GGGCCGACATTGTCGACTACAACCCGTCTCTGGAGCACGCCACGCCTCCAGCGACAACGG 2640
A D I V D Y N P S L E H A T P P A T T A

2641 CTGGTGGCAGCAGCTCAAAGAACGGTAGCGGTCACCATCACTAGCGGCATCTTCTCTTC 2700
G G S S S K N G S G H H H *

2701 TCCAGGCGCCGTCGTGTTGTGTTTCGACTGTGTGTGCCATCCCCTCACGCAGGCGGCAC 2760

2761 ACGCGGGTCATGAGTGGGAAAGAGATGTGTGGAGGTGAGGAAATAGCGAACGGTGGAAGC 2820

2821 GGGAAATGCGTGGCTGGCGAGGGCGAGACAGCGGGAGGAGAGGCCATGACGGGTGCACAGC 2880

2881 CGCGTCAAATCTCATTTTTCCGTCTTCCACGCGTGTGACGCGGTGGGTGTGCGAGTACCAT 2940

2941 GGAGGTGGAGCGCGCTCCGCGCACACGATGGACACATGCACCTTCACGCACCAACAGAC 3000

3001 GCTCAGTCGCGACGCCTACAGAGCGGGGCCGACGTGCGTACGGAAATATTTAGATGGAG 3060

3061 CGCGCGCCTGGATGGCGCTACTCTCTCCCCCTCCCCTCCCCTTCCCCCACCACCACCAC 3120

3121 CACCACCACACCCTCGATTTGCCTTTCTCTTCTACCTTATCCGATGCGGTGCTTCTT 3180

3181 CTTTTCCCCTGTGCGAGCGTATCTGCATGTGTGGTGGCGGGCACGAGGAGCACGTTATCG 3240

3241 TCCTTCTACACACCCCGTCCACACCCGACGCACACACGCGCACGCACGCGTATAACCAGTGTG 3300

3301 TGTTAGGGGAGGGGAGAAGAGGGGAGGGGAGGGGATATCTGTACAAGTGTCTCCCCCTC 3360

3361 TCTTCCCTCTCCGTCTGTCTTTCTCTCTCCCTGTGTGTGTGTATGTGTGTGTGTTGCGTT 3420

3421 TATTATTACCACTGCGCAGCCTTGTGTAAGCGTGTGGTGGTGGTGGTCTGCCCTCCCCCT 3480

3481 CCCCTCCCCTCCCCTTCTTCTTCCATCCACTCCCTGGTAGGGCGCCGTCCCCTCTTCGAGT 3540

3541 GTGTTTCTTCGTGCGTGTGTTTTCCGTCTTCTCATCACGTACGCACGCGCACATCATTTT 3600

3601 GTTTGGTTGGTTGTCCGTTGTTGTTTTCTTCTCTCTCTCCCCTCCCCCATCGACTTTCTT 3660

3661 GGTTTGCCTGCTTGCCTCACGCTGCCGTGCGGTGTGGTGGTGGTGGTCTGGTGGTGGTGGT 3720

3721 CCGTGCCTCAGCGACCGCTGCCAAACTGGTCCCAGGGAGGCGGAAGCGGGGATGACCGGC 3780

3781 GATGAACCATGCCGGCGGTACTCTCCGTGGTGGACGTTGTTGTTTGTCCCTTTTTTACT 3840

3841 TATTTTGTTTTTTTAGATCGGTTCCCTACGGCATGTTGCTGGCTCTCTTTTGGCCCTCC 3900

3901 TCCCCTCCCCTCCCCTCCTCTTTACTTGGTGGTCCCTTCACATTTGGTTGCCCGTGTCT 3960

3961 TCATGTACATAACCGCACCCCTCCCCCTCCCTCCTTCCCTCCTCCCCCTTCGTGGAACG 4020

4021 GGACGCCTCTTCGTTCTTCTTCTTGTGTGGACTTCAGTCTGGTCTGGTGGTGGTGGT 4080

4081 GGTGCTGGTGGTGGTGGTGGTGGTGGTGGTGGTGGTGGTGGTGGTGGTGGTGGTGGTGGT 4140

4141 CTTTTGCTTGGGGCCGCTCTGCCGTTCCCTGCAATCGGAACGGCAGAGCG 4189

Alignment of LmxMPK3 and homologous proteins

				1	14
LmxMPK3				MHKS	NQELSVPKVV
TbMPK3			CE.TI.
TcMPK3				..D.CE.TI.
CrMPK3		MADPGAQPV	PAPQSAEEPV	TGGLQESVEV	TASGKLDYSN
StMPK3	MDASAPQMDT	MMPDVAAPAV	QQPPPPPPQL	PG--MDNIPA	TL-----SHG
DdMPK3				MPP	PPTS DTSNFN
	15		▼		△ 63
LmxMPK3	GDFKVYNVSG	SPFEVPSKYT	L-LKILGMGA	YGIACSCLDG	DTGEKVSIIK
TbMPK3	.G.....G.	.E....R...	-.....NE	E.Q.....
TcMPK3L.....	.Q....R....	-.....T..NE	E.K....V..
CrMPK3	REYNQFLC.	.L..C.A..L	-PI.PI.K..	..VV..AKNL	.NQ...A...
StMPK3	.R.IQ..IF.	NI...TA..K	PPIMPI.K..	..V..A.NS	E.N.N.A...
DdMPK3	DN-IS.F.Y.	.Q.T..RR.S	I-V.CI.H..	..VV..AK.N	L.....A...
			I		
	64				113
LmxMPK3	CRDVF RDVED	GKRVLREIDM	MRFFHHENLL	NVVN ILPPLK	CEYHSFEDVY
TbMPK3	..E....LD.	.R.....VA.R.....	H.MD....M.	-G.NE.R...
TcMPK3L..A.Q.....	HIMD....M.	-S.TE.R...
CrMPK3	IANA.DN.I.	A..T...KL	L.HLQ...IV	QIKD.I..TN	RD--A.K.L.
StMPK3	IANA.DNKI.	A..T...KL	L.HMD...IV	AIRD.I..PQ	R.--A.N...
DdMPK3	<u>ISKA.DNLK.</u>	<u>T..T...HL</u>	<u>L.H.K...I</u>	<u>SIKD..K.NS</u>	<u>K.--Q....</u>
	II	III		IV	
	114				163
LmxMPK3	VVTPLMDVDM	NVVLRSRQVL	EESHMQYFVY	QILRGLKYLH	SANVAHRDLK
TbMPK3	I....K....T.VR..I.G.....
TcMPK3	I....K....E.	TGA.VR....G.....
CrMPK3	..YE...T.L	HQII..P.A.	SND.S...L.	.L.....I.	...IL.....
StMPK3	IAYE...T.L	HQII..N.G.	S.E.C...L.I.	...L.....
DdMPK3	<u>I.SE...T.L</u>	<u>HQIIT.P.P.</u>	<u>SDD.C....</u>	<u>.M....HI.</u>	<u>...L.....</u>
	V		VIa		VIb
	164			↓ ↓	212
LmxMPK3	PANLVTNISC	ELKIIDFGLS	RSVDVPYSE-	LTDYVITRWY	RPPELLLENT
TbMPK3D...TI.HHD-S
TcMPK3D.T.N.TM..Y.-N
CrMPK3	.S..LV.AN.	D...C...A	.TSTSNER.F	M.E..V....	.A....SCS
StMPK3	.S..LL.AN.	D...C...A	--VTSETDF	M.E..V....NSS
DdMPK3	<u>.S..LI.ED.</u>	<u>L...C.L.A</u>	<u>.VE.ATHQGF</u>	<u>M.E..A....</u>	<u>.A..VI.SWN</u>
		VII		VIII	
	213				259
LmxMPK3	NYSTAVDIWS	VGCIFAEMYN	RKPVFPGRNT	MDQLRMIAQH	IGKPPAS---
TbMPK3	Y.D.....M....L....	I....L.CT.RD---
TcMPK3	Y.T.....M....TLR....	L....L.CT.SE---
CrMPK3	G.T..I.V..LLG	...L...KDY	VH..SL.TKV	..S.SEEELG
StMPK3	D.TA.I.V..M.LMD	...L...DH	VH...L.MEL	..T.SEAEME
DdMPK3	K.TK.I....LLG	...L.Q.KDY	IH.ITL.IET	..S.SSEEDIC
		IX		X	
	260				306
LmxMPK3	IVEHREALEK	LNELP---GG	SLNIPKLVPG	LAGNTEGIDF	LSKMWTLDPS
TbMPK3	M..SA.....	..Q.---D.	E.DMG....	.T-SAD....	..Q..E...R
TcMPK3	M.NNP...D.	.HG.---D.	..EVTE....	.T-DP.A..I	.T...E...A
CrMPK3	FITSEK.KRY	IRS..RSE--	RVDFGQ.W.H	V--TKTAL.L	ID..LVF..T
StMPK3	FL-NEN.KRY	IRQ..LYR--	RQSFTKEF.H	V--.PAA..L	VE..L.F..R
DdMPK3	NIANEQ.RQF	IRS.NMG NQP	KV.FANMF.K	A--.PDA..L	<u>.ER.LYF...</u>
				XI	

	307	▼		356
LmxMPK3	KRPTAADMLA	HPYLAHLHDE	EDEPACPCPF	LWAHESTPMG VSELRRAFWA
TbMPK3	...S..EL.R	..FM.P....	V...V..TS.	A.PY.MQE.S LDS.....D
TcMPK3	..QS..EL.Q	..F..A....	Q...E..TL.	S.PY.QKE.N D.L.....E
CrMPK3	..I.VEQA.ES...V	S...V..T..	TFDFD.EHLT PDVV.EVILQ
StMPK3	R.I.VE.A..S...I	S...I.MT..	NFDF.QHALT EEQMKELIYR
DdMPK3	..L.VEEA...	...FQS...P	S...I.LHK.	SLNF.AWDLN RDL.KELIYN
	357		388	
LmxMPK3	DIVDYNPSLE	HATPPATTAG	GSSSKNGSGH	HH
TbMPK3	E.CSF..H.A	SQI.KGA	(371)	
TcMPK3	E.CAF..Q.K	SQM...SP	(372)	
CrMPK3	.MAELHT	(389)		
StMPK3	ESIAF..EYQ	RM	(396)	
DdMPK3	EMLA.H.EDP	Q.PYYTDLNN	PNFNLSRIQS	SSELFNLLQQ QKQPIHQQVN
LmxMPK3				
TbMPK3				
TcMPK3				
CrMPK3				
StMPK3				
DdMPK3	QQSIKINN	(415)		

I - XI = conserved MAP kinase subdomains; ▼ = border of kinase core structure; Δ = invariant lysine; ↓ = TXY activation motif; . = identical residues; - = gap.

Numbering corresponds to LmxMPK3.

Tb = *T. brucei*; TbMPK3 (TIGR; Tb08.10J17.940); Tc = *T. cruzi*; TcMPK3 (TIGR; Tc00.1047053509553.60); Cr = *C. reinhardtii*; CrMPK3 (NCBI; AB035141); St = *Solanum tuberosum*; StMPK3 (NCBI; BAB93529); Dd = *Dictyostelium discoideum*; DdMPK3 (NCBI; A56042; Gaskins *et al.*, 1994).

8.1.2 PFR-2C

L. mexicana PFR-2C amino acid sequence (NCBI; AAB17719)

MSIAADMAYP	AEAAAAADV	EVSDVTLEAA	RKQKIHNKLL	KTACLSNEEF	IQDLHVS	DWS	60
ETQKQKLA	HEKAAEL	AESGTKWALT	EAYDVQKLMR	VAGLEMSVRE	LYKPEDK	PQF	120
MEIVALKKT	NELKQHPNKT	RTVSLTATID	NGVVKMEKAE	EELRQSQLDA	SDLAKVP	VPV	180
LKSLEDCMNV	TVVQTALQGN	EDQIAAQLAS	IEKACEIRDV	AIADGEMAIA	EEQYI	KAQL	240
LEHLVELVAD	KFRIIGQTED	ENKSFDR	IAD TQKRAFQETA	ALKD	GKRR	LK	300
HDAIQKADLE	DAEALKRYAT	QKEKSEQLIA	ENVDRQEDAW	RKIQELER	AL	QRLGTERFEE	360
VKRRIEENDR	EERRRVEYQQ	FLDVCGQHKK	LLELSVYNCD	LALRCSGMVE	EFVAESCS	SAI	420
KARHDKTGDE	LAELRLQEHQ	EYLEAFRR	LY KTLGQLVYKK	EKRLEE	IDRQ	IRTSHIQLEF	480
AIETFDPNAK	KHSDLKKELY	KLRAQVEEEL	EMLKDKMAQA	LEMFGPTEDA	LHQAGIE	FVH	540
PAEEVEDGNL	NRRSKIVEYR	AHLAKQEEVK	IAAEREELKR	TKVLQAQQYR	GKT	VQQITE	599

L. mexicana PFR-2C nucleotide sequence (NCBI; LMU45884)

ATGAGCATCG	CTGCGGACAT	GGCGTACCCG	GCCGAGGCCG	CCGCGGCGGC	GGATGTGCCG	60
GAGGTGAGCG	ACGTCACGCT	GGAGGCTGCG	CGCAAGCAGA	AGATCCACAA	CCTGAAACTG	120
AAGACGGCGT	GCCTGTTCGAA	CGAGGAGTTC	ATCCAGGACC	TGCACGTGTC	CGACTGGAGC	180
GAGACGCAGA	AGCAGAAGCT	CGCTGCGGCG	CACGAGAAGG	CCGCGGAGCT	GCTTGCCGCG	240
GCGGAGAGCG	GGACGAAGTG	GGCGCTGACG	GAGGCGTACG	ACGTGCAGAA	GCTGATGCGC	300
GTGGCCGGGC	TGGAGATGTC	CGTGCGCGAG	CTGTACAAGC	CGGAGGACAA	GCCGCAGTTC	360

ATGGAGATCG	TCGCGCTGAA	GAAGACGCTG	AACGAGCTGA	AGCAGCACCC	GAACAAGACG	420
CGGACCGTGT	CGCTGACGGC	GACGATCGAC	AACGGCGTCG	TGAAGATGGA	GAAGGCGGAG	480
GAGGAGCTGC	GGCAGTCGCA	GCTGGATGCG	TCGGACCTGG	CGAAGGTGCC	GGTGCCTGTG	540
CTGAAGAGCC	TGGAGGACTG	CATGAACGTG	ACTGTTGTGC	AGACTGCGCT	GCAGGGCAAC	600
GAGGACCAGA	TCGCGGCGCA	GCTCGCCTCG	ATCGAGAAGG	CGTGCAGAT	CCGCGACGTC	660
GCGATTGCGG	ACGGCGAGAT	GGCGATCGCG	GAGGAGCAGT	ACTACATCAA	GGCGCAGCTG	720
CTGGAGCACC	TTGTGGAGCT	CGTGGCGGAC	AAGTTCGGGA	TCATTGGGCA	GACGGAGGAC	780
GAGAACAAGA	GCTTCGACCG	GATCGCGGAC	ACCCAGAAGC	GCGCGTTCCA	GGAGACTGCT	840
GCGCTGAAGG	ACGGGAAGCG	GCGGCTGAAG	GGGCGGTGCG	AGGACGACCT	GCGCAGCCTG	900
CACGACGCGA	TCCAGAAGGC	GGACCTTGAG	GACGCCGAGG	CGCTGAAGCG	CTACGCGACG	960
CAGAAGGAGA	AGAGCGAGCA	GCTCATCGCG	GAGAACGTGG	ACCGGCAGGA	AGACGCGTGG	1020
CGCAAGATCC	AGGAGCTGGA	GCGCGCGCTG	CAGCGCCTGG	GGACGGAGCG	CTTCGAGGAG	1080
GTGAAGCGGC	GGATCGAGGA	GAACGACCGC	GAGGAGCGGC	GCCGCGTGGA	GTACCAGCAG	1140
TTCCTGGACG	TGTGCGGGCA	GCACAAGAAG	CTGCTGGAGC	TGTCCGTGTA	CAACTGCGAC	1200
CTTGCGCTGC	GGTGTCTCCG	CATGGTGGAG	GAGTTCGTGG	CGGAGAGCTG	CAGCGCGATC	1260
AAGGCGCGGC	ACGACAAGAC	GGGCGACGAG	CTGGCGGAGC	TGCGGCTGCA	GGAGCACCAG	1320
GAGTACCTGG	AGGCGTTCCG	GCGGCTGTAC	AAGACTCTCG	GGCAGCTTGT	GTACAAGAAG	1380
GAGAAGCGTC	TGGAGGAGAT	CGACCGCCAG	ATCCGGACGT	CGCACATCCA	GCTGGAGTTC	1440
GCGATCGAGA	CGTTCGACCC	GAACGCGAAG	AAGCACTCGG	ACTTGAAGAA	GGAGCTGTAC	1500
AAGCTGCGCG	CGCAGGTGGA	GGAGGAGCTG	GAGATGCTGA	AGGACAAGAT	GGCGCAGGCG	1560
CTGGAGATGT	TCGGCCCCGAC	GGAGGACGCG	CTGCACCAGG	CGGGCATCGA	GTTCGTGCAC	1620
CCCGCGGAGG	AGGTGGAGGA	CGGCAACCTG	AACCGCCGCA	GCAAGATCGT	GGAGTACCGC	1680
GCGCACCTTG	CGAAGCAGGA	GGAGGTGAAG	ATCGCCGCGG	AGCGCGAGGA	GCTGAAGCGC	1740
ACGAAGGTGC	TGCAGGCCCA	GCAGTACCGC	GGCAAGACGG	TGCAACAGAT	CACCGAGTAG	1800

8.1.3 LmxKin32

LmxKin32 motor domain nucleotide sequence (96% identical to the *L. major* homologue LmjF32.0680)

ATGGAATT CG	TGAAAGCGAA	CTCCGGGG CG	GAGAACATCC	GCGTCGTCAT	CCGCTGCCGC	60
GACATCCTCC	CGTACGAGGC	GGAGCGCGGC	GACAAGGCGC	TCGTTCCGGCT	CGATCTGGCA	120
ACGAACCAGG	TGGTGGTGCA	GCACCCCATC	GGCGACGCCG	ATGTGTTTGC	CTTCGACGCC	180
GTTTACAACA	ACTCCTTCAC	CCAGCGCGAC	ATCTTCCTGC	AGGAGGTGCA	GCCTCTGGCG	240
GATGCGGTGC	TGCAAGGCTA	CAACGCTACC	GTCTTCGCTT	ACGGTCAATC	CGGGTCTGGT	300
AAGACGCACA	CGATGACAGG	TAAGCTGAGC	CAGCGGAACA	TGTGGGGTAT	GATGCCGCAG	360
GTAGTTGACT	ACCTCTTCTC	CGAGATCAAG	AAGCTCACGT	CGTCCACGAA	GACCTTCAAG	420
GTGAAGGTGT	CCTACGTGGA	GCTATAACAAC	GGCAAGTCGC	GCGACTTGCT	CTCCTCAAAG	480
CAGGTTAACC	TGGAGATCAA	GCAGAATACG	TCCAAGAACT	TCTACGTGAA	GGGTGCAGAG	540
ATGCCAGAGG	TGACCAGCTT	CGAGGATGCC	ATCAAATGGT	TCAACGCCGG	TACGGAGAGG	600
CGACAGACGG	CCTCGACCGA	CCTCAATGAC	ACAAGCAGCC	GCAGTCACTC	ACTCTTCACA	660
GTGCAGATTG	AGCACTTCGA	CTTCGAGAAC	GACCCGAGCT	CGCCGATCGT	CATGACGAGC	720
AAGATCAATG	TGGTCGATTT	GGCCGGGTCG	GAGAAGCTCA	GCAAGACGAA	CGCGACTGGC	780
GAGACGGCAA	AAGAAGGCTG	CAACATCAAT	CTGTCCCTGT	CCGCACTGGC	CACGGTGATC	840
GACACCATCG	TGAAGGGGGC	AAAGCACATT	CCGTACCGCG	GCTCGCCGCT	GACGATGCTG	900
CTGAAGGATT	CCTTGGGGGG	TAATGCCAAG	ACAGTCATGT	TCGCAAACGT	CGGCCCTTCC	960
GATAAGAATC	TGTCCGAGAC	GATCTCGACG	CTCCGGTTTCG	CGCTGCGCGC	<u>AAAGCAGATC</u>	1020
<u>GAAAACAAGC</u>	<u>CTAGGGTCTA</u>	G				1041

Oligonucleotide sequences - based on *L. major* and containing inserted restriction sites - are underlined. Start codon and stop codon used for recombinant expression are bold.

LmxKin32 motor domain amino acid sequence (100% identical to the *L. major* homologue LmjF32.0680)

```

MEFVKANSGA ENIRVVIRCR DILPYEAERG DKALVRLDLA TNQVVVQHPI GDADVFAFDA 60
VYNNSTQRD IFLQEVQPLA DAVLQGYNAT VFAYGQSGSG KTHMTGKLS QRNMWGMMPQ 120
VVDYLFSEIK KLTSSSTKTFK VKVSYVELYN GKSRLDSSK QVNLEIKQNT SKNFYVKGAE 180
MPEVTSFEDA IKWFNAGTER RQTASTDLND TSSRSSHSLFT VQIEHFDFEN DSSPIVMTS 240
KINVVDLAGS EKLSKTNATG ETAKEGCNIN LSLSALATVI DTIVKGAKHI PYRGSPLTML 300
LKDSLGGNAK TVMFANVGPS DKNLSETIST LRFALRAKQI ENKPRV 346

```

Amino acids translated from the *L. major*-based oligonucleotide sequences are underlined. Additional amino acids generated by inserted restriction sites are bold. The potential D-domains are discontinuously underlined. The potential PXSP and SP phosphorylation motifs are red.

8.1.4 LmjDC2

Alignment of LmjDC2 (CAB55364) and LmxDC2

```

LmjDC2      MSVVAAKKKGAVSDTLRRSQIADGILGAQDQGARQQEQILHITTEENNQIKKEISAISGTH 60
LmxDC2      MSVVAAKKKGAVSDTLRRSQIADGILGAQDQGARQQEQILRITEENDQIKKEISALSSGTH 60
*****.*****:****:*****:*****:****

LmjDC2      YDYVKADKLASLQSDVDGLERRYQFEKMRKNDLTKRYQLARIDLLHSRKMKGGINVEKEQ 120
LmxDC2      YDYVKADKLASLQSDVDGLERRYQFEKMRKNDLTKRYQLARIDLLHSRKMNGGVNVDKEQ 120
*****.*****:*.**:***

LmjDC2      AVAVQRQVDILESRLDQTLGQFNDALSYNKELRDRIDVIREERRVFLRVHVKRMEDDLKTK 180
LmxDC2      AAVVQRQVDILESRLDQTLGQFNDALSYNKELRDRIDVIREERRVFLRVHVKRMEDDLKTK 180
*.*****

LmjDC2      KRLMAEHIEKSNRDMDDRDAQLREVERLRAALAEQRQAYTNQLRDLDTAMMDIKAMRDGQ 240
LmxDC2      KRLMAEHIEKSNRDMDDRDAQLREVERLRAALAEQRQAYTNQLRDLDTAMMDIKAMRDEQ 240
*****

LmjDC2      TEMQLELEAREYEFGERMGDTKAARAQEEADTSRRAIGASVSGNGEDPASTTGEEDEDD 300
LmxDC2      TEMQLELEAREYEFDERMGDTKSARTQEEADTSRRAIGASVSGNGEEPASTTGEEDEDD 300
*****.*****:*.**:*****:*****

LmjDC2      THTLLCVERESATITSILAQIKDDLQTDDDDELRTKYLHTGDLNFSMYKYVNELSAKKEA 360
LmxDC2      THTLLCVERESATITSILAQIKDDLQTDDDDELRAKYLHTGDLNFSMYKYVNELSAKKEE 360
*****.*****

LmjDC2      LKDSIRDLQRLLEEDDSERQHRILIKGLEEELAGTESKLDEMNCATVQLRDAVQRTAAT 420
LmxDC2      LKDSIRDLQRLLEEDDSERQHRALIKGLEEELAGTESKLDEMNSATMQLRDAVQRTAAT 420
*****.*****

LmjDC2      AEDVYAHIGCPQMADGAVEGEERCTEANMKQFLGTIEERATHILIAFQRHHQFSANSRTS 480
LmxDC2      AEDVYAHIGCPQMAGGAVEGEERCTEANMKQFLGTIEERATHILIAFQRHHQFSTNSRTS 480
*****.*****:*****

LmjDC2      VASSSRVTRDTQSPKEAVQNLEEDNALTANTTDSPHGETLQMAEDWEVEESPIMPIAPQ 540
LmxDC2      VTSSLRFRDPPSPKETVQNLEEDNALTANTTDSPHGETLQMVEDWEVEESPIMPIAPQ 540
*:** *.** . *****:*****.*****

LmjDC2      TAHSAVSARNLVRMELPSASLAGGTTDRDSSLYADQDDDHIISHEDIRKQMEARLATMR 600
LmxDC2      TPHSAVSARNLVRMELPSASLAGGTTDRDNSLYADQDDDHIVSHEEIRKQMEIRLATMR 600
*.*****.*****:***:*****

LmjDC2      EREERNQRKKKDAAQKAK 618
LmxDC2      EREERNQRKKKDAGQKAK 618
*****.****

```

Lmj = *L. major*, Lmx = *L. mexicana*.

* = identical residues; : = conserved residues; . = semi-conserved residues.

The potential SP phosphorylation motifs are red.

8.1.5 LmxGS

Alignment of LmxGS, LmjGS (LmjF06.0370) and CrGS (NCBI; AAB01817)

LmxGS	-----MSSSNQ--TVRVTYIWLSGKDSHHDIRSKDRT	31
LmjGS	-----MSSSNQ--TVRVTYIWLSGKDSHHDIRSKDRT	31
CrGS	MAAGSVGVFATDEKIGSLDQSITRHFVSTVTDQQGKICAEYVWIGG--SMHDVRSKSR	58
	:* : ..* .: . *:*.* * **;***.**	
LmxGS	MYLSQENVAKHPKELLANGVFPVWNFDGSSTGQAKGLDTEILLKPVNAFPCCLPRTSSKI	91
LmjGS	MYLSQENVAKHPKDLLANGVFPVWNFDGSSTGQAKGVDTEILLKPVNAFPCCLPRTSSKI	91
CrGS	LST---IPTKPED-----LPHWNYDGSSTGQAPGHDSEVYLIPRSIFKDPFRGGDN--	106
	: :..*:*: :* **;***** * *:*: * * . * : ..	
LmxGS	PWILVLAECYLP-----SGKPTRDNSRATARETFEQCPPEHPWFGLEQEYFIMG	141
LmjGS	PWILVLAECYLP-----SGEPTRDNSRATARETFEQCPPEHPWFGLEQEYFIMG	141
CrGS	--ILVMDCYEPKVNPDGTLAAPKPIPTNTRFACAEVMEKAKKEEPWFGIEQEYTLINA	164
	:..* * : :* *:* .: *.:*.. :*.*;***** :..	
LmxGS	DGR-PYGWPAHGFPAPKAYCSTGSKSAWGRKFCQHYEVCLEMGLNISGTNAEVTPGQ	200
LmjGS	DGR-PYGWPAHGFPAPQAYCSTGSKSAWGRKFCQHYEVCLEMGLNISGTNAEVTPGQ	200
CrGS	ITKWPLGWPKGGYPAPQGPYYCSAGVAIGRDVAEVHYRLCLAAGVNI SGVNAEVLPSQ	224
	: * ** *:*:*:*.* **;*: * * ..: *.:* * :*****.*** *.*	
LmxGS	WEFQVGPCEGLEMGDQLTVARWVLLRLLLEEEGLDADYHAKPIQGDWNGSGLHTNFSTEST	260
LmjGS	WEFQIGPCEGLEMGDQLTVARWVLLRLLLEESLDADYHAKPIQGDWNGSGLHTNFSTEST	260
CrGS	WEYQVGPCEGITMGDHMWSRYIMYRVCEMFNVEVSFDPKPIPGDWNGSGGHTNYSTKAT	284
	:*:*:*:*:*: *:*:*: :*:*: : * * ..:..... ***** **:*:*:*:	
LmxGS	R-AENGLEVIHQYIDRLSKTVSKDIIIFYGSENNKRLTGTHETSKVSEFSAGVTRCTSIR	319
LmjGS	R-AENGLEVIHQYIDRLSKTVSKDIVFYGSENNERLTGKHETSKVSEFSAGVTRCTSIR	319
CrGS	RTAPDGWVKVIQEHCAKLEARHAVHIAAYGEGNERRLTGKHETSMSDFSWGVANRGCSIR	344
	* * :* :*:*:*: :*. : . * ** .*: *****.***.:** **..* ***	
LmxGS	IPNAVASEGKGYMEDRRPAGDADPYLVTSRLFASCIGLETPSLDLASPTHERDWMRNAFK	379
LmjGS	IPNAVASEGKGYMEDRRPAGDADPYLVTSRLFASCIGLETPSLDLASPTHEKDWMRNAFK	379
CrGS	VGRMVPVEKSGYEDRRPASNLDAYVVTRLIVETTILL-----	382
	: . * . * .** *****.: *:*:*: .: : * *	

Lmx = *L. mexicana*; Lmj = *L. major*, Cr = *C. reinhardtii*.

* = identical residues; : = conserved residues; . = semi-conserved residues; - = gap.

The 14-3-3-binding motif is underlined. Identified phosphorylation sites are blue.

The potential S/TP phosphorylation motifs are red.

8.1.6 LmjHS and LmxHS

LmjHS amino acid sequence (LmjF36.1150)

MTEYAGTQTT	RHAQSLKSTL	PASETRGSM	AATALPSMRD	IGVYPRALPP	LGENEACSNN	60
NTTCSIQHDF	DSSAAGNVRT	TAAMGATVPA	SSFCTCTDK	DPSGGLPLLR	VGNSAPP <u>PLT</u>	120
<u>PTALVTTLPA</u>	LSGQHALHCP	RNATASTG <u>SP</u>	RVPVGLTRAS	LQHHDENDAC	PHLQSTGQGD	180
EAALRSSQRA	CSLAPTENYV	NQLADQRPAL	AVEQGPRRGE	A <u>TP</u> SLHAAPS	RSDNTEVDLL	240

ARQLVQHTVL	WSSMCDSVSG	CAS P ARGRRG	EVVKSTLRAG	SVGTGSGACP	HEATATVPVL	300
STTAATSSPS	CVGILNSTNV	HSSHHDKTDN	ATAGS S PLTY	ADNPTLSTRE	TFPIPRCCPD	360
DLLRGDDKIW	IPGKPLRIAY	VTWNMASKRP	RTGEVSAHCI	YRNAHLVVVG	TQENGPYVMS	420
NKRQRRWTKI	VSHACLGGQY	ELVGQHMMWA	VQMLVFARRR	DVAHYISRAH	ASHVKTGLLN	480
GLGGNKGGVA	VGLVLSL TPK	DAAPPHRAKA	HLTITSATRA	PPLKSKTSGA	RGTSIKGSAI	540
TP QKPDSSMV	TGRETSAAFV	LSKSSADCGA	GAPPPVMRNP	YMLHDADDEY	GKLLRKRSLP	600
DANSTGNFFC	DDGDTVLEND	GVF S PAEMMS	RNTLSELTTE	HADADHSHRH	TQRSENGTDR	660
QERGGGDDDD	ASSDGRPDSV	TP NYMTLLFI	TAHLTAHQGA	VRNRNKDYRK	IVYGLQLGRR	720
GPYRKFFKLL	LGRKKVLEGD	DEEEASDEDD	EADCWEDNNP	EEGVMPRLRP	VVSGVERKRR	780
MRRDVTTEFD	LTFGGDLNY	RINGTRKAIE	YVIQHHSNIR	SILINNDQLS	LERARGKVFQ	840
RFQEGDLLFR	PTYKYEVSA	GGFTLNEYNF	SQKKNRMPAY	CDRILYKKRM	SSAARRITIR	900
LYTDVNPVRS	SDHRPVVALF	DIGTRAYTG				929

The PREDIKIN-predicted substrate heptapeptide is underlined. The potential D-domain is discontinuously underlined. The potential PXTTP and S/TP phosphorylation motifs are red.

Alignment of LmjHS, LmxHS and homologous proteins

LmjHS	MTEYAGTQ TR HAQSLKSTLP-----ASET	TRGSMPAATALP	SMRDIGVYPRAL	PPLIGEN	54
LinHS	MTEYAGTQATRHAESVKS TP P-----TSQ	TRGSMPAATALP	STRDIGVYPRSL	PPLGGS	54
LmxHS	MTEYAGSQT TR QAQSVKS TP L-----ANQ	TRVSM AATALP	STSDIEMYPRAL	PPLARN	54
LbrHS	MKEHHGTQGT KH PPSVES TP L S LPPLPAVQARG-	MQANSIGPSAG	KGGVDRA TP TAAASK		59
TbHS	-----				
TcHS	-----				
LmjHS	EACSNNTTCSIQHDFDSSAAGNVRTTAA	MATVPASSFCSTCTDKDPSGGLP	LLRVGNS	114	
LinHS	GAGSNNTTCTRHDFFPSAAGNVNTTAA	MATFPSSFRSTLTDRDPSRGP	SLLRVSDP	114	
LmxHS	GAWSDNNTACSAQYNVDPSAAGNVSTTTAT	GAAFPDSS S PSTRNDRDPSRGP	LRLGVSDP	114	
LbrHS	EACS Y NGSTCCTRDNTNALAADNGRAITAI	IGPTS-----RALPDDSLSR-----	RTYDP	108	
TbHS	-----				
TcHS	-----				
LmjHS	APP PL TPALVTTLPALSGQHALHCPRNATA	STG S PRVPVGLTRASLQHHDENDAC	PHLQ	174	
LinHS	APP PL TPAPATTAPTLSGQHVLCPRKPA	AAS T GGPRMPVCLTSASVQSHDENDAC	PHSQ	174	
LmxHS	AP S PLTSTAS P NTAPALSGQVLHFP	PRKPAGSTGAPRMPIGLTSVSLKN	PEENDTCPQLQ	174	
LbrHS	AC P SP P PESFVTVVPDQPLQRLR	LPSQSSARAG-ARISADLAKSSLQ	NTTEEDVAYPSVQ	167	
TbHS	-----	-----MVVALLSCPFPFSSVVV	FVTLW	23	
TcHS	-----				
LmjHS	STGQGD <small>EA</small> LRSSQRACSLAPTENYVNQLADQR	PALAVEQGPRRGEAT P SLHAAPSRSDN	234		
LinHS	STGEGDEA <small>AP</small> RRSSQRAC S PAPTE <small>DYANQ</small> HADRRLARTVEQGPRRGEAT P RLHAAPSRSDN	234			
LmxHS	STGQGD <small>EA</small> ARRSSQKACNPAPTE <small>DYVHK</small> CADCRPPLTAEQRPRGRESTAALHAPP	SRSDN 234			
LbrHS	NTRQSENTALLPTQRTCESLSREARVDPADPQ	STVPVEQDHRKSERKSCPLSASSSSEH	227		
TbHS	KEGGGASHQNPPLSFSLCSGCRGGMRAE	GDHVAEGAENTTAT S PGPGSVRESSK S PK-	82		
TcHS	-----	-----MDANSIGAGFTQVRVHDEE	VERESENKGPLTCCFKELHEITK-	43	
LmjHS	TEVDLLARQLVQHTVLWSSMCDSVSGCAS P ARGRRGEVVKSTLRAGSVGTGSGACP	HEAT	294		
LinHS	TEVDLLARQFVQRTVLWSSICNCASGGES P ARCRDELVKSTVTVTVSVGTGSGACS	HEAT 294			
LmxHS	TEVDFLARQFVQRTVLWSSMCNCVSQRE S PAHRNRDELVKSTLNRNVSVGAGSSACL	HEVT 294			
LbrHS	ANLESVTRQFTRHSVMRQSLCAPASIHK S PTLHFAGESGNSAWYTVGAHANNGCCSH	DAT 287			
TbHS	-----	-----SRSRCH S PRNGRRG-----RSKR	101		
TcHS	-----	-----SEVSVLG PAT PFEV-----HSVS	62		
LmjHS	ATVPVLSTTAAT S SPSCVGI LNSTNVSSHHDKTDN	ATAGS S PLTYADNPTLSTRET	TFPI	354	
LinHS	ATVPIFSTTAAKSSQSCVGI LNSANVQSSHRDE	TENGTAGSFPLTRANNPALSTRET	TFPI 354		
LmxHS	ASVPVFSKTAGASSRSCVGVNSTSVHSSH	RDETDNGALGD S PSTHADNPALSTRET	TFPI 354		
LbrHS	ASMPVDCATVSACS RSP VEAEFTTNEHTRHRN	KIDTTLADGTLVSGAETTFTPTRET	TFPI 347		
TbHS	GSVQHT P PRNSVRDPSAI PKQLDIDAMQVA	IATSLPRLDQFCDEFHSI PFVIRNET	FPV 161		
TcHS	SSFFAVSHNEGE-----	-----CHLHDRIDQYYDDRHTVP	FSEIEETFPV 102		

```

LmjHS      PRCCPDDLLRGDDKIWI PGKPLRIAYVTWNMASKRPRTEGEVSAHCIYPNAHLVVVGTQEN 414
LinHS      PRCCPDDLLRGDGKMWTPGKPLRIAYVTWNMASKRPRTEGEVSAHCIYPNAHLVVVGTQEN 414
LmxHS      PRCCPDDLLRGDDKIWAPGKPLRIAYVTWNMASRRRPRTEGEISAYCIYPNAHLVVVGTQEN 414
LbrHS      PRYCLDDLLRGEDKIWAPGKPLRIAYISWNMASKRSRVGEVSAYCIHPNAHLVVVGTQEN 407
TbHS       P----DSLKRNS---WIPGEVLRVAYITWNMAHAKPDFYRVSKYCI CPNAHLVVVCTQEN 214
TcHS       P----VSLPEEK---WIPGKPLRI SYVSWNMAHRRPNFEDVAGHC IHPNAHI IAVCTQEN 155
*      . * . . * ** : **::**::*** :. : : ** *****:.* ****

LmjHS      GP-YVMSNKRQRRWTKIVSHACLGGQYELVGQHHMWAVQMLVFARRRDVAHYISRAHASH 473
LinHS      GP-YVMSNKHQRRWTKIVSQACLGGQYELVCQHHMWAVQMLVFARRRDVAHYISRAHASH 473
LmxHS      GP-YVSSNEHQRRWTKIVSQVCLGGQYELVGKHHMWAVQMLVFARRRDVAHYISRAHASH 473
LbrHS      GP-YLISNKLQRRWAKTVSQVCLGGQYELVGKHHMWAVQMLVFARRRDVVHYISRSHTAH 466
TbHS      GCNWYAKKKQQRQWRDHITQACLKNSYELVGCNSLWYIHMLVYARKHVDVAPHVGHVEKAK 274
TcHS      GS-YVRVKKEQRQWERHVRHNCLHGEYVLVGRKELWYIQLLVYARKKDVASVYVGYSDASS 214
*      :      :: **:*      : : ** ..* ** : : * ::**::***::** . : . :

LmjHS      VKTGLLNGLGNGKGGVAVGLVLSLTPKDAAPPBRAKAHLTITSATRAPPLKSKTSGARGT 533
LinHS      VKTGLLNGLGNGKGGVAVGLVLSLTPKDAAPPBRAKAHLATASAPQAPPLKSKASGARGT 533
LmxHS      VKTGVLNGLGNGKGGVAVGLVLSLTPKDAAPPBRAKAHLTASVPQTLPLKSKTAWSRVM 533
LbrHS      VKTGLLNGLGNGKGGVAVGLVLSLTPKDIELSQQATTLRGPTDILLTPLLEKVTSTTRDT 526
TbHS      VRTGIGNGLGNGKGGVGIALSISTEFCRNALSDPRGHRRG-----ARASKQQRQ 323
TcHS      VKTGIANGLGNGKGGVAVALSIAMTV--SPLQMVPGRRKG-----ENTSHTEGS 261
*::** : *****:.* : : : : : : : : : : : : : : : : : : : : : : : :

LmjHS      SIKGSAITPQKPDSSMVTGRETSAAFMLSKSSADCGAGAPPVPMRNPYMLHDADDEYGKL 593
LinHS      PIKRSATTPQNLDSMVKGREISAGFMLSKSSADCAVGI PPMVMSNPYMLHDADGEYGKL 593
LmxHS      PMKRAATTPQNLDSMVAGRESSAAFMMSSKSSANRSVEI PPAITSDPYMLHDADDEYGEL 593
LbrHS      PVKQAATSPPLTVGSPMIPSSKNCFFVVPKFSAAAGSVASYSPLLCEPRIVPDLDEYGT 586
TbHS      DISCSHMNPI----- 333
TcHS      --TSSVFSR----- 269
. : .*

LmjHS      LRKRSLPDANSTGNFFCDDGDTVLENDGVFSPAEMMSRNTLSELTTEHADADHSHRHTQR 653
LinHS      LQQHSLPDGNSTGNLFCDDGDTVLENDGVFSPAEMMSRNTSSELTTEHADAEHSHRHTQH 653
LmxHS      LHKRSFPDGNSTGNFFFDNSDVTVDNDGAFSPAEVISRNTSSDLTTEHGDDHSDCHTQR 653
LbrHS      LDGRSLADGNSTPSLYNDE-EGVLDDDESVPSP LGNNSRTASLDSF SERLEAHFAQRRRYQ 645
TbHS      -----
TcHS      -----

LmjHS      SENGTRDQERGGDDDDASSDGRPDSVTPNYMTLLFITAHLTAHQGAVRNRNKDYRQIVY 713
LinHS      SENDMDRQERGGDDDD-ASSDGRPDNVTPNYMTLLFITAHLTAHQGAVSNRNKDYRQIVY 712
LmxHS      SENGMDRHERCGGDDDD-ASSDGPDRVTPNYMTLLFITAHLTAHQGAVSNRNKDYRQIVY 712
LbrHS      LDNGISQRQDGGVDDDDASNDGTEPKDTPNYMTLLFITAHLAAHQGAVRNRNKDYEQIVY 705
TbHS      -----ECGGG----DSDLHSALPQPARFTILFVGAHLAAHQDAVGLRNRNDRYRNVK 380
TcHS      -----EGGPCSVHVGDDVNFASAPPRITLLFVGAHLSAQKGVHMRNKDYISIVR 320
.      . . . * :*:** : **:* ** . * **:* ** .**

LmjHS      GLQLGRRGPYRKFFKLLLGRKKVLEGD--DEEE-----ASDED----- 749
LinHS      GLQLGRRGPYRKFFKLLLGRKKVLDGD--DEEE-----ASDED----- 748
LmxHS      GLQLGRRGPHRKFFKLLLGRKKVLEGD--DEE-----ASDED----- 747
LbrHS      GLRLGRRGPYRKFFNQLLERRKVLLEGAE-----EGSEN----- 743
TbHS      MLHVGLRGKFKFPHASIR-RSRALACCPDTE SARGLNITEDQATRQNAVCSNGGCKAMN 439
TcHS      SLRVGSQGR---HKALF-RERFLHECPFNEE-----LKDVDGGDNNEVLVSG-----C 364
*::* :* . : * : * : * : * : :

LmjHS      --DEADCWEDNNPEEGVMPLRLPVPVSGVERKRMRRDVTEEFDLTFFGGDLNYRINGTRK 807
LinHS      --DEADYWEDNNPEEGVMPLRLPVPVSEVEHKRKMRRDVTEEFDLTFFGGDLNYRINGTRK 806
LmxHS      --DEADCWEDNSPEEGVTPRLRPAVSGVEQKRKTRRDVTEEFDLTFFGGDLNYRINGTRK 805
LbrHS      --NADHDWADTDYSEGVTPRLRPMVSAVAPNRKMRRDVTEEFDLTFFGGDLNYRINGTRK 801
TbHS      GSAAVSNERDEDDGGPVGIMKLPFCMKNQPOE-ERRDATDEFDLVFFGGDLNYRDLGTSK 498
TcHS      GNGVGDCEGDVECCSSDLSMLRPLVAQSNFDSR-LYRDVTEDEFDLVFFGGDLNYRINGTRK 423
. * . : : ** .. **:* ***:*****:*** *

```


Lmj = *L. mexicana*; Lmj = *L. major*.

* = identical residues; : = conserved residues; . = semi-conserved residues.

Amino acids translated from the *L. major*-based oligonucleotide sequences are doubly underlined. The PREDIKIN-predicted substrate heptapeptide is singly underlined. The potential D-domain is discontinuously underlined. The potential PXTIP and S/TP phosphorylation motifs are red.

8.1.7 IFT57

Alignment of IFT57 homologues

```

LmjIFT57      -----
LinIFT57      -----
LmxIFT57      -----
LbrIFT57      -----
TbIFT57      MS-EETQPQSTEPKSGSGVIIDDGTMDDLIDKLRILRYETEFPCPRVKPPFKPLSKYYFS 59
TcIFT57      MSQEEILQQATGPSFPGKGVIVDDGTMEDLIDKLRILRYEKDFCPRVKPPFKPLSKYYFS 60

LmjIFT57      -----MNIAIANI 8
LinIFT57      -----MNIAIANI 8
LmxIFT57      -----MNIAIANI 8
LbrIFT57      -----MNIAIPNI 8
TbIFT57      GPSTIDNPNAQFYYFTSLCSWLMGLSGRNFEPPGQFDDPNATATNILMELRGMNITAPNL 119
TcIFT57      GPSSIDNPNAQFHYFTSLCSWLMGLAGHNFEPGQFDDPNATSTNILGELRAMNISAPNL 120
                                     ***: .*:

LmjIFT57      APTRLKQGSGEAVLAVLSALVNAALSSTGYGFQPIDYGQVERYDELAAVADAEDAQQGE-D 67
LinIFT57      APTRLKQGSGEAVLAVLSALVNAALSSTGYDFQPIDYGQVGRYDELAAVADAEDAQQGE-D 67
LmxIFT57      APTRLKQGSGEAVLAVLSALVNAALSSTGYGFQPIDYGQVERYDELATVADAEDAQQGE-D 67
LbrIFT57      APTRLKQGSGEAVLAVLSALVNAAISGAGYDFQPIDYSQVSRYDELAAVADAEDAQQGA-D 67
TbIFT57      APNRLRQASGEAVLTVLSLLADHAILSKGLSIRAIDYSNIEKFDELEGATDGDENYIGIGD 179
TcIFT57      APNRIHQGSGEAVLTVLSVLSHDHALLKKGFTVRSVDYTNVEKYDELGDGVTDADDDNGIGE 180
**.*:.*.*****:*** * : * : * . : :*** : : :*** .*:.: : * :

LmjIFT57      EIEDNVVIDSDDDDEVYVRAVSGNRSKNDADRPPTPKVDVEEWKMEVERVAPLLQVRQS 127
LinIFT57      EIEDNVVIDSDDDDEVYVGA VSGNRSKSDADRPPTPKVDVEEWKMEVERVAPLLQVRQS 127
LmxIFT57      EIEDNVVIDSDDDDEVYVRAVSGNRAAKSDADRPPTPKVDVEEWKMEVERVAPLLQVRQS 127
LbrIFT57      EIEDNVVIDSDDDDEVYVRAVSGSRNAKSDADRPPTPKVDVEEWKMEVERVAPLLQVRQS 127
TbIFT57      EVEDNVMIDSDDDDELYVRAT-VGGKSGKEDTGIPVESEINADEWNLEVERVGPLLHVKSE 238
TcIFT57      EVEDNVMIESDDEEELYVRAT-GERLVKEDAGVPLESEINAEEWNLEVERVGPLLQVRSD 239
*:****:*:****:**** * . * : *.*: * . : : : : : : : : : : : : : : : :

LmjIFT57      SLDDWRSRIESATVLLKAVENMYPDVKQMLERLAGDMDKSRDRIQKREQTLAQQFSDQVE 187
LinIFT57      SLDDWRSRIESATVLLKAVENMYPDVKQMLERLAGDMDKSRDRIQKREQTLAQQFSDQVE 187
LmxIFT57      SLDDWRSRIESATVLLKAVENMYPDVKQMLERLAGDMDKSRDRIQKREQTLAQQFSDQVE 187
LbrIFT57      SLDDWRSRIESATVLFKAVENMYPDVKQMLERLASDMDKSRDRIQKREQTLAQQFSDQVE 187
TbIFT57      AIQDWRSRIENAAIILKAVEKMYPEVRQMLQRMSDDLEKSKDRIQKREQTLAQQFSDQVE 298
TcIFT57      ALQDWRSRIESAGVLLRAVEKMYPEVKQMLQHVADDLEKSRDRIQKREQTLAQQFSDQVE 299
: : : : : : : * : : : : : : : : : : : : : : : : : : : : : : : : : : :

LmjIFT57      DYRVKLRRELNTSRDSANVAQQTVQQMTVELNQISELLDQTKRDIAERQAKISDTTPLIQV 247
LinIFT57      DYRVKLRRELNTSRDSANVAQQTVQQMTVELNQISELLDQTKRDIAERQAKISDTTPLIQV 247
LmxIFT57      DYRVKLRRELNTSRDSANVAQQTVQQMTAELNQISELLDQTKRDIAERQAKISDTTPLIQV 247
LbrIFT57      DYRVKLRRELNTSRDSANVAQQTVQQMSVELNQISELLDQTKRDIAERQARISDTTPLIQV 247
TbIFT57      DYRVKLRRELNSSQDAANIASQSVQQLSAELNQVSGLLDQVKRDIEEREAKLSDTSPLMQV 358
TcIFT57      DYRVKLRRELNTSQDSANMASQSVQQLSAELNQLSGLLDQVKRGIEDREAKISDTTPLMQV 359
*****:*:****:*.*:*:*:*:*:*:*:*:*:*:*:*:*:*:*:*:*:*:*:*:*:

```

```

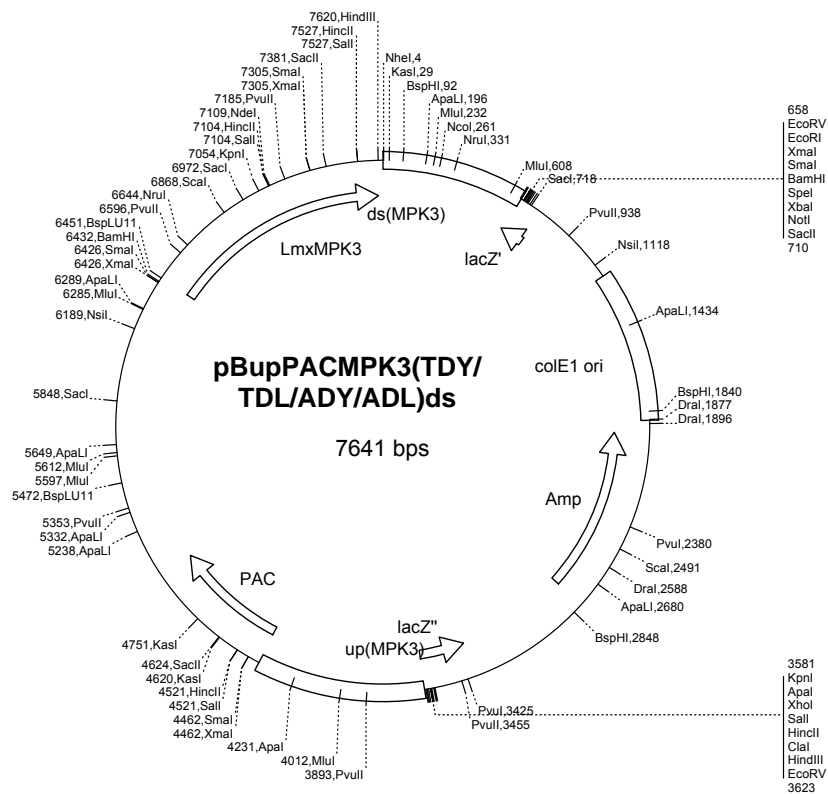
LmjIFT57      KEAVVKVQAEIKLMSLRIGILQNGVLQHVMKQTKARREGPTAEGTEMYSGEIMFS 302
LinIFT57      KEAVVKVQAEIKLMSLRIGILQNGVLQHVMKQTKARREGPTVEGTEMYSGEIMFS 302
LmxIFT57      KEAVVKVQAEIKLMSLRIGILQNGVLQHVMKQTKARREGPTVEGKEMYSGEIMFS 302
LbrIFT57      KEAVVKVQAEIKLMSLRIGILQNGVLQHVMKQTKARREGQAIERADMYNGGIMFS 302
TbIFT57       KDAAVKVRAEIKQMSLRIGILQHTVLHYVMKQTKAKREGTANTSGGDEWEETDYM 413
TcIFT57       KDAVTKVRAEIKQMSLRIGVLQHAVLHYVMKQTKAKREGLNGLGLDDWEEIESM 414
*:...*:*** *****:***: **::*****:***

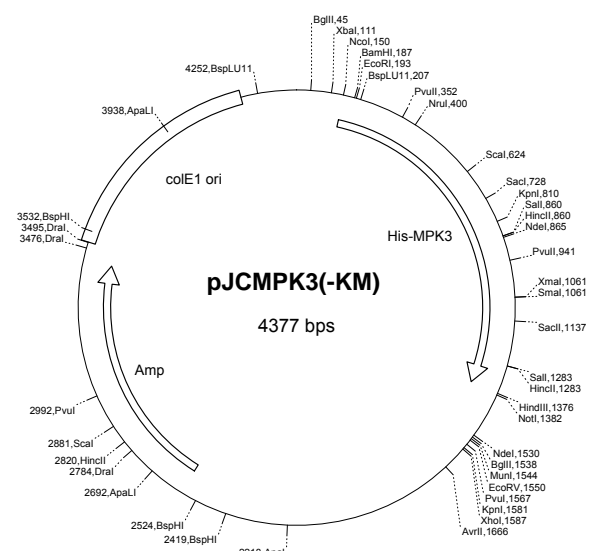
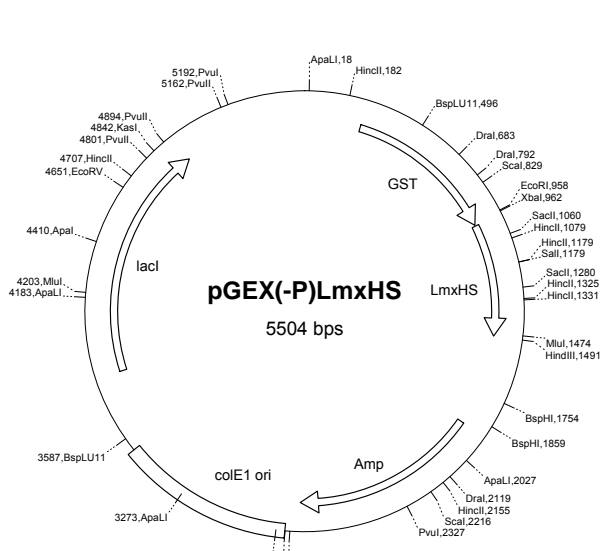
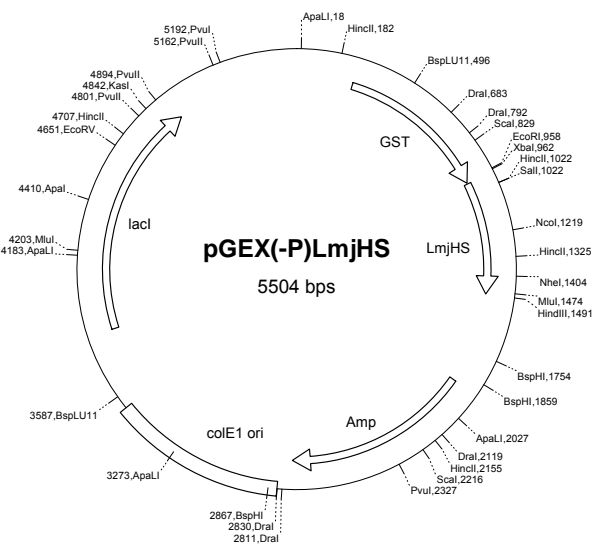
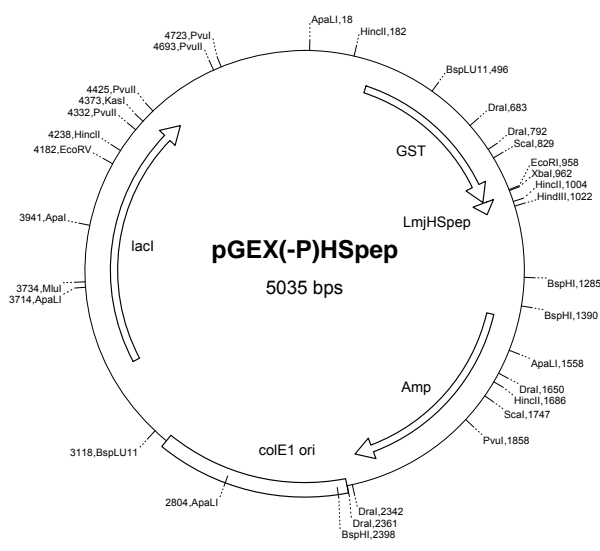
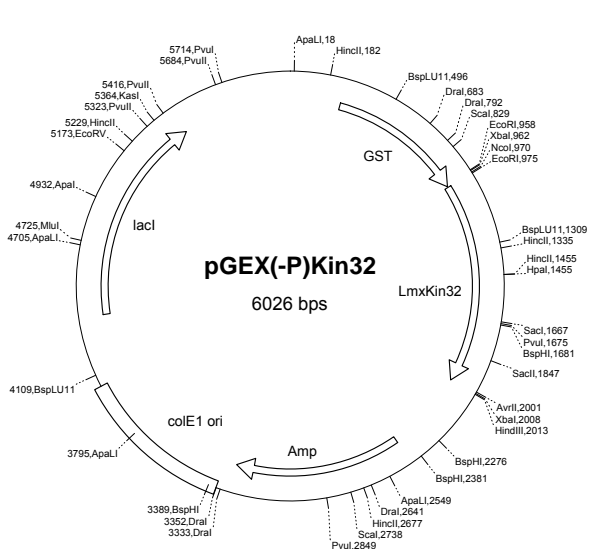
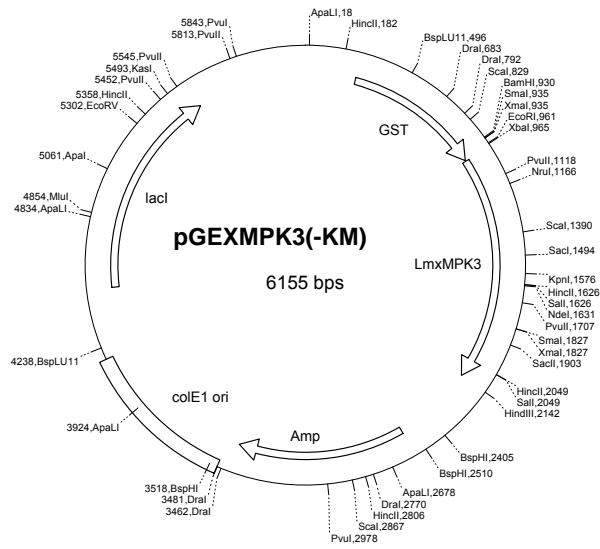
```

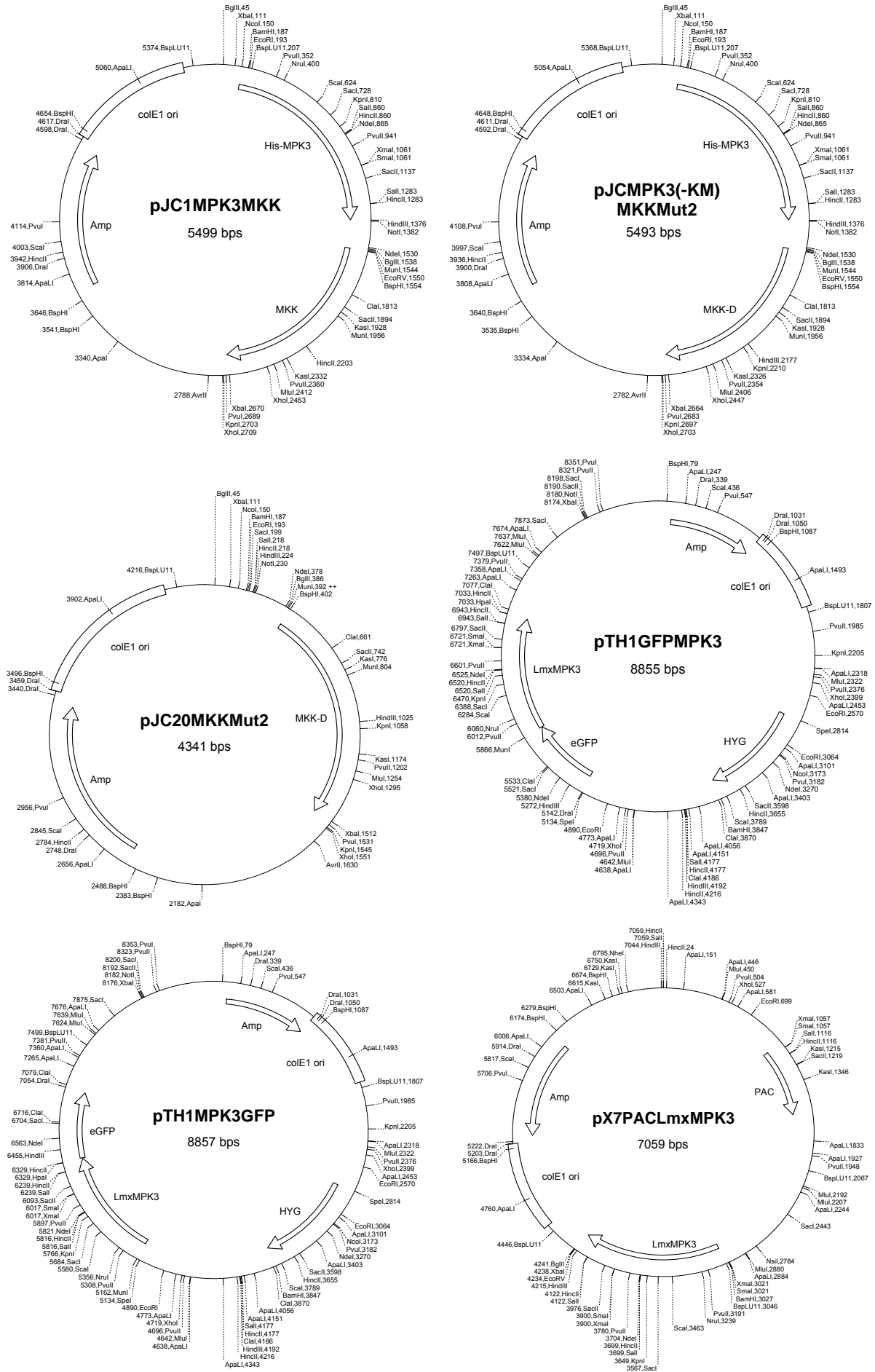
Lmj = *L. major*; LmjIFT57 (LmjF33.0620; Gouveia *et al.*, 2007); Lin = *L. infantum*; LinIFT57 (LinJ33_V3.0670); Lmx = *L. mexicana*; Lbr = *L. braziliensis*; LbrIFT57 (LbrM33_V2.0660); Tb = *T. brucei*; TbIFT57 (TIGR; Tb10.26.0670); Tc = *T. cruzi*; TcIFT57 (TIGR; Tc00.1047053507711.10).

* = identical residues; : = conserved residues; . = semi-conserved residues; - = gap.
The potential PXT/P and S/T/P phosphorylation motifs are red.

8.2 Plasmid maps

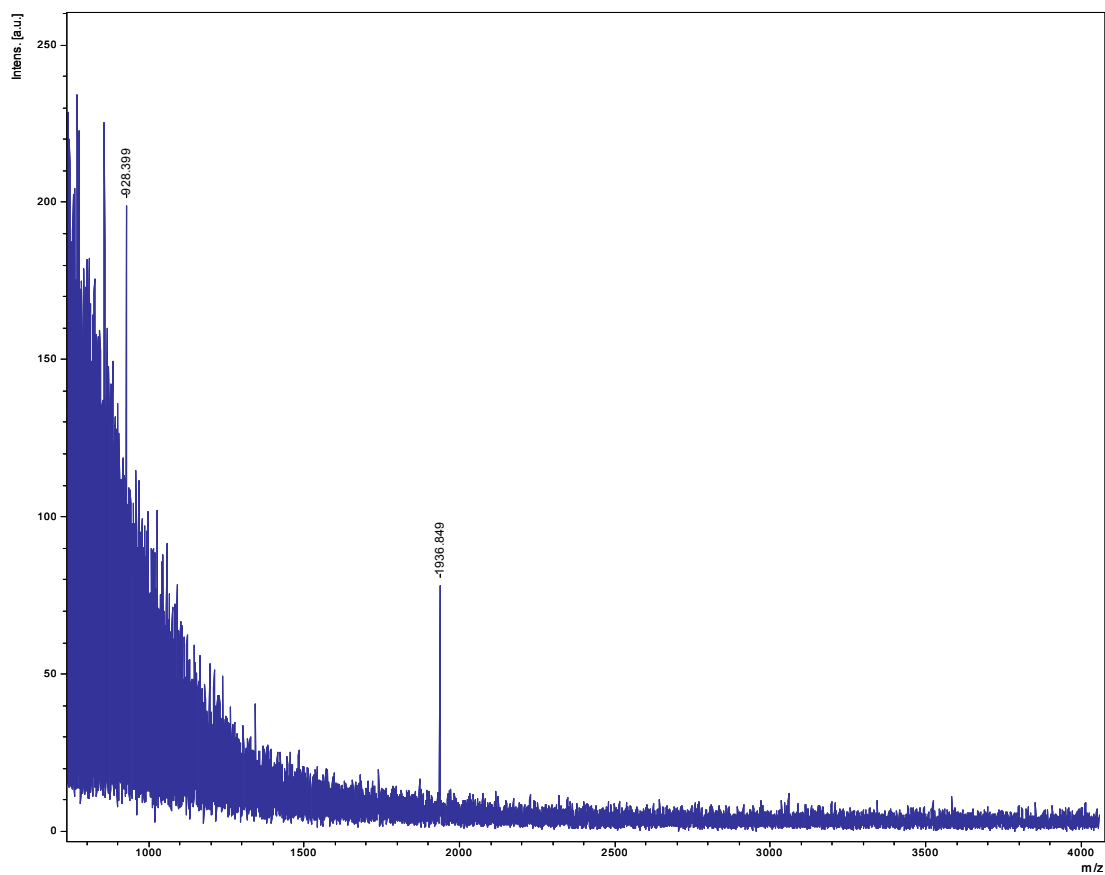




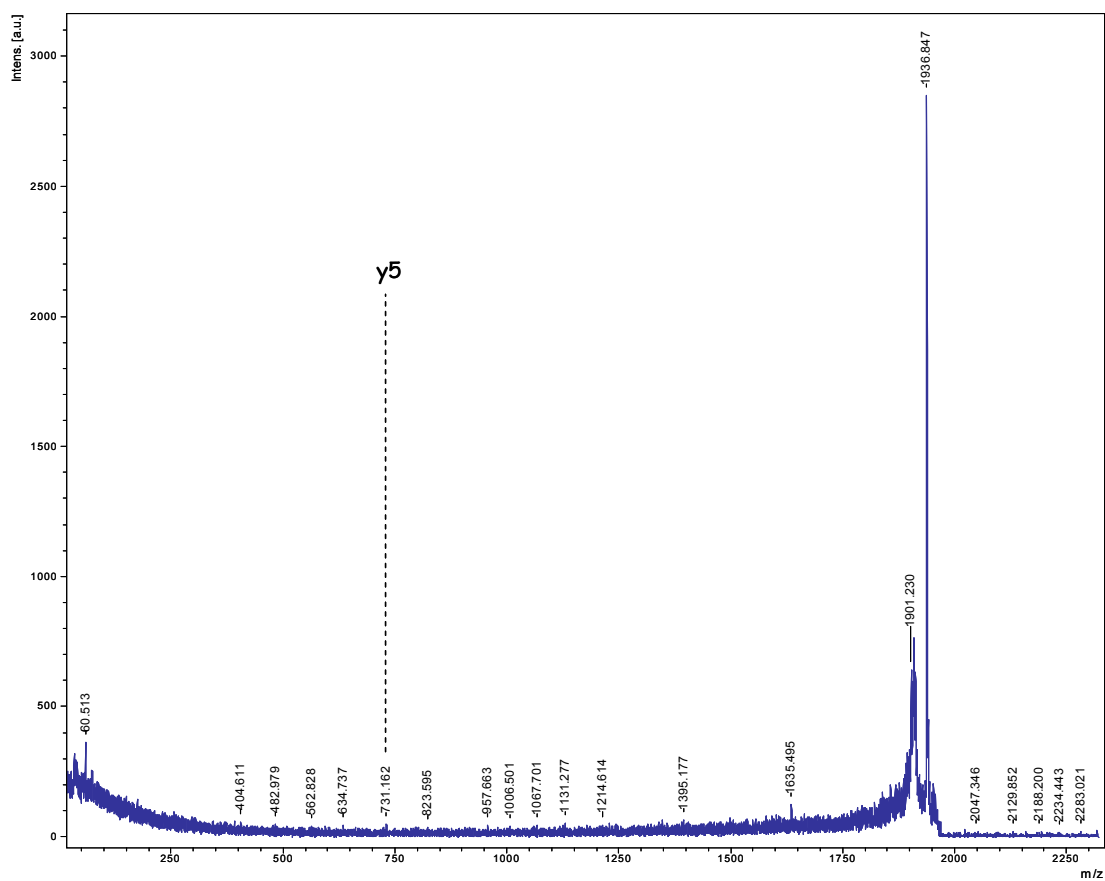


8.3 MALDI-TOF MS and MS/MS spectra

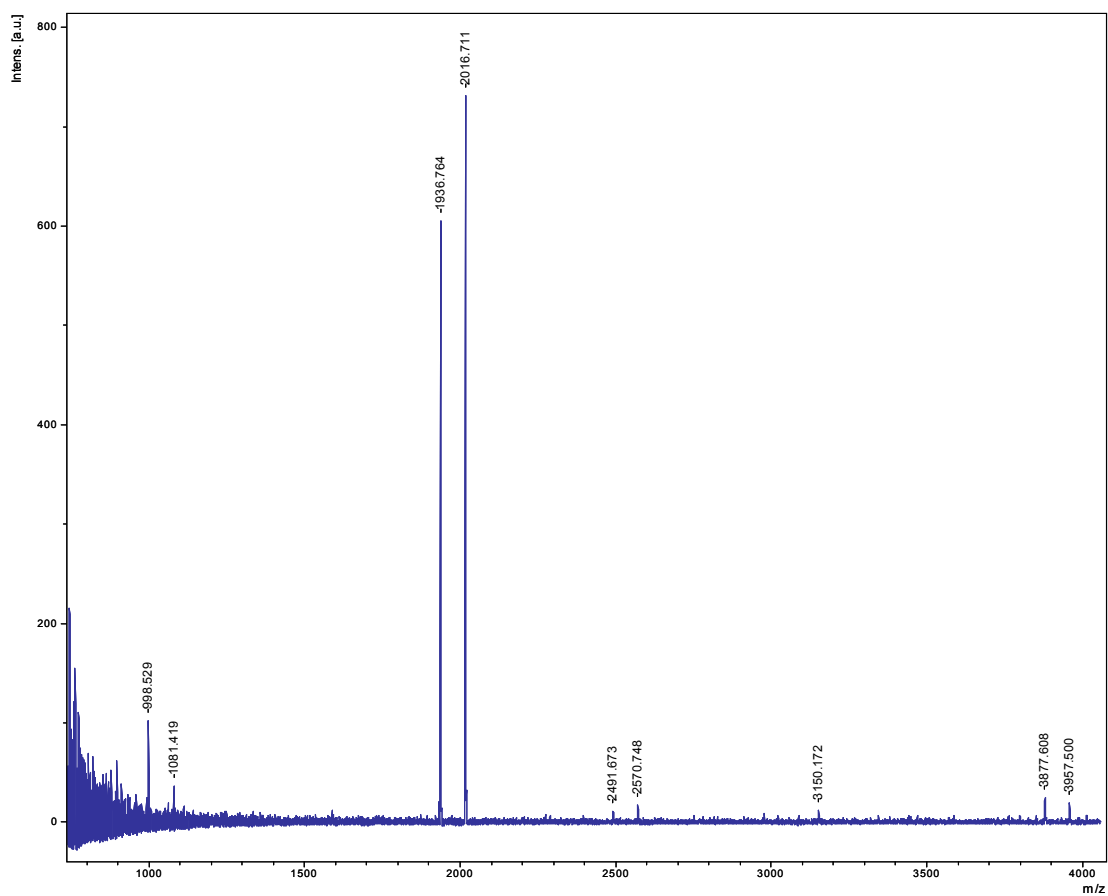
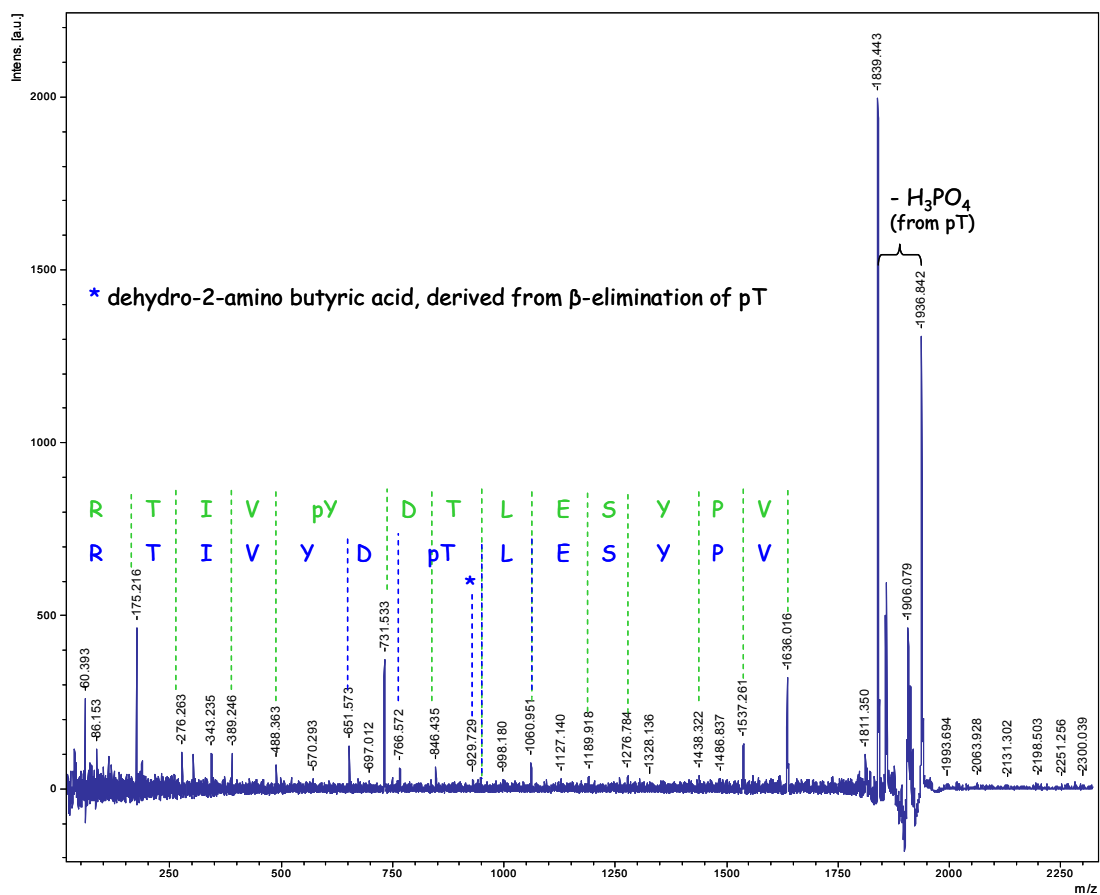
MALDI-TOF MS of His-LmxMPK3 phosphopeptides

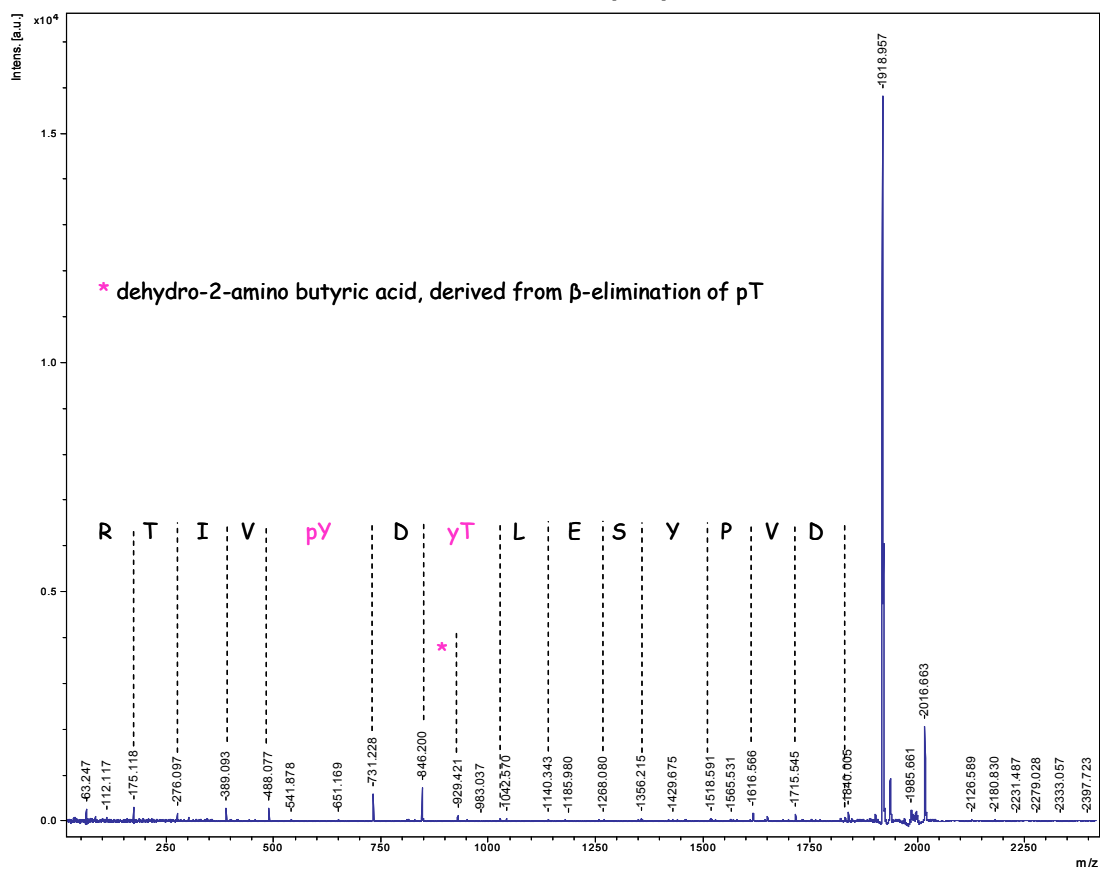


MS/MS of 1936.849; LmxMPK3 ¹⁸⁵SVDVPYSELTDpYVITR²⁰⁰

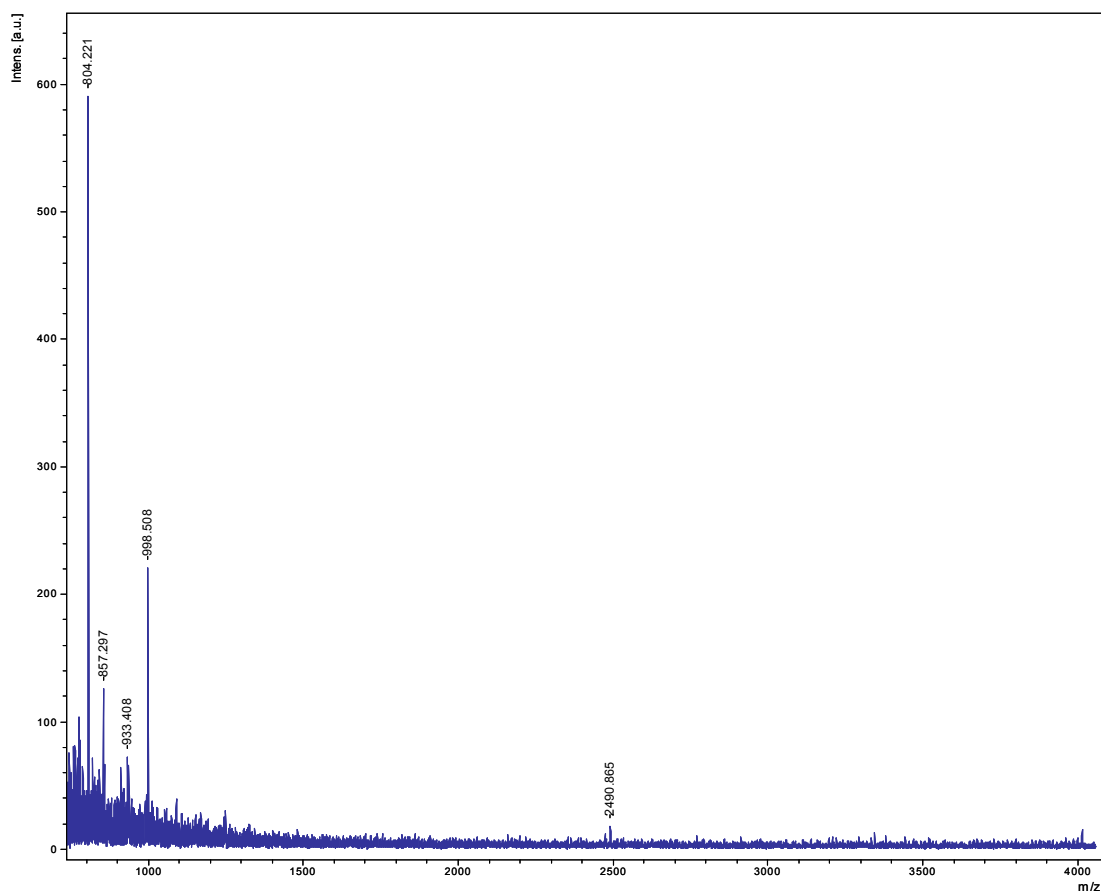


MALDI-TOF MS of His-LmxMPK3/(LmxMKK-D) phosphopeptides

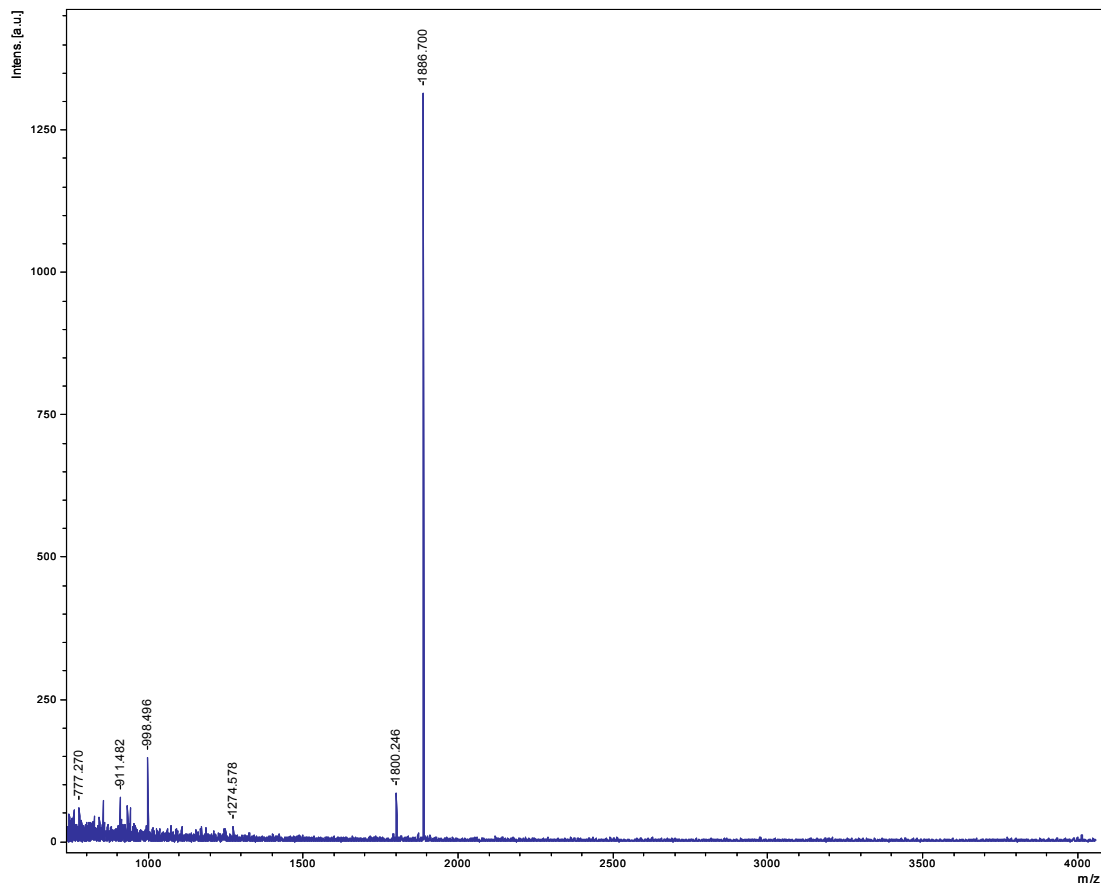
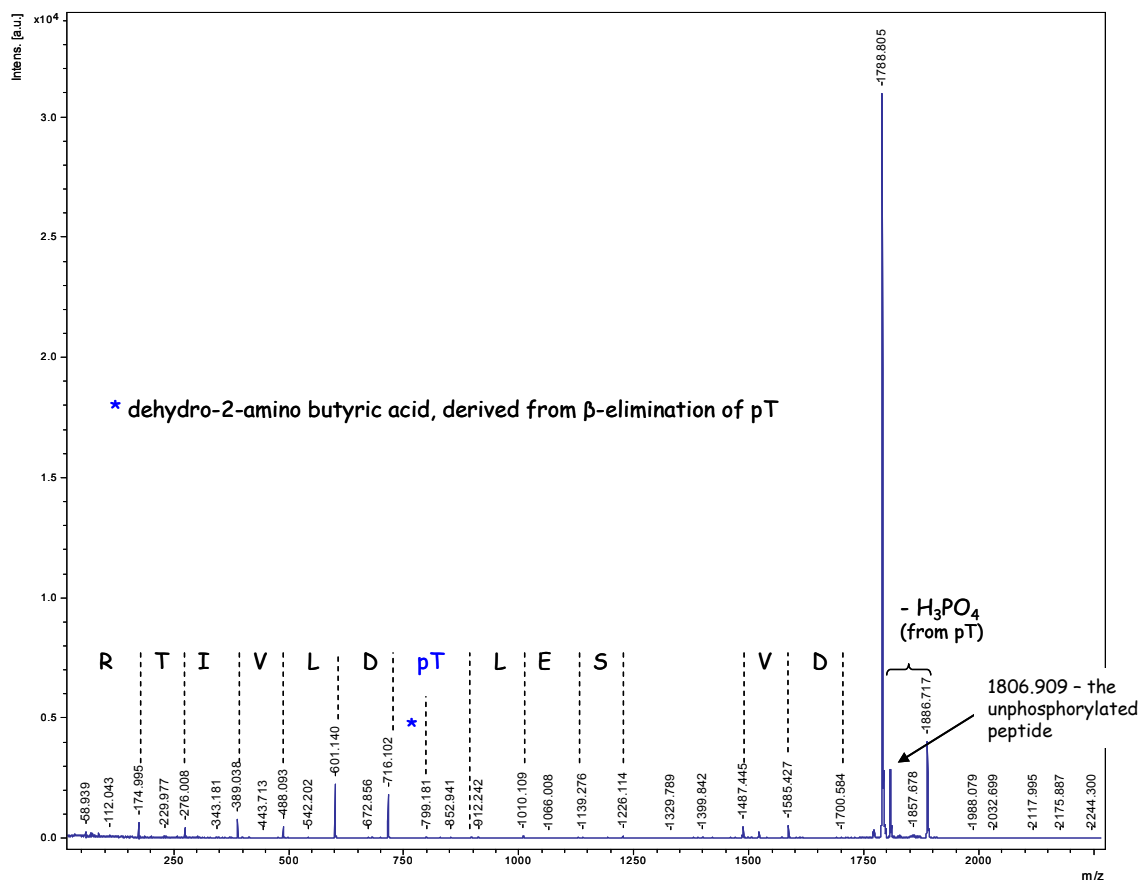
MS/MS of 1936.764; LmxMPK3 ¹⁸⁵SVDVPYSELpTDYVITR²⁰⁰ and ¹⁸⁵SVDVPYSELTDpYVITR²⁰⁰

MS/MS of 2016.711; LmxMPK3¹⁸⁵SVDVPYSELpTDpYVITR²⁰⁰

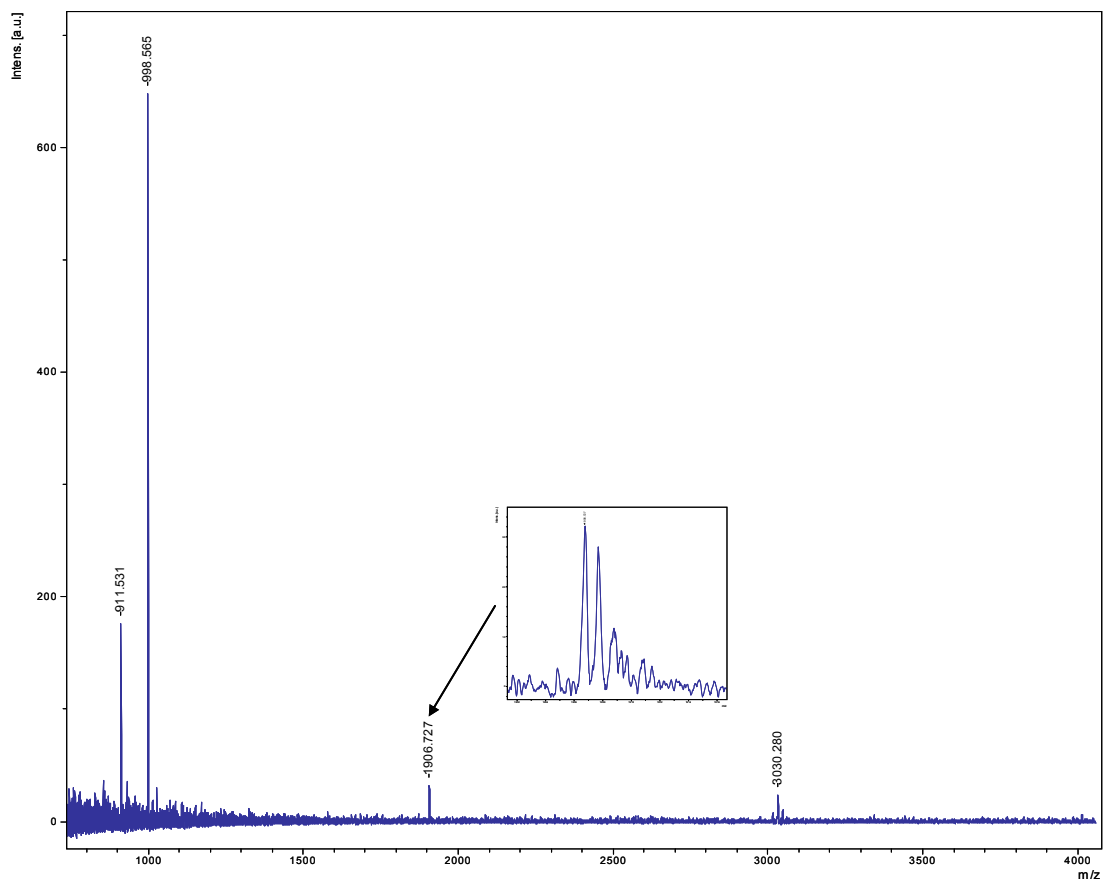
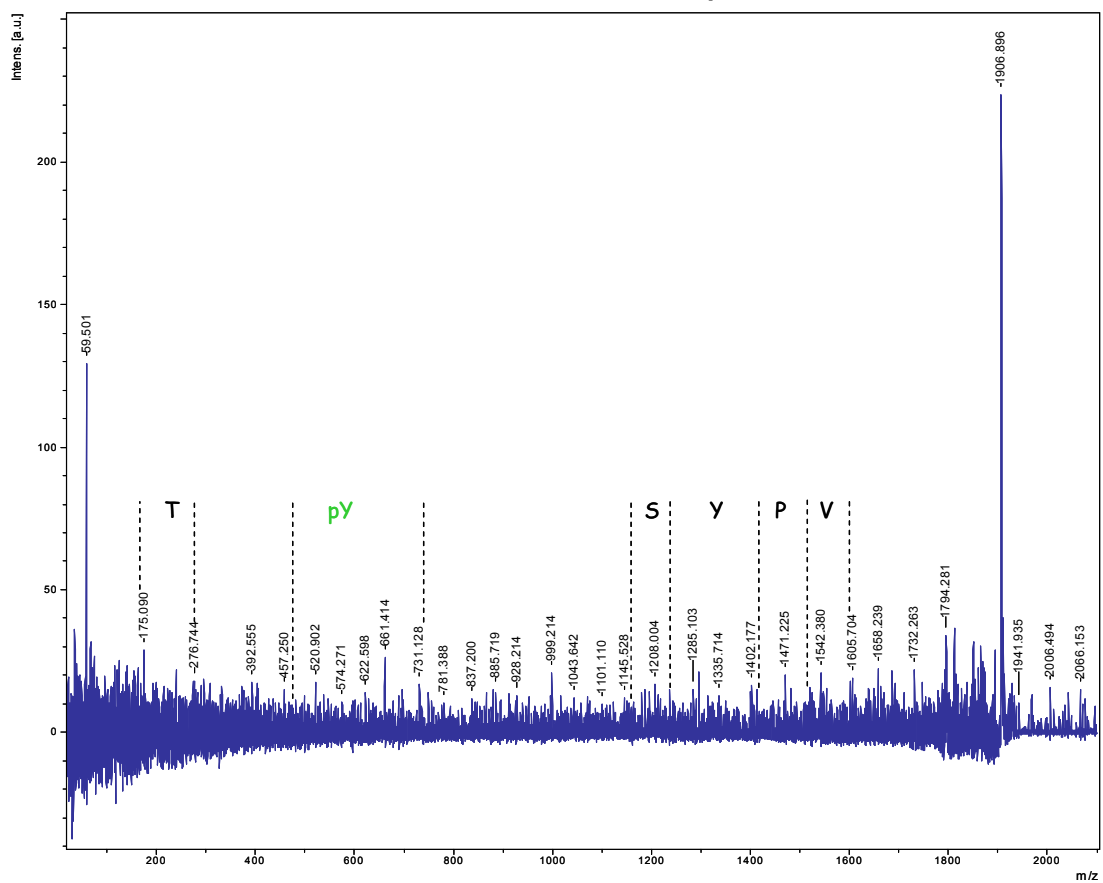
MALDI-TOF MS of His-LmxMPK3-TDL phosphopeptides



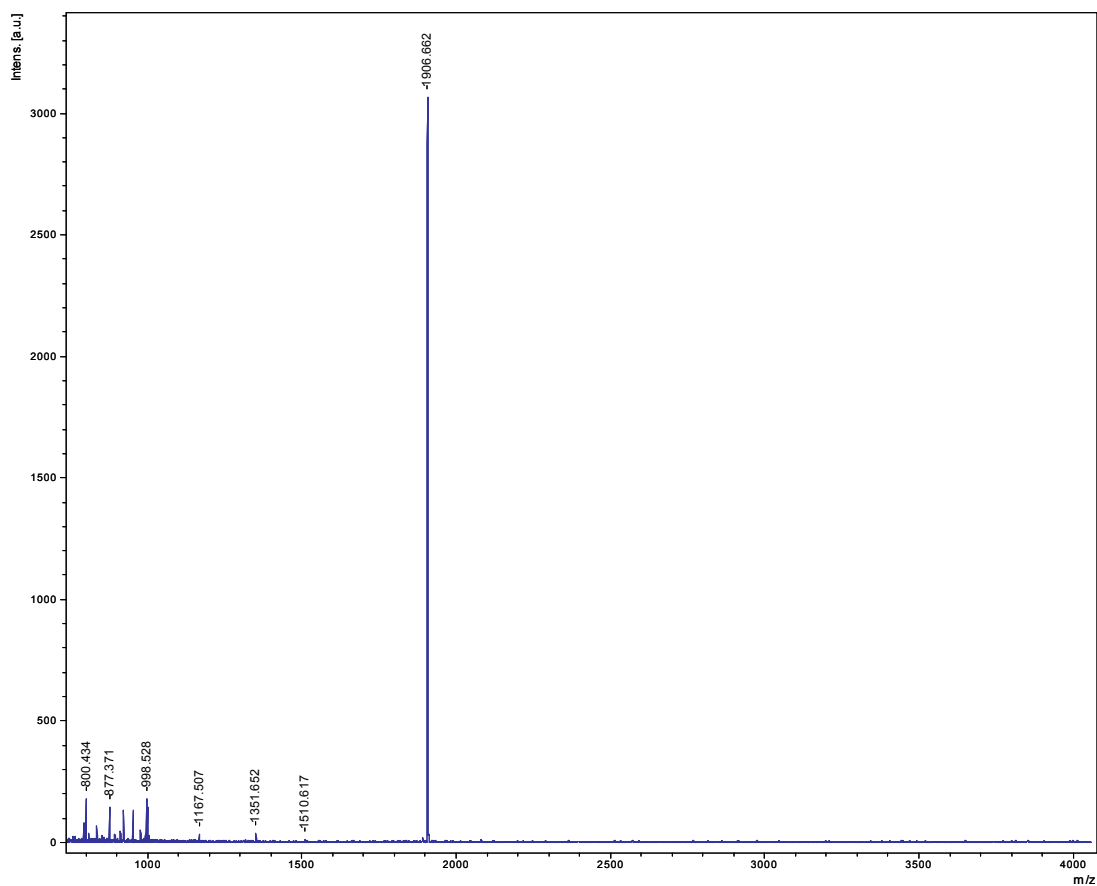
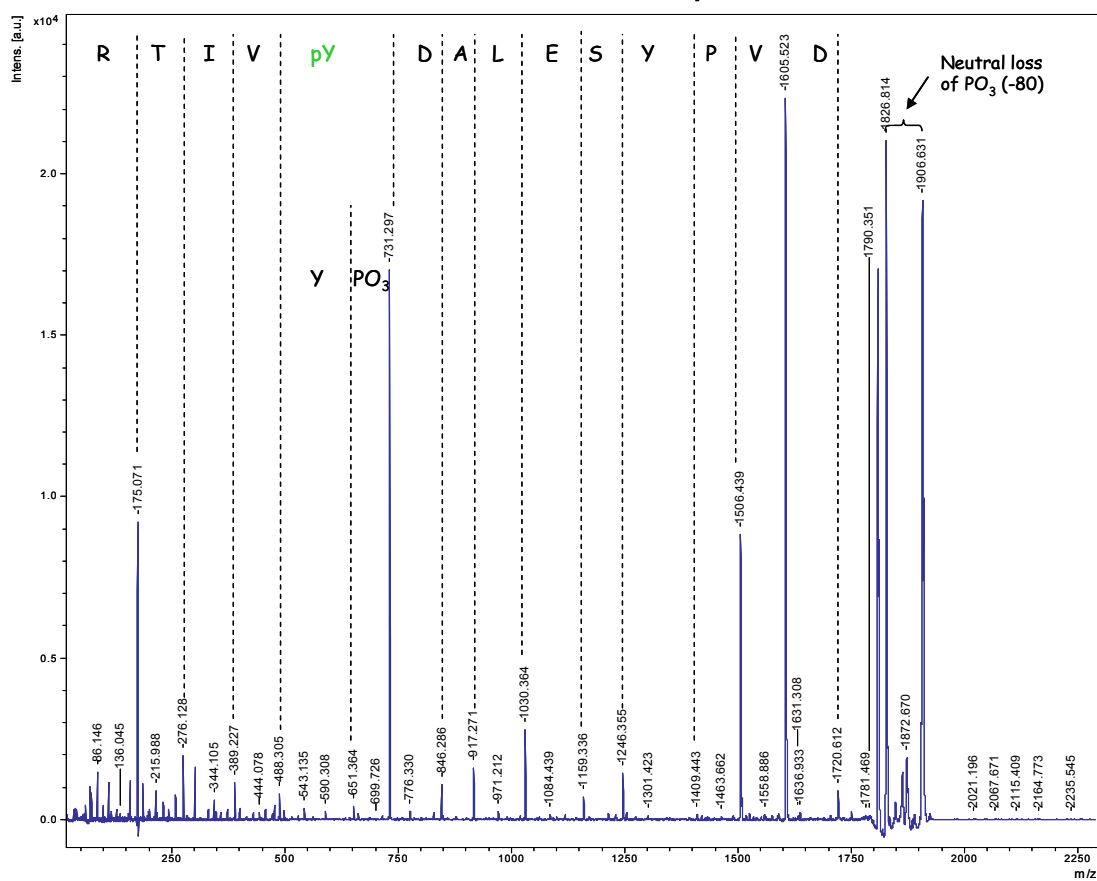
MALDI-TOF MS of His-LmxMPK3-TDL(/LmxMCK-D) phosphopeptides

MS/MS of 1886.700; LmxMPK3-TDL ¹⁸⁵SVDVPYSELpTDLVITR²⁰⁰

MALDI-TOF MS of His-LmxMPK3-ADY phosphopeptides

MS/MS of 1906.727; LmxMPK3-ADY ¹⁸⁵SVDVPYSELADpYVITR²⁰⁰

MALDI-TOF MS of His-LmxMPK3-ADY(/LmxMKK-D) phosphopeptides

MS/MS of 1906.662; LmxMPK3-ADY ¹⁸⁵SVDVPYSELADpYVITR²⁰⁰

Acknowledgements

I would first like to thank my supervisor Dr. Martin Wiese for the opportunity to carry out this project in his group, first at the Bernhard Nocht Institute in Hamburg, later at the University of Strathclyde in Glasgow (UK). Thank you for the continuous support as well as for the fruitful discussions and ideas.

I would also like to acknowledge Prof. Dr. Iris Bruchhaus for her willingness to read and assess this work.

I want to thank the Arthur and Aenne Feindt foundation for the generous financial support of the main part of the project. I also acknowledge the financial assistance of the University of Strathclyde during my time in Glasgow; a special thanks to Prof. Dr. Graham Coombs who arranged this support.

Furthermore, I would like to thank Christel Schmetz (BNI) for the electron microscopical analyses and Claudia Sander-Jülch (BNI) for the FACS of the parasites. Great thanks also to Heidi Rosenqvist from the University of Southern Denmark in Odense for the MS/MS analysis. I appreciated your helpfulness and patience to explain all the MS/MS spectra to me! I would like to acknowledge Prof. Dr. Petr Volf and coworkers from the Charles University in Prague for carrying out the sand fly transmission studies. I want to thank Dr. Joachim Clos (BNI) who kindly provided the co-expression vector pJCduet. Moreover, I would like to thank Prof. Dr. Jeremy Mottram from the University of Glasgow who generously offered me to use their microscopes and Daniela Tonn who always arranged the microscope booking and access for me.

I thank all past and present members of the Wiese group for the great teamwork and for making the place fun to work in! Great thanks to Anne MacDonald for her practical support, especially for the sample preparations for the electron microscopy. I would like to thank Anne S. for a fantastic cooperation on the “flagellar length” field and Inga, my bench neighbour, for a lot of good advice and mental support! A special thanks to Mona, Nadja and Stefan for all the lively discussions and for making Glasgow feel like home! Annette and Mareike, thank you for all the amusing conversations! I would also like to thank our trainees Nadine, Valea and Nils for their good work!

Finally, I would like to thank my sisters, Hanna and Lisa, and my parents for their continuous support and encouragement. Great thanks to my parents who helped me with moving to and back from Glasgow. Most importantly, I want to thank Dominik for his patience and for always cheering me up, and my friends for listening to me.